



IntechOpen

# River Basin Management

*Edited by Daniel Bucur*





---

# RIVER BASIN MANAGEMENT

---

Edited by **Daniel Bucur**

## River Basin Management

<http://dx.doi.org/10.5772/61557>

Edited by Daniel Bucur

### Contributors

Ata Amini, Muhammad R. Mustafa, Khamaruzaman B. W. Yusof, Soheila Zareie, Pezhman Taherei, Ertuğrul Karaş, Matjaž Glavan, Polona Ojsteršek Zorčič, Marina Pintar, Mihaela Constantin, Michio Sanjou, Adélia Nunes, Wei Shan, Ying Guo, Zhaoguang Hu, Jana Moravcová, Pavel Ondr, Jiri Pecenka, Jakub Polensky, Vaclav Bystricky, Tomas Pavlicek, Luis Mejia-Ortiz, Marilu Lopez-Mejia, Antonio Chale-Chim, Yazmin Perera-Pech, Keith Crandall, Oscar Frausto-Martinez, Luis Carlos Santander-Botello, Luca Franzi, Alessandro Pezzoli, Angelo Besana, Joe Magner, Modreck Gomo, Alla Kolesnikova, Elena Lapteva, Svetlana Degteva, Anastasija Taskaeva, Alexej Kudrin, Yulia Vinogradova, Fluza Habibullina, James L Seago, Willow B Eyres, Matthew F Volny, Soojun Kim, Igor Cretescu, Zsafia Kovacs, Sorin Mihai Cimpeanu

### © The Editor(s) and the Author(s) 2016

The moral rights of the and the author(s) have been asserted.

All rights to the book as a whole are reserved by INTECH. The book as a whole (compilation) cannot be reproduced, distributed or used for commercial or non-commercial purposes without INTECH's written permission.

Enquiries concerning the use of the book should be directed to INTECH rights and permissions department ([permissions@intechopen.com](mailto:permissions@intechopen.com)).

Violations are liable to prosecution under the governing Copyright Law.



Individual chapters of this publication are distributed under the terms of the Creative Commons Attribution 3.0 Unported License which permits commercial use, distribution and reproduction of the individual chapters, provided the original author(s) and source publication are appropriately acknowledged. If so indicated, certain images may not be included under the Creative Commons license. In such cases users will need to obtain permission from the license holder to reproduce the material. More details and guidelines concerning content reuse and adaptation can be found at <http://www.intechopen.com/copyright-policy.html>.

### Notice

Statements and opinions expressed in the chapters are those of the individual contributors and not necessarily those of the editors or publisher. No responsibility is accepted for the accuracy of information contained in the published chapters. The publisher assumes no responsibility for any damage or injury to persons or property arising out of the use of any materials, instructions, methods or ideas contained in the book.

First published in Croatia, 2016 by INTECH d.o.o.

eBook (PDF) Published by IN TECH d.o.o.

Place and year of publication of eBook (PDF): Rijeka, 2019.

IntechOpen is the global imprint of IN TECH d.o.o.

Printed in Croatia

Legal deposit, Croatia: National and University Library in Zagreb

Additional hard and PDF copies can be obtained from [orders@intechopen.com](mailto:orders@intechopen.com)

River Basin Management

Edited by Daniel Bucur

p. cm.

Print ISBN 978-953-51-2604-1

Online ISBN 978-953-51-2605-8

eBook (PDF) ISBN 978-953-51-6666-5

# We are IntechOpen, the world's leading publisher of Open Access books Built by scientists, for scientists

**3,800+**

Open access books available

**116,000+**

International authors and editors

**120M+**

Downloads

**151**

Countries delivered to

Our authors are among the  
**Top 1%**

most cited scientists

**12.2%**

Contributors from top 500 universities



**WEB OF SCIENCE™**

Selection of our books indexed in the Book Citation Index  
in Web of Science™ Core Collection (BKCI)

Interested in publishing with us?  
Contact [book.department@intechopen.com](mailto:book.department@intechopen.com)

Numbers displayed above are based on latest data collected.  
For more information visit [www.intechopen.com](http://www.intechopen.com)





# Meet the editor



Daniel Bucur is currently a professor of Land Improvement at the Pedotechnics Department, University of Applied Life Sciences and Environment in Iasi, Romania. He completed his doctorate at the Technical University of Iasi in 1998. His major research areas include water excess removal, irrigation, soil erosion control, climate changes, and sustainable land management. In recent years, he has been in charge of many national and international research projects, including Soil Erosion and Conservation Measures, Effect of Sewage Sludge Application on Quality Indices of Soil Vulnerable to Degradation, Sustainable Development of Soil Resources from the Areas with Drainage Works, and Impact of the Hydro-climatic and Pedo-geomorphological Risks on the Environment in Small Catchment. He has published more than 150 papers in reviewed journals, 5 book chapters, and 9 books apart from more than 30 unreviewed papers and reports.





---

# Contents

---

## **Preface XI**

- Section 1 Regional Impacts of Climate Change on Hydrological Extremes 1**
- Chapter 1 **Landslides Caused by Climate Change and Groundwater Movement in Permafrost Mountain 3**  
Wei Shan, Ying Guo, Zhaoguang Hu, Chunjiao Wang and Chengcheng Zhang
- Chapter 2 **River Basin Management in the Past and at Present and its Impact on Extreme Hydrological Events 35**  
Jana Moravcová, Václav Bystřický, Jiří Pečenka, Jakub Polenský, Tomáš Pavlíček, Nikola Nováková and Pavel Ondr
- Chapter 3 **Streamflow Response to Climate Variability and Land-Cover Changes in the River Beça Watershed, Northern Portugal 61**  
Adélia. N. Nunes and Patrícia Lopes
- Chapter 4 **Hydrological Drought Analysis Based on Copula Theory 81**  
Jaewon Kwak, Soojun Kim, Duckhwan Kim and Hungsoo Kim
- Chapter 5 **Drought Analysis and Water Resources Management Inspection in Euphrates–Tigris Basin 97**  
Ata Amini, Soheila Zareie, Pezhman Taheri, Khamaruzaman Bin Wan Yusof and Muhammad Raza ul Mustafa
- Chapter 6 **Flood Lamination Strategies for Risk Reduction 113**  
Luca Franzì, Alessandro Pezzoli and Angelo Besana

<b>Section 2</b>	<b>Sustainable Land Use Planning in the River Basins</b>	<b>133</b>
Chapter 7	<b>Sustainable Land Use Planning Model in Rural Basins</b>	<b>135</b>
	Ertuğrul Karas	
Chapter 8	<b>Modelling Agri-Environmental Measures for Minimizing Soil Erosion While Protecting Valuable Agricultural Land</b>	<b>165</b>
	Matjaž Glavan, Polona Ojsteršek Zorčič and Marina Pintar	
<b>Section 3</b>	<b>River Engineering and River Basin Development</b>	<b>191</b>
Chapter 9	<b>Riverine-Based Aquifers and Riparian Exchange: A Conceptual Discussion</b>	<b>193</b>
	Modreck Gomo and Joe Magner	
Chapter 10	<b>Monitoring of Surface Water Status in the Lower Danube Basin</b>	<b>205</b>
	Igor Cretescu, Zsófia Kovács and Sorin Mihai Cimpeanu	
Chapter 11	<b>Turbulence Diffusion Mechanism in Submerged Vegetation Flows</b>	<b>225</b>
	Michio Sanjou	
<b>Section 4</b>	<b>River Ecosystems Management and Conservation</b>	<b>249</b>
Chapter 12	<b>Selected Structural Features of the Riverine Plants, <i>Trapa natans</i> (Lythraceae) and <i>Justicia americana</i> (Acanthaceae)</b>	<b>251</b>
	James L. Seago, Willow B. Eyres and Matthew Volny	
Chapter 13	<b>Biodiversity of Floodplain Soils in the European North-East of Russia</b>	<b>271</b>
	Alla Kolesnikova, Elena Lapteva, Svetlana Degteva, Anastasia Taskaeva, Alexey Kudrin, Yulia Vinogradova and Fluza Khabibullina	
Chapter 14	<b>Freshwater Prawns (Palaemonidae: Macrobrachium) with Abbreviated Larval Development in Rivers of Mexico: Uses, Management, and Conservation Opportunities</b>	<b>295</b>
	Luis M. Mejía-Ortíz, Marilú López-Mejía, Antonio Chale Chim, Yazmín Perera-Pech, Keith A. Crandall, Oscar Frausto-Martínez and Luis C. Santander-Botello	

---

## Preface

---

In many regions of the world, soil and water management has been always a major problem due to the insecurity and climatic variations. Along with the society development, the human actions in the natural environment—at first isolated and insignificant—have gradually increased so lately; anthropogenic intervention on relatively large areas has become decisive in the manifestation of soil erosion processes, for instance, its effects exceeding as breadth and intensity ones of natural factors of erosion. Through industrial development and urban life, man intervenes directly on local climate; by soil tillage, man mobilizes annually a huge mass of soil, transforming radically the aeration, hydric and thermal regime conditions, biological processes, etc. Man changes the geographical landscape—with multiple consequences on the regimes of watercourses and of the topoclimates—landforms shaping, deforests and afforests large areas of land, etc.

In addition, the climate changes in recent decades complicated the watershed management in many areas of the world. In this context, the scientific investigations on the issue of sustainable use of water, soil, and natural capital as a whole, from the hydrographical basins, are timely and important.

This book is structured into four sections, which group different aspects of the addressed matter, consisting of fourteen chapters.

The first part presents hazards resulting from hydrological extremes in different regions of the world, from the landslide caused by climate warming in the permafrost mountain in Northeast China, to the hydrological drought analysis in the Euphrates-Tigris Basin and severity-duration-frequency relationships of droughts over south part of Korean Peninsula, and the flood risk management in the Po Basin from Italy. It is also argued that the impacts of climate variability and land use/cover change on streamflow are challenging and crucial to the management of water resources in the Mediterranean river basins.

The impact of the management of river basin practices in the Czech Republic, on water quality and on the retention capacity, with reference to the occurrence and consequences of both floods and periods of drought was analyzed.

A special importance is given to the sustainable use of the land. Thus, in the second part of the book, a sustainable land use planning model for the semiarid basins and agri-environmental measures in order to maintain the soil losses by erosion in tolerable limits are presented. On the basis of a multi-scale modeling and management approach, an effective decision support tool for evaluating better management options for sustainable development in the rural watershed in Turkey and Slovenia was provided.

A conceptual discussion of the aquifers that typically occur along river channels and the riparian exchange of water as influenced by valley and channel type and management are presented in the third part of the book. The monitoring and analysis of cross-border river water quality are the subject of the same part of the book.

Environmental problems in river basin have been recently highlighted as public interest, and thus many researchers tried to reveal mass and momentum transfers associated with the wind waves, turbulence diffusion, and coherent vortex. Related to this issue, an interesting study focused on fundamental hydrodynamic characteristics and related turbulent diffusion properties in the vegetated open-channel flows.

The last part of the book presents issues related to river ecosystem management and conservation. Aquatic, stoloniferous plantlets with floating leaves and nodal, adventitious roots of *Trapa natans*, and emergent, stoloniferous, rooted plants of *Justicia americana* from the Oswego River, New York, USA, were investigated in order to illustrate the kinds of anatomical adaptations of native and invasive eudicot species to their riverine habitats. River floodplains are unique nature landscapes. In contrast to zonal communities on watersheds, soil biota of river floodplains is studied in less degree. In compensation, an interesting study is conducted in the floodplain forests in the European North-East of Russia that shows high diversity of soil biota in alluvial forest soils.

Considerations about the use, management, and conservation opportunities of the freshwater prawns in Mexico rivers conclude the issues included in this book.

Each chapter has the extension adapted to the addressed issues, updated content with the data in the literature and with the scientific results of the authors.

It should be stressed that each chapter has the extension adapted to the addressed issues, updated content with the data in the literature and with the scientific results of the authors.

Without claiming that it is an exhaustive presentation of the complex issue of watershed management, we believe that this book can be successfully used by students, academics, researchers, and field professionals and that it can serve as a basis for new scientific approaches.

**Prof. Dr. Daniel Bucur**

University of Applied Life Sciences and Environment in Iasi  
Romania

---

# Regional Impacts of Climate Change on Hydrological Extremes

---



---

# **Landslides Caused by Climate Change and Groundwater Movement in Permafrost Mountain**

---

Wei Shan, Ying Guo, Zhaoguang Hu,  
Chunjiao Wang and Chengcheng Zhang

Additional information is available at the end of the chapter

<http://dx.doi.org/10.5772/63068>

---

## **Abstract**

Climate change induced warming results in permafrost degradation. Melting permafrost subsequently leads to an increased incidence of landslides. The study area was within the northwest section of the Lesser Khingan Range in northern China along the Bei'an-Heihe Highway. We analyzed the impact of climate change on landslide movement in the permafrost zone via a combination of geological survey and meteorological data. The average annual temperature of the study area has increased by 3.2°C in last 60 years, and permafrost degradation is severe. Loose soil on the hillside surface provides appropriate conditions for the infiltration of atmospheric precipitation and snowmelt, and seepage from thawing permafrost. As it infiltrates downwards, water is blocked by the underlying permafrost or dense soil, and infiltrates along this barrier layer toward lower positions, forming a potential sliding zone. The combination of high density resistivity (HDR) methods based on soil resistivity values, ground-penetrating radar (GPR) methods based on characteristics of radar wave reflection, respectively, and geological drilling can be utilized to determine the regional stratigraphic distribution. This will allow the exact location of the landslide sliding surface to be precisely determined. Field test results indicate that radar reflectivity characteristics and the resistivity values of the soil in the landslide mass is significantly different from surrounding soil. There are sudden decreases in the apparent resistivity values at the sliding surface location. In addition, the radar exhibits strong reflection at the sliding surface position, with a sudden increase in the amplitude of the radar wave. Drilling results indicate that the soil has high water content at the location of the sliding surface of the landslide mass in the study area, which is entirely consistent with the GPR and HDR results. Thus, abnormal radar wave reflection and abrupt changes in apparent resistivity values can be used in practice to identify the location of landslide sliding surfaces in this region. We produce a detailed analysis of a representative landslide within the study area. Displacement monitoring locations were positioned at the trailing edge of the landslide mass and on the landslide mass surface.

We then used this data to determine the relationships of landslide movement with both ground temperature and the trailing edge pore water pressure. The results suggest seasonal variation in the landslide movement process and characteristics of an annual cyclical trend. Landslide movement can be described by intermittence and low angles. The slip rate and the timing of slide occurrence exhibit relationships with the trailing edge pore water pressure of the landslide mass. The seepage of thaw water into the landslide mass will impact the trailing edge pore water pressure of the landslide mass. This phenomenon is identified as the primary cause of landslide movement.

**Keywords:** climate change, groundwater movement, permafrost, landslides, mountains

---

## 1. Introduction

The area north of 47° N in northeast China exhibits widespread permafrost. This represents the sole high-latitude permafrost region in China. This region also represents the second largest permafrost region in China [1–3]. In recent years, the southern boundary of this high-latitude permafrost region has gradually moved to the north as a result of climate change. Permafrost proximate to the southern boundary exhibits accelerated degradation and a distribution that is discontinuous and island-like [4–6].

Climate change refers to the temporal alteration of the baseline state of climate. The mean global surface temperature has been increasing throughout the last century. The rate of warming during 1957–2007 was almost double the rate during 1957–2007 [7]. Temperatures in a majority of the permafrost regions throughout the world have risen since the early 1980s. The recorded temperature rise has reached 3°C in some regions in northern Alaska, and the rise has reached 2°C in the northern regions of Europe and Russia. During the period of 1975–2005, there were significant reductions in the range and thickness of the permafrost layer in the northern area of Russia [8]. Climate change and its impact are an important research issue receiving extensive global attention.

A number of studies have demonstrated that climate change in China has presented the same tendency as the global trend [9]. The temperature increase rate in China for the last 54 years was approximately 0.25°C/10a. This value far exceeds the hemispheric and global average rates of warming. Northeast China is among the national areas exhibiting the most notable warming and permafrost degradation [10].

Accumulated snow and vegetation have extremely significant impacts on the thawing process of the underlying seasonal frozen ground and permafrost [11]. Temperature shifts caused by snow, vegetation, water, topography, atmospheric inversion, and other local factors can be substantial in the Great and Lesser Khingan Ranges of northeast China and the Outer Baikal region of Russia. This results in the “Khangin–Baikal type” permafrost that differs from high-altitude and polar permafrost distributions [12, 13]. The form and process of high-latitude permafrost degradation in northeast China are also affected by the occurrence conditions. Therefore, the form and process of degradation in this region differ from their analogs in high-altitude and polar [14].



Landslide events tied to extreme weather and climate change have increased in recent years [15], and have gradually received attention from national governments and relevant international academic organizations [16, 17]. In particular, landslides in cold areas are becoming a hot issue in landslide research [18, 19].

Landslides are geological phenomena that naturally occur in mountainous areas. The triggering mechanism and evolution of landslides are closely tied to environmental factors and geological conditions. Landslides are influenced by geological forces, lithologic structure, and other crustal internal factors as well as by land cover, topography, human activities, precipitation, and environmental conditions. The temporal and spatial distribution of landslides exhibits characteristics of continuation, uncertainty, intermittency, and irreversibility. Landslides are the result of environmental and geological changes and their occurrence can dramatically alter the geology of an area [20]. Scientists have applied various methodologies to analyze the relationships between climate change in cold areas and landslide evolution and mechanisms [21]. These studies have discussed the landslides induced by permafrost and glacier degradation and their impact on the geology, topography, biodiversity, and water resources. Climate has also been investigated as a main factor influencing the landslide evolution in cold regions [22–28]. However, the preponderance of these studies were conducted at large-scales due to a lack of observational data [29]. To date, there have been no studies on the movement characteristics, mechanisms, and patterns of landslides caused by the combined effects of extreme weather events and permafrost thawing.

In the present study, we designate the area surrounding the intersection of the Bei'an to Heihe Highway with the northwest region of the Lesser Khingan Range as the study area. We conducted field measurements, a geological survey, and an engineering survey. These data sets were plotted on a geological cross section and a topographic map of the landslide area. We investigated the impact of climate change on geological environment, permafrost thaw, and landslide mechanisms in the study area via meteorological data from Sunwu County (30 km from the study area) provided by the China Meteorological Data Sharing Service System (<http://cdc.cma.gov.cn/home>). In order to conduct a comprehensive analysis of the impact of climate change on the landslide movement process and the pore water pressure, we utilized point displacement on the landslide mass, trailing edge ground temperature, and pore water pressure data sets collected from the landslide area of the Landslide K178 + 530. In addition, in this paper we apply a combination of geophysical techniques (HDR and GPR) and traditional methods (drilling and mapping) to Landslide K178 + 530 that occurred in the Lesser Khingan Range of northeast China. Landslides occur frequently in this region due to atmospheric precipitation and permafrost degradation. We aim to determine the thickness and internal structure of the study landslide and thereby ascertain the applicability of GPR and HDR for these regional types of landslide.

## 2. Background

The study area ranges between 127° 17' 31"–127° 21' 24" east longitude and 49° 30' 57"–49° 41' 50" north latitude (**Figure 1**). In this area, the northwest section of the Lesser Khingan Range

intersects the Bei'an-Heihe Highway at the border between Sunwu County and the Aihui District. The area is located on the southern fringe of China's high-latitude permafrost region and has typical periglacial landforms. The island-like permafrost in this region is the result of residual paleo-glacial deposition and is currently in the degradation stage. The geological conditions are extremely unstable.



**Figure 1.** High-latitude permafrost distribution in Northeast China (data from Zurich University, Switzerland), and the location of study area.

## 2.1. Climate conditions

The study area is positioned in the transition area between the cold-temperate zone and the northern area of the middle temperate zone. The area is subject to monsoons as well as alternating influences from high and low pressures originating from inland and the ocean. Generally, the study area experiences dry, cold, and long winters as well as hot, humid, and short summers. It is classified as a continental monsoon climate zone.

In the study area, the average annual temperature is within the range of  $-2$  to  $1^{\circ}\text{C}$ , with an extreme minimum of  $-48.1^{\circ}\text{C}$  and an extreme maximum of  $38.6^{\circ}\text{C}$ . The average annual precipitation is within the range of 530–552 mm, with a maximum of 800 mm. Precipitation is mostly concentrated from July to September during the summer. The precipitation that falls during this period accounts for 61–67% of the total yearly precipitation. The first snow fall is typically in mid-October, and the final snow fall is often in late March or early April of the following year. The annual average wind speed is 2.7–4.0 m/s. The minimum annual evaporation is 850 mm and the maximum annual evaporation exceeds 1000 mm. The average annual total radiation is  $1148 \text{ kcal/cm}^2$ , with a minimum of  $1039 \text{ kcal/cm}^2$  and a maximum of

1229 kcal/cm<sup>2</sup>. The average annual sunshine is 2500 h, with a minimum of 2200 h and a maximum of 2800 h.

## 2.2. Permafrost distribution

The climate in Northeast China is subject to the Siberia-Mongolia high-pressure system. This region has a widely distributed inversion layer. This layer has important impacts on the regional distribution and development process of permafrost. Meanwhile, the majority of forest area in China is distributed in the northeast region. In this area, permafrost coexists and is influenced by wetlands, grasslands, and forests. Forests, mosses, shrubs, and other ground covers reduce absorption of solar radiation, thereby decreasing ground and air temperatures. The valleys, low-lying river terraces, shady slopes, and wetlands provide suitable conditions for slow permafrost degradation as well as the development of island-like permafrost.

In the study area, the seasonal frozen ground reaches its maximum depth at the end of May. The recorded maximum depth of seasonal frozen ground is in the range of 2.26–2.67 m. In the mountains, the maximum depth of seasonal frozen ground can exceed this range. The thawing period of seasonal frost is April to September. All the seasonal frost in dry areas thaws by early July. However, seasonal frosts do not completely thaw in swampy areas with thick peat and humus zones until the end of October. Island-like permafrost is mainly distributed in valley areas and on shaded slopes.

## 2.3. Climate change in the study area

Due to global climate change, the study area is among the regions in northeast China that have experienced the largest temperature increases during the past 50 years. Sunwu County meteorological data indicate that during the past 60 years, change in temperature was the most significant among all climate indicators. Using meteorological data from Sunwu County,

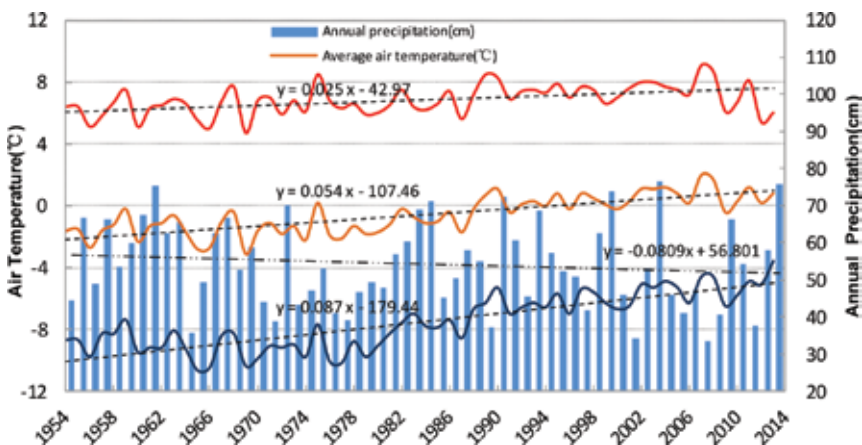


**Figure 2.** Annual average maximum temperatures, average temperatures, average minimum temperatures and average precipitation in Sunwu County (1954–2013).

**Figure 2** shows the yearly average temperatures, average maximum temperatures, average minimum temperatures, and average precipitation from 1954 to 2013. Linear regression indicates that during the 60 year period from 1954 to 2013 the annual average temperature increased by 3.2°C; the average annual minimum temperature increased by 5.2°C (69.04%); the average annual maximum temperature rose by 1.5°C (21.99%); and the average annual precipitation decreased by 4.85 cm (8.93%). The average annual minimum temperature increase was 3.45 times the increase in the average annual maximum temperature.

The permafrost distribution map generated from the Enhanced Thematic Mapper (ETM+) data collected in 2009 via the Landsat7 satellite (**Figure 3**) indicates that the landslide locations match the permafrost distribution to a high degree [30]. We therefore conjectured that these landslides were the result of thawing permafrost.



**Figure 3.** Permafrost distribution map in K176 + 500–K180 + 000 section of Bei'an-Heihe Highway.

#### 2.4. Climate change and landslides

Climate change in the study area has led to permafrost degradation, and engineering projects have exacerbated the permafrost degradation process [31]. In 1999, a planning survey conducted for the secondary road from Bei'an to Heihe indicated that along the entire road length there were 17 permafrost road segments [32, 33]. However, a survey conducted right before the construction of the Bei'an-Heihe Highway in 2009 showed that there were only six permafrost road segments remaining; the other 11 segments had been completely degraded.

The survey conducted in 2009 showed that within 10 m of the left of the roadbed in the K177 + 400 to K179 + 200 section there were four landslides with a total volume that exceeded 20,000 m<sup>3</sup> (**Figure 6**). In addition, there were numerous landslides within 3 km of this road section (**Figure 4**).

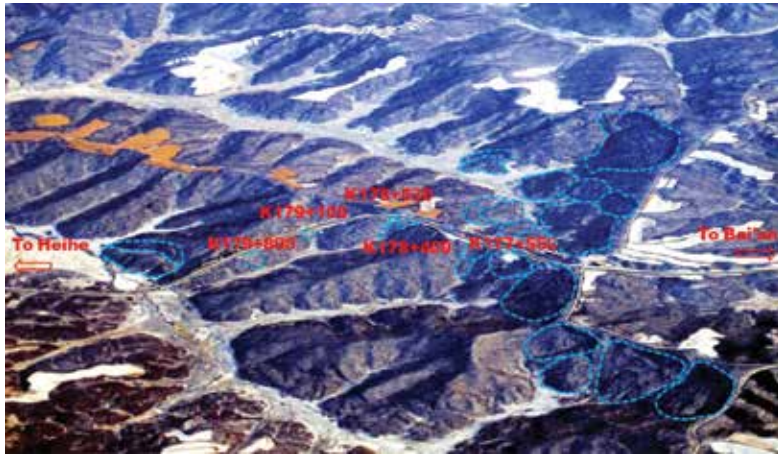


**Figure 4.** Full view of K175 + 500–K180 + 200 section of Bei'an-Heihe Highway (blue line is the boundary of the landslides, the orange area is corn field).



**Figure 5.** Satellite photos of K176 + 500–K179 + 900 section of Bei'an-Heihe Highway (Google earth). (A) Landslide in K178 + 530 section (in 2000); (B) satellite photos of K178 + 530 (2004.6); and (C) satellite photos of K178 + 530 (2010.9).

The phase change of water during the thawing of permafrost has a significant impact on the soil's mechanical properties [34]. Permafrost degradation causes a multitude of geological engineering issues for road construction. In 1999, the Bei'an-Heihe secondary road construction began. A landslide was caused by thawing of permafrost in the roadbed during August 2000 in the K176 + 900 to 178 + 200 section. This necessitated the abandonment of this section due to instability over the entire roadbed. The road had to be redirected along the left side of the ridge (**Figure 5A**).

### 2.5. Topography and geological structure

The study area encompasses a hilly landscape with rolling terrain. The slope is typically within the range of 10–20°. The upper sections of the slopes are usually within the range of 25–30° but can reach up to 40°. The area can also be divided into hills and valley bottomland. The altitude range over the entire area is 210–330 m. A 2010 survey also showed that, in the section between K177 + 400 and K179 + 200, there were four landslides within 10 m of the left of the roadbed with a total surface area of over 2000 m<sup>2</sup> (Figure 6). The four landslides are located at the A, B, C and D position, respectively. C illustrates Landslide K178 + 530. Figure 6 shows the geologic and geomorphic map of the landside road area of the study area plotted from the field survey conducted in June 2010.

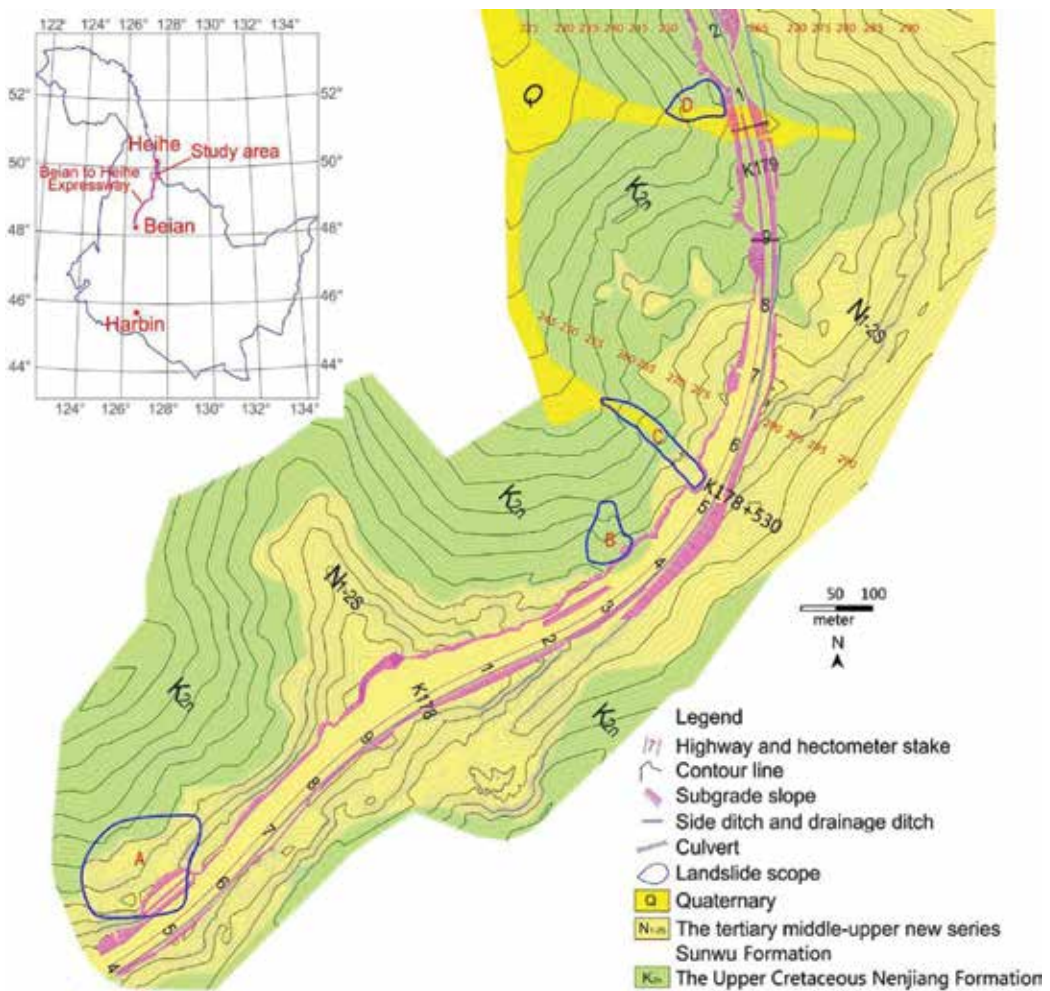


Figure 6. Geological map of K177 + 400–K179 + 200 section of Bei'an-Heihe Highway.

The geology of the study area can be characterized as belonging to the Khingan-Haixi fold belt. Beginning at the surface and moving down, the stratigraphy is composed of powdery sandstone, silty mudstone, Tertiary pebbly sandstone, and Cretaceous mudstone. The Lesser Khingan Range experienced block uplift during a period from the late Tertiary to the early Quaternary. Due to leveling and long-term erosion, loose sediment has gradually thinned at the summit and on the slopes of hills. The current residual layer is typically only 1–2 m thick. The loose deposits mainly accumulate with a thickness of approximately 10 m in the valley and basin areas between mountains. The soil is mainly composed of mild clay, clayey silt, and gravelly sand. The ground is covered with a relatively thick layer of turf and grass peat. The surface vegetation is composed of woodland and grassland, and there are inverted trees in the woodlands.

Landslide K178 + 530 is positioned at the widened embankment on the left side of the Bei'an-Heihe Highway (**Figure 7**). The surface soil and the roadbed soil slide together along the valley, and the maximum slippage is 200 m distance from the road. This landslide mass is 20–30 m wide and covers an area of approximately 6000 m<sup>2</sup>. The distance between the leading and trailing edges is 200 m. The height of the trailing edge is 285 m, and the height of the leading edge is 254 m. The landslide trailing edge has an arc-shaped dislocation that is positioned within the widened embankment.



**Figure 7.** Landslide scene photos: (a) Panoramic view of landslide (in November 2014); (b) the trailing edge of landslide (in June 2010); and (c) the leading edge of landslide (in October 2013).

For prospecting purposes, four boreholes were drilled into the K178 + 530 section. The borehole depths were within the range of 14–26 m, and the distribution of boreholes is presented in **Figure 8**. The drilling revealed the soil profile as follows, from bottom to top: Cretaceous mudstones, siltstones, Tertiary pebbly sandstones, and Quaternary loose Embankment:

yellow, primarily composed of loosely mixed Tertiary pebbly sandstones, sandy mudstones, and Cretaceous mudstones; the soil is plastic when saturated with water and loose when dry. Clay: yellow, plastic and with high rigidity and strength when dry. The downstream region of the landslide mass has a depth distribution within the range of 0–6.7 m. The upstream region of the landslide mass has a depth distribution within the range of 1.5–3.8 m. There are numerous sandwiched grit layers, and one of these layers is approximately 1–10 cm thick. These layers greatly enhance the soil water seepage capacity.

Tertiary pebbly sandstones: distributed in the embankment within the range of 2.0–3.4 m depth. The upstream region of the landslide mass is within the range of 3.8–4.5 m depth. This area is mainly composed of weathered feldspar stone and mineral sands that are well-graded with high permeability. Fully weathered siltstones: yellow, distributed in the upstream region of the landslide mass at a depth of 4.5–9.7 m, sandy, of bedding structure and poor water seepage capacity.

Fully weathered mudstone: yellow or gray-green and pelite. They exhibit a layered structure and poor water seepage capacity. They are easily softened by water. Strongly weathered mudstones: dark gray, pelite, of layered structure, weakly cemented rock. Moderately weathered mudstones: brown, black and gray, pelite, layered structure.

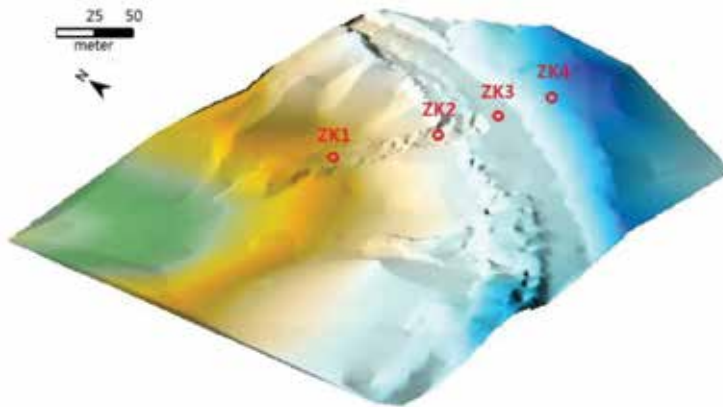


**Figure 8.** Drilling borehole layout on Landslide K178 + 530 and the geomorphological map of the landslide area (using SURFER software to draw the geomorphological map based on GPS terrain data in June 2010).

### 3. Geophysical research methods

In this paper we present combination geophysical techniques of HDR and GPR on the landslide K178 + 530 on the Bei'an-Heihe Highway in Lesser Khingan Range of northeast China. The survey lines were established, as shown in **Figure 9**.



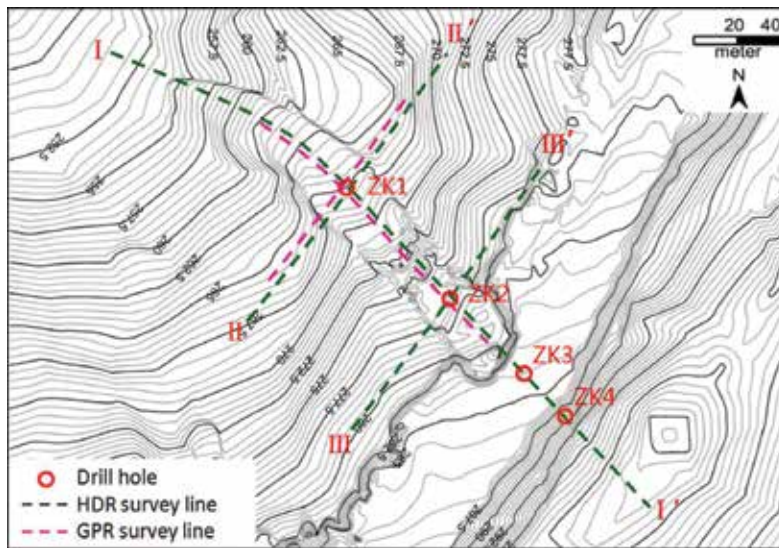


**Figure 9.** The layout of the Landslide K178 + 53 geophysical survey lines. (1) HDR survey lines. A total of three HDR survey lines, i.e., I-I', II-II' and III-III', were established on the Landslide K178 + 530 road section. Line I-I' passed through the center of the landslide mass and was oriented along the sliding direction. The survey line start point was 40 m from the leading edge of the landslide mass. The survey line passed the drilling boreholes ZK1, ZK2, ZK3 and ZK4 in sequence. The survey line has a total length of 357 m (300 m horizontal distance). Line II-II' was oriented to be perpendicular to the sliding direction and began 110 m away from the trailing edge. Point ZK1 was the midpoint of this line with a total length of 177 m. Along this line, 1–60 numbered electrodes were arranged in order from left to right. Line III-III' was also oriented perpendicular to the sliding direction but was had a start position 50 m away from the trailing edge. Point ZK2 served as the midpoint of this transect with a total length of this survey 177 m. A similar set up of electrodes was also deployed in this transect. The data collection date is September 3, 2012. (2) GPR survey lines: we set up two survey lines with the locations that corresponded to the HDR survey lines. However, the start and end points were different. The HDR survey lines were longer than the GPR survey lines. The two survey lines (I-I' and II-II') had lengths of 150 m and 118 m, respectively. The data collection date is October 1, 2013.

### 3.1. HDR method

The WGMD-9 Super HDR system produced by the Chongqing Benteng Digital Control Technical Institute (Chongqing, China) was utilized in this study. Within this system, the WDA-1 super digital direct current electric device is used for control host and measurement. Centralized two-dimensional HDR measurements can be generated via the optional WDZJ-4 multi-channel electrode converter, electrodes, and centralized high-density cables. The RES2DINV software was used to perform the inversion of the apparent resistivity data sets. This software package generates a two-dimensional model of the subsurface via apparent resistivity pseudo-sections [35]. A Wenner configuration was employed to acquire the relevant data. The method utilizes the inversion of pseudo-section data via smoothness-constrained least squares [35–37]. The subsurface in this algorithm is subdivided into rectangular blocks with constant resistivity. The resistivity of each block is then assessed via an iterative scheme that minimizes the difference between calculated and observed pseudo-sections using an iterative scheme. The smoothness-constraint leads to results with smooth resistivity changes.

The derived pseudo-sections can be generated either via finite-element or finite-difference methods [38, 39]. In this study, we employed the finite element scheme due to the changes in the study area topography.

We utilized the smoothness-constraint least squares method in the inversion model. Fundamentally, this method is used to constantly adjust the model resistivity through model correction to reduce the difference between the calculated apparent resistivity and the measured resistivity, and to describe the degree of fit between the two using the mean square error. The smoothness-constraint least squares method, which has been widely applied, has a number of advantages, such as adaptability to different types of data and models, relatively small noise influence on the inversion data, rapid inversion, high sensitivity to deep units, and a small number of iterations. In tests utilizing the HDR method, the maximum exploration depth of the survey lines was determined to be 30 m and the spacing between unit electrodes was 3.0 m.

We established three HDR survey lines on the Landslide K178 + 530 road section, i.e., I–I', II–II' and III–III' (**Figure 9**). The date of data collection is September 3, 2012.

### 3.2. GPR method

The GPR instrument used was the RIS-K2 FastWave Ground Penetrating Radar produced by IDS Corporation (Italy). We utilized an unshielded dual radar antenna that operated at low-frequency 40 MHz. The time window of detection was set at 600 ns, the sampling rate was set at 1024, and a 0.05 m data acquisition track pitch was employed. Two GPR survey lines were set up (**Figure 9**) with orientations that coincided with the HDR survey lines, but termination points of the GPR survey lines were different. The two survey lines (I–I' and II–II') had lengths of 150 m and 118 m, respectively. The date of data collection is October 1, 2013. Raw GPR data were processed via the REFLEXW software produced by Sandmeier Scientific Software (Karlsruhe, Germany). The coordinates of each trace were calculated at equal distances. The surface signal reflection was set to time zero. Noise and low frequency parts of the spectrum were filtered by applying bandpass and dewow methods. In the following step of processing, we eliminated temporally consistent signals via a background removal technique. Topographical correction was then performed. The picks were exported along with the two-way travel time attribute. The propagation velocity of the wave in this case appears to be approximately 0.10 m/ns.

## 4. Results, analysis, and discussion of HDR

### 4.1. Survey line I–I'

The apparent electrical resistivity profile data for line I–I' as collected on September 3, 2012 is presented in **Figure 10**. The figure clearly shows distinct layering in the soil resistivity values of the landslide mass. The RES2DINV software is able to extract the resistivity curve value for any transect point. This allows further analysis of the relationship between soil resistivity

changes and depth. **Figure 11** presents the curves of soil resistivity vs. depth at boreholes ZK1 and ZK2.

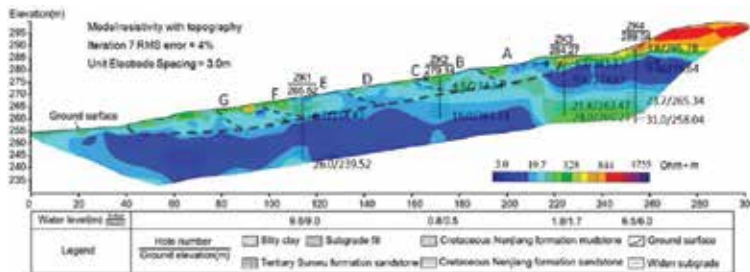


**Figure 10.** Comparison of drilling results and electrical resistivity profile of the survey line I-I'. Geological drilling date is in June 2010, HDR detection date is on September 3, 2012. The dashed thick black line indicates the position of the major sliding surface, and the dashed thin black lines illustrate the secondary sliding surfaces.

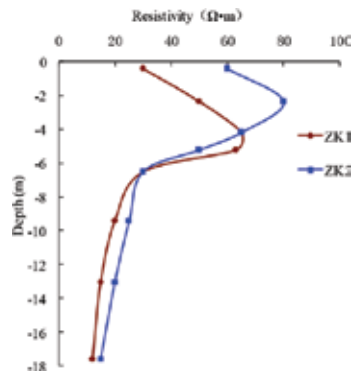


**Figure 11.** The electrical resistivity curves at positions ZK1 and ZK2.

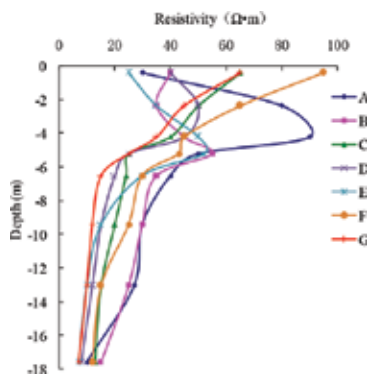


**Figure 12.** The electrical resistivity curves at different points on the survey line I-I'.

The ZK1 borehole is located 115 m from the beginning point of the HDR survey line. At a depth of 0–2.1 m, the soil is rather loose silty clay and is composed of approximately 15% grass roots and other organic matter. The resistivity values at this depth are in the range of 25–45 Ohm m. At the 2.1–6.7 m depth, the soil is primarily silty clay with localized weathered sand layers. The resistivity values for this depth are within the range of 45–65 Ohm m. Within the range of 6.7–8.0 m depth, the soil is composed of yellow mudstone. It is difficult for the water to infiltrate downward as the permeability coefficient is small. This forms a layer where water easily gathers. There are relatively low resistivity values in this layer, i.e., 20–30 Ohm m. At a depth of 8.0–26 m, the soil is gray mudstone, close to or below the water table. The resistivity value is relatively low, i.e., 10–25 Ohm m. As shown in the curve, silty clay contacts mudstone at a depth of 6.7 m, and resistivity exhibits apparent layering, the resistivity value decreased suddenly.

The ZK2 borehole is located 175 m from the beginning point of the survey line. At depths in the range of 0–4.5 m, the soil is somewhat loose. The resistivity values in this layer are within the range of 45–80 Ohm m. The surface embankment soil is dominated by silty clay (depth 0–3.8 m) and gravelly sand (depth 3.8–4.5 m) with resistivity values within the range of 60–80 Ohm m and 45–60 Ohm m, respectively. At the 4.5–9.7 m depth range, the soil is siltstone and primarily composed of relatively small particles. This layer exhibits poor permeability, forming a watertight layer where water can easily gather. The resistivity values are within the range of 25–35 Ohm m. At the 9.7–14.6 m depth range, the soil is composed of sandstone, and the resistivity values are within the range of 15–25 Ohm m. As the gravelly sand contacts the siltstone at a depth of 4.5 m, the resistivity value decreases suddenly.

The RES2DINV software was used to generate the soil resistivity curves along survey line I–I' at points A, B, C, D, E, F and G (**Figure 10**). The horizontal distances between the starting point and the points A, B, C, D, E, F and G of line I–I' are 80 m, 100 m, 120 m, 140 m, 160 m, 180 m and 200 m, respectively. The obtained soil resistivity curves are shown in **Figure 12**. At position A, the soil resistivity value decreased abruptly at a depth of 4.5 m. In other words, the soil resistivity values exhibited abrupt stratification at this depth. It can thus be determined that the sliding surface is located at a depth of 4.5 m. Similarly, the depths of the sliding surface at points B, C, D, E, F and G on line I–I' were determined to be 5 m, 4.7 m, 5.5 m, 6.5 m, 6 m, and 5.5 m, respectively.

The above resistivity curves and HDR profiles illustrate that the soil resistivity values are clearly different and exhibit an abrupt stratification above and below the sliding surface of the landslide mass. The locations of the major sliding surfaces along the line I–I' were deduced according to this typical sliding surface characteristic. These are illustrated with the thick dashed black line in **Figure 10**. The sliding power originated from the trailing edge of the landslide and the sliding type was propelled sliding. The minimum slip rate occurred at the leading edge. The maximum slip rate was at the trailing edge, followed by the intermediate portion of the landslide [40]. Secondary sliding in the landslide mass occurred as a result. Combining the results of the drilling exploration as well as the changes in the soil resistivity values of different positions in the landslide mass and, the secondary sliding surface was obtained, as shown via the thin dashed black line in **Figure 10**.

#### 4.2. Survey line II-II'

The apparent electrical resistivity profile measured along survey line II-II' is presented in **Figure 13**. **Figure 14(a)** shows the soil resistivity curves of points C, D, ZK1, E and F of line II-II'. The distances between points C, D, ZK1, E and F and the beginning point of the survey line are 80 m, 85 m, 90 m, 95 m and 100 m, respectively. Based on **Figures 13** and **14(a)**, we can know the changes in the soil resistivity values, there are apparent resistivity layering at the depths of the sliding surfaces, the resistivity value decreased suddenly. According to this characteristic of the sliding surface, the positions of the sliding surfaces along line II-II' were deduced, as shown by the black dotted line in **Figure 13**. Based on the changes in the soil resistivity values, it can be inferred that the depths of the sliding surfaces at positions C, D, ZK1, E and F on line II-II' were 4 m, 6 m, 6.5 m, 5.5 m and 3.5 m, respectively. **Figure 14(b)** illustrates the soil resistivity curves at the A, B, G and H locations (all outside the landslide mass) along the II-II' survey line. The distances between the start point of the survey line and the points A, B, G and H were 40 m, 60 m, 110 m and 130 m, respectively. As can be seen in **Figure 14(b)**, the soil resistivity values of the stable soil body outside the landslide only showed stratification in the surface loose layer. As depth increased, the resistivity basically exhibited a monotonic decline, and there was no abrupt stratification.

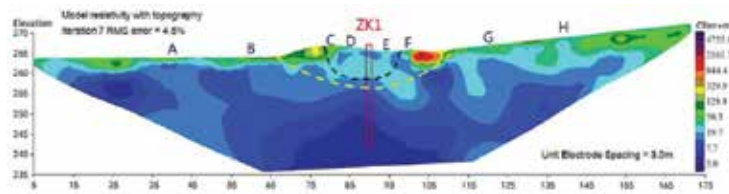


**Figure 13.** Survey line II-II' electrical resistivity profile. HDR collection date of September 3, 2012. The dashed black line represents the current sliding surface. The dashed yellow line illustrates the sliding surface position of the paleo-landslide.

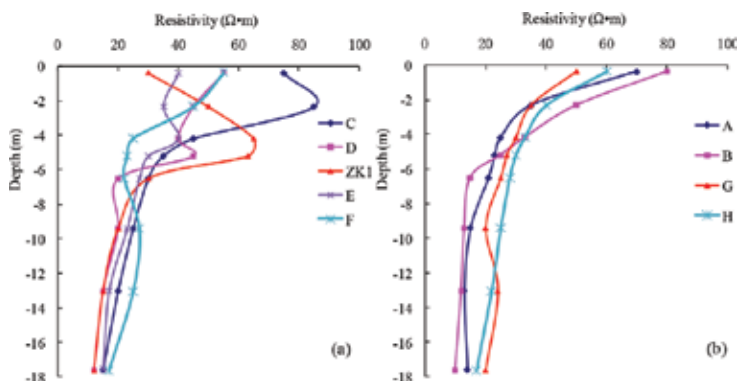


**Figure 14.** The electrical resistivity curves at different points on the survey line II-II' (points C, D, ZK1, E and F are all on the landslide mass, points A, B, G and H are all outside the landslide mass).

This landslide represents a recurring landslide that has once again slipped [40]. The dashed black line in **Figure 13** illustrates the current sliding surface. By combining the geological survey at the site, and the resistivity change characteristics, we can infer the location of the sliding surface for the paleo-landslide, as illustrated by the dashed yellow line in **Figure 13**.

## 5. Results, analysis, and discussion of GPR

### 5.1. Survey line I-I'

The profile determined by the GPR survey line I-I' is illustrated in **Figure 15** (due to the constraints under field conditions, this GPR survey line can only be used to measure this long section). The layer picking option (phase follower) of the REFLEXW software can identify a continuous reflector (the thick dashed red line in **Figure 15**). The radar-wave reflection intensity differed significantly from the reflection intensity of the surrounding medium. The strong reflected-wave signal exhibits characteristics of a distinctive horizon. The signal presents a low-frequency high-amplitude sync-phase axis. We conclude that this represents the sliding surface. The sliding surfaces exhibit good continuity and essentially reflect the landslide mass development depth range [41, 42].

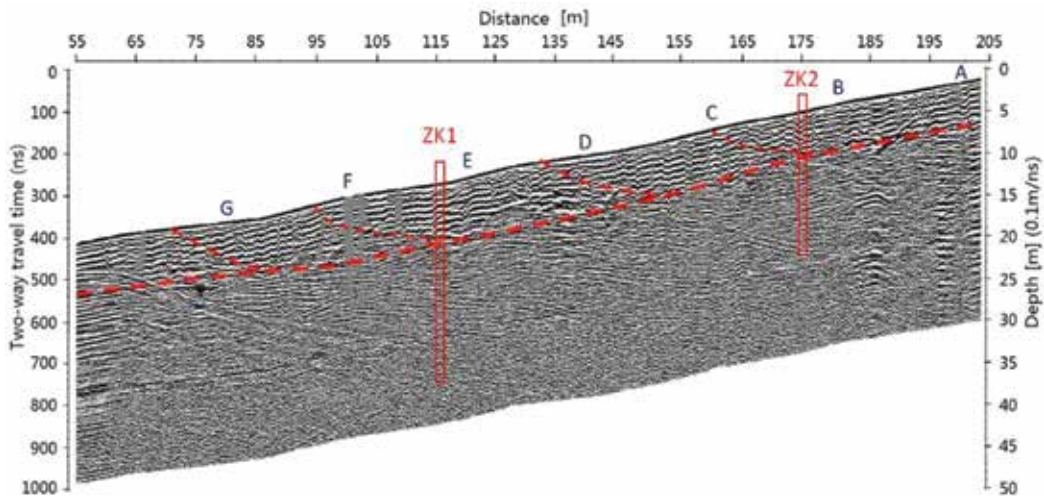


**Figure 15.** The GPR profile of the survey line I-I'. The radar antenna was a low-frequency 40-MHz unshielded dual antenna, the measuring date is October 1, 2013. The thick red dashed line show the position of the major sliding surface, the thin red dashed lines show the secondary sliding surfaces. (see text for discussion).

Using REFLEXW radar data processing software, the radar waves amplitude values of all the data acquisition track points in the profile at different depths can be extracted. In order to better understand the changes in the reflected radar wave intensity, we plotted the radar-wave amplitude curves for positions A, B, ZK2, C, D, E, ZK1, F and G (as depicted in **Figure 15**) on

the survey line I-I' (**Figure 16**). Greater reflected radar wave intensity is indicated by a higher radar-wave amplitude value [41,43]. As shown in **Figure 16**, most curves showed relatively large amplitudes in the depth range of 0–2.5 m as the surface soil body is quite loose at this depth. At position A, the radar-wave amplitude increased substantially and abruptly at a depth of 4.5 m. We can conclude that the soil moisture content was relatively high at this position based on the characteristic differences between different types of soil bodies with regard to their radar-wave reflection [41,43]. We can therefore deduce the location of the sliding surface of the landslide mass. Likewise, an abrupt increase in radar-wave amplitudes occurred at

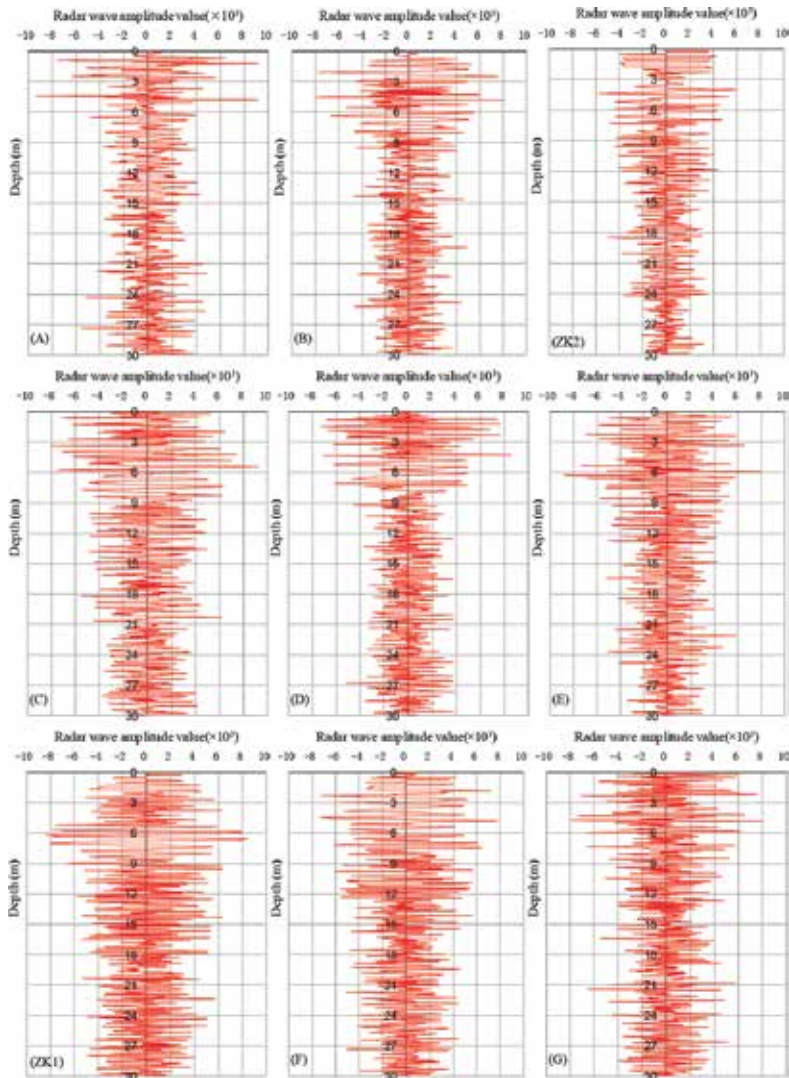


**Figure 16.** The radar-wave amplitude curves on the survey line I-I'. Positions A, B, ZK2, C, D, E, ZK1, F and G are all on the survey line I-I' (as shown in Figure 15).

depths of 4.7 m, 4.7 m, 5.5 m, 5.5 m, 6.7 m, 6.5 m, 5.6 m and 5 m on line I-I' at positions B, ZK2, C, D, E, ZK1, F and G, respectively, and the position of the sliding surface can be inferred. This is very close to the position of the sliding surface as denoted by thick the red line in **Figure 16**.

## 5.2. Survey line II-II'

The GPR profile recorded for survey line II-II' is presented in **Figure 17**. The dotted red line is the low-frequency high-amplitude sync-phase axis, and we conclude that this represents the profile's sliding surface. This axis illustrates the landslide mass development depth range.

Using REFLEXW radar data processing software, we can obtain the radar-wave amplitude curves at positions A, B, C, D, ZK1, E, F, G and H (as shown in **Figure 17**) on the survey line II-II', as shown in **Figure 18**. As can be seen from **Figure 18**, because the surface soil body is rather loose in this area, most curves showed relatively large amplitudes in the depth range of 0–2.5 m. D, ZK1 and E are all on the landslide mass, in positions D, ZK1 and E, a sudden and substantial increase in the radar-wave amplitude occurred at depths of 3.5 m, 6.5 m and 3.2 m, respectively, exhibiting abrupt changes. According to the differences in characteristic radar-wave reflection for different classes of soil bodies [41, 43], we inferred a relatively high soil moisture content at this location. This also implies the location of the landslide sliding surface. The deduced position of the sliding surface is about the same as that denoted by the red dashed line in **Figure 17**. Positions A, B, G and H were all located outside of the landslide mass. Except in the surface layer, i.e., in the depth range of 0–2.5 m, there were abrupt changes in the radar-wave amplitudes; at deeper depths, no abrupt changes were observed in the radar-wave amplitude curves.

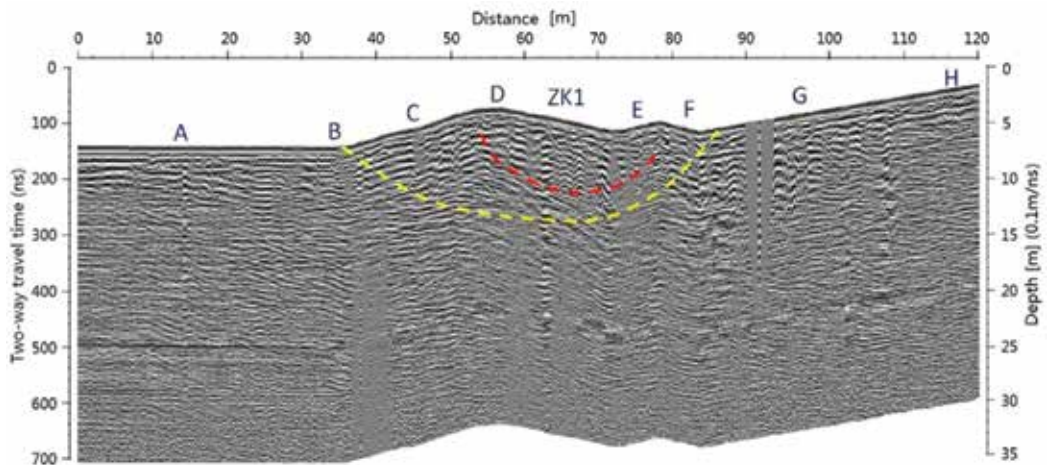


**Figure 17.** The GPR profile of the survey line II-II'. GPR detection date is on October 1, 2013. The red dashed line shows the current sliding surface. The yellow dashed line shows the position of the sliding surface for the paleo-landslide.



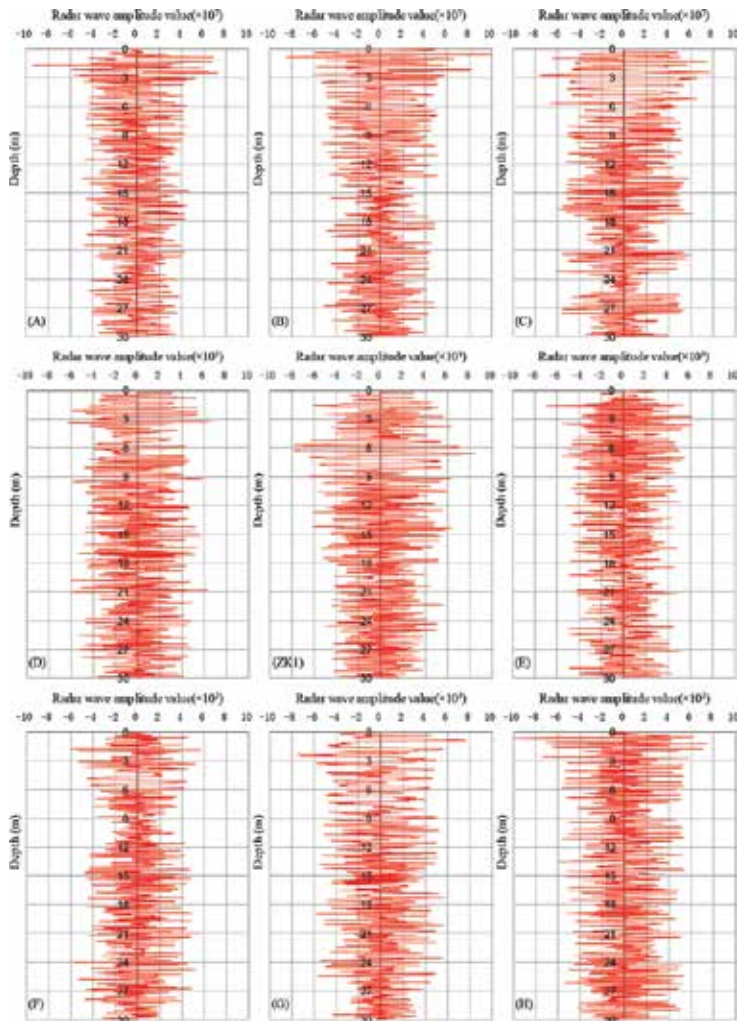


**Figure 18.** The radar-wave amplitude curves on the survey line II-II'. Positions A, B, C, D, ZK1, E, F, G and H are all on the survey line II-II' (as shown in **Figure 17**).

As shown in **Figure 18**, in positions C, D, ZK1, E and F, the amplitude values showed substantial increases at depths of 6 m, 9.5 m, 9 m, 7 m and 3.5 m, respectively, exhibiting abrupt changes. These locations can be utilized to infer the sliding surface location of the paleo-landslide (illustrated in **Figure 17** with yellow dashed lines). Meanwhile, the magnitude of the sudden alteration in the radar-wave amplitudes at the sliding surface location of the paleo-landslide was less than the magnitude at the current sliding surface location.

The results of the GPR indicate relatively high soil moisture content at the sliding surface of the landslide mass. The drilling data also indicate very high moisture content of the sliding surface in the study area. These drilling results are in complete agreement with the results obtained from the HDR profile and the GPR profile.

## 6. Underlying mechanism of landslide development

A geological survey of the study area in May 2010 revealed permafrost in the shaded slopes on the two sides of the landslide [40]. Permafrost locations were identified by drilling into the profile of the survey line III–III' (Figure 19). The HDR method was also used on June 2, 2010 for prospecting along survey line III–III'. Permafrost layer range in the profile of the survey line III–III' can be inferred based on soil resistivity characteristics (in [41]). Figure 20 presents the apparent electrical resistivity profile of survey line III–III' collected in June 2, 2010 (as shown by the black dotted line).



**Figure 19.** The photo of high temperature permafrost. Sampling location is in the survey line III–III', at 40 m position on the X axis, the drilling time is in May 2010.

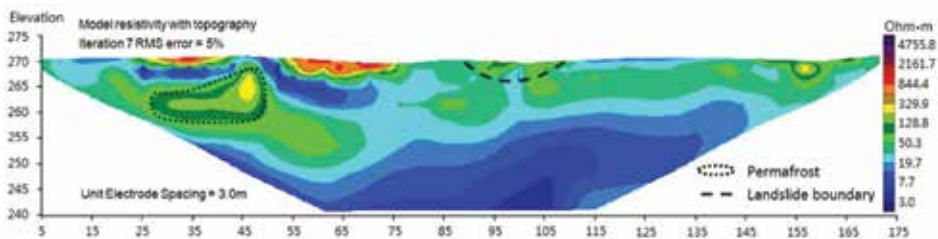


**Figure 20.** The electrical resistivity profile of the survey line III–III' (2010-6-2).

Due to permafrost melting and concentrated summer rainfall, the landslide mass started to slip near the end of July in 2010 [40]. Borehole drilling and site survey data establish Landslide K178 + 530 as a shallow creeping consequent landslide. Water infiltration generated from concentrated summer precipitation in conjunction with water seepage produced from permafrost melting increase the local moisture content within the soil of hillsides. In the northwest section of the Lesser Khingan Range in China, this is the main cause of landslide formation. During the rainy season and the spring melting season, instability can easily occur. The relatively high number of bulging cracks on the landslide mass facilitates the infiltration

and accumulation of water. The highly permeable surface soil, sand and gravel layer, and the silty clay with a weathered sand interlayer produce an expedient route for water infiltration. The mudstone and siltstone layers beneath exhibit low permeability and produce watertight layers. Water generated from melting snow, precipitation, and permafrost melting is hindered by the impermeable layer during its downward infiltration, and the local moisture content sharply increases. Water therefore infiltrates along the interface of the permeable layer and the impermeable layer. This generates a slip zone. Combining the geophysical and drilling data, the position of the sliding surface can be determined, as shown by the red line in **Figure 21**.

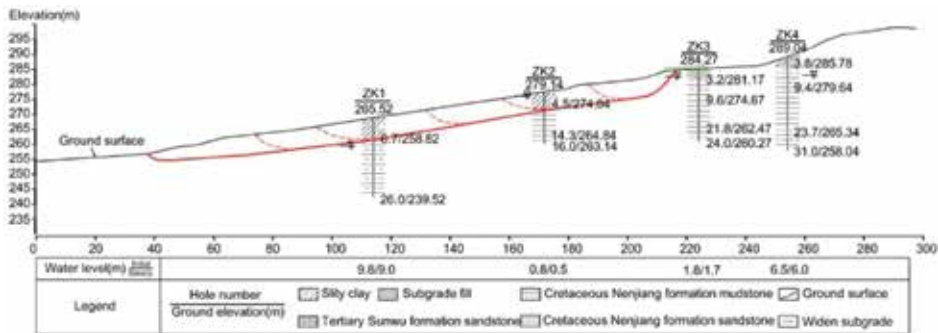


**Figure 21.** The stratigraphic distribution of section K178 + 530 (the thick red dashed line shows the position of the major sliding surface, the thin red dashed lines show the secondary sliding surfaces).

## 7. Landslide movement monitoring

Comprehensive examination and dynamic monitoring of the slip movement were performed for a representative landslide that could threaten the roadbed. This was done on the basis of geological survey and topographic measurements of the study area with the aim of investigating the impact of permafrost thaw on landslide movement.

Landslide K178 + 530 on the Bei'an-Heihe Highway (**Figure 6C**) is among the closest landslides to the roadbed and exhibits the most rapid slip rate. Due to the unavailability of monitoring and survey data prior to 2009, we could not determine the date of the initial slip. A satellite photo taken on June 15, 2004 indicates a straight-line distance of 101.26 m between the trailing edge and the leading edge of the landslide mass (**Figure 5B**). A satellite photo taken on September 12, 2010 indicates that the straight-line distance between the trailing and leading edges had increased to 145.05 m (**Figure 5C**). During this six year period, there was 43.79 m of movement in the leading edge of the landslide, whereas there was basically no movement in the position of the trailing edge.

**Figure 22** presents the locations of the geophysical measurement lines, the drilling points, and monitoring points for ground temperature, displacement, and pore water pressure. The points ZK1, ZK2, ZK3, ZK4, E, and F in the figure denote the positions of the drilling, and lines I and

III denote the high-density resistivity measurement line and the ground-penetrating radar (GPR) measurement line, respectively. During the drilling in holes E and F, permafrost was found at a depth 2.2 m below the ground surface, and the permafrost thicknesses at points E and F were 3.7 m and 2.4m, respectively. The area of permafrost distribution in **Figure 22** is inferred according to **Figure 3**.

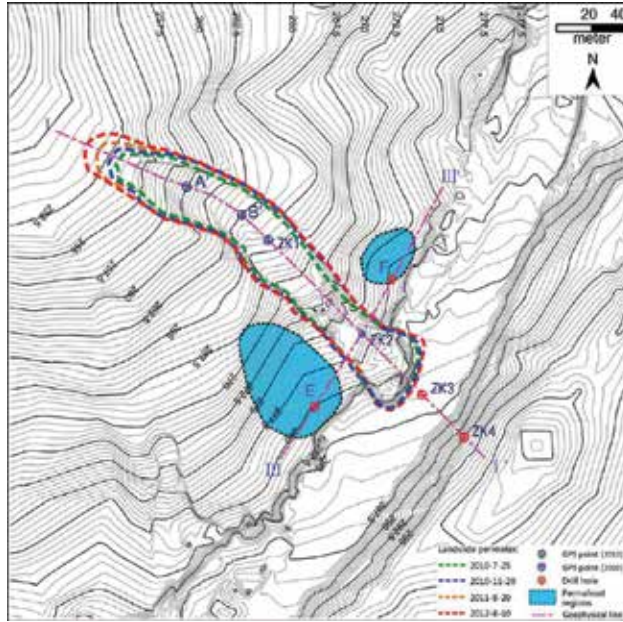


**Figure 22.** Distribution of the drillings, the geophysical measurement lines and points for monitoring displacement, ground temperature, and pore water pressure in Landslide K178 + 530.

Through drilling, GPR, and high-density resistivity prospecting; the profiles of Landslide K178 + 530 in cross section H along the sliding direction and in cross section G perpendicular to the slide direction were obtained (**Figures 23 and 24**).

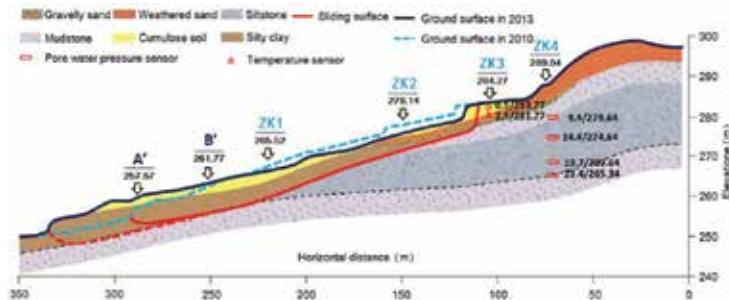


**Figure 23.** The profiles of Landslide K178 + 530 along the sliding direction.

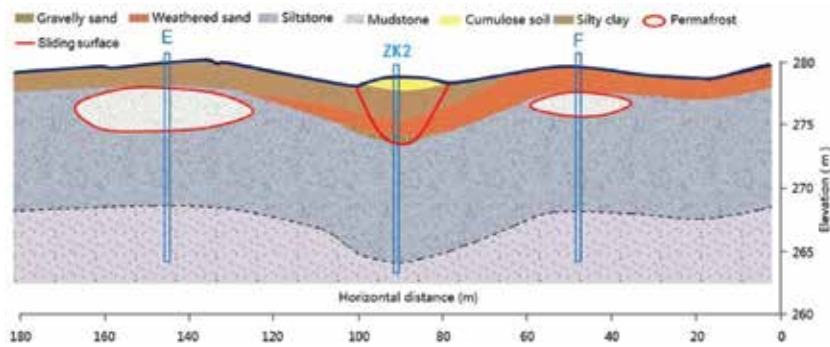


**Figure 24.** The profiles of Landslide K178 + 530 perpendicular to the slide direction.

In the boreholes ZK1 and ZK2 (**Figure 22**), we buried plastic displacement measurement piles that were 400 cm long with an above-ground height of 30 cm. The top of the pile was utilized to quantify the landslide mass slope displacement. ZK3 was used as the monitoring point for the ground temperature. Thermistor soil temperature sensors were set up at 0.5 m intervals from 0.5 m to 2.5 m below the ground surface. ZK4 served as the monitoring point of pore water pressure; in the borehole, steel-wire soil pore water pressure sensors were set up at 3.8 m, 9.4 m, 19.4 m, and 23.7 m depth. The relevant parameters were regularly monitored starting in July 2010.

We utilized a Real Time Kinematic-Global Positioning System (RTK-GPS) to monitor the movement of data collection points on the landslide surface. Point ZK1 horizontally slid by 69.03 m from July 2010 to August 2014, and its elevation decreased by 7.95 m. Point ZK2 horizontally slid by 113.97 m, and its elevation decreased by 17.37 m. From these values, we conclude that the angle between the horizontal plane and the slope dropped from  $8.07^\circ$  to  $6.02^\circ$ . Points A' and B' in **Figures 22** and **23** illustrate the locations of points ZK1 and ZK2 after sliding, respectively. These positions reflect data collected in August 2014.

**Figure 25** illustrates the daily average atmospheric precipitation and ground temperature at point ZK3 on Landslide K178 + 530 at depths of 0.5 m and 2.0 m. The ground temperature data represents monitoring data collected in the study area. The daily average atmospheric precipitation and temperature represent the meteorological data collected via the Sunwu County weather station.

To facilitate the analysis of data, we defined the soil freeze period as the period from the time when the thermistor sensor at 0.5 m below ground surface detected temperature below  $0^\circ\text{C}$  in the autumn to the time when the thermistor sensor at 2.0 m below ground surface detected temperature changing from below to above zero degree Celsius in the spring. This period is displayed in light blue in **Figure 25**. We calculated the cumulative atmospheric precipitation for soil non-freeze and freeze periods, and these are illustrated in **Figure 23** via the dark blue bars. During the frozen soil period, snowmelt water and atmospheric precipitation cannot typically infiltrate to deep soil layers due to the seasonal frozen soil layer and **Figure 26** illustrates the pore water pressure recorded 19.4 m below the ground surface at point ZK4. At

the time of drilling, water was first observed for point ZK4 at a depth of 3.8 m. However, the stable water level recorded during the study period was within the range of 15.8–16.6 m. Unsaturated soil was recorded at 3.8 m and 9.4 m below the ground surface during the study period. Measurements from the pore water pressure sensor placed at a 23.7 m depth were unstable near the end of the study period. Data collected from the sensor placed at 19.4 m depth were therefore utilized to reflect pore water pressure at point ZK4.

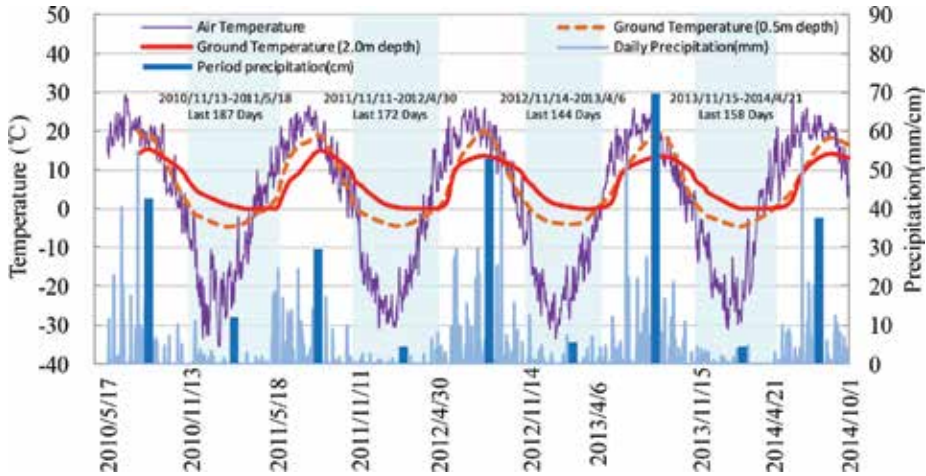


Figure 25. Daily average air temperature/precipitation/soil temperature in the depth of 50 cm, 200 cm in K178 + 530 section of Bei'an-Heihe Highway.

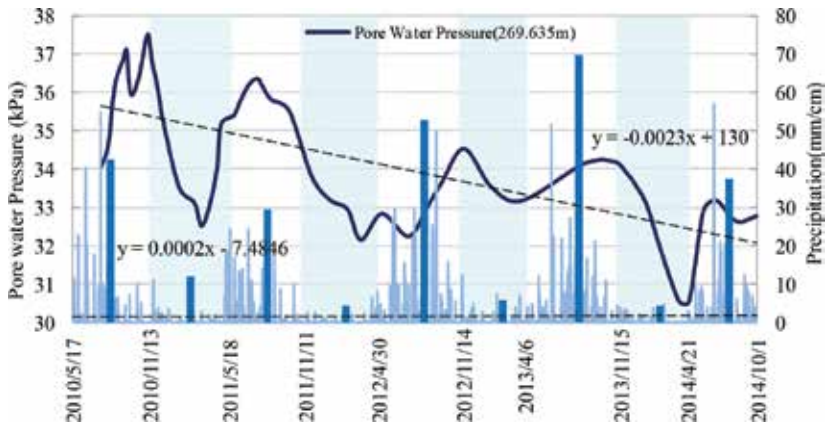
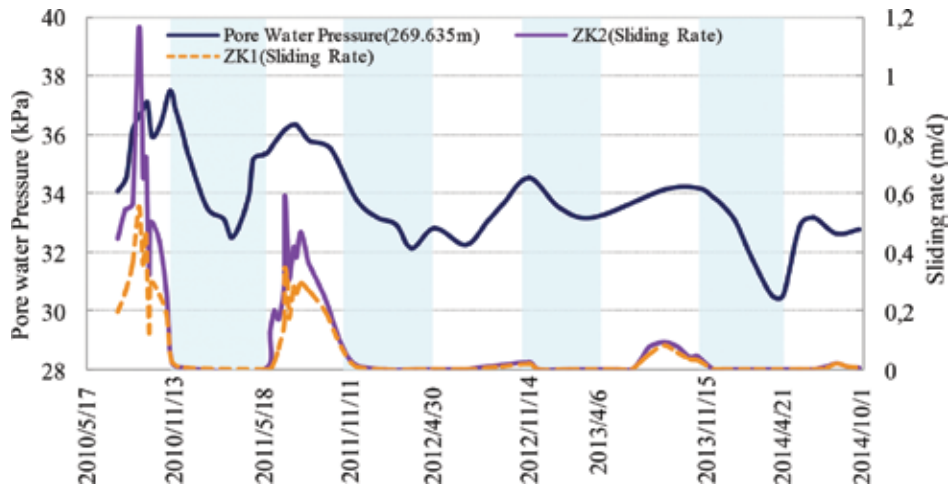


Figure 26. Daily precipitation and pore water pressure in the depth of 19.4 cm of ZK4 point in K178 + 530 section of Bei'an-Heihe Highway.

Figure 27 shows the displacement rates at point ZK1 and point ZK2 as well as the pore water pressure at point ZK4 over time. Displacement values collected via the RTK-GPS real-time

dynamic deformation monitoring system were divided by the time interval to obtain displacement rates.



**Figure 27.** Horizontal displacement rates at point ZK1 and point ZK2 on the landslide mass and pore water pressure at point ZK4 (19.4 m depth) in K178 + 530 section of Bei'an-Heihe Highway.

## 8. Results, analysis, and discussion of data

The permafrost distribution determined by the present study is consistent with previous investigations [44, 45]. In the current study, we analyzed meteorological data from Sunwu County (collected 30 km to the south from the study area) to examine the climate change. The causes of landslide in the study area were evaluated preliminarily by means of permafrost distribution, geological survey of the study area, and topography. The roadbed instability that occurred during August 2000 in the section K176 + 900 to 178 + 200 of the Bei'an-Heihe secondary road was used as a case study.

The meteorological data from Sunwu County indicate that the variation in atmospheric precipitation was 8.93% during the 60 year period from 1954 to 2013. In the study area, this variation had a negligible long-term impact on the thermal state of the soil. As depicted in **Figure 2**, the increase in the average annual maximum temperature was substantially lower than the increase in the average annual minimum temperature. This indicates that the primary cause of the temperature increase was due to a reduction in the soil heat demand from the atmosphere and a rise in the soil's ability to radiate heat rather than an increase in the amount of direct radiation [46]. The latent heat of permafrost thaw caused the difference in the amplitude of temperature rise between the average annual minimum temperature and the average annual maximum temperature. The fact that these amplitudes differed by 47.05% over a 60 year period indicates rapid degeneration of the permafrost in the study.

Permafrost is not found in the section K176 + 900 to 178 + 200 (where overall roadbed instability occurred) of the previous Bei'an-Heihe secondary road (**Figure 3**). This is because the roadbed instability occurred in August 2000, while the ground temperature data used for **Figure 3** represent e ETM+ data collected by Landsat7 in 2009. The permafrost in this road section had entirely degraded entirely after nine years. In **Figure 3**, there are permafrost areas along the road on both sides of point ZK2, i.e., the right side of the K178 + 530 road section. However, no permafrost was found in borehole ZK2. Additionally, no aberrant data was detected below point ZK2 within 15 m along line III via the GPR and high-density resistivity methods. This suggests the absence of permafrost. This could be due to severe degradation of permafrost at this location was at a stage of severe degradation. In other words, the phase transition of soil moisture had already occurred with the associated transition to warm permafrost or melting permafrost. It could also be associated with the resolution of the ETM+ data from the Landsat7 satellite.

**Figure 25** shows the relatively concentrated time period of the initial soil freezing in the study area. This typically fell in within 11 November to 15 November. However, the thawing period required for seasonal frost exhibited large annual variations at the same measurement point. This could be related to the level of winter snowfall and autumn precipitation in the previous year. It could also be related to the soil water thermal condition proximate to the maximum seasonal frost depth. However, these potential relationships require further investigation.

As shown in **Figure 26**, the pore water pressure at point ZK4 exhibited annual periodic changes. The pore water pressure began to increase in the spring of each year, reached the maximum value in the summer, and then subsequently decreased. At an interannual time scale, there was an overall downward trend in pore water pressure. This trend exhibited no correlation with atmospheric precipitation. Linear analysis indicates that the atmospheric precipitation in the study area rose by 0.318 mm during the study period, however, the pore water pressure at point ZK4 declined by 3.675 kPa. This resulted in a 36.75 cm decrease in its groundwater level. The groundwater reduction level was 1155 times the rise in atmospheric precipitation for the same period.

The slip rates measured at points ZK1 and ZK2 agree well with the pore water pressure results from point ZK4. During the study period, the landslide mass began to slip with thawing of seasonal frost and snowmelt each spring due to the gradual increase in the pore water pressure of the soil. The pore water pressure reached annual the peak during the concentrated rainfall of the summer, and the slip rate of the landslide obtained its maximum value at the same time. The soil pore water pressure gradually decreased with the landslide movement, and the sliding of the slope gradually stalled. The landslide movement exhibited notable seasonal activity and annual periodicity.

**Figures 23** and **27** illustrate consistent trends in the slip rates of points ZK1 and ZK2 on the landslide mass. The displacement of point ZK2 was 1.65 times the movement at point ZK1 during the monitoring period. We conjecture that the displacement at point ZK1 might be due to force coming from the rear area of the landslide mass. For the period of 2010–2014 the annual maxima of pore water pressures at point ZK4 were 37.52 kPa, 36.37 kPa, 34.53 kPa, 34.14 kPa, and 33.19 kPa, respectively. The maxima decline each year, and the decline in amplitude was



relatively large in 2012. The maximum slip rates of point ZK2 from 2010 to 2014 were 115.7 cm/d, 59 cm/d, 2.55 cm/d, 9.63 cm/d, and 2.2 cm/d, respectively. Rapid sliding primarily occurred in the summer of 2011 and in 2010. There were decreases in the slip rate each year, and the largest reduction occurred in 2012. However, there was a slight rise in the slip rate in the summer of 2013. The underlying cause of these phenomena may be related to thawing permafrost which supplemented water to the landslide mass at points E and F (**Figure 22**), which are exterior to the lateral edge of the slope at point ZK2. Additionally, these phenomena could be related to the level of summer precipitation. As shown in **Figure 26**, the summer atmospheric precipitation in 2013 reached the largest value for the entire monitoring period (672 mm). This level was 14.33 mm higher than the second largest summer precipitation (which occurred in 2012) and it was 1.46 times the average summer atmospheric precipitation for the entire monitoring period. We therefore concluded that the slip rate of Landslide K178 + 530 during the monitoring period was mainly impacted by pore water pressure at the trailing edge of the landslide mass. At the same time, the slip rate was also impacted by the level of summer precipitation. Furthermore, the thawing of permafrost at the lateral edge of the slope was related to the pore water pressure at the trailing edge of the landslide mass. As permafrost thawed each year, its volume was reduced. This trend gradually decreased the pore water pressure at the trailing edge of the slope. Consequently, there were gradual decreases in the slip rate of the landslide mass each year.

## 9. Conclusion

In this study, we performed a comprehensive analysis via data on the study area climate as well as ground temperature, displacement, and pore water pressure data that were collected at transect points along Landslide K178 + 530 on the Bei'an-Heihe Highway. We arrived at the following main conclusions based on this analysis:

The northwest section of China's Lesser Khingan Range is positioned along the southern boundary of the high-latitude permafrost region. This area has been subject to temperature increases due to global climate change. The increase in yearly average minimum temperature is 3.45 times the increase in the average yearly maximum temperature. Permafrost degradation in the region is quite significant. There will be additional temperature increases in this region due to permafrost degradation. These patterns will also result in an acceleration of the northward migration of the southern boundary of the permafrost region.

Permafrost thaw results in increases in the number of landslides in the northwest section of China's Lesser Khingan Range. This subsequently results in regional topographical changes. Anthropogenic activity can accelerate the thawing of permafrost.

Infiltration of concentrated summer precipitation and water seepage from thawing permafrost both increase the moisture content in the soil of local hillsides. In the northwest section of the Lesser Khingan Range in China, this is the main casual factor for landslides.

Landslide movement in the northwest section of China's Lesser Khingan Range begins in the summer season with concentrated precipitation. The movement gradually stops when the soil freezes in the autumn. The landslide movement exhibits clear seasonal and annual periodicity.

The thawing process of permafrost on and near the landslide mass control the landslide slip rate and movement process in the northwest area of the Lesser Khingan Range. As the permafrost thaws each year and the volume is correspondingly reduced, there is an associated decrease in its ability to supplement water to the landslide mass. This results in a decrease in the landslide slip rate each year until it reaches zero. The landslides then tend towards stability.

The soil resistivity values above and below the sliding surface of the landslide mass are clearly different and exhibit an abrupt stratification. There is apparent resistivity layering at the position of the sliding surface in the landslide mass, the resistivity value decreased suddenly. In the profile of the GPR, the sliding surface is expressed as a low-frequency high-amplitude sync-phase axis, and there is an associated rapid rise in the radar wave amplitude. In practice, the abnormal abrupt changes in the GPR and HDR results can be used in this region to identify the sliding surface location of shallow landslides.

The results from the three methods we used to investigate landslides in the study area, i.e., HDR, GPR, and drilling, generally agree with regard to the sliding surface position. This indicates that the GPR and HDR methods are economical, rapid, and reliable methods for prospecting in landslide areas. These methods can be applied to shallow landslides in high-latitude permafrost regions for accurate and rapid identification of the sliding surface position. These techniques can also aid in the generation of accurate data for engineering projects to ensure that appropriate measures are adopted.

## **Acknowledgements**

We thank the Science and Technology Project of the Chinese Ministry of Transport (2011318223630) and the International Landslide Research Program (IPL-167) for funding support. We are also grateful to an anonymous referee who helped improve the manuscript.

## **Author details**

Wei Shan\*, Ying Guo, Zhaoguang Hu, Chunjiao Wang and Chengcheng Zhang

\*Address all correspondence to: shanwei456@163.com

Institute of Cold Regions Science and Engineering, Northeast Forestry University, Harbin, China

## References

- [1] Guo D X, Wang S L, Lu G, Dai J B, and Li E Y. Regionalization of permafrost in the Da and XiaoXing'anling Mountains in northeastern China. *Journal of Glaciology and Geocryology*. 1981; 3: 1–9.
- [2] Zhou Y W, Wang Y X, Gao X W, and Yue H S. Ground temperature, permafrost distribution and climate warming in northeastern China. *Journal of Glaciology and Geocryology*. 1996; 18: 139–147.
- [3] Sun G Y, Yu S P, and Wang H X. Causes south borderline and subareas of permafrost in Da Hinggan Mountains and Xiao Hinggan Mountains. *Scientia Geographica Sinica*. 2007; 27: 68–74.
- [4] Jin H J, Li S X, Wang S L, and Zhao L. Impacts of climatic change on permafrost and cold regions environments in China. *Acta Geographica Sinica*. 2000; 55: 161–173.
- [5] Wei Z, Jin H J, and Zhang J M. Prediction of permafrost changes in Northeastern China under a changing climate. *Science China: Earth Sciences*. 2010; 41: 74–84. DOI: 10.1007/s11430-010-4109-6.
- [6] He R X, Jin H J, Lv L Z, Yu S P, Chang X L, Yang S Z, Wang S L, and Sun G Y. Recent changes of permafrost and cold regions environments in the northern part of North-eastern China. *Journal of Glaciology and Geocryology*. 2009; 31: 525–531.
- [7] Solomon S, Qin D, and Manning M. Summary for policymakers. *Climate Change 2007: The physical science basis (Contribution of Working Group I to the Fourth Assessment Report of the Intergovernmental Panel on Climate Change)*. Intergovernmental Panel on Climate Change. 2007 ([www.ipcc.ch/](http://www.ipcc.ch/)).
- [8] IPCC. Summary for policymakers. Working group I contribution to the IPCC fifth assessment report climate change 2013: the physical science basis. Cambridge, UK. Cambridge University Press; 2013.
- [9] Ding Y H, Ren G Y, and Shi G. National assessment report of climate change (I): climate change in China and its future trend. *Advances in Climate Change Research*. 2006; 2: 3–8.
- [10] Shi P J, Sun S, and Wang M. Climate change regionalization in China (1961-2010). *Science China: Earth Sciences*. 2014;44: 2294–2306. DOI: 10.1007/s11430-014-4889-1.
- [11] Chang X L, Jin H J, Yu S P, Sun H B, He R X, Luo D L, Sun G Y, and Lu L Z. Influence of vegetation on frozen ground temperatures the forested area in the Da Xing'anling Mountains, Northeastern China. *Acta Ecologica Sinica*. 2011; 31: 5138–5147.
- [12] Zhou Y W, and Guo D X. Principal characteristics of permafrost in China. *Journal of Glaciology and Geocryology*. 1982; 4: 1–19.

- [13] Chang X L, Jin H J, and He R X. Review of permafrost monitoring in the northern Da Hinggan Mountains, Northeast China. *Journal of Glaciology and Geocryology*. 2013; 35: 93–100.
- [14] Jin H J, Wang S L, and Lv L Z. Features of permafrost degradation in Hinggan Mountains, northeastern China. *Scientia Geographica Sinica*. 2009; 2: 223–228.
- [15] Arndt D S, Blunden J, and Willett K. State of the Climate in 2011 Special Supplement to the Bulletin of the American Meteorological Society. *Bulletin of the American Meteorological Society*. 2012; 93(7).
- [16] Eu-Fp7. A summary for policymakers. PD Investigación. ACQWA: Assessing Climate impacts on the Quantity and quality of Water. A large integrating project under EU Framework Programme 7 (FP7). 2008.
- [17] Sassa K, Yin Y, and Canuti P. The Third World Landslide Forum, Beijing, 2014. *Landslides*. 2015; 12(1): 1–16 (<http://iplhq.org/category/home/>)
- [18] Sassa K. ICL strategic plan 2012–2021 – To create a safer geo-environment. *Landslides*. 2012; 9(2): 155–164 (<http://iplhq.org/category/home/>).
- [19] Guo Y, Canuti P, Strom A, Hideaki M, and Shan W. The First Meeting of ICL Landslides in Cold Regions Network, Harbin, 2012. *Landslides*. 2013; 10: 99–102. DOI: 10.1007/s10346-012-0369-x.
- [20] Shan W, Guo Y, Zhang C C, Hu Z G, Jiang H, and Wang C J. Climate-change impacts on embankments and slope stability in permafrost regions of Bei'an-Heihe Highway. *Landslide Science for a Safer Geoenvironment*. 2014; 1: 155–160. DOI: 10.1007/978-3-319-04999-1\_18.
- [21] Shan W, Guo Y, Wang F, Marui H, and Strom A. *Landslides in cold regions in the context of climate change* (Springer: Environmental Science and Engineering). ISBN 978-3-319-00866-0. ISBN 978-3-319-00867-7 (eBook). 2014;105–109. DOI: 10.1007/978-3-319-00867-7
- [22] Grab S W, and Linde J H. Mapping exposure to snow in a developing African context: implications for human and livestock vulnerability in Lesotho. *Natural Hazards*. 2014; 71: 1537–1560. DOI: 10.1007/s11069-013-0964-8.
- [23] Ballantyne C K, Sandeman G F, Stone J O, and Wilson P. Rock-slope failure following Late Pleistocene deglaciation on tectonically stable mountainous terrain. *Quaternary Science Reviews*. 2014; 86: 144–157.
- [24] Nussbaumer S, Schaub Y, Huggel C, and Nat AW. Risk estimation for future glacier lake outburst floods based on local land-use changes. *Hazards and Earth System Sciences*. 2014; 14: 1611–1624. DOI: 10.5194/nhess-14-1611-2014.
- [25] Haerberli W. Mountain permafrost – research frontiers and a special long-term challenge. *Cold Regions Science and Technology*. 2013; 96: 71–76.

- [26] Kliem P, Buylaert J P, Hahn A, Mayrd C, Murray A S, Ohlendorf C, Wastegård S, Zolitschka B, and Team T P S. Magnitude geomorphologic response and climate links of lake level oscillations at Laguna Potrok Aike, Patagonian steppe. *Quaternary Science Reviews*. 2013; 71: 131–146.
- [27] Fischer L, Hugge C, Kaab A, and Haerberli. Slope failures and erosion rates on a glacierized high-mountain face under climatic changes *Earth Surf. Landforms*. 2013; 38: 836–846. DOI:10.1002/esp.3355
- [28] Starnberger R, Drescher S R, Reitner J M, Rodnight H, Reimer P J, and Spötl C. Late Pleistocene climate change and landscape dynamics in the Eastern Alps: the inner-alpine Unterangerberg record (Austria) *Quaternary Science Reviews*. 2013; 68, 17–42.
- [29] Stoffel M, Tiranti D, and Huggel C. Climate change impacts on mass movements – case studies from the European Alps. *Science of the Total Environment* 2014; 22014: 1255–1266.
- [30] Wang C J, Shan W, Guo Y, Hu Z G, and Jiang H. Permafrost Distribution Study Based on Landsat ETM+ Imagery of the Northwest Section of the Lesser Khingan Range. *Landslide Science for a Safer Geoenvironment*. 2014a; 3: 529–534. DOI: 10.1007/978-3-319-04996-0\_81.
- [31] He R X, Jin H J, Chang X L, Lv L Z, Yu S P, Yang S Z, Wang S L, and Sun G Y. Degradation of permafrost in the northern part of Northeastern China: Present state and causal analysis. *Journal of Glaciology and Geocryology*. 2009; 31: 829–834.
- [32] Zhang Y, Wu Q B, and Liu J P. Distribution characteristics of the permafrost in the section from Heihe to Bei' an in the Xiao Hinggan Mountains. *Journal of Glaciology and Geocryology*. 2001;23:312–317.
- [33] Wang B, Sheng Y, and Liu J P. Distribution and degradation of permafrost in Xiao Hinggan Mountains along the Heihe-Dalian Highway. *Journal of Glaciology and Geocryology*. 2001; 23: 302–306.
- [34] Wang S H, Qi J L, Yin Z Y, Zhang J M, and Ma W. A simple rheological element based creep model for frozen soils. *Cold Regions Science and Technology Cold Regions Science and Technology*. 2014; 106: 47–54. DOI: 10.1016/j.coldregions.2014.06.007.
- [35] Loke M H, and Barker R D. Rapid least-squares inversion of apparent resistivity pseudosections using a quasi-Newton method. *Geophys Prospect*. 1996; 44: 131–152.
- [36] Tripp A C, Hohmann G W, and Swift C M. Two-dimensional resistivity inversion. *Geophysics*. 1984; 49: 1708–1717.
- [37] Sasaki Y. Resolution of resistivity tomography inferred from numerical simulation. *Geophys Prospect*. 1992; 40: 453–463.
- [38] Coggon J H. Electromagnetic and electrical modelling by the finite element method. *Geophysics*. 1971; 36: 132–155.

- [39] Dey A, and Morrison H F. Resistivity modelling for arbitrarily shaped two-dimensional structures. *Geophys Prospect*. 1979; 27: 106–136
- [40] Shan W, Hu ZG, Guo Y, Zhang C C, Wang C J, Jiang H, Liu Y, and Xiao J T. The impact of climate change on landslides in southeastern of high-latitude permafrost regions of China. *Frontiers in Earth Science*. 2015; 3(7): 1–11. doi: 10.3389/feart.2015.00007
- [41] Telford W M, Geldart L P, and Sheriff R E. Applied geophysics. *Geological Journal*. 1992; 27(1): 97. DOI: 10.1002/gj.3350270119.
- [42] Daniels D J. The Institution of Electrical Engineers, London, United Kingdom, editors. *Ground Penetrating Radar*. 2nd ed. London: IEE Radar; 2004.
- [43] Benedetto A, Benedetto F, and Tosti F. GPR applications for geotechnical stability of transportation infrastructures. *Nondestructive Testing and Evaluation*. 2013; 27(3): 253–262.
- [44] Wang C J, Shan W, Guo Y, Hu Z G, and Jiang H. Permafrost distribution study based on Landsat ETM+ Imagery of the northwest section of the lesser Khingan Range. *Landslide Science for a Safer Geoenvironment*. 2014; 3: 529–534. DOI: 10.1007/978-3-319-04996-0\_81.
- [45] Wang C J, Shan W, Guo Y, Hu Z G, and Jiang H. Permafrost distribution research based on remote sensing technology in northwest section of Lesser Khingan Range in China. *Engineering Geology for Society and Territory*. 2015; 1: 285–290. DOI: 10.1007/978-3-319-09300-0\_53.
- [46] Chen J, Sheng Y, and Cheng G D. Discussion on protection measures of permafrost under the action of engineering from the point of earth surface energy balance equation in Qinghai Tibetan Plateau. *Journal of Glaciology and Geocryology*. 2006; 28: 223–228.

---

# River Basin Management in the Past and at Present and its Impact on Extreme Hydrological Events

---

Jana Moravcová, Václav Bystřický, Jiří Pečenka,  
Jakub Polenský, Tomáš Pavlíček,  
Nikola Nováková and Pavel Ondr

Additional information is available at the end of the chapter

<http://dx.doi.org/10.5772/63398>

---

## Abstract

River basin and small watercourse river basins should be seen as interdependent and interconnected elements and components. Activities within the river basin can affect water conditions in terms of quality and quantity. Nevertheless, river basin management has an impact on other areas, such as on the social or economic conditions.

Hydrological extremes as floods and droughts are natural phenomena, which cannot be avoided. Their irregular occurrence and variable range adversely affect the perception of the risk it poses, which complicate the systematic implementation of preventive measures. Given this, it is necessary to choose a comprehensive, coordinated and systematic process of planning, control, organization, leadership and management within the river basin.

One way to ensure optimal integrated river basin management is currently hydrological modelling. Hydrologic models are simplified quantitative relationship between input and output parameters of a system. Simulations of these models are then used primarily to assess the impact of proposed changes in the use of scenarios in the basin and the various water management strategies.

The aim of this chapter is to evaluate the current management of selected river basin. The main focus is on finding the fact whether the management of the selected river basin can be designated as integrated river basin management, which takes into account all of the above elements. Retention capacity of the basin is then related to the occurrence and consequences of extreme hydrological situations.

**Keywords:** river basin, management, flood, drought, hydrological modelling

---

## 1. Introduction

Most of the earth's surface, besides dry or permanently frozen areas can be divided into the river basin of surface waters. When natural river basin area is too large for the rational management planning in their area, these are often divided into several subsections according to the hydrological characteristics [1].

Social responsibility is one of the most promising approaches to river basin management. This concept is based on three key ideas.

1. The owners of the land should be included in the management of natural resources

None of the individual owners do not have sufficient information, legal competence, funding and other resources for the satisfactory managing of natural resource management. For this reason, it is clearly preferable that the individual owners cooperate management areas farmed.

2. Physical resources need some forms of management and organization

Individual natural resources need to be managed in the long-term steady manner which ensures a uniform approach to their management. This method of control is only possible through the involvement of landowners in the long-term functioning of organizations such as associations of owners, user organizations, cooperatives, information networks and associations.

3. Management of natural resources is a learning process

Management of natural resources requires the development of new knowledge, attitudes and skills so that managers could adequately cope with the changes and uncertainties [2].

The need for a focused integrated river basin management of large rivers is a matter of the past century. This need arises due to increasing human activities in the river basin areas of major rivers [3].

The river basin area should be seen as interdependent and interconnected elements and components that can as well as various activities within a river basin affect water levels or can have an impact on other areas, such as on the social or economic conditions [1].

Due to this fact, it is necessary to choose a comprehensive, coordinated and systematic process of planning, control, organization, leadership and management within the basin, which will be based on the knowledge that the water in the landscape-ecological perspective is one of the primary components of landscape structure; it is an integral part ecosystem as well as socioeconomic resource [4]. Its quality depends on the way of use [5]. Such an approach reflecting the multidisciplinary nature in the context of the overall socioeconomic development and other interests relating to the use and protection of water resources, for example, in the field of water supply and sewerage systems, agriculture, industry, residential development, water works, transportation, recreation, fishing and other activities, while emphasizing the need for coordination between sectors and proposing adaptation of different systems planning and management within individual basins, is named as an integrated river basin management.



Basically, an integrated management is defined as interdependence and connections of socioeconomic, environmental and technical aspects [6].

Most proper functioning and effectiveness of integrated river basin management occur during extreme hydrological events such as floods or drought [3].

Flood protection is a very important global issue. Globally, floods represent about one-third of the total number of natural disasters. These have resulted in more deaths than all other natural disasters combined, causing property damage and economic losses representing about a third of the total damage and economic losses caused by all natural disasters [7].

The flood is a hydrological phenomenon that occurs as a result of rainfall, snow melting, or other weather events in various combination of human activity, which manifests itself most dramatic increase in surface water runoff, increasing groundwater levels, temporary flooding of the earth's surface or erosion processes. Flooding is defined as a temporary significant increase in water flow, caused by the sudden enlargement of the flow or by temporarily reducing the watercourse profile trough, for example, ice constipation. During these events, water floods the areas outside the watercourse and may cause damage. Floods are divided on natural floods, which are caused by natural phenomena, and special flood caused by other factors [8].

Conversely, drought is very vague, but in meteorology frequently used concept, basically meaning the lack of water in the soil, plants or even in the atmosphere. Uniform criteria for defining quantitative exist with respect to various aspects of meteorological, hydrological, agricultural, soil, bioclimatological and many other conditions with regard to damages in various fields of national economy [9].

A properly functioning integrated river basin management should in these emergency situations ensure the coherence of individual components addressing this critical situation through information channels and ensure the timely and continuous information transfer between these components for effectively dealing with the crisis [3].

The aim of this chapter is on the example of river systems in the Czech Republic introduce historical and contemporary approach to the management of river basins. Its effectiveness is demonstrated mainly on approach to crisis management by droughts and floods. This chapter is a practical demonstration of the effects of changes in the river basin on hydrological characteristics.

## **2. Management of river basins in the Czech Republic**

Water flows in the Czech Republic are divided into significant watercourses in the length of 16,326 km and small watercourses in the length of 86,553 km. Major rivers, and about half the designated small watercourses, are managed by state owned enterprises, that is, Vltava River Basin, state enterprise; Eger River Basin, state enterprise; Elbe River Basin, state enterprise; Oder River Basin, state enterprise and Morava River Basin, state enterprise. Another major administrator of approximately 6.6% of small streams is state-owned company Forests of the

Czech Republic, Ministry of Defense, the management of national parks and other private and legal persons [7].

Flood situation, as well as drought, poses the greatest threats to natural disasters in the Czech Republic. This is mainly due to the geographic location of the Czech Republic. Despite the relatively low altitude of the area, Czech Republic is known as the roof of Europe, mainly because of the location of the river basin edge of three major European rivers—the Elbe, Oder and Danube, on Klepý Mountain (1144 m a.s.l.) in Jeseníky Mountains. The main sources of water in this area are thus precipitation [10].

For good planning of flood protection and improvement of the landscape water regime during periods of drought, it is necessary to know the extent and the possible occurrence of flood situations and drought in historical context. Information about extreme historical hydrological situations is composed partly from calculations of mathematical models that are verified by the actual course of floods and historical monitoring of the impacts of floods and droughts on the individual components of the environment [9].

## 2.1. Flood situations

The longest and most complete evidence of flood conditions is preserved flood for the upper reach of the Vltava River. From immemorial, time floods were frequent and regular phenomenon, as evidenced by the occurrence of 136 large floods in this from the beginning of the eleventh century. Among the largest floods that were at least initially documented by hydrological records were floods in the years 1118, 1141, 1159, 1272, 1310, 1315, 1342, 1445, 1463, 1481, 1501, 1675, 1770–1772 and 1890. Between catastrophic floods, there are included floods from July 1432, by which almost all the mills on the river Vltava and other rivers were destroyed, flood in 1581, when the dam of Staňkovský pond was broken, flood in 1582, when high water flooded the whole region of Netolice and Bechyně. These large floods were caused primarily by rainfall during the summer. An example of the catastrophic winter floods caused by snow melting, or a combination of snowmelt and rainfall floods is one of February 1784, at which many pond dams were damaged, the floods of March 1845, which occurred after a long winter with plenty of snow and intense ice phenomena on watercourses [11].

On the Berounka River basin, one of the largest tributaries of the Vltava, flooding is historically documented for much shorter time. Recorded and reported are only the great floods of 1845, similar to the upper Vltava caused by the sudden melting of large masses of snow, combined with persistent and heavy rainfall, the flood of 1872 in the upper river basin area of the Berounka, which is not fully documented, but according to the preserved record, it was a very short sharp rain in several hours with a very high intensity, and the flood of 1890 caused by several days of rain in the Pilsen region [12].

On the lower section of the Vltava, flood conditions are usually the result of stopping the flood wave from the upper basin. Equally important fact is also overlap with flood waves of the main tributaries, such as the Sázava River. An example of such a flood is the aforementioned situation resulting from 1845 due to the spring thaw. Similar examples are then floods of 1890, 1917 and 1920, which were significantly contributed by water from Sázava [10].

A similar situation exists in the monitored river basin Eger, where the records are from the period after installing the gauge on the river in 1862. In that year, there was recorded significant winter flooding. The records also show that in this basin apart from isolated events of 1919 and 1981 occurred in practice until 2002, no significant flooding [13].

Compared detailed monitoring of the situation on the Czech territory, the territory of the Morava River basin is evidenced significantly less important historic flood conditions. The best-documented situations include the years 1363, 1480, 1598, 1620, 1714, 1883 and 1891 [14].

During the recent past, a significant event in the history of the whole country, were mainly two summer floods in the 1997 and 2002 and winter flood of 2006 [15].

In the long term can be deduced from the observed data, especially the fact that in the Czech Republic, floods usually occur randomly, but in a comprehensive multi-year episodes. Historically, river basin managers responded to this fact by modifications in economy, and above all by modifications of watercourses in river basins [16].

## **2.2. Periods of drought**

Historic drought usually affects the entire Czech Republic. About how the drought is significant in various areas decides especially the local long-term precipitation conditions. In addition, the dry season is usually accompanied by above-average temperature conditions, which further aggravate the water balance. The earliest record of the drought is in the Kosmas Chronicle, where he writes that the winter between 1090 and 1091 was warm and snowless. Dry periods occur in every century, and unlike floods there cannot be searched regularity [17].

In the area of upper Vltava River basin significant droughts can be identified according to the flow indicators in the years 1971, 1972, 1983, 1936, 1958, 1961, 1990, 1999 and 2003 [11].

In the Eger and the lower Elbe River basin occurred, except for the above-mentioned period, significant dry periods in the summer of 1973 spilling over into the spring months of 1974. The local drought manifested itself even in the summer of 1976, 1983 and the spring of 1984. Other major drought, which was the longest recorded, has been documented in this area since 1990, with the exception of the spring 1992 until the spring of 1993. In some localities, overlap was observed until the end of the summer 1994 [13].

For Moravia are the most important periods of drought for surface waters documented in the years 1962, 1992, 1994–1995 and 2004 [15]. Already this observation shows that in the eastern part of the Czech Republic, the issue of drought is less pronounced than in the Czech part of the republic, especially the northwest parts (Eger River basin) [13].

## **2.3. River basin management in response to extreme hydrological events**

Integrated river basin management consists mainly in the protection of area from floods and from the negative effects of drought and improves the water regime of the landscape through a variety of measures directed if the local situation allows into the places with particular problems [9]. Basic measures are divided into three areas:

(1) Increase of natural river basin retention

Increase of natural river basin retention can achieve nature-friendly measures on watercourses in the river basin area. These measures consist of the revitalization of watercourses, erosion measures, biotech and agro-technical changes and procedures and increasing of water retention within river basin by land consolidation.

(2) Technical flood protection

Flood protection by technical elements is focused exclusively on the built-up area where it is necessary to find the optimal solution design. The solution may be increasing of the watercourse capacity in urban areas, construction of dams, increased capacity on stream and other objects. The most effective way of dealing with the formation of a sufficiently large storage space in the form of polders or areas designated for flood overflows. To achieve the maximum effect of flood, protection is necessary to create the perfect combination of measures increasing natural retention and technical measures.

(3) Flood prevention

Preventive measures are mainly legislative measures, flood protection plans, forecasting and warning service, regulation of the use of floodplains or manipulation rules of waterworks [3].

*2.3.1. Measures in the watercourse channels*

Basins in the Czech Republic have always been the subject of numerous anthropogenic modifications. The interference with the natural character of the river basin occurred at various levels—from changes in use of the river basin, strengthening river channel, construction of river basin facilities in the profile of the watercourse, flow path geometry modifications and changes in riparian vegetation. These interventions are largely reflected not only in the river network, but also play role during the runoff process. This fact is of utmost effect during extreme hydrological events such as floods or drought, which may result in changes in the rate of progress of flood waves or their concurrence. This leads to major changes in the extent of flood damage and losses to the health and lives of the population [18].

The main causal flow adjustments were and still are the protection of property and built-up areas from the effects of floods. Another reason for the flow modification was efficient use of the force of water flows for agriculture, transport and industry. A large part of watercourses of all sizes and categories in the past undergone some degree of technical adjustments. The first change in the nature of streams have been documented since the middle ages, in the form of the construction of dams and other artificial backwater for improving the use of energy from flowing water. These adjustments were associated mainly with building the traditional mills but also the mills for processing of metallic ores in crushing mills for glassworks, mills processing harvested timber or processing wool and fabrics. Fundamentally flow adjustments are connected with industrial revolution, which brought the expansion of steam-powered machinery in the late nineteenth century. With the development of settlements and the rise of industrialism arose effort to use energy and transport potential of the waterways and to protect

property from the effects of floods. These measures first hit the significant flows in lowland areas with high population and industry density [7].

Completely separate category in historical changes and adjustments of the rivers and their river basin are the adjustment associated with boating activities, or to transport material, especially along rivers. In the Czech Republic, the largest piece of such technical constructions is canals. From the still existing water works, we can mention Schwarzenberg channel and Vchynicko–Tetovský channel in Šumava Mountains. Along with other waterworks in the form of small water reservoirs called Clause used to serve for transport of harvested timber by the water for further processing. Both canals will be subsequently described in a case study in this chapter [11].

Another, now defunct water work is Fláje Channel in Erzgebirge from 1624. This channel, which is about 160 years older than above-mentioned channels in Šumava Mountain, was used to transport timber from the area of Fláje in the Saxon town Clausnitz. The channel was in operation only until the end of 1872. After that the channel was cut out, and today, it is virtually non-functional [13].

Special utilization was the last of canals built on one of the largest rivers in the Czech Republic called Bata's Channel on the Morava River. This water project, built in the years 1934–1938, was determined not to transport wood, but to transport the mined lignite. Unlike the above three canals, this was partly conducted riverbed Dřevnice and Moravia, and so it is not a purely artificial waterway [14].

An important milestone and a stimulus for change in the river basin areas was the so-called “provincial” flood in 1890, which hit the bulk of the country. Nevertheless, the control of small streams was already laid six years before. It was the so-called Amelioration Act from 1884. In many areas, the modification of water flows was brought through the land reform in the years 1919–1935. These adjustments primarily affected major rivers, but also small streams in the agricultural landscape. Modifications consisted mainly in straightening and damming streams as possible to prevent further flood conditions. It was often a modification of water flows inside the town, for example, in Pilsen rivers Mže and Radbuza. A series of alterations to streams was carried out in the framework of public works for the prisoners of the First World War and the unemployed during the economic crisis. These adjustments also affected the river basin of mountain waterways all over the country, for example, Úpa or Blanice river basin. The great flood in 1890 also gave an impulse to show the first stone masonry dams like Mariánské Lázně Dam from 1896, Kamenička and Harcov Dams from 1904, Pařížov Dam from 1913 or the Les Království Dam from the 1919 [10, 13, 16].

Straightening and regulation of flows are most often spoken in connection with the period of the socialist regime since the late 1950s of the twentieth century till the end of the 1980s of the twentieth century. This is many times related to extensive and often insensitive interventions into the network of watercourses which is connected very often with the intensification of agriculture collectivization and industrial and mining activities. An example is the huge range of water flows collected in the pipes, the proportion of drained land or completely transformed river basins such as Bílina River [7].

At that time, there was also a significant measure in the fight against drought. The idea of creating a network of backwater on the Vltava River to improve water management and shipping and energy purposes dates from the late nineteenth century. In response to the aforementioned significant period of dry years around the year 1947, the Czech Republic started to implement previously established concept of large water reservoirs. The task of these reservoirs was primarily to create enough storage capacity in the event of another dry year. At the same time, however, the dam should play a role in energy and to some extent the flood. Examples of these dams are a system known as the Vltava cascade, which currently consists of eight dams and one submerged weir degree on the Vltava River. System, as we know it today, was built from 1930 (water reservoir Vrané) to 1992 (waterworks Hněvkovice and Kořensko). In the beginning, there was the purpose of constructing the navigability of the river Vltava and obtaining energy from water source. Nevertheless, the largest water works was between the years 1951–1966 (Lipno, Orlický, Slapy and Kamýk) as a result of the catastrophic drought which affected the entire region of the Republic and had an impact mainly on water supply and agricultural production [11].

Currently, the solution of protection against extreme events on watercourses and water reservoirs addressed through action plans basin. Direct flood protection is ensured through adjustments riverbeds, whether it is meaningful and appropriate implementation of the regulation on large waterworks or through a revitalization action on small watercourses in the agricultural landscape. In connection with the protection of the area from flooding, it is also creating new retention reservoirs that are able to transform and slow down the passage of flood waves in river basins. Very often, it is the water works without a constant level, in the form of dry reservoirs and polders. An important part of flood protection is also clear and unambiguous definition of flood zones and adherence to a set of management of these areas. Thus, the stage would especially be protected against building of houses. This fact is unfortunately often underestimated or sometimes even non-compliance. The severity of the consequences of major and minor flooding is often intensified by just these buildings in floodplains. The extent of development in floodplains considerably increased since the 1940s of the nineteenth century, when they first began to extensively use hydropower for industrial purposes. In addition, construction activity in the vicinity of watercourses is usually cheaper than in hilly terrain above the rivers. It cannot be said that the company did not realize the danger of flooding. After several times mentioned provincial flood in the late nineteenth century, a technical concepts of flood protection were created, based on the construction of levees and dams. The problem is not the concept of direction to prevent floods as such but to reduce the consequences of irresponsible assets located in flood plains [7, 18].

In connection with protection against drought in recent times, increasingly mentions the possibility of repeating the solution from the middle of the last century, through the construction of new water reservoirs in the country at major watercourse. The bulk of these efforts are channelled into streams in mountain and foothill conditions. One option is the possibility of restoring the previously existing water reservoirs (e.g., the so-called klauzy, reservoirs for improving the flow of navigable canals for floating timber, for example, in a mountainous area of Šumava Mountain). The second option is the identification of new sites suitable for creating

storage space, for example, planned waterwork Nove Heřmínovy. Total about 200 potential sites for the construction of new water reservoirs are currently identified in the Czech Republic by Management of river basin. When constructing new dams serving for accumulation of water in the dry season, it is still important to keep in mind their further use for example in flood protection. Even the best water work can be potentially dangerous and can threaten the management of the river basin. An example might be a tear loose dam on the Bílá Desná in Jizské Mountains in 1916, or worsening flood flows below the dam Slezská Harta or Vír Dam in 1997 [16].

Besides protecting of river basins from flood and drought belongs to the concept of integrated river basin management also navigability of waterways. Currently, navigability is ensured only on part of the Elbe and Vltava. With longer-lasting periods of drought, there appear more and more problems with maintaining minimum flows to these traditional sailing routes. Currently in the management of river basins included in these two rivers navigability of Elbe up to Pardubice and navigability of the Vltava River between Prague and České Budějovice. Both projects entail considerable investment to build locks and overcome various height levels weirs and dams reservoirs [10].

### *2.3.2. Measures in the area of river basin*

Integrated river basin management not only focuses solely on actual water flows but also focuses on the whole river basin area. In such locations, it is defined and then the most important question of the development of the use of the various areas in terms of agricultural and non-agricultural activities.

If we divide the territory of the Czech Republic in terms of agricultural production to favorable and less favorable locations, there will be recorded entirely different evolution in the use of these areas [19].

Before Second World War, there were the biggest changes in land use, especially in the areas of traditional intensive agricultural production, especially in the area of lowlands. In the context of agricultural production, these were mainly conversion of grassland to cropland and the intensification of its use. In the non-agricultural sector, it was mainly in these areas recorded an increase in built-up areas. In other production areas, no significant changes were recorded, with the exception of the least-favored mountain areas, where at the beginning and during of Second World War the process of production extensiveness began [20].

In this period, the Czech Republic noted a number of significant historical events. This was primarily the completion of the industrial revolution and the associated industrial and transportation expansion of the state, such as the construction of the railways. Secondly, it was mainly the two World Wars and bound to them above described land reform [21].

Despite the large number of significant changes both political and legal, this period is marked by the smallest changes in land use. This fact is mainly due to the fact that people especially in the early centuries were not willing to significantly change their habits and traditional farming methods [18]. In the Czech Republic, during that period was the development and use of land equal in all areas, including mountain and foothill areas. The reason was the desire

for independence and self-sufficiency of food. This fact has not changed even the first agrarian reform after the First World War, rather to encourage this trend [22]. The reason for the shift of agricultural activities from big manufacturers is that they were able to deliver products at the national and international market for small-scale production and whose only task was to secure the aforementioned self-sufficiency. Conclusion especially post-war period marked by presidential decrees and the subsequent expulsion of large masses of the population from border sites heralded changes in land use for the next period [23].

The beginning of the period around the end of the nineteenth century is marked by increasing the area of arable land. At the end of the century, the percentage of arable land was the highest ever recorded—more than 50% of the country. Arable land was used for newly planted crops mainly technical, such as the sugar beets and potatoes. New areas of arable land were acquired primarily at the expense of pastures and meadows, but also at the expense of new water areas that were drying out. One of the reasons for the constant search for new land for growing crops was low efficiency and intensity of agriculture [19].

Around the beginning of the twentieth century, the application of the results of industrial and technological revolution made possible to reduce the area of arable land and convert these areas into other categories [18]. At the same time, there was also a slight decrease in pasture area. The reason is mainly the less need for livestock, which was replaced by machine forces. Positive on the whole change was the of increase valuable areas of woods and meadows. We cannot also forget the increasing urbanization in this period as well as the construction of railways. All this has led to a significant increase in built-up areas [24].

After the end of Second World War, significant breakthrough occurred in the evolution of land use. In areas with poor agricultural productivity continued the established trend of decreasing of production, mainly due to population displacement and also due to the greater involvement of agricultural technology [25]. For this reason, there was a cancellation of a large area of arable land and its conversion to permanent grasslands, where there was a presumption at least livestock production. Where even this kind of agricultural production, there were arable areas converted to forests [26]. The conversion to other land was often administrative. This fact is not recorded only in our country, although there is accentuated by the political situation, but also in other parts of Europe, where the marginalization of mountain areas was also under the pressure of increased mechanization of agricultural production. This fact can be documented by the example of Italy [1], Slovenia [27], Austria [28] and other alpine countries [29]. Even in highly traditional production areas in the lowlands, situation for agricultural production was not favorable. This was mainly due to development of industrial activities and the related construction of new industrial and residential buildings. For these activities, substantial occupation of agricultural land was carried out, even the finest soils [30].

This trend started in the period after 1948, but not ended after the revolution and still persists. Areas in mountain and foothill areas are increasingly being converted to grassland and forest areas. Lowland locations mainly in the vicinity of large cities have become interesting for investors and are often used for further development of residential and commercial buildings [7].



In general, we can say that in the long term, the agricultural land was converted to non-agricultural land more in less productive areas than in the traditional areas of agricultural production [22]. The most significant changes in these areas occurred in the period of communism, the loss of farmland, especially in mountainous areas amounted to 35%. This decrease can be primarily attributed to a reduction in arable land and the conversion of arable land to other non-productive categories. An interesting changes were in the acreage of grassland, which in 1989 throughout the country significantly decreased [31]. After 1990, however, there is the significant increase. Magnifying acreage of grassland, however, does not show the whole country evenly. The increase is more pronounced in the less favored areas (over 20%), probably under pressure of subsidy policies, while in lowland areas is only an increase of several percent [22]. A similar trend is then recorded in other parts of Europe [32, 33].

The period between 1948 and 1990 is marked at the beginning by displacement of the German population and the allotment procedures. This situation, however, was overshadowed by subsequent reforms in agriculture and political changes in the country. The main impetus for change in land use was mainly the formation of agricultural cooperatives and related collectivization of agricultural production. In addition, especially in border areas came the influence of building of the so-called iron curtain and the associated restrictions [7].

On a national point of view, this further loss of areas of agricultural land. The reason is the aforementioned policy changes, but also changes in the farming itself [19].

In the first place, it was left a large amount of agricultural land in the border areas is typical for this period. The reasons for this fact are twofold: land close to national borders has become inaccessible, or accessible only to permit. Therefore, there was not possible to continue to manage, even extensively [20]. Plots were left to spontaneous succession or converted to forest complexes. Border area and outside this band, however, suffered from other problems. The main drawback is the large slope of the land, relatively high fragmentation of land ownership, and inadequate soil moisture and the non-suitable conditions for intensive agricultural production. Because of these shortcomings, there is not possible without significant interference to apply modern technology and mechanization [25]. Plots were therefore often abandoned, left fallow or converted to other categories of use, such as meadows, pastures and forests. As already mentioned, much land was transferred to the category of other area [34].

Changes in farming practices and agricultural production brought another major change in land use. This change was extensive construction of agricultural buildings to a range of urban and rural areas, or within open countryside. This is the construction of various storage and handling areas and especially new large-scale production complexes for livestock production such as cowsheds, piggeries and large poultry [35].

There were changes related to the development and industrialization of the country, especially towards heavy industry. For these purposes, there was carried out large-scale occupation of farmland mainly in lowland areas around major rivers. Occupied areas were built up by industrial areas [19].

In connection with the construction, it cannot be forgotten the big farmland appropriation for the construction of new residential areas of the major cities. This was largely in building blocks of flats around agglomerations [36].

After 1990, the period of transformation from a centrally planned economy to a market economy country began. This period is marked by significant shifts in ownership of agricultural and non-agricultural land in restitution reforms [18].

The reason for this change in land use is disintegration of agricultural cooperatives, the transfer of land to private farmers, but also nationwide reduction of state support for agricultural production and the partial replacement of the support subsidizing non-agricultural activities in the country. As in previous years and now, there is a conquest of agricultural land for construction purposes. This phenomenon is mainly connected to the concept of suburbanization, that is, the expansion of built-up areas around agglomerations of large cities for residential and commercial purposes [37]. This is basically the construction of satellite towns, transshipment terminals, warehouses and shopping centers on the so-called greenfield. Paradoxically, after the pre-1990 period in our country, there appear a large number of areas designated as the so-called brownfields [38, 39]. These are the sites that have been used either for agricultural production, industry or the military, and now left abandoned and unused. Unfortunately, these built-up areas are in most cases left to decay and place of their use is still the appropriation of new areas of agricultural land [40].

### 3. Case study of the river Otava

To demonstrate the impact of changes in the management of river basins, especially in connection with the use of the river basin, was selected Otava River, its upper reaches to the city of Susice. This area has long been inhabited and used for many different aspects of human activity. The study will cover the changes that have occurred in the area since the mid-twentieth century (before this time was practically river basin management since the mid-nineteenth century unchanged) to the present.

Otava River is beginning in the Pilsen region in the southwest of the Czech Republic. It is a left tributary of the Vltava River originates at the confluence of smaller watercourses Vydra and Křemelná at Čeňkova saw in Šumava Mountains. The entire basin of water flow consists of a large number of sub-basins of natural waterways and also one man-made shipping channel.

Otava River basin is quite rugged. Especially, the southern part of the area is predominantly mountainous. Geographically, it falls into the area of the Sumava Mountains and the foothills of Sumava Mountains, with an average altitude of 1003 m above sea level. Watershed average slope XXX°.

From a geological point of view metamorphic rocks (gneisses and migmatite) and magmatic Moldanubicum rocks (granite and granodiorite) are dominated. The magmatic types of rock are mainly in the top parts of the mountains. Peat bogs also frequent occurred in the uppermost

part of the river basin. Sand and gravel are then located mainly around watercourses. In the flatter northern part of the river basin, there are also disseminated limestone and erlan islands.

From the pedological point of view, forest land in the form podsoles completely dominates due to the high percentage of forested land. Cambisols, stagnosols and in permanently wet areas with high ground water gleysols occur mostly on agricultural lands. Modal fluvisols are developed around watercourses. Mainly in the northern half of the river basin, there are located small patches of leptosols.

From the climatic point of view, the Otava River basin falls mostly in cold climatic area with long-term average annual air temperature of 3.7°C (average temperature in January—4.4°C and an average July temperature of 12.5°C). The northern plains of the basin are located in the temperate climatic zone, characterized by an average annual temperature of 7.2°C (average temperature in January—2.5°C and an average July temperature of 17.0°C). Rainfall totals are very diverse with long-term average annual value for mountain areas 1486 mm and for the flat part 631 mm.

### 3.1. Material

The first of two parts, of which the Otava River is composed, Vydra is created by the confluence of three rivers in the mountain village Modrava at an altitude of 978 m above sea level. The largest and longest of these flows are Roklanský (Mlýnský) stream, which rises at an altitude of 1264 m above sea level and collect water from numerous other streams and bogs as Javoří stream or Rokytká. The basin of Rokytká stream was in the middle of the last century important with water tank for the free navigation of timber. One of the largest of them, Roklanský tank should hold up volume 14,000 m<sup>3</sup>. Another tank was built on a tributary Rokytká. This tank was holding back up to 18,000 m<sup>3</sup>. Virtually in all river basins of other tributaries, the dam was also built, which was called Klauzy (Novohutský stream—15,000 m<sup>3</sup>, Studený stream—3000 m<sup>3</sup>, Javoří stream—16,000 m<sup>3</sup>). The second component of the waterways from which consists Vydra River is also Luzenský or Modravský stream that originates at the confluence Luzenský and Březnický stream near the path to Březník. At the end of Luzenský valley, there is one of the largest navigable reservoir Březnický dam with a height of 4 m and a total accumulation space of 21,000 m<sup>3</sup>. Luzenský stream receives water from the nearby mountains and bogs, the largest of which is the Cikánská moor stream draining the same name peat bog. Just before the confluence with the waterways were two corridors lead into the bed of the now noticeable tanks Ptačí a Černohorská. The last of the sub-tributaries of Vydra River is Filipohutský stream that collects water from Tetřevské and Filipohutské moor.

After the above-mentioned confluence of three major rivers, even as Vydra, the river has considerable energy and adopt progressively more right-hand and left-hand tributaries, the most important of which is the right flowing Hamerský stream and left smaller flowing Popelský stream, Hrádecký stream and Zhužský stream. After 12 km, Vydra after the confluence with Křemelná at an altitude of 627 m above sea level at Čeňkova saw changes in the Otava River.

The important point is called Rechle, gate bridge, is located 2.2 km from the establishment of Vydra River at court Antýgl. At this point, there is the beginning of artificially built Vchynicko–Tetovský channel. The canal was designed and built by Ing. Josef Rosenauer between the years 1799–1801, as second after the Schwarzenberg channel built between the years 1788–1821. After branching out, Rechelský bridge at an altitude of 937 m above sea level surpassed water from the Vydra River by original 14 km long route and 255 m elevation to the Křemelná River at an altitude of 682 m above sea level. In the original arrangement, the channel ends with a wooden structure slip to Křemelná River.

The other watercourse from which the Otava River is formed is Křemelná River. Křemelná River rises at an altitude of 1050–1170 m above sea level on the slope of the ridge between Pancíř and wetlands under Jedlová mountain. The total length of the river is about 30 km, and after overcoming total 463 m altitudinal gradient it casts of Vydra at Čeňkova saw. Compared to Vydra River, Křemelná River is leisurely, meandering watercourse. Because of this, it was used in the past as an energy source for many aquatic power plants, mills and smelters and glass rising. The river Křemelná has four significant right-sided tributaries, Slatinný stream, Jezerní stream, Prášilský stream and Sekerský stream. First mentioned tributary brings into the Křemelná River water from a large wetland fen under Pancíř, which is located near the source of Křemelná River. At the same time, there are other small streams such as Sklářský stream, Černý stream or Drozdí stream. The latter, Jezerní stream flows from the smallest of the Šumava lakes, lake Laka. The penultimate tributaries, Prášilský stream overcomes a 12-km route quite significant elevation of 400 m from the village Prášily to the confluence with Křemelná. Just before the confluence takes on Prášilský stream of water from the Jezerní Brook, who, unlike his namesake, flows from the Prášilské lake. Sekerský stream flowing from the Jezerní hřbet is the last tributary of Křemelná River.

### 3.2. Methods

To quantify changes in direct runoff height in a different river basin management under the same designed rainfall events was used curve number (CN) method, because in the Czech Republic and abroad, this method is often used, among other things, for assessing the impact of changes in land use on the size of the direct runoff [41].

The runoff curve number (also called a curve number or simply CN) is an empirical parameter used in hydrology for predicting direct runoff or infiltration from rainfall excess. The CN method was developed by the USDA Natural Resources Conservation Service, which was formerly called the *Soil Conservation Service* or SCS. The runoff CN was developed from an empirical analysis of runoff from small catchments and hillslope plots monitored by the USDA. It is widely used and is an efficient method for determining the approximate amount of direct runoff from a rainfall event in a particular area.

The basic input to CN method is designed rainfall event ( $P$ —[mm]) assuming uniform distribution over the entire river basin area. For rainfall–runoff event for a given time is assumed that the ratio between the current retention ( $F$ —[mm]) and maximum potential retention of the basin ( $S$ —[mm]) is the same as the ratio between the direct runoff ( $Q$ —[mm])

and the rainfall without initial abstraction ( $P - I_a - [mm]$ ). Initial abstraction is expected to be  $0.2 \cdot S$  [42]. Using balance equations was derived from these assumptions following equation:

$$Q = \frac{P - 0.2 \times S}{P + 0.8 \times S}, \text{ where } P \geq 0.2 \times S$$

Instead of potential retention described method uses runoff CNs that transform the retention, so that the CN ranges from 0 to 100. Transformation for the variable in mm is following:

$$CN = \frac{25400}{S + 254}$$

Runoff CNs are according [43] determined by:

- hydrologic soil groups (HSGs) divided into four groups A, B, C, D according to the minimum infiltration rates of soils without vegetation cover when thoroughly wetted,
- soil moisture at the beginning of the event,
- land use, that is, the type of vegetation cover, tillage and application of erosion control methods.

To categorize, land use was used the results of Corine Land Cover project, for the years 1970, 1990, 2000, 2006 and 2012.

To categorize, the soils into the HSGs were used method described in [44], which adapts the CN method for steeper area. When categorizing soil into HSG was therefore taken into account not only the infiltration capacity of soils, but also the water retention capacity of the soils and the slope of the territory derived from the digital terrain model. Everything was calculated in software ArcGIS 10.1 in raster format. Data of the infiltration rates and water retention capacities were taken from the "Research Institute for Soil and Water Conservation" in Prague, digital terrain model was constructed in ArcGIS 10.1 based on the contours of the model Zabaged (The geographic base data of the Czech Republic from the "Czech Office for Surveying, Mapping and Cadastre").

For each combination of different HSG categorizations with land use were subsequently determined values of CN and subsequently from these (three), CN values were calculated the mean for each pixel. Since the infiltration rate can be considered as the most important soil characteristic to create direct runoff from rainfall event (primarily in planes), the resulting map of CN values (**Figure 1**) was formed as the maximum CN value determined from HSG by infiltration and average values CN of HSG by all the used categorizations. This emphasized the influence of a low infiltration rate of soils in the flat area and influence of water retention capacity and the slope of the territory in areas with steeper terrain [44].

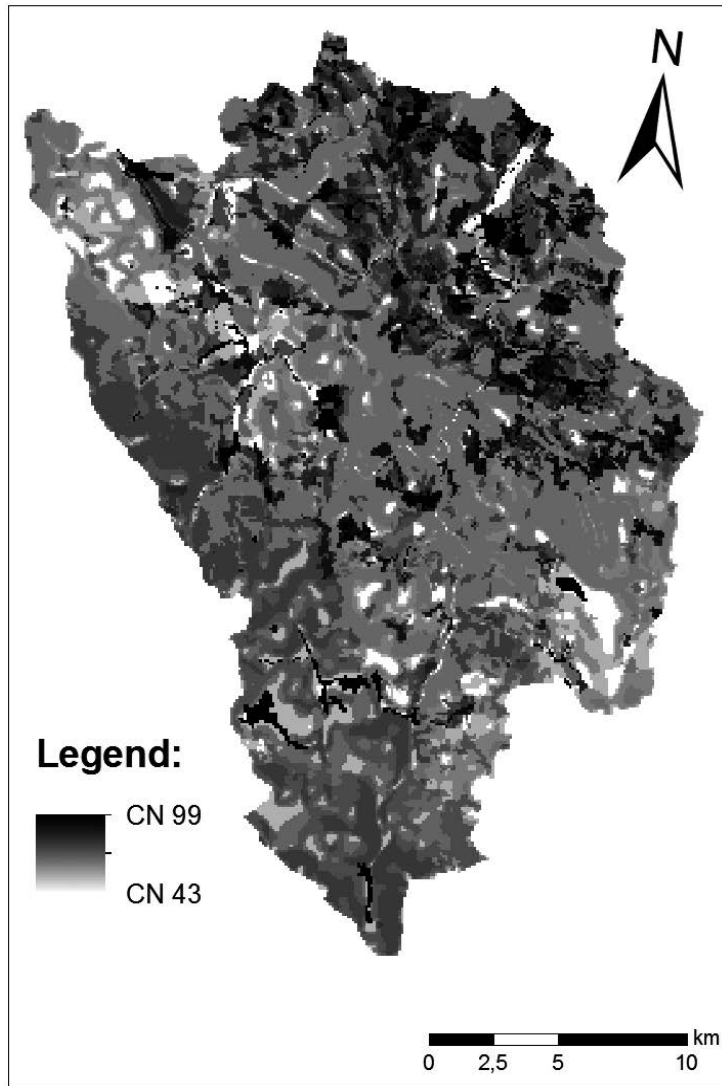


**Figure 1.** Example of the map of final CN values in the 2012.

In this study, for the calculations of direct runoff, designed rainfall events were used with the annual exceedance probability of  $p = 0.1$ ;  $p = 0.02$  and  $p = 0.01$  (return period of  $N = 10$ ,  $N = 50$  and  $N = 100$  years—that is, 10-year, 50-year and 100-year rainfall). Calculation of the  $N$ -year designed rainfall evenly distributed over the entire river basin area (assumption of CN method) were done by interpolation (spline method) in software ArcGIS 10.1 of the  $N$ -year rainfall in the rain gauge stations within the Otava River basin and its surroundings. The 24-hour designed rainfall for each return period is as follows:  $N10 = 82.6$  mm,  $112.2$  mm =  $N50$  and  $N100 = 125$  mm.

ArcGIS 10.1 was subsequently calculated (using the formulas given above) the values of the direct runoff (mm) and its volumes ( $\text{m}^3$ ) for each input CN raster for the years 1970, 1990, 2000, 2006 and 2012, and for each designed rainfall events (10-year, 50-year and 100-year). **Figure 2** is an example of the resulting direct runoff volume raster in  $\text{m}^3$  calculated for the 10-year rainfall and land use in 2012.

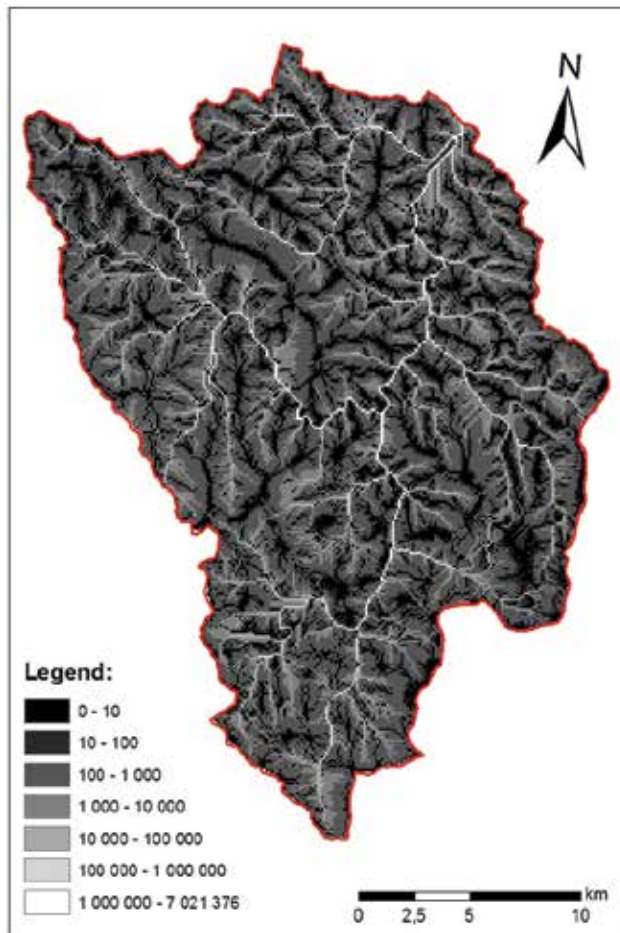


**Figure 2.** Direct runoff volume [ $\text{m}^3$ ] for 10-year rainfall in 2012.

### 3.3. Results and discussion

#### 3.3.1. Changes in river basin management

The subject area was under the observation period and often radically altered. As a reference datum, there was the year 1970, which represents the state before until the mid-eighteenth

century. It should be noted that the use of territory has changed significantly nearly in the entire surface. Changes are practically constant, and at two basic levels.

1. Conversion of arable land with varying intensity at different management of intensive and extensive grassland
2. Deforestation of large areas of indigenous mostly spruce monocultures and their transfer to the shrub and herbaceous vegetation covering the surface with a discontinuous vegetation

The first-mentioned change in the area is related to the transfer of arable land to various forms of permanent grassland. This change was caused mainly by economic as well as environmental reasons. The first significant change was recorded in 1990. The conversion of cropland to permanent grass cover was related to the change of the political situation in the whole of Central and Eastern Europe. Under pressure of this fact and also under pressure from neighboring countries and consequently the European Union, there have been some partial changes in land use [23]. These changes were reflected off the site of interest, especially in the ongoing reduction in the percentage of arable land throughout the country in the period after 2004. This trend is supported still setting state subsidy policy and the European Union [45]. The main driving force that brought about changes in the conversion of cropland to permanent grass cover was the creation of agri-environment grant scheme. Conversion of arable land has continuing problems with degradation of arable land by erosion, compaction, etc. [46]. The measure is divided into six titles, because grassing can be made by three kinds of mixtures. Then, there can be distinguished grassing of parts near water or in protective zones of water sources and grassing outside these areas. Species-rich mixture is appearing for the first time and represents a certain alternative to tighter regional blends. The aid is effective and permanent protection of soil against erosion, water pollution prevention, increasing species diversity and attractiveness of the landscape. Changes in agricultural commodity markets also brought a reduction in livestock, particularly cattle for milk production. These breeds were either cancelled without refund or farmers switched to less intensive cattle sucker ongoing grazing manner. For this reason, there is a constant increase in the acreage of grassland at the expense of other categories of agricultural land [47].

The second described change—loss of forest areas—was first recorded in 1990. It was a change to a smaller portion of the territory over the coming decades. The cause must be sought in the past. During the eighteenth century, when the last big wave of settlement, there was a large loss of forest area. Due grazing in the forest and favoring mining hardwood was negatively affected species richness [48]. In addition, the clear-cutting for the needs of glassworks and subsequent afforestation of even-aged spruce monocultures is causal primarily wind calamity of October 1870. After this, natural disaster areas were promptly reforested by trees. Spruce seedlings were imported for this purpose from all parts of the former State and their genetic composition differs from the original Šumava spruces [49]. This led to a weakening of natural populations of native spruce that were already years adapted to local conditions. The result is often highly unstable growth with reduced resistance to diseases and pests like against bark beetle [50]. Another negative influence for resilience of forests was caused by the discharge of



pollutants and acid deposition into the atmosphere [51]. Pollution took place from the beginning of the Industrial Revolution until the 1980s of the twentieth century. In our country, stronger steps against atmospheric pollution were taken after 1989. As a result of these changes, the forest is weakened, decreasing vitality, and substantially increases the risk of possible damage by disturbances [50]. The most significant disturbance on the area of interest is considered the influence of wind and insects [52]. Based on historical sources, the important fact is that a wind storm or gale in the past in the Bohemian occurred quite frequently, but their frequency varied over the centuries [53, 54]. Currently, it is more frequent, but their appearance and in the future to be reckoned with frequent wind warps at high speeds [55].

Loss of forests between 1970 and 1990 has its cause in the first place outside the area of interest. During the years 1983 and 1984, the areas of neighboring Bavarian National Park were affected by two powerful winds, which damaged large areas of valuable forest ecosystems in the first zone of the national park [52, 54]. Heavily damaged forest in non-intervention part of the Bavarian National Park has become a breeding ground for the rapid development of the bark beetle, which subsequently began to spread into the surrounding forests. Czech part of Šumava was hit by bark beetle in 1990 [54]. Monocultural local spruce forest significantly contributed to the rapid development of the bark beetle in Šumava, which reduces the ability of spruce forests to withstand the stresses caused by strong winds [56].

Already so weakened and reduced stands of forest were damaged even more. The next big hit in the Šumava mountain spruce came on the night of 18–19 January 2007 when the Bohemian Forests caught wind of hurricane force, named Kyrill. The highest recorded wind force in national park was  $176 \text{ km h}^{-1}$ . Thus, strong winds caused extensive damage to forests in dozens of square kilometers [55]. It fell victim to around one million cubic meters of wood.

Windstorm hit the most senior parts of the Šumava National Park. The subsequent massive loss of forested areas between 2006 and 2012 took care of warm and dry late winter and early spring, which caused a very rapid onset of bark beetles [57].

A total of about 217,000 trees in the forests of the National Park Šumava left without treatment. Raw windbreaks have become a source of spread of spruce bark beetles in the area. Mining infested trees in 2010 exceeded historical maximum and reached the highest value in the history of the Šumava National Park. Even in forests left to spontaneous development was the death of hundreds of thousands of adult pines [56].

### *3.3.2. The effect of changes in river basin management to direct runoff*

The resulting values of the heights of runoff and runoff coefficients for individual design rains are shown in **Tables 1** and **2**.

The results suggest the influence of land use changes that have occurred in the river basin in the past, and the formation of runoff. However, the differences in values of runoff are not remarkable. The highest differences were, based on model, between 2006 and 2012. In this period, the large areas near the river basin borders were deforested due to the combination of bark beetle calamity, windstorm and excavation of remnants of forest. In fact, it was the replacement of forest by land cover, which can be characterized as a scrub and herb layer on

the forest floor. CN value therefore varies, but the soil is permanently covered with vegetation and soil infiltration properties themselves remain almost identical. By the 100 year designed rainfall distinction is the highest and a difference in direct runoff height is 1.4 mm, which in units of volume is almost 750,000 m<sup>3</sup>. The change is therefore evident, but not significant.

Year/designed rainfall	N10 (82.6 mm)	N50 (111.2 mm)	N100 (125.0 mm)
2012	13.6	28.0	35.3
2006	12.9	26.8	33.9
2000	13.0	27.0	34.1
1990	13.8	28.00	35.2
1970	13.8	28.00	35.2

**Table 1.** Direct runoff [mm] for designed rainfall with periodicity 10, 50 and 100 years.

Year/designed rainfall	N10 (82.6 mm)	N50 (111.2 mm)	N100 (125.0 mm)
2012	16.5	25.0	28.2
2006	15.6	23.9	27.1
2000	15.7	24.1	27.3
1990	16.7	25.0	28.2
1970	16.7	25.0	28.2

**Table 2.** Direct runoff coefficient [%] for designed rainfall with periodicity 10, 50 and 100 years.

Other changes in land use are differences in heights and volumes of runoff smaller, but even here it can be seen the positive impact of some changes. For example, reduction of direct runoff between 1990 and 2000 for all forms of the rainy season can be put into the context with the grassing of arable land after 1990. In contrast, surprisingly identical values of direct runoff model were calculated in 1970 and 1990, although there had been significant changes in the landscape. However, the loss of arable land, pasture and forest has been “offset” by the increase of meadows and bushes, so that was a mix of changes variously distributed across the river basin with almost no difference for creating direct runoff throughout the river basin.

These results confirm the findings of [58], who based on the long-term observation and statistical analysis suggests that it is virtually impossible that changes in land use (if we exclude drastic interventions such as the permanent removal of vegetation cover from soil or the establishment of impervious surfaces) can permanently significantly change the long-term average height of runoff from the river basin. Similarly, Hanel et al. [59] argue that by larger basins whose area is in the tens or hundreds km<sup>2</sup> and which are not predominantly agriculturally used changing flood runoff volume and flow due to changes in land use is almost unreal. Because in this study there are modelled extreme precipitation events (N = 10 to N = 100 years), the results also confirm the claim [60] that the use of the land has only a marginal impact in the development of flash floods. Also Hanel et al. [59] add that for flooding from extreme rainfall is the effect of land use on runoff volume and flow weaker compared with the

importance of causal precipitation. This confirms [61], claiming that during the major floods in 2002 (which also took place at the catchment evaluated in this study), the influence of total rainfall on the height of the flood flow was completely dominant.

This conclusion does not mean that changes in land use and other measures decreasing surface runoff should be avoided. Changes in land use from arable land to grassland or forest naturally improves soil protection against erosion in the river basins and can have a significant impact on flood flow height and peak flow in smaller catchment area, especially for short-term floods.

The above-described changes are reflected in the characteristics expressed in relative terms (runoff coefficients—**Table 2**). Moreover, it is seen that the coefficients of runoff during designed rainfall  $N = 10$  to  $N = 100$  years are in the range of about 15–30%. This confirms the findings of Kašpárek et al. [62] that the runoff coefficients of flood flow even by a very intensive and large precipitation are close to the value of 30%. Similar values are seen on the charts published by Kašpárek et al. [61], which suggests that in exceptional floods in 2002 runoff coefficients were maximally to 30% in the river basin areas larger than 400 km<sup>2</sup> with total rainfall amount varying from 80 to 150 mm.

## Acknowledgements

This publication was created with the contribution of a grant of the University of Southern Bohemia in Ceske Budejovice 081/2016/Z. The water in the cultural landscape in a period of climate change.

## Author details

Jana Moravcová\*, Václav Bystřický, Jiří Pečenka, Jakub Polenský, Tomáš Pavlíček,  
Nikola Nováková and Pavel Ondr

\*Address all correspondence to: moravcova.janca@seznam.cz

University of South Bohemia in České Budějovice, Faculty of Agriculture, Department of  
landscape management, Studentská, České Budějovice, Czech Republic

## References

- [1] Andreoli, M., Brunori, G., Campus, F., Tellarini, V. I sistemi agricoli in aree marginali. Aspetti socio-economici. (Agricultural systems in marginal areas. Socio-economical aspects.) Firenze: Mugello-Alta Romagna-Garfagnana-Alto Reggiano; 1989. 460 p.

- [2] Mostert, E. Social learning in European river-basin management: barriers and fostering mechanisms from 10 river basins. *Ecology and Society*. 2007;12(1):17–32.
- [3] Downs, P. W., Gregory, K. J., Brookes, A. How integrated is river basin management? *Environmental Management*. 1991;15(3):299–309.
- [4] Knight, D., Shamseldin, A., editors. *River basin modelling for flood risk mitigation*. Boca Raton: CRC Press; 2005. 608 p.
- [5] Shim, K. -C., Fontane, D. G., Labadie, J. W. Spatial decision support system for integrated river basin flood control. *Journal of Water Resources Planning and Management*. 2002;128(3):190–201.
- [6] Molle, F. River-basin planning and management: The social life of a concept. *Geoforum*. 2009;40(3):484–494.
- [7] Sklenička, P. *Základy krajinného plánování (Basics of landscape planning)*. Prague: Naděžda Skleničková; 2003. 314 p.
- [8] Palmer, M. Climate change and the world's river basins: anticipating management options. *Frontiers in Ecology and the Environment*. 2008;6(2):81–89.
- [9] Jaspers, F. G. W. Institutional arrangements for integrated river basin management. *Water Policy*. 2003;5(1):77–90.
- [10] Povodí Vltavy, s. p. Lower Vltava river basin plan [Internet]. 2009. Available from: <http://www.pvl.cz/planovani-oblasti-vod/dolni-vltava> [Accessed: 20.1.2016]
- [11] Povodí Vltavy, s. p. Upper Vltava river basin plan [Internet]. 2009. Available from: <http://www.pvl.cz/planovani-oblasti-vod/horni-vltava> [Accessed: 3.1.2016]
- [12] Povodí Vltavy, s. p. Berounka river basin plan [Internet]. 2009. Available from: <http://www.pvl.cz/planovani&hyphen;oblasti-vod/berounka> [Accessed: 30.1.2016]
- [13] Povodí Ohře, s. p. Eger and Lower Elbe river basin plan, [Internet]. 2009. Available from: <http://www.poh.cz/VHP/vhp.htm> [Accessed: 2.1.2016]
- [14] Povodí Moravy, s. p. Morava river basin plan [Internet]. 2009. Available from: <http://www.pmo.cz/pop/2009/morava/end/index.html> [Accessed: 15.1.2016]
- [15] Povodí Moravy, s. p. Dyje river basin plan [Internet]. 2009. Available from: <http://www.pmo.cz/pop/2009/dyje/end/index.html> [Accessed: 5.2.2016]
- [16] Povodí Labe, s. p. Upper and Middle Elbe river basin plan [Internet]. 2009. Available from: <http://www.pla.cz/planet/projects/planovani/hlavni.aspx> [Accessed: 11.2.2016]
- [17] Povodí Odry, s. p. Oder river basin plan [Internet]. 2009. Available from: [http://www.pod.cz/planovani/cz/plan\\_oblasti\\_povodi\\_odry.html](http://www.pod.cz/planovani/cz/plan_oblasti_povodi_odry.html) [Accessed: 1.2.2016]

- [18] Sklenička, P. Temporal changes in pattern of one agricultural Bohemian landscape during the period 1938–1998. *Ekologia-Bratislava*. 2002;21(2):181–191.
- [19] Bičík, I., Jeleček, L., Kabrda, J., Kupková, L., Lipský, Z., Mareš, P., Šefrna, L., Štych, P., Winklerová, J. *Vývoj využití ploch v Česku (Development of land use in the Czech Republic)*. Prague: Czech geographical society; 2010. 250 p.
- [20] Bičík, I., Götz, A., Jančák, V., Jeleček, L., Mejsnarová, L., Štěpánek, V. Land use/land cover changes in the Czech Republic 1845–1995. *Geografie–Proceedings of Czech geographical society*. 1996; 101(2):92–109.
- [21] Bičík, I., Jeleček, L., Štěpánek, V. Land-use changes and their social driving forces in Czechia in the 19th and 20th centuries. *Land Use Policy*. 2001;18(1):65–73.
- [22] Novotná, M. *Problémy periferních oblastí (Problems of peripheral areas)*. Praha: Univerzita Karlova; 2005. 251 p.
- [23] Bičík, I. Land use in the Czech Republic 1845–1948–1990. Methodology, interpretation, contexts. *Acta Universitatis Carolinae Geographica*. 1998;32(1):247–255.
- [24] Kuskova, P., Gingrich, S., Krausmann, F. Long term changes in social metabolism and land use in Czechoslovakia, 1830–2000: An energy transition under changing political regimes. *Ecological Economics*. 2008;68(1–2):394–407.
- [25] Kabrda, J., Bičík, I., Šefrna, L. Pudy a dlouhodobé změny využití ploch Česka (Land and long-term land use changes in the Czech Republic). *Geografický časopis (Geographical magazine)*. 2006;58(4):63–87.
- [26] Jeleček, L. Využití pudního fondu České republiky 1845–1995: hlavní trendy a širší souvislosti (Utilisation of the Czech Republic 1845–1995: major trends and the wider context). *Proceedings of Czech geographical society*. 1995;100(2):276–291.
- [27] Gabrovec, M., Petek, F., Kladnik, D., Fridl, J. Land use changes in the 20th century in Slovenia. *Slovenia a Geographical Overview*. 2001;25(2):41–52.
- [28] Krausmann, F., Haberl, H., Schulz, N. B., Erb, K. -H., Darge, E., Gaube, V. Land-use change and socio-economic metabolism in Austria – Part I: driving forces of land-use change: 1950–1995. *Land Use Policy*. 2003;20(1):1–20.
- [29] Macdonald, D., Crabtree, J. R., Wiesinger, G., Dax, T., Stamou, N., Fleury, P., Lazpita, J. G., Gibon, A. Agricultural abandonment in mountain areas of Europe: Environmental consequences and policy response. *Journal of Environmental Management*. 2000;59(1): 47–69.
- [30] Jeřábek, M., (Editor). *Geografická analýza pohraničí České republiky (Geographical analysis of borderland of the Czech Republic)*. Prague: Sociological institute of Czech academy of Science; 1999. 179 p.

- [31] Bičík, I., Jeleček, L. Political events factoring into land-use changes in Czechia in the 20(th) century. *Understanding Land-Use and Land-Cover Change in Global and Regional Context – Proceedings of International conference*. 2005:165–186.
- [32] Acs, S., Hanley, N., Dallimer, M., Gaston, K. J., Robertson, P., Wilson, P., Armsworth, P. R. The effect of decoupling on marginal agricultural systems: implications for farm incomes, land use and upland ecology. *Land Use Policy*. 2010;27(2):550–563.
- [33] Rounsevell, M., Ewert, F., Reginster, I., Leemans, R., Carter, T. Future scenarios of European agricultural land use: II. Projecting changes in cropland and grassland. *Agriculture, Ecosystems & Environment*. 2005;107(2):117–135.
- [34] Sklenička, P., Hladík, J., Střeleček, F., Kottová, B., Lososová, J., Číhal, L., Šálek, M. Historical, environmental and socio-economic driving forces on land ownership fragmentation, the land consolidation effect and the project costs. *Agricultural Economics-Zemedelska Ekonomika*. 2009;55(12):571–582.
- [35] Jeleček, L., Burda, T., Chromý, P. Historická geografie a výzkum vývoje struktury půdního fondu Česka od poloviny 19. století (Historic geography research and development of Czech land resources structure from the mid-19th century). *Historická geografie*. 1999:261–270.
- [36] Pacione, M. Models of urban land use structure in cities of the developed world. *Geography. (Historical Geography)*. 1999; 34(2):261–270.
- [37] Lipský, Z., Kalinová, T. Landscape structure changes in urbanized areas: Case study from the Prague outskirts. *Ekologia-Bratislava*. 2001;20:110–117.
- [38] Brito, M. G., Costa, C. N., Vendas, D. Methodological approach for ground contamination assessment and remediation of brownfields. *WSEAS Transactions on Power Systems*. 2007;4(3):288–293.
- [39] Kuráž, V. The function of urban land, agricultural land protection and regeneration of brownfields. *Vodní hospodářství. (Water management)*. 2011;64(10):377–380.
- [40] Sýkora, L., Ourednek, M.,. Sprawling post-communist metropolis: commercial and residential suburbanization in Prague and Brno, the Czech Republic. *Employment Deconcentration in European Metropolitan Areas - Proceedings of National conference*. 2007;209–233.
- [41] Kašpárek, L., Peláková, M. Analýza citlivosti změn objemu přímého odtoku a infiltrace do půdy při potenciálních změnách užívání pozemku (Sensitivity analysis: How do land use changes affect water infiltration and direct runoff?). *Vodní hospodářství (Water management)*. 2014;64(10):8–12.
- [42] Janeček, M., Kovář, P. Aktuálnost "metody čísel odtokových křivek—CN" k určování přímého odtoku z malých povodí (Actuality of "runoff curves numbers method - CN" to determine the direct runoff from small watersheds). *Vodní hospodářství. (Water management)*. 2010;64(7):187–190.

- [43] Janeček, M. Ochrana zemědělské půdy před erozí (Agricultural land protection against erosion). Prague: ISV nakladatelství; 2002. 254 p.
- [44] Šercl, P. Metoda CN křivek—pruběžná zpráva na ČHMÚ Praha. Rozvoj a testování modelovacího systému pro predikci povodňových odtoků v malých povodích (The method of CN curves—Interim Report for the Czech Hydrometeorological Institute in Prague. Development and testing of modeling system for predicting flood runoff River Basin Management small watersheds). Report of project VaV 1D/1/5/05, DHI Hydroinform and ČHMÚ Prague for year 2005. 2006:50 p.
- [45] Kouřilová, J., Pšenčík, J., Kopta, D. Dotace v zemědělství z hlediska komplexního pohledu a s přihlédnutím k ekologickému zemědělství (Subsidies in agriculture from the perspective of a comprehensive view and with regard to organic farming). České Budějovice: University of Southern Bohemia publishing - Economical Faculty; 2009. 241 p.
- [46] Sklenička, P. Agro-Ecological Zoning and Conversion of Czech Agriculture. *The Land*. 1999;3(1):1–20.
- [47] Csaki, C., Lerman, Z. Land reform and farm restructuring in East Central Europe and CIS in the 1990s: Expectations and achievements after the first five years. *European Review of Agricultural Economics*. 1997;24(3–4):428–452.
- [48] Hrib, M., Kopp, J., Křivánek, J., Kyzlík, P., Moucha, P., Němec, J., Oliva, J., Pelc, F., Pešková, V., Roček, I., Řezáč, J., Slabá, M., Vančura, K., Vašíček, J., Zahradník, P., Zatloukal, V. *Lesy v České republice (Forests in the Czech Republic)*. Prague: Consult; 2009. 399 p.
- [49] Mánek, J. Elektroforetická laboratoř NP Šumava, její role a výsledky při výzkumu genetické diverzity smrku ztepilého na Šumavě a v ČR (Electrophoretic laboratory Sumava NP, its role and the results of the research of the genetic diversity *Picea abies* in Šumava and the Czech Republic). *Aktuality šumavského výzkumu (Actualities of Sumava research)*. 2001;10(2):129–133.
- [50] Fanta J. Rehabilitating degraded forest in Central Europe into self-sustaining forest ecosystems. *Ecological Engineering*. 1997;8(4):289–297.
- [51] Kopáček, J., Turek, J., Hejzlar, J., Šantruček, H. Canopy leaching of nutrients and metals in mountain spruce forest. *Atmospheric Environment*. 2009;45(34):5443–5453.
- [52] Jonášová, M., Prach, K. Central-European mountain spruce (*Picea abies* (L.) Karst.) forests: regeneration of tree species after a bark beetle outbreak. *Ecological Engineering*. 2000;23:15–27.
- [53] Dobrovolný, P., Brázdil, R. Documentary evidence on strong winds related to convective storms in the Czech Republic since AD 1500. *Atmospheric Research*. 2003;67–68:95–116.

- [54] Skuhrový, V. Lýkožrout smrkový (*Ips typographus* L.) a jeho kalamity (*Ips typographus* L. and its calamities). Prague: Agrospoj; 2002. 196 p.
- [55] Kolečka, J., Klimánek, M., Mikita, T., Svoboda, J. Polomy na Šumavě způsobené orkáne Kyrill a spoluúčast reliéfu na poškození lesa (Windbreaks in Šumava caused by the windstorm Kyrill, and relief participation on forest damage). *Geomorphologia Slovaca et Bohemica*. 2010;5(1):16–28.
- [56] Jonášová, M., Prach, K. The influence of bark beetles outbreak vs. Salvage logging on ground layer vegetation in Central European mountain spruce forests. *Biological Conservation*. 2004;141(6):1525–1535.
- [57] Steyrer, G., Tomiczek, C. Orkanschäden und Witterung begünstigen Borkenkäfer. *Forstschutz Aktuell*. 2007;40:3–5.
- [58] Kašpárek, L. Shrnutí poznatku o vlivu fyzicko-geografických charakteristik povodí na základní charakteristiky prutoku (Summary of findings on the effect of physical-geographical characteristics of the basin at the base flow characteristics). In: Blažková, Š., editors. *Vybrané výsledky projektu Labe IV 2003–2006, Hydrologická tematika se zaměřením na retenci vody v povodí (Selected results of the project Labe IV 2003–2006, The hydrological thematises, focusing on the retention of water in the basin)*. Praha: Čsvts; 2007. p. 52–64.
- [59] Hanel, M., Kašpárek, L., Mrkvičková, M., Horáček, S., Vezina, A., Novický, O., Fridrichová, R. Odhad dopadu klimatické změny na hydrologickou bilanci v ČR a možná adaptační opatření (Estimated impacts of climate change on the hydrological balance in the Czech Republic and possible adaptation measures). Prague: VUV T. G. Masaryka Praha; 2011. 64 p.
- [60] Hattermann, F. F., Huang, S., Vetter, T., Kron, W., Burghoff, O., Merz, B., Bronstert, A., Krysanova, V., Gerstengarbe, F. -W., Werner, P. Hauf, Y. Flood Risk from a Holistic Perspective—Observed Changes in Germany. In: Kundzewicz, Z. W., editors. *Changes in Flood Risk in Europe*. IAHS Special Publication ed. New York: IAHR Press; 2012. p. 212–237.
- [61] Kašpárek, L., Krátká, M. Analýza vlivu fyzicko-geografických charakteristik na tvorbu povodňového odtoku a sestavení publikace o povodni 2002 (Analysis of the impact of physical-geographical characteristics of the formation of flood runoff and flood compilation publications, 2002). VÚV T. G. Masaryka Praha, závěrečná zpráva. 2004;
- [62] Kašpárek, L., Eckhardt, P., Hanel, M. Možnosti zmírnění současných dusledku klimatické změny zlepšením akumulární schopnosti v povodí Rakovnického potoka (pilotní projekt) (Possibilities of alleviating the effects of climate change by improving storage ability of the basin Rakovnický stream (pilot project)). VÚV T. G. Masaryka Praha, periodická zpráva o řešení projektu. 2010;



---

# Streamflow Response to Climate Variability and Land-Cover Changes in the River Beça Watershed, Northern Portugal

---

Adélia. N. Nunes and Patrícia Lopes

Additional information is available at the end of the chapter

<http://dx.doi.org/10.5772/63079>

---

## Abstract

This work analyses changes in the River Beça basin streamflow, an area with a typically Mediterranean climate, since the second half of the last century, evaluating trends in annual, monthly and extreme streamflow in the River Beça basin and relating them to precipitation variability and changes in land use and vegetation. Annual streamflow and precipitation are highly irregular, both in intra and inter annual terms. During the period analysed, which covers the last six decades, a consistent negative trend was observed, both in mean annual streamflow and amount of annual precipitation. The results also demonstrate that precipitation greatly influences streamflow dynamics, accounting for around 85% of the variability observed in mean annual streamflow. In addition, the results show that the changes detected in land use/cover may have affected the water discharges of the river, although it is difficult to evaluate the magnitude of impact. The findings demonstrate that the impacts of climate variability and land use/cover change on streamflow are challenging and crucial to the management of water resources in Mediterranean river basins.

**Keywords:** Streamflow, Precipitation, land use/cover change, River Beça, Northern Portugal

---

## 1. Introduction

Water is a natural resource which has great economic, environmental and social value and is fundamental to the livelihood and welfare of human beings and the earth's ecosystems. A decrease in streamflow can have severe consequences for the water supply, both for ecosys-

---

tems and societies. Thus, management of the river basin is a key factor affecting the volume of water required to cope with the increasing demands of the population and several specific activities such tourism, agriculture and the energy sector, which directly depend on water resources.

Climate and land use/cover changes can have a profound influence on hydrological processes. The effect of climate variables, such as precipitation, temperature and evapotranspiration, is crucial to understanding the availability of water in any given territory [1]. Nowadays, it is recognised that the climate system is being subjected to natural as well as man-made changes [2], affecting the global cycle as well as the quantity and quality of water resources [3–5]. Observation of the climate in mainland Portugal from the 1970s onwards shows that the mean annual temperature has increased in all regions by about 0.5°C per decade, more than twice the global warming rate [6]. With regard to precipitation, analyses of spatial variability and trends in annual and monthly precipitation based on data from 42 stations in mainland Portugal during the period 1960–2011 show that annual precipitation has decreased in all stations and that this trend is statistically significant for most of the time series (70% of the stations showed negative trends with at least a 0.1 significance level) [7]. In many cases these changes in climatological variables can be identified as the cause of trends detected in the hydrological time series [8–25].

Moreover, in order to understand water resources, which are closely related to the production of runoff, at regional/local level the role of the whole tributary basin should be taken into consideration, particularly with regard to land use and plant cover [17, 18]. Several authors have reviewed catchment experiments to determine the effect of vegetation change on water yield [26–30]. In general, they concluded that surface runoff and river discharge tend to increase when natural vegetation (especially forest land) is cleared [31, 32], since deforestation reduces canopy interception storage, transpiration, and infiltration capacity [33]. Conversely, compared with a deforested area, a dense forest cover implies less surface runoff, due to the interception of the rain by leaves and the water requirements of the trees themselves [16, 17, 19–23, 34–37].

On the other hand, in Portugal, important socio-economic and political changes in the 1970s led to migration from the countryside. In fact, the introduction of modern agriculture, the opening up of international markets and the lowering of crop prices, market-oriented cultivation of cereals became unprofitable in most marginal areas of the country. As a consequence, several areas were abandoned, especially in marginal, semi-mountainous and mountainous areas, which significantly reduced the cultivated land and resulted in important transformations to the landscape, characterised by the spread of natural vegetation, including both shrub and forest land. Moreover, the implementation of CAP measures in Mediterranean countries has reinforced the extensification of farming in the “Less-Favoured Areas” (i.e., abandonment or marginalization and collapse of traditional farming systems), which has been going on for the last decades. Changes in land use characteristic of extensification include fewer cultivated fields, more shrub patches, larger areas of natural pastures, and the abandonment of some patches, followed by the development of stratified bush communities [37].

Thus, water resources in the Portuguese mountains, as well as in the Mediterranean mountains in general, are facing the effects of a changing climate, higher temperatures and lower precipitation, together with the consequences of a socioeconomic process that has led to the abandonment of rural activities and consequent changes in land use and land cover [20, 38].

It is therefore important to understand the hydrological responses to these changes in order to develop sustainable catchment management strategies. In fact, management is a key element in terms of the volume of water required to cope with increasing demand [39]. This factor is crucial in countries with a Mediterranean climate, such as Portugal, where the greatest demands for water are concentrated in the summer months (associated with tourism, irrigation and the return of emigrants for holidays), namely the season when it is least available [17].

The main aim of this study was to investigate the changes in the River Beça basin streamflow since the second half of the last century. Two objectives were defined: (i) to determine changes and trends in annual, monthly and extreme streamflow in the River Beça basin; (ii) to estimate the effects of climate variability and human activities, particularly those related to changes in land use and cover change, on streamflow. The environmental conditions of this basin are typical of Mediterranean mountain regions and the river is not regulated, thus presenting a natural regime.

## 2. Study area

Located in the North of Portugal, the Beça watershed is a third-order watershed that flows into to the Tâmega River (**Figure 1**), a tributary in the northwest sector of the Douro basin. The substratum mainly comprises two important lithic types: granitic rocks (granitoids) and metasedimentary rocks (schists and graywackes). The soils are classified as humic cambisols.

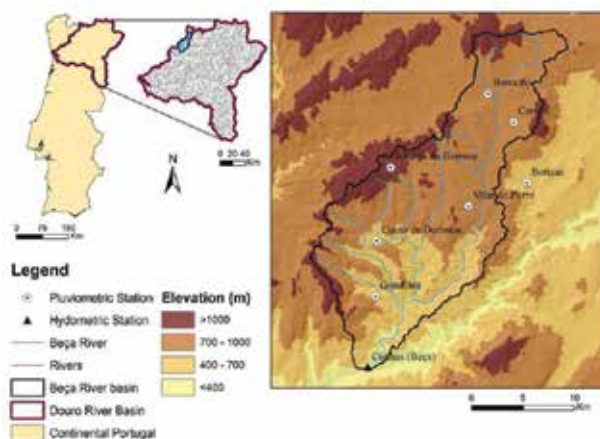


**Figure 1.** Location of the Beça River watershed.

It is characterized by a rugged topography, in which the altimetric gradient exceed 800 m asl, and drains over 338 km<sup>2</sup>.

Like other Mediterranean river systems, there is a marked variability in the inner and inter annual streamflow responses of the River Beça. **Table 1** presents the monthly and annual variability. It is no surprise that autumn and winter (the humid season) river flows account for the majority of runoff (around 80%), followed by a relatively long dry period. During the remaining six months of the year, 17% of the streamflow occurs during the spring and only 3% in the summer season. The river flow is also characterized by large disparities between wet and dry years (with a maximum of 21.5 m<sup>3</sup>s<sup>-1</sup> and a minimum of 1.3 m<sup>3</sup>s<sup>-1</sup>, St. deviation of 4.6 m<sup>3</sup>s<sup>-1</sup>). This situation presents a major problem for water resources management.

The mean annual rainfall is around 1150 mm yr<sup>-1</sup>. The area is also characterized by great inter-annual variability in precipitation, with a standard deviation of 458.8 mm. Thus, there is marked seasonality, with rainfall dominant in autumn-winter and concentrated in the period October-May, whereas July and August are very dry months (**Table 1**).

River flow (m <sup>3</sup> s <sup>-1</sup> )	O	N	D	J	F	M	A	M	J	J	A	S	Year
Maximum	28.2	43.3	64.7	70.7	75.2	78.6	30.1	25.8	11.5	5.9	3.3	7.2	21.5
Mean	4.2	9.5	16.7	19.2	18.3	14.2	9.5	6.4	3.6	1.5	0.7	1.1	8.7
Minimum	0.5	0.5	0.5	0.5	0.6	0.6	0.7	0.5	0.5	0.4	0.4	0.4	1.3
St. deviation	5.9	9.5	15.8	16.1	16	13.5	6.8	5.1	2.6	1.3	0.4	1.1	4.6
<b>Prec. (mm)</b>													
Maximum	382.5	474.9	827.0	474.5	582.8	618.5	328.6	251.0	221.5	88.7	97.0	196.0	2411.2
Mean	106.4	144.2	172.6	155.8	135.5	119.8	93.9	81.1	45.1	17.1	20.4	54.9	1146.7
Minimum	1.0	0.0	7.0	1.0	5.2	0.0	6.5	1.9	0.0	0.0	0.0	1.3	336.4
St. deviation	90.1	110.5	175.1	118.6	127.6	123.0	71.4	55.3	43.4	18.9	20.8	45.4	458.8

**Table 1.** Variations in monthly streamflow and precipitation in the study area.

### 3. Methodology

The streamflow data used in the study was obtained from the Portuguese National Institute for Water (INAG), which has kept records for the last six decades in daily time steps (m<sup>3</sup>s<sup>-1</sup>). Annual, monthly and daily data were examined for the period 1950/51–2010/11, using data from a hydrological station in Cunhas, located near the lower point of the catchment area (222 m asl) by the mouth of the River Beça. The streamflow follows a natural, unmanaged regime. A number of different statistics were chosen to describe the characteristics of the streamflow and test for any change in the flow regime at the streamflow gauging station. Trends were also calculated for selected quantiles of discharge, namely the <10th and >90th percentiles, in order

to evaluate the differences between low and high-flow regimes during the six decades analysed.

Rainfall data was also obtained from the INAG. Although precipitation data was collected from seven rainfall gauges distributed within the study area, only the data series for the Cervos rain gauge (842 m asl) was used. The Cervos station was the only one that had collected rainfall data for over five decades (1950/51-2008/09) and is classified as offering high quality and reliability. The annual rainfall data at this station also showed a statistically highly significant correlation with the annual precipitation of all other stations (with a Pearson-correlation coefficient of over  $r = 0.77$ ). The data from this station was therefore considered representative of the average rainfall for the whole of the watershed.

Two non-parametric methods (Mann-Kendall and Sen's slope estimator) were applied to detect trends in the annual and monthly precipitation and streamflow variables. As the Mann-Kendall (MK) trend test [40, 41] can detect trends in a time series without requiring normality or linearity [42], it is highly recommended by the World Meteorological Organization [43] and therefore widely used to detect trends in hydrological and meteorological series [44].

According to the MK trend test, the null hypothesis  $H_0$  is that the data in a time series  $\{Y_i, i = 1, 2, \dots, n\}$  is independent and identically distributed over random variables and the hypothesis  $H_1$  implies is that there is a trend in the series. The MK trend test starts by computing the test statistic  $S$  given by equation 1:

$$S = \sum_{i=1}^{n-1} \sum_{j=i+1}^n \text{sgn}(Y_j - Y_i) \tag{1}$$

where  $\text{sgn}()$  is the signum function. The  $S$  statistic, in cases where the sample size  $n$  is larger than 10, is assumed to be asymptotically normal, with  $E(S)=0$  and

$$\text{Var}(S) = \frac{n(n-1)(2n+5) - \sum_t t(t-1)(2t+5)}{18} \tag{2}$$

where  $t$  refers to the extent of any given tie and  $\sum_t$  states the summation over all ties (equation 2). The standard normal variate  $Z$  is computed by Equation 3:

$$z = \begin{cases} \frac{(S-1)}{\sqrt{\text{Var}(S)}} & \text{if } S > 0 \\ 0 & \text{if } S = 0 \\ \frac{(S+1)}{\sqrt{\text{Var}(S)}} & \text{if } S < 0 \end{cases} \tag{3}$$

Therefore, in case  $|Z| \leq Z_{1-\alpha/2}$  in a two-sided test for trend, the null hypothesis  $H_0$  should be accepted at the  $\alpha$  level of significance. A positive value of  $S$  denotes an “upward trend”, while a negative value of  $S$  indicates a “downward trend”.

The Sen slope estimator is useful in cases where the trend is assumed to be linear, depicting the quantification of change per unit of time [45, 46]. De Lima et al. [47] highlight the use of this estimator in cases where there are missing values or other gaps in the data, as it remains unaffected by outliers or gross errors. The slope estimates  $Q_i$  of  $N$  pairs of data are calculated as (equation 4):

$$Q_i = \frac{x_j - x_k}{j - k} \text{ for } i = 1, 2, \dots, N \quad (4)$$

where  $x_j$  and  $x_k$  are data values at times  $j$  and  $k$  ( $j > k$ ) respectively. The Sen slope estimator derives from the above  $N$  values of  $Q_i$  and equals their median. When there is only one datum in each time period, then  $N = n(n - 1)/2$ , where  $n$  corresponds to the number of time periods. The  $N$  values of slopes are ranked from the smallest to largest and if  $N$  is odd, the Sen slope estimator is calculated as equation 5:

$$Q_{median} = Q_{[N+1]/2} \quad (5)$$

On the other hand, if  $N$  is even, the estimator is produced by equation 6:

$$Q_{median} = \left( Q_{[N/2]} + Q_{[N+2/2]} \right) / 2 \quad (6)$$

A simple relationship between streamflow and rainfall was also established, excluding temperature since several studies have shown that this variable is not significant in explaining the variance observed in streamflow [17, 22, 48].

In order to evaluate changes in land use and land cover, two different cartographic sources were used:

- i. A map of the soil, land use and capacity of the Nordeste Transmontano region, 1980, 1:100,000 [49],
- ii. A map of land use in Portugal, 2007, 1:25000 (source: Direção Geral do Território; <http://www.dgterritorio.pt/>)

As the two sources have different land use/cover classifications, a simplified legend was established by combining classes, in order to capture the main land use/cover changes. A simple description of the land use and cover classes identified in the River Beça basin are described in **Table 2**.

Land use/cover	Description
Urban areas	Includes built-up land and other recreational areas (gardens, parks, etc.)
Agricultural areas	Areas used for cultivating both annual (vineyards, olives) and perennial (cereals) crops
Agroforestry systems	Areas used as pasture and grassland, as well as mosaic farmland.
Forest and woodlands	Areas covered with dense trees that form almost complete canopies (70%–100%). This category includes forest plantations, mainly pinus, and mixed forest, largely associated with the regeneration of “autochthonous” species such as oak trees.
Shrubland	Areas covered with shrubs, small trees and bare land that has very little or no grass cover (exposed rocks)

**Table 2.** Description of the land use/cover classes identified in the Beça watershed.

## 4. Results

### 4.1. Trends in annual and monthly precipitation and streamflow

The annual mean rainfall and streamflow over the period for which records exist were 1150 mm and 8.7 m<sup>3</sup> s<sup>-1</sup> respectively. Significant inter-annual variations in rainfall and streamflow are shown in **Figure 2**, corroborated by the respective coefficients of variations, namely 40% for rainfall and 52% for streamflow, showing that streamflow was generally more variable than rainfall.

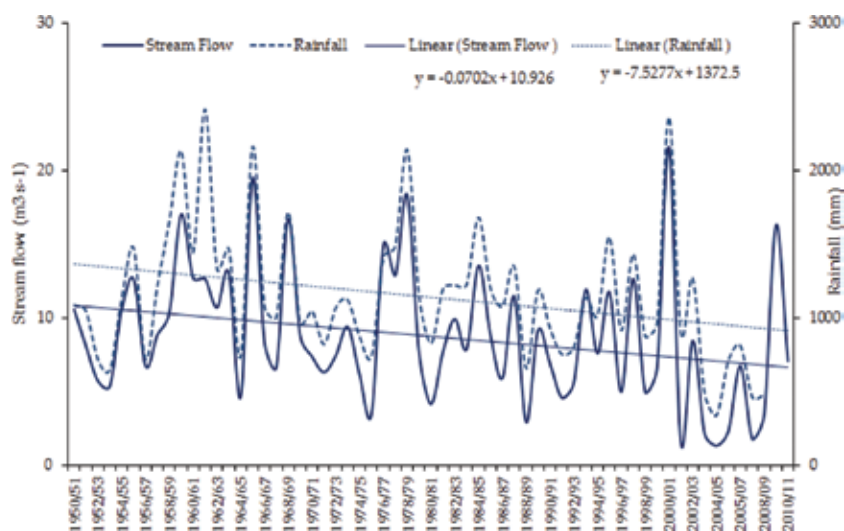


**Figure 2.** Inter-annual variability of rainfall and mean stream flow at the Cervos and Cunhas station.

Linear trend curves were fitted to the annual rainfall and mean annual streamflow to evaluate the long-term temporal changes (**Figure 2**). These linear regression models show that over the

60-year period both annual rainfall and streamflow decreased, 7.5 mm and  $0.07 \text{ m}^3 \text{ s}^{-1}$  respectively per year. These annual rates of change accounted for 32% and 39% of the variation in the rainfall and streamflow rates of change for the study period. The results of the Mann-Kendall method confirm the significant negative annual trend for both variables with a significance level of 5% (**Table 3**).

Rainfall			Stream flow		
Mann-Kendall score (S)	P-value	Sen's slope	Mann-Kendall score (S)	P-value	Sen's slope
O -14.000	0.931	-0.024	-50.000	0.755	-0.004
N -161.000	0.283	-0.952	-168.000	0.287	-0.048
D -73.000	0.629	-0.367	-70.000	0.660	-0.029
J -198.000	0.186	-0.971	-84.000	0.597	-0.056
F -246.000	0.100	-1.283	-380.000	0.016	-0.192
M -420.000	0.005	-2.000	-690.000	0.0001	-0.270
A -116.000	0.440	-0.370	-544.000	0.001	-0.140
M -65.000	0.668	-0.194	-600.000	0.000	-0.098
J -481.000	0.001	-0.783	-666.000	0.0001	-0.069
J -20.000	0.861	-0.008	-626.000	0.0001	-0.015
A 165.000	0.271	0.135	-489.000	0.002	-0.004
S -43.000	0.778	-0.082	-589.000	0.000	-0.008
Y -331.000	0.027	-7.925	-382.000	0.015	-0.79

Positive values in the table indicate an upward trend and negative values a downward trend.

**Table 3.** Results of the Mann-Kendall test and Sen's slope for monthly and annual precipitation and streamflow (figures shaded in grey indicate significant trends).

Analysis of changes in monthly precipitation and mean flow provides much greater temporal detail, and can help reveal and explain the cause of changes in annual patterns [50]. **Table 3** provides the calculations for the Mann-Kendall statistics and p-values derived for each month for precipitation and stream flow.

The results show that all of the months reveal a downward trend, with the exception of August rainfall which has a positive trend that is not statistically significant. It is interesting to note that rainfall only exhibited significant negative trends ( $p$ -value  $< 0.05$ ) for the months of March and June, whereas stream flow demonstrated statistically significant decreasing trends between February and September. These negative trends in streamflow affected the late winter period and the whole of the spring and summer seasons.

Following the M-K test, the Sen slope estimator was also used to calculate the change per unit of time for the trends observed in all the precipitation and stream flow time series. The outputs are presented in **Table 3**, where a negative sign represents a downward slope and a positive



sign indicates an upward one. On a monthly basis, only August rainfall confirms an upward slope. During the winter season (January, February and March) downward approximates of 4.4 mm/hydrologic year were recorded. As this concerns the monthly stream, the decreases were more significant between February and April.

#### 4.2. Changes in the pre- and post-1980 period

Noticeable differences in streamflow and precipitation were recorded when comparing the statistics for the pre- and post-1980 period. As **Table 4** shows, the mean annual streamflow for the pre- and post-1980 period was 10.1 m<sup>3</sup>s<sup>-1</sup> and 7.4 m<sup>3</sup>s<sup>-1</sup> respectively, meaning a decrease of 2.7 m<sup>3</sup>s<sup>-1</sup> (-26.7%). The greatest decreases (-50%) in streamflow were recorded in February and March, followed by June (-43.5%), July (-36.8%), May (-34.6%) and April (-33.9%). Conversely, an increase in the daily mean streamflow can be observed in October (+33%) and December (+8.8%). With regard to precipitation, a significant decrease can be observed in February (-49.2%), March (-47.4 %) and June (-40.8%) whilst slight increases were recorded in August (+25.4%), September (17.9%) and October (5.9%).

Streamflow mean (m <sup>3</sup> s <sup>-1</sup> )	O	N	D	J	F	M	A	M	J	J	A	S	Year
1950-1980	3.6	10.4	16.0	19.8	24.6	19.0	11.5	7.8	4.6	1.9	0.8	1.1	<b>10.1</b>
1980-2011	4.8	8.6	17.4	18.7	12.3	9.5	7.6	5.1	2.6	1.1	0.6	1.0	<b>7.4</b>
≠ in m <sup>3</sup> s <sup>-1</sup>	1.2	-1.8	1.4	-1.1	-12.3	-9.5	-3.9	-2.7	-2.0	-0.7	-0.2	-0.1	<b>-2.7</b>
≠ in %	<b>33.3</b>	<b>-17.3</b>	<b>8.8</b>	<b>-5.6</b>	<b>-50.0</b>	<b>-50.0</b>	<b>-33.9</b>	<b>-34.6</b>	<b>-43.5</b>	<b>-36.8</b>	<b>-25.0</b>	<b>-9.1</b>	<b>-26.7</b>
Rainfall mean (mm)	O	N	D	J	F	M	A	M	J	J	A	S	Year
1950-1980	103.4	146.6	182.9	178.7	178.7	156.3	92.8	81.6	56.4	18.0	18.1	50.5	<b>1264.0</b>
1980-2011	109.5	141.8	161.9	132.1	90.8	82.2	95.0	80.5	33.3	16.1	22.7	59.5	<b>1025.3</b>
≠ in mm	6.1	-4.9	-21.0	-46.6	-87.9	-74.1	2.1	-1.1	-23.0	-1.9	4.6	9.0	<b>-238.7</b>
≠ in %	<b>5.9</b>	<b>-3.3</b>	<b>-11.5</b>	<b>-26.1</b>	<b>-49.2</b>	<b>-47.4</b>	<b>2.3</b>	<b>-1.4</b>	<b>-40.8</b>	<b>-10.8</b>	<b>25.4</b>	<b>17.9</b>	<b>-18.9</b>

**Table 4.** Daily mean flow for the pre- and post-1980 period.

#### 4.3. Changes in extreme flows

In order to evaluate the differences between low and high-flow regimes during the six decades analysed, trends were also calculated for the quantiles of discharge < 10th and > 90th percentiles (<0.54 and >20.9 m<sup>3</sup>s<sup>-1</sup> respectively). As **Figure 3A** shows, the annual 10th percentile of daily discharge has increased significantly (M-K score: 615.000; P-value: 0,000; Sen's slope: 0.774), particularly in the last decade. Conversely, the number of daily annual classified with maximum discharges of > 90th percentiles is decreasing (**Figure 3B**). This tendency is not statistically significant according to the M-K test and Sen's slope (M-K score: -263.000; p-value: 0.103; Sen's slope: -0.322).

This pattern indicates that baseflows have been decreasing (which suggests that hydrological drought is increasing), whilst extreme hydrological events are tending to decrease in frequency and/or magnitude.

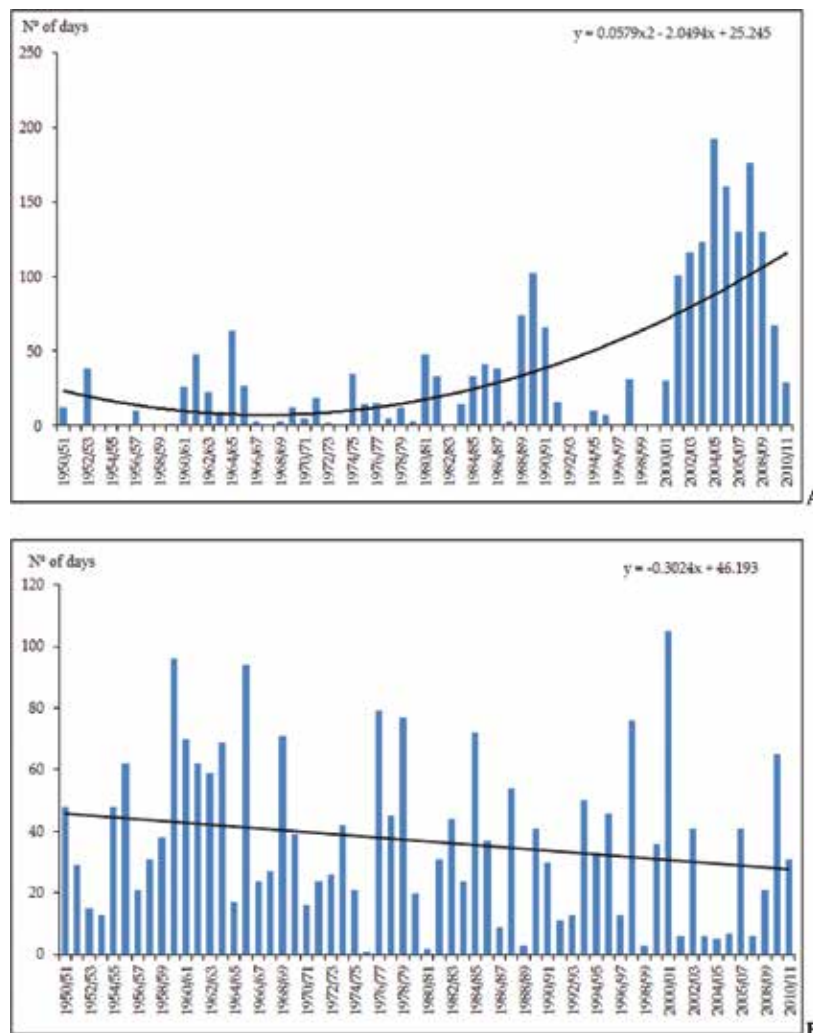
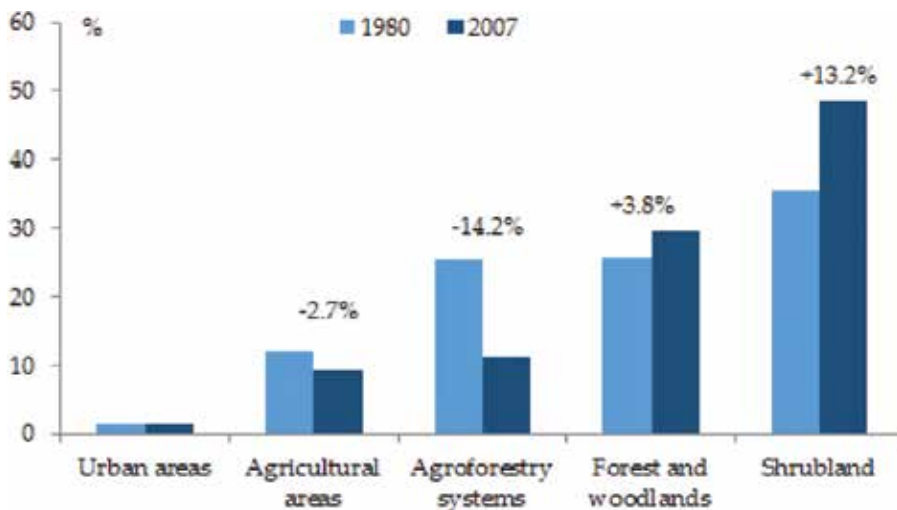


Figure 3. Number of days, per year, included in the <10th (A) and > 90th (B) percentiles.

#### 4.4. Analysis of land use/cover change

As indicated by the two land use maps (Figure 4), the major changes within the last 30 years are changes from agriculture and agroforestry to semi-natural vegetation (shrubland). In fact, agricultural activities dominated land use in marginal areas of Portugal for many decades. In the 1960s, over half of the agricultural area utilized was divided between non-irrigated cereals

(the dry system) and unseeded fallow rotations. In recent decades, the marked decrease in cropland and agrosystems in the entire catchment area (-17%) is mainly due to poor conditions for agriculture (a Mediterranean climate, undulating relief, and poor, shallow soils), uncompetitive farm structures (with small, scattered plots), the peripheral location of the area, the lack of alternative employment sectors, a reduction in livestock and the large number of elderly farm owners. This process of farmland abandonment was triggered by the migration of significant numbers of the population to certain European countries and the Portuguese urban centres and, more recently, as part of the set-aside strategy of the EU common agricultural policy [51].



**Figure 4.** Changes in land use/cover in the River Beça basin, 1980–2007.

The subsequent abandonment of cultivated and pasture land has increased the spread, growth and consolidation of compact wood and shrub masses, which registered an upward trend of 17%. This spread is the result of secondary succession in abandoned pastures and croplands and more frequent disturbances in Mediterranean forests, such as increasing fire recurrence.

#### **4.5. Interactions between hydroclimatic variables and the possible effect of changes in land use/cover**

It is clear that the River Beça hydrological regime is largely influenced by the temporal distribution of rainfall (**Figure 5**). Thus, the relationship between annual streamflow and total precipitation shows a significant correlation coefficient of 99% ( $R^2 = 0.846$ ), meaning that the changes in precipitation lead to reductions in streamflow. However, the correlations between regional precipitation and discharge have only changed slightly throughout the study period. A higher correlation was found between precipitation and streamflow in the post-1980 period ( $R^2 = 0.895$ ) in comparison to the pre-1980 period ( $R^2 = 0.784$ ).

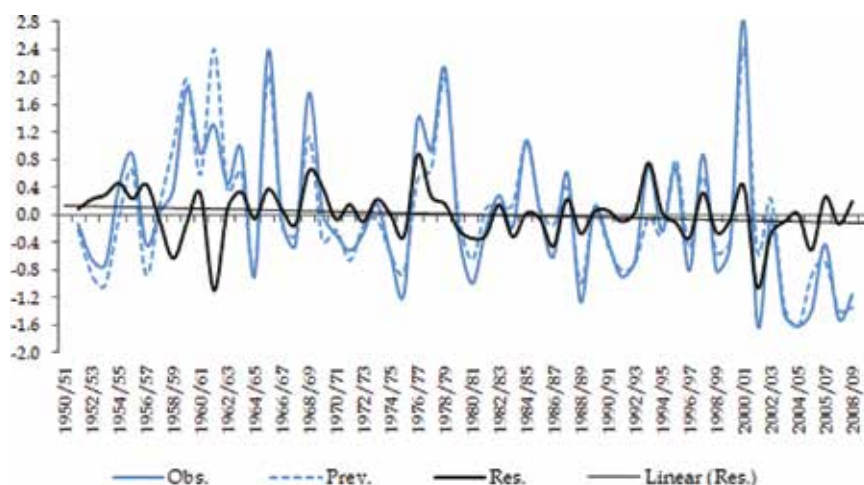


Figure 5. Evolution of observed and predicted streamflow and temporal trend of the residuals.

Given the fact that the relationship between the variables has changed slightly during the period studied, together with the temporal tendency denoted by the residuals, the product of the year-by-year correlation between rainfall and discharge suggests that the changes in land use/cover in the study area might have affected water resources. As the figure shows, although the residuals were randomly distributed over time, a downward trend can be observed which is almost significant at the 5% level ( $p$ -value= 0.051), suggesting a gradual decrease in the stream yield for a given precipitation.

## 5. Discussion

Annual precipitation and streamflow can be described as highly irregular, both in intra and inter annual terms. During the period analysed, namely the last 6 decades, a consistent negative trend was observed, both in the amount of annual precipitation and the mean annual streamflow in the Beça basin. Our results also demonstrate that precipitation greatly influences streamflow dynamics, explaining around 85% of the variability observed in the mean annual streamflow. A significant decrease in precipitation, particularly during the wet period, can have severe consequences for the hydrological cycle and water supply, both for ecosystems and societies. In fact, a change in precipitation quantity results in changes in runoff and affects the groundwater recharge rates which, in turn, have an impact on the water supply to the local population. In terms of agricultural demand, both rainfed crops and irrigated cultures may face a soil-moisture deficit associated with lower precipitation. The post-1980 period was significantly drier in comparison with the pre-1980 period.

Decreasing precipitation and streamflow in southern Europe, particularly in Spain and Portugal, has been linked to an increasingly positive North Atlantic Oscillation Index (NAOI) [52, 53]. As the negative phase of these indices is associated with frontal conditions that trigger

rainfall in the Mediterranean basin, the more frequent occurrence of positive phases after 1970 may explain the drying trends reported for several regions, as well as for Portuguese territory as a whole [54, 55]. Moreover, the analyses of the effects of the NAO on precipitation confirm the major influence of the winter NAO on precipitation in the Mediterranean mountain areas, particularly in the mountains of the Iberian Peninsula [56].

These results concur with the findings of other researchers working on a regional level, who have reported a decline in precipitation and streamflow in the Mediterranean basin. For example, in their study of the behaviour of four direct tributaries of the River Douro (Águeda, Huebra, Uces and the Tormes) in the south-west sector of the Douro basin, Ceballos et al. [17] detected that water discharges have decreased appreciably in three of the basins analysed. This decrease exceeds 50% in some cases and was directly linked to the decrease recorded for rainfall, with a significant correlation coefficient of 99% ( $r=0.85$ ) between both variables, which confirms the notion that a reduction in precipitation plays an important role in the reduction of discharges.

Similar results were found by Morán-Tejeda et al. [19, 20] in analysing the evolution of runoff and fluvial regimes in catchments located in the mountains surrounding the River Douro basin. The results show a general negative trend for annual runoff which is related to a decrease in precipitation and rising temperatures in winter and spring. The effects of land-cover expansion on runoff evolution could be only partially demonstrated, which confirms the difficulty in obtaining a detailed understanding of the interaction between hydrology and land-use at catchment scale in Mediterranean environments. Ceballos et al. [17, 18] also verified that the changes detected in forest land have not affected the water discharges of the rivers and related this to the changes observed in the vegetation cover, which are below the threshold for detecting the effect of the forest on water. In fact, the magnitude of the impact caused by changes in land use/cover varies significantly according to the extent of the vegetation cover and the type of vegetation (shrub or forest type), which have different levels of evapotranspiration [57].

In evaluating water yield evolution across the whole Ebro basin, López-Moreno et al. [22] also found a marked decrease in river discharges in most of the sub-basins. In this case, the changes in water yield are associated with an increase in evapotranspiration rates in natural vegetation, which had expanded as a consequence of land abandonment in areas where agricultural activities and livestock pressure had declined. In fact, the analysis of the time evolution of residuals from empirical models that relate climate and runoff in each sub-basin provided evidence that climate alone does not explain the decrease in river discharge which was observed.

For the Portuguese territory, previous studies on tributaries of the River Douro (the Côa and Sabor rivers) [58, 59] detected significant decreases in streamflow which were also related to changes in annual precipitation and land use/cover. A study of the high Côa river catchment area which aimed to evaluate and compare the hydrological response of soils subject to different land uses and vegetation types (cereal crop, fallow land or short-term abandonment, shrubland, recovering autochthonous vegetation, arable land afforested with *Pinus pinaster* and arable land transformed into pastureland), which represent situations commonly found

throughout central and northern Portugal [37], showed a decrease in runoff, together with an increase in soil cover with vegetation. The results concur with those observed by different authors in a variety of environments [60, 61].

The results obtained for the River Beça basin show that the changes detected in land use/cover may have affected the water discharges of the river, although it is difficult to evaluate the magnitude of the impact.

In fact, two main factors (climate, especially precipitation, and land use/plant cover) govern fluvial discharge variations in streamflow and generally reproduce the variations in precipitation. Quantifying the isolated and integrated impacts of land use/cover change and climate change on streamflow is therefore challenging, as well as crucial to optimum management of river basin water resources [25].

In addition to the downward trend for streamflow, the significant positive trend observed in low flow, particularly in summer, also has some parallels with previous work, which has detected a general drying in Europe in summer [50]. This increasing low flow trend may cause major disasters and severe social and economic losses [62].

## 6. Conclusion and further research

As in other Mediterranean mountain areas, water resources in the River Beça basin are affected by climate change, lower precipitation and higher temperatures, together with the impacts of changes in land use/land cover associated with major socioeconomic changes that result in land abandonment. It has been widely accepted that climate variability and changes in land cover or land use are two critical drivers which influence watershed hydrological changes. It is therefore important to separate their relative contributions to hydrological change so that their individual effects can be examined. Moreover, other variables should be included, such as evapotranspiration and plant canopy characteristics, in order to understand the watershed hydrological response better. In addition to river flow variations caused by climate variability and changes in land use/cover, the hydrological impact of major wildfires should also be analysed. In fact, several wildfires have occurred in the area since the 1980s. It is generally accepted that wildfires reduce infiltration and increase surface runoff by removing the surface litter and vegetation. Thus, wildfires can significantly change hydrological processes and the landscape's susceptibility to major flooding. Burned catchment areas are therefore at increased hydrological risk and respond faster to rainfall than unburned catchment areas.

However, assessment of the relative effects of land use and cover changes and climatic variability on hydrology is rather limited in Portugal and more case studies are therefore needed, focusing on both small and large watersheds, before general conclusions can be drawn.

The limited hydrometeorological data available at national level, the quality or "fitness use" of this data, inadequacy of spatial and temporal datasets, insufficient temporal data, and data sequences with gaps or incomplete sets are common obstacles in time series analysis which compromise process modelling, since it is essential to have serially complete data. Likewise,

it is difficult to collect data on changes in land use or land cover on large spatial scales over extended time periods.

This should therefore be a priority for future research, since they it is of prime importance both to hydrological modelling and the planning/management of water resources. A greater effort should be made to focus on the reconstruction of serially incomplete data records for basins with short streamflow records or ungauged river basins, as well as climatic data series. In addition, other statistical methods such as the trend analysis method, sensitivity-based approach and elasticity method should be used to quantify the effects of climatic variability first, then estimate the influence of land use/cover change from the total variations in streamflow.

Furthermore, it is imperative for scientists, politicians and managers to coordinate their efforts, since maintaining the water supply in the face of increasing demand presents a challenge, given that climate projections for the end of the twenty-first century suggest a reduced capacity for runoff generation due to rising temperatures and lower precipitation.

## Acknowledgements

This work was funded by the CEGOT (Centre for Studies in Geography and Spatial Planning), which is financed by national funds via the FCT - Foundation for Science and Technology - under the COMPETE project, reference POCI-01-0145-FEDER-006891 (FCT project: UID/GEO/04084/2013).

## Author details

Adélia. N. Nunes<sup>1,2\*</sup> and Patrícia Lopes<sup>2</sup>

\*Address all correspondence to: [adelia.nunes@fl.uc.pt](mailto:adelia.nunes@fl.uc.pt)

1 Centre for Studies in Geography and Spatial Planning (CEGOT), Portugal

2 Department of Geography and Tourism, Faculty of Arts, University of Coimbra, Coimbra, Portugal

## References

- [1] Dunne T, Leopold LB. *Water in Environmental Planning*. W.H. Freeman and Company, New York; 1978.

- [2] Kondratyev KY, Cracknell AP. Observing Global Climate Change. Taylor and Francis Ltd., London; 1998. p. 562.
- [3] Chiew FHS, Whetton PH, McMahon TA, Pittock AB. Simulation of the impacts of climate change on runoff and soil moisture in Australian catchments. *Journal of Hydrology*. 1995; 167 (1–4): 121–147. DOI: 10.1016/0022-1694(94)02649-V
- [4] Chiew FH, McMahon TA. Modelling the impacts of climate change on Australian streamflow. *Hydrological Processes*. 2002; 16: 1235–1245. DOI: 10.1002/hyp.1059
- [5] IPCC. Climate Change 2014. In Core Writing Team, Pachauri RK and Meyer LA, editors. Synthesis Report. Contribution of Working Groups I, II and III to the Fifth Assessment Report of the Intergovernmental Panel on Climate Change IPCC, Geneva, Switzerland; 2014. p. 151.
- [6] Miranda P, Valente M, Tomé A, Trigo R, Coelho M, Aguiar A, Azevedo E. The Portuguese climate in the 20<sup>th</sup> and 21<sup>st</sup> centuries. In Santos FD and Miranda P, editors. *Climate Change in Portugal. Scenarios, Impacts and Adaptation Measures*, ed., Gradiva Publications, Lisbon, Portugal; 2006. pp. 45–113.
- [7] Nunes A, Lourenço L. Precipitation variability in Portugal from 1960 to 2011. *Journal of Geographical Sciences*. 2015; 25 (7): 784–800. DOI: 10.1007/s11442-015-1202-y
- [8] McCabe GJ, Wolock DM. A step increase in streamflow in the conterminous United States. *Geophysical Research Letters*. 2002; 29 (24): 2185. DOI: 10.1029/2002GL015999.
- [9] Mansell MG. The effect of climate change on rainfall trends and flooding risk in the west of Scotland. *Nordic Hydrology*. 1997; 28: 37–50.
- [10] Shorthouse C, Arnell N. The effects of climatic variability on spatial characteristics of European river flows. *Physics and Chemistry of the Earth (B)*. 1999; 24 (1–2): 7–13. DOI: 10.2478/quageo-2013-0006
- [11] Pfister L, Humbert J, Hoffmann L. Recent trends in rainfall-runoff characteristics in the Alzette river basin, Luxembourg. *Climatic Change*. 2000; 45 (2): 323–337. DOI: 10.1007/s10584-006-9195-2
- [12] Hisdal H, Stahl K, Tallaksen LM, Demuth S. Have streamflow droughts in Europe become more severe or frequent? *International Journal of Climatology*. 2001; 21: 317–333. DOI: 10.1002/joc.619
- [13] de Wit MJM. Effect of Climate Change on the Hydrology of the River Meuse. Report 104, Wageningen University Environmental Sciences, Netherlands; 2001.
- [14] Burn DH, Elnur M. Detection of hydrological trends and variability. *Journal of Hydrology*. 2002; 255: 107–122. DOI: 10.1016/S0022-1694(01)00514-5
- [15] Christensen NS, Wood AW, Voisin N, Lettenmaier DP, Palmer RN. The effects of climate change on the hydrology and water resources of the Colorado river basin. *Climatic Change*. 2004; 62: 337–363. DOI: 10.1023/B:CLIM.0000013684.13621.1f



- [16] Ceballos A, Morán-Tejeda E. Evolution of water discharges in a mountain basin from the Central System: headwaters of river Tormes (1941-2004). *Cuadernos de Investigación Geográfica*, University of La Rioja, Spain. 2006; 32: 7–28. DOI: 10.1007/s00382-013-1885-7
- [17] Ceballos A, Morán-Tejeda E, Luengo-Ugidos MA, Llorente-Pinto JM. Water resources and environmental change in a Mediterranean environment: the south-west sector of the Duero river basin (Spain). *Journal of Hydrology*. 2008a; 351: 126–138. DOI: 10.1016/j.jhydrol.2007.12.004
- [18] Ceballos A, Morán-Tejeda E, Luengo-Ugidos MA, Llorente-Pinto JM. A Water discharges in River Douro headwaters: relationship with climate variability and changes in vegetation cover. *Territorium*, Portugal. 2008b; 15: 15–28.
- [19] Morán-Tejeda E, Ceballos A. Water resources and environmental changes in mediterranean headwaters. In: Efe R, Cravins G, Ozturk M, Atalay I, editors. *Natural Environment and Culture in the Mediterranean Region*. Cambridge Scholars Publishing, United Kingdom; 2008. pp. 271–288.
- [20] Morán-Tejeda E, Ceballos A, Llorente-Pinto JM. Hydrological response of Mediterranean headwaters to climate oscillations and land-cover changes: the mountains of Duero basin (Central Spain). *Global and Planetary Change*. 2010; 72(1–2): 39–49. DOI: 10.1016/j.gloplacha.2010.03.003
- [21] Morán-Tejeda E, Zabalza J, Rahman K, Gago-Silva A, López-Moreno I, Vicente-Serrano S, Lehmann A, Tague CL, Beniston M. Hydrological impacts of climate and land-use changes in a mountain watershed: uncertainty estimation based on model comparison. *Ecohydrology*. 2015; 8 (8): 1396–1416. DOI: 10.1002/eco.1590
- [22] López-Moreno JI, Vicente-Serrano SM, Morán-Tejeda E, Zabalza J, Lorenzo-Lacruz J, García Ruíz JM. Impact of climate evolution and land-use changes on water yield in the Ebro basin. *Hydrology and Earth System Science*. 2011; 15: 311–322. DOI: 10.5194/hess-15-311-2011
- [23] López-Moreno JI, Zabalza J, Vicente-Serrano SM, Revuelto J, Gilaberte M, Azorin-Molina C, Morán-Tejeda E, García-Ruiz JM, Tague C. Impact of climate and land use change on water availability and reservoir management: Scenarios in the Upper Aragón River, Spanish Pyrenees. *Science of the Total Environment*. 2014; 493: 1222–1231. DOI: 10.1016/j.scitotenv.2013.09.031
- [24] Peña-Arancibia JL, van Dijk AIJM, Guerschman JP, Mulligan M, Bruijnzeel LA, McVicar TR. Detecting changes in stream flow after partial woodland clearing in two large catchments in the seasonal tropics. *Journal of Hydrology*. 2012; 416–417: 60–71. DOI: 10.1016/j.jhydrol.2011.11.036
- [25] Chawla I, Mujumdar PP. Isolating the impacts of land use and climate change on streamflow. *Hydrology and Earth System Sciences*. 2015; 19: 3633–3651. DOI: 10.5194/hess-19-3633-2015

- [26] Bosch JM, Hewlett JD. A review of catchment experiments to determine the effect of vegetation changes on water yield and evapotranspiration. *Journal of Hydrology*. 1982; 55: 2–23.
- [27] Stednick JD. Monitoring the effects of timber harvest on annual water yield. *Journal of Hydrology*. 1996; 176 (1/4): 79–95. DOI: 10.1016/0022-1694(95)02780-7
- [28] Sahin V, Hall MJ. The effects of afforestation and deforestation on water yields. *Journal of Hydrology*. 1996; 178 (1/4): 293–309. DOI: 10.1016/0022-1694(95)02825-0
- [29] Vertessy RA. The impacts of forestry on streamflows: a review. In: Croke J, Lane P, editors. *Forest Management for the Protection of Water Quality and Quantity*. Proceedings of the Second Erosion in Forests Meeting. Warburton, 4–6 May, Cooperative Research Centre for Catchment Hydrology, Report 99/6; 1999. pp. 93–109.
- [30] Vertessy RA. Impacts of plantation forestry on catchment runoff. In: Sadanandan N, Nabia, EK, Brown, AG, editors. *Plantations, Farm Forestry and Water Proceedings of a National Workshop*, 20–21 July, Melbourne; 2000. pp. 9–19.
- [31] Laurance WF. Forests and floods. *Nature*. 2007; 449: 409–410. DOI: 10.1038/449409a
- [32] Bradshaw CJA, Sodhi NS, Peh KS-H, Brook BW. Global evidence that deforestation amplifies flood risk and severity in the developing world. *Global Change Biology*. 2007; 13: 1–17. DOI: 10.1111/j1365-2486200701446x
- [33] Clark, C. Deforestation and floods. *Environmental Conservation*. 1987; 14(1): 67–69. DOI: 10.1017/S037689290001112
- [34] Joffre R, Rambal S. How tree cover influences the water balance of Mediterranean rangelands. *Ecology*. 1993; 74: 570–582. DOI: 10.1038/npgels0003196
- [35] Zhang L, Dawes WR, Walker GR. Response of mean annual evapotranspiration to vegetation changes at catchment scale. *Water Resources Research*. 2001; 37(3): 701–708. DOI: 10.1029/2000WR900325
- [36] Brown AE, Zhang L, McMahon TA, Westen AW, Vertessy RA. A review of paired catchment studies for determining changes in water yield resulting from alterations in vegetation. *Journal of Hydrology*. 2005; 310: 28–61. DOI: 10.1016/j.jhydrol200412010
- [37] Nunes AN, Almeida AC, Coelho COA. Impacts of land use and cover type on runoff and soil erosion in a marginal area of Portugal. *Applied Geography*. 2011; 31(2): 687–699. DOI: 10.1016/j.apgeog201012006
- [38] Martínez-Fernández J, Sánchez N, Herrero-Jiménez J, Carlos M. Recent trends in rivers with near-natural flow regime: The case of the river headwaters in Spain. *Progress in Physical Geography*. 2013; 37(5): 685–700. DOI: 10.1177/0309133313496834
- [39] Iglesias A, Garrote L, Diz A, Schlickerrieder J, Martin-Carrasco F. Rethinking water policy priorities in the Mediterranean Region in view of climate change. *Environmental Science & Policy*. 2011; 14: 744–757. DOI: 10.1016/j.envsci2011102

- [40] Mann, HB. Non-parametric tests against trend. *Econometrica*. 1945; 13: 163–171.
- [41] Kendall, MG. *Rank Correlation Methods*. 4th ed. Charles Griffin, London; 1975.
- [42] Wang W, Chen X, Shi P, van Gelder PHAJM. Detecting changes in extreme precipitation and extreme streamflow in the Dongjiang River Basin in southern China. *Hydrology and Earth System Sciences*. 2008; 12(1): 207–221, DOI: 10.5194/hess-12-207-2008
- [43] Mitchell JM, Dzerdyevskii B, Flohn H, Hofmeyr WL, Lamb HH, Rao KN, Wallen CC. *Climatic Change*. (Report of a working group of the Commission for Climatology). WMO No. 195, Switzerland, 1966. 79 p.
- [44] Zhang Q, Liu C, Xu CY, Xu YP, Jiang T. Observed trends of annual maximum water level and streamflow during past 130 years in the Yangtze River basin, China. *Journal of Hydrology*. 2006; 324(1–4): 255–265. DOI: 10.1016/j.jhydrol.2005.09.023
- [45] Sen PK. Estimates of the regression coefficient based on Kendall's tau. *Journal of American Statistical Association*. 1968; 63: 1379–1389. DOI: 10.1080/01621459196810480934
- [46] Gilbert RO. *Statistical Methods for Environmental Pollution Monitoring*. Wiley, NY; 1987.
- [47] De Lima MIO, Marques ACP, De Lima JLMP, Coelho MFES. *Precipitation Trends in Mainland Portugal in the Period 1941–2000: The Fourth Inter-Celtic Colloquium on Hydrology and Management of Water Resources*. Guimarães, Portugal; 2005.
- [48] Beguería S, López-Moreno J, Lorente A, Seeger M, García-Ruiz J. Assessing the effect of climate oscillations and land-use changes on streamflow in the Central Spanish Pyrenees. *Ambio*. 2003; 32(4): 283–286. DOI: 10.1579/0044-7447-324283
- [49] Agroconsultores e Coba. *Soil Charter, land use chart and Land Suitability chart from the Northeast of Portugal, scale 1:100 000*, University of Trás-os-Montes e Alto Douro, Vila Real, Portugal, 1991.
- [50] Stahl K, Hisdal H, Hannaford J, Tallaksen LM, van Lanen HAJ, Sauquet E, Demuth S, Fendekova M, Jódar J: Streamflow trends in Europe: evidence from a dataset of near-natural catchments. *Hydrology and Earth System Sciences*. 2010; 14(12): 2367–2382. DOI: 10.5194/hess-14-2367-2010
- [51] Almeida AC, Nunes A, Figueiredo, A. *Land use and cover change in inland of center and north of Portugal*. University of Coimbra Press, Portugal; 2009. 99 p.
- [52] Trigo RM, Pozo-Vazquez D, Osborn TJ, Castro-Diez Y, Gamiz-Fortis S, Esteban-Parra, MJ. North Atlantic oscillation influence on precipitation, river flow and water resources in the Iberian peninsula. *International Journal of Climatology*. 2004; 24: 925–944. DOI: 10.1002/joc.1048

- [53] López-Moreno J, Vicente-Serrano SM. Positive and negative phases of the wintertime North Atlantic Oscillation and drought occurrence over Europe: A multitemporal-scale approach. *Journal of Climate*. 2008; 21: 1220–1243. DOI: 10.1175/2007JCLI1739.1
- [54] Trigo IF, Davies TD, Bigg GR. Decline in Mediterranean rainfall caused by weakening of Mediterranean cyclones. *Geophysical Research Letters*. 2000; 27: 2913–2916. DOI: 10.1029/2000GL011526
- [55] Trigo RM, da Camara C. Circulation weather types and their impact on the precipitation regime in Portugal. *International Journal of Climatology*. 2000; 20(13): 1559–1581. DOI: 10.1002/1097-0088(20001115)20:13<1559::AID-JOC555>3.0.CO;2-5
- [56] López-Moreno JI, Vicente-Serrano SM, Morán-Tejeda E, Lorenzo-Lacruz J, Kenawy A, Beniston M. Effects of the North Atlantic Oscillation (NAO) on combined temperature and precipitation winter modes in the Mediterranean mountains: observed relationships and projections for the 21st century. *Global Planet Change*. 2011; 77: 62–76. DOI: 10.1016/j.gloplacha.2011.03.003
- [57] Cui X, Liu S, Wei X. Impacts of forest changes on hydrology: a case study of large watersheds in the upper reaches of Minjiang River watershed in China. *Hydrology and Earth System Sciences*. 2012; 16: 4279–4290. DOI: 10.5194/hess-16-4279-2012
- [58] Nunes A. Water resources in the river Côa basin: relationships with climate variability and changes in land use. *Iberografias, Portugal*. 2007; 10: 71–86.
- [59] Nunes A. Water resources in the river Sabor basin: recent evolution and relations with socio-environmental changes. VI Iberian Congress on Water Management and Planning, Vitória-Gasteiz; 2008. 10 p.
- [60] Bochet E, Rubio JL, Poesen J. Relative efficiency of three representative matorral species in reducing water erosion at the microscale in a semi-arid climate (Valencia, Spain). *Geomorphology*. 1998; 23: 139–150. DOI: 10.1016/S0169-555X(97)00109-8
- [61] Durán Zuazo VH, Francia Martínez JR, Rodríguez Pleguezuelo CR, Martínez Raya A, Carcéles Rodríguez B. Soil-erosion and runoff prevention by plant covers in a mountainous area (SE Spain): implications for sustainable agriculture. *Earth and Environmental Science*. 2006; 26 (4): 309–319. DOI: 10.1007/s10669-006-0160-4
- [62] Tian P, Zhao G, Li J, Tian K. Extreme value analysis of streamflow time series in Poyang Lake Basin, China. *Water Science and Engineering*. 2011; 4 (2): 121–132. DOI: 10.3882/j.issn.1674-2370.2011.02.001

---

# Hydrological Drought Analysis Based on Copula Theory

---

Jaewon Kwak, Soojun Kim, Duckhwan Kim and  
Hungsoo Kim

Additional information is available at the end of the chapter

<http://dx.doi.org/10.5772/64244>

---

## Abstract

Drought has been a more frequent phenomenon of major concern all over the world. From the perspective of water resources management, one of the biggest problems associated with drought analyses is a lack of quantitative estimation for the target drought amount. The objective of this study is to examine the establishing process for the severity-duration-frequency (hereafter referred as “SDF”) curves on climate change. The standardized truncation level that defines hydrological drought was estimated and a bivariate frequency analysis for drought duration and severity was derived. The SDF curves were also estimated. The methodology suggested in this study could be used as elementary data for water resources managements.

**Keywords:** hydrological drought, frequency analysis, run theory, copula

---

## 1. Introduction

In recent times, drought has become one of the major concerns because it has occurred more frequently all over the world. Droughts are caused by the shortage of rainfall, affecting water resources in both urban and rural areas, and they cause the greatest damage among all the natural disasters [1]. For the Korean peninsula, a drought occurs approximately once every 2 years and the costs and losses due to drought are also increasing dramatically [2]. Generally, drought has been grouped by type as meteorological, hydrological, agricultural, and socio-economic drought [3]. Among these, hydrological drought causes real damage to economic sectors, because it is an actual deficiency of water in hydrological storage systems, such as stream-flow, reservoir and lake levels, groundwater, power generation, irrigation, and recreation. In order to develop measures for the mitigation of hydrological droughts, it is important to quantify

---

the probabilistic characteristics of droughts. Therefore, there are many ongoing investigations for hydrological droughts quantitative estimation and considering future climate change.

A number of studies have been conducted on the analysis and estimation of hydrological drought. These studies can be divided into several topics. Some studies have employed hydrological drought indices for quantitative estimation, such as cumulative streamflow anomaly that a cumulative departure of streamflow from mean conditions [4–6], surface water supply index (SWSI) that is a suitable measure of hydrological drought for the mountainous region, where snow contributes significantly to the annual streamflow [4, 7, 8], or Palmer hydrological drought severity index (PHDI) that uses the identical water balance with soil moisture model [5, 7, 9, 10]. Other studies also conducted hydrological drought analysis using deterministic approach such as the extreme dependency score that is an informative assessment of skill in deterministic forecasts [11], or stochastic model [12, 13]. The other, other studies were conducted on probabilistic approach for hydrological drought monitoring [14–16], or forecasting [17–19]. In detail, since Yevjevich [20], many studies on univariate analysis have been conducted based on the run theory [21]. These studies assumed run length and sum to be independent identically distributed random variable and have analytically derived statistical characteristic of hydrological drought, such as probability distributions, return periods, accumulated deficit, and moments of drought durations [22]. By contrast, the studies about multivariate drought analysis are relatively small, because they require considerably more data and sophisticated process, which are limited in their applicability [23]. Some studies have employed bivariate gamma, exponential, and extreme distribution for drought analysis, but they have limitations that drought characteristics have to have same distribution type. Therefore, many studies have been undertaken, because they can be overcome by the copula theory, which was suggested by Sklar [24]. The drought surmised that the increased with climate change, there are also many on-going studies about drought are conducted [26] with Global Climate Models and Regional Climate Model (hereafter referred as ‘GCM’ and ‘RCM’) [25–31]. Considering that the GCM/RCM is one of the effective ways for future projection, drought frequency analysis based on the copula theory and GCM/RCM could be a good alternative for water resources managements or planning.

The objective of this chapter is therefore to briefly examine the establishing process for the SDF curves on climate change based on the studies of Kwak et al. [32, 33]. For this, the joint probability distribution of drought characteristics using copula theory was examined, and established that the derive process the drought SDF curves for presents and future projected period using GCM/RCM. These established concepts and processes could be the basic methodology for water resources planning.

## 2. Methodologies

### 2.1. Drought definition with run theory

Generally, drought is a prolonged deficiency of precipitation including snow, a deficiency that results in water shortage for some activity or for some group, or a period of abnormally dry

weather sufficient to cause a serious of hydrological imbalance [34]. Drought has been defined in a number of ways and hydrologic drought is related to below-normal streamflow, lake, and groundwater levels. Yevjevich [20] defined drought using the run theory and suggested a way to calculate drought variables (drought duration, severity, and inter-arrival time).

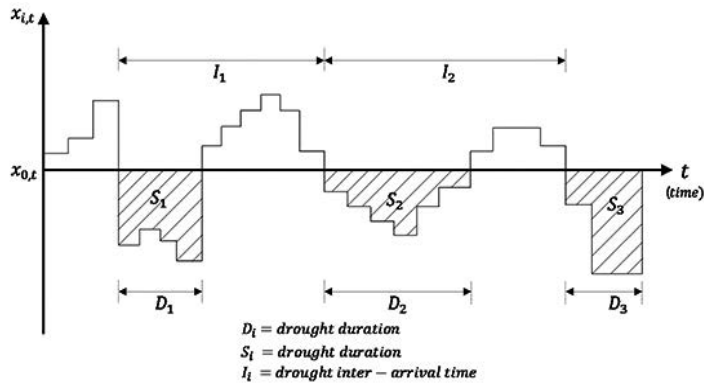


**Figure 1.** Drought characteristics using the run theory.

As shown in **Figure 1**, each drought variables are defined by truncation level that can be determined as a constant value or a time-varying function. Specifically, according to the truncation level  $x_0$ , the time period when the streamflow falls below  $x_0$  defines “duration ( $D_1, D_2, \dots$ ),” and the accumulated shortage amount of the streamflow during drought duration and the interval time period between two drought occurrences defines drought severity ( $S_1, S_2, \dots$ ) and inter-arrival time ( $I_1, I_2, \dots$ ), respectively. Therefore, the proper truncation level is the most challengeable problem, and it has been widely used to estimate statistical drought model and analysis [25, 26, 35–37] due to their applicability.

## 2.2. Copula theory

One of the challenges of the multiple variable analysis of drought is the different type of distribution due to their characteristic that variables are highly correlated with each other [32]. Therefore, the copula function that was suggested by Sklar in 1959 [24] was thought to be an effective alternative to consider the dependence structure between drought variables [22, 23]. The copula function was used to measure the correlation between multiple variable such as the coefficient of correlation, but it also has the advantage that can be used in any type of distributions. Especially, it is more appropriate than the correlation coefficient in the case of variables, which tend to indicate the same directivity [33].

As Sklar’s theorem, there is a copula function  $C$  with a dependence structure of probability distribution  $F(x_1, \dots, x_n)$  with  $n$ -dimensional function having marginal distributions  $F_1(x_1), \dots, F_n(x_n)$ , and it can be represented as

$$F(x_1, x_2, \dots, x_n) = C(F_1(x_1), F_2(x_2), \dots, F_n(x_n)) \tag{1}$$

where  $F_i(x_i)$  is the marginal distribution of each variables. When each marginal distribution  $F(x_1, x_2, \dots, x_n)$  is satisfied to be continuous random, the copula function also can be represented as

$$C(x_1, x_2, \dots, x_n) = F(F_1^{-1}(x_1), F_2^{-1}(x_2), \dots, F_n^{-1}(x_n)) \tag{2}$$

When  $u_i = F_i(x_i) \in [0,1]$  and  $F_1^{-1}$  is the inverse function of  $F_1$ , the partial differentiation of both Eqs. (1) and (2) with respect to  $x_1, \dots, x_n$  can be yielded as follows:

$$f(x_1, \dots, x_n) = c(F_1(x_1), F_2(x_2), \dots, F_n(x_n)) \prod_{i=1}^n f_i(x_i) \tag{3}$$

$$c(u_1, u_2, \dots, u_n) = \frac{f(F_1^{-1}(u_1), F_2^{-1}(u_2), \dots, F_n^{-1}(u_n))}{\prod_{i=1}^n f_i(x_i)}$$

Using Eq. (3), the multivariate probability density function that considers the relationship between marginal probability distribution can be obtained. It also shows that the copula function is the ratio of joint probability distribution function and the product of marginal probability distributions (see **Table 1**).

Copula Family	Copula function, $C(F_1(x_1), F_2(x_2))$	Generator function $\psi_a(t)$	Generator	Parameter ( $\alpha$ )
Clayton	$(\max\{F_1(x_1)^{-1} + F_2(x_2)^{-1} - 1; 0\})$	$\frac{1}{\alpha}(t^{-\alpha} - 1)$		$\alpha \in [-1, \infty]$
Frank	$\frac{-1}{\alpha} \log\left(1 + \frac{(\exp(-\alpha F_1(x_1)) - 1)(\exp(-\alpha F_2(x_2)) - 1)}{\exp(-\alpha) - 1}\right)$	$-\log\left(\frac{\exp(-\alpha t) - 1}{\exp(-\alpha) - 1}\right)$		$\alpha \in [\mathbf{R}]$
Gumbel	$\exp\left(-\left((-\log(F_1(x_1)))^\alpha + (-\log(F_2(x_2)))^\alpha\right)^{\frac{1}{\alpha}}\right)$	$-\log(t)^\alpha$		$\alpha \in [1, \infty]$
Independence	$F_1(x_1)F_2(x_2)$	$-\log(t)$		
Ali Mikhail Haq	$\frac{F_1(x_1)F_2(x_2)}{1 - \alpha(1 - F_1(x_1))(1 - F_2(x_2))}$	$\log\left\{\frac{1 - \alpha(1 - t)}{t}\right\}$		$\alpha \in [-1, 1]$

**Table 1.** Archimedean copula family;  $C$  is the copula function,  $t$  denotes the drought event,  $a$  is the copula parameter, and  $F_1$  and  $F_2$  denote maginal distributions [38].



The occurrence probability with copula function can be represented to be the return period, that is, the average time of occurrence of hydrological events of certain intensity. The return period was calculated from univariate frequency analysis using the following equations:

$$1/T = \frac{E(L)}{\{1 - F_1 - F_2 \dots F_n + C(F_1, F_2, \dots, F_n)\}} \quad (4)$$

where  $L$  is the inter-arrival time between drought events,  $E(L)$  is the average inter-arrival of occurrences, and  $F_1$  and  $F_2$  are the cumulative probability distribution functions of drought duration and severity, respectively.

### 3. Drought frequency analysis

#### 3.1. Study area and data

The upstream of the Namhan River is a main stream of Han River, with a drainage basin of 2,442.22 km<sup>2</sup>, located in the middle-eastern part of Korea. The upstream of the Namhan River is unregulated with flows between 8.0 and 1,000.0 m<sup>3</sup>/s at the Yeongwol water-level station, which is the outlet of the study area, and shows extreme flow rate in the typhoon season during June to September. The streamflow data were obtained from 1967 to 2008 with flow meter sampling at hourly interval. Also, other hydrological properties of the study area were extracted from a 3 × 3-km grid digital elevation model (DEM), land-cover, and land-use map [39]. The collected streamflow data are shown in **Figure 2**. Drought duration, severity, and inter-arrival time were defined for streamflow data from the upstream of the Namhan River using the run theory.

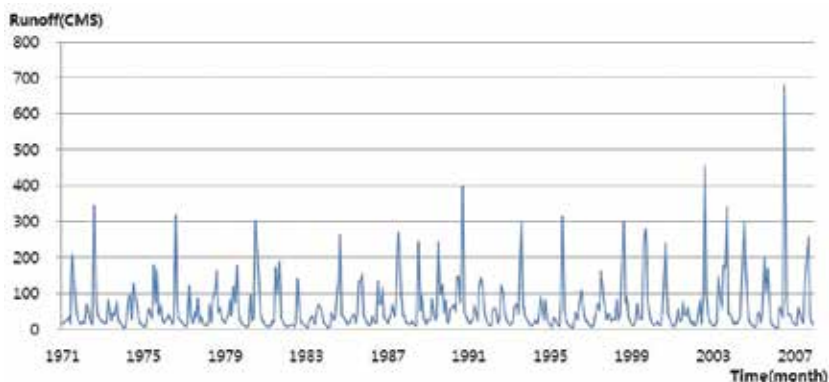


**Figure 2.** Monthly streamflow upstream of Namhan River, Korea (1967–2008).

### 3.2. Derive drought event based on run theory

The truncation level is defined as a fixed constant or a time function of streamflow that falls below the relevant level. It is one of the important challenges to estimate the proper bivariate frequency analysis because it determines the drought characteristics. Some studies employed the monthly mean value of streamflow, which is widely used due to their applicability, as the truncation level [23, 40–43]. The median value that has advantage with abnormal extreme value is also widely adopted [44, 45]. However, the mean and median values of streamflow are not proper, because the ratio between the minimum and maximum flow is over 300 in the river of Korea. In this case, the standardized truncation level should be a good alternative [46]. Generally, 0.5 (median value), 0.7, 0.8, 0.9, and 0.95 are commonly employed as the standardized truncation level, and Korea is adopting the concepts of Low Flow and Minimum Flow in the field of water resources planning; it is equal as 0.75 and 0.97 [47]. Also, the monthly streamflow in Korea shows significantly seasonal effect, so there are less or more occurrences of droughts than expected. Therefore, the truncation levels are defined for each month with monthly standardized truncation level (see **Figures 3–5**).

Each standardized truncation level was examined in comparison with major drought records in South Korea [48], and 0.75 is selected as the proper truncation level. The mean monthly truncation level was considered relatively improper, because it led to too large and deeper drought events. The defined droughts are 2.12 months of average drought duration, 22-mm/month severity, and 8.8 month of inter-arrival time (see the **Figure 3**). The events from December 1981 to July 1982 were estimated as the most severe drought with a 109.5-mm severity and an 8-month duration, and their damage were estimated about 643 million USD as of the year 2000 [48].

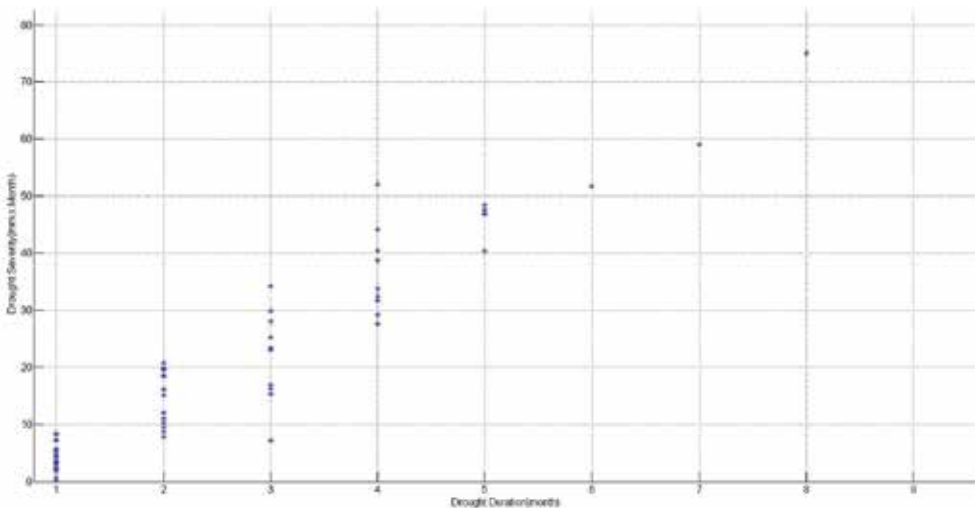


**Figure 3.** Drought event of the upstream of the Namhan River (1967–2008) with 0.75 standardized truncation level for each month.

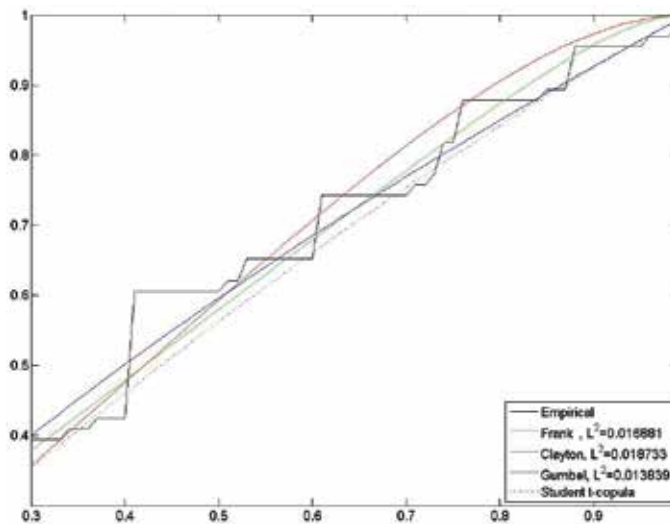


Figure 4. K-criterion plot for copula families.

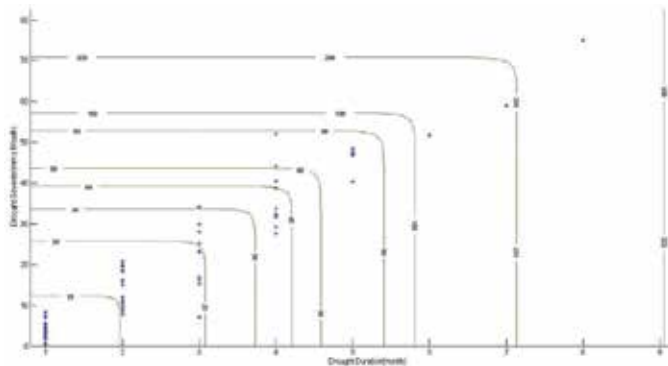


Figure 5. Contours of bivariate probabilities of drought severity and duration from streamflow upstream of Namhan River.

### 3.3. Bivariate drought analysis based on copula

Each marginal distribution of drought duration and severity is essential to estimate bivariate frequency analysis. The drought duration was determined to have the “exponential” distribution, and the drought severity the “gamma” distribution with 95% confidential level with the Probability Plot Correlation Coefficient (PPCC) [49] distribution goodness-of-fit test. Furthermore, the parameters of the Archimedean family copulas (Frank, Clayton, and Gumbel) were estimated by the method of moments according to their relationship with Kendall’s tau [50], which was found adequate for estimating parameters for small sample sizes [51]. Also, the minimum quadratic distance ( $L^2$ ) between empirical and theoretical values of

the *K* criterion, which described the most appropriate copula [51], was estimated for each copula (see the **Figure 4**).

The Gumbel copula, which generally fitted well throughout ( $L^2 = 0.0138$ ), was selected for bivariate drought analysis for the study area. The copula parameter was estimated as 3.599.

With the bivariate probabilities, it is possible to combine the drought duration and severity, and express them in terms of the same return period. For example, the severest drought lasted for 8 months from December 1981 to July 1982 and was 75.51-mm severity, which is approximately 280 years of return period (see **Figure 5**). The conventional method of deriving intensity-duration-frequency (IDF) curve was applied to drought events and was compared with the copula method, and the results are shown in **Figure 6**, and it can be used as the elementary data for water resources planning. For instance, if a decision maker or an agency determined a 3-month duration with a 20-year return period, then the design deficiency of a dam or a reservoir is 26.0 mm, which is about  $63.6 \times 10^6 \text{ m}^3$ .

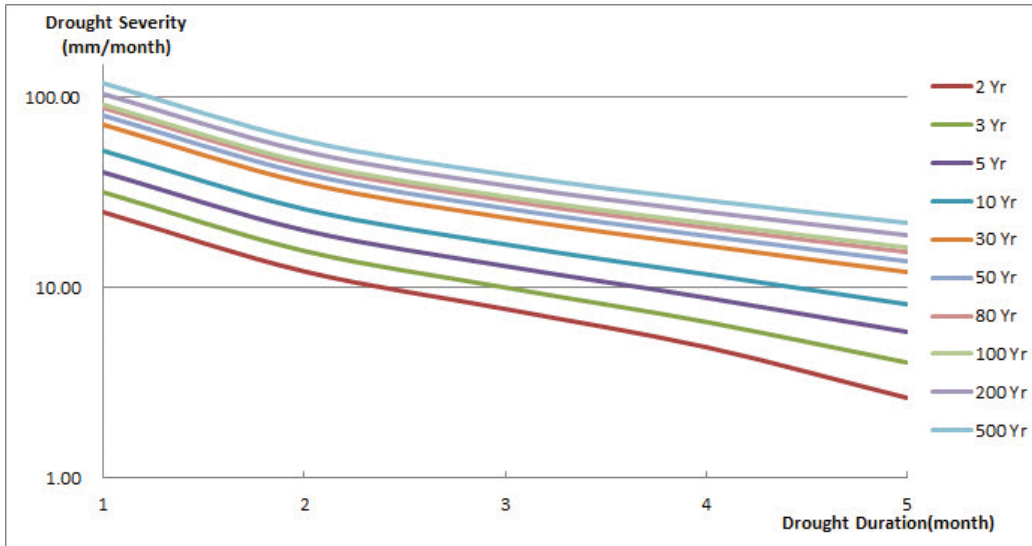


**Figure 6.** Drought SDF curve for the upper Namhan River basin.

#### 4. Bivariate drought analysis on climate change and SDF curve

One of the difficulties to analyze the hydrological drought is streamflow data, which is the result from hydrological response of basins. GCMs representing physical processes in the atmosphere, ocean, cryosphere, and land surface simulate the response of the global climate system [52]. Therefore, they need other techniques to obtain projected streamflow in the future, and long-term hydrological model using meteorological data was commonly used. Also, there

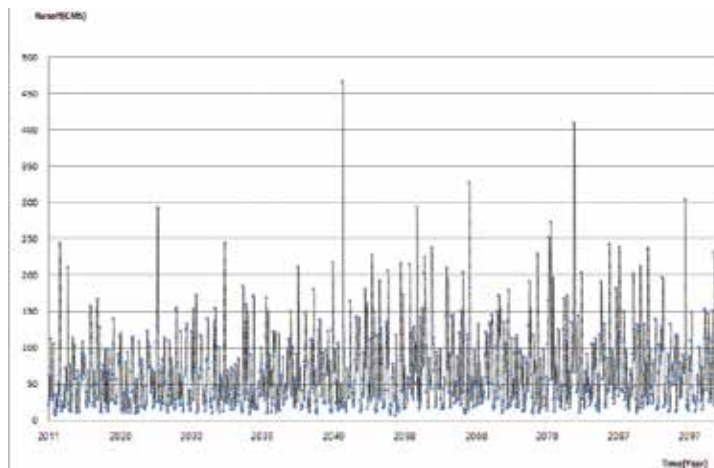


**Figure 7.** Simulated daily streamflow in the upper Han River basin.

are many climate models in use, and Korea Meteorological Administration (KMA) RCM climate model was selected as the suitable GCM by reviewing the applicability of 25 climate models provided by Intergovernmental Panel on Climate Change (IPCC) [53]. Also, socioeconomic scenarios are also needed to simulate meteorological data, and A1B climate change scenario was selected as the suitable scenario [54]. The meteorological data until 2100 years on the upper Namhan River basin were projected using climate model and scenarios. The modified TANK model [55] was constructed as the long-term hydrological model, and was calibrated and validated with observed meteorological data. Based on the projected meteorological data and hydrological model, the streamflow data until 2100 years were simulated (see **Figure 7**).

To analyze short- and long-term trends of the drought, each case was defined as every 30 years; Obs Case for 1967–2007; Case 1 for 2011–2039; Case 2 for 2040–2069; Case 3 for 2070–2100. The

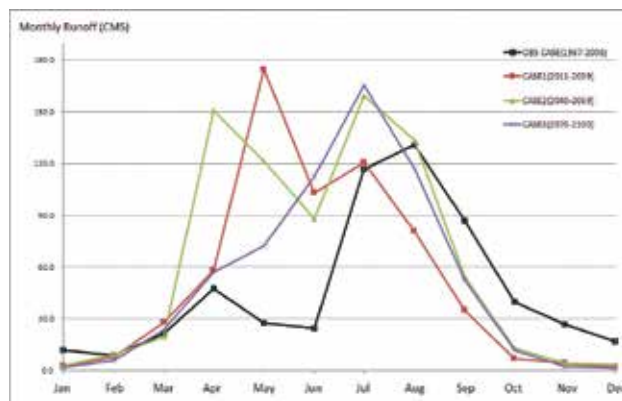


**Figure 8.** Monthly mean streamflow for each case.

projected monthly mean streamflow is shown in **Figure 8**, and it presents that the streamflow is highly increased from March to June and decreased from September to December.

The projected drought event can be obtained through the truncation process with simulated streamflow and 0.75 standardized truncation levels. Moreover, it can also be estimated as the return period and SDF curves with the same process as described in Section 3.

The SDF curves that are derived from climate change model can be used for water resources planning as the elementary data. For example, in **Figure 9**, when the agency determined for design drought has a 30-year return period and a 3-month duration, the design amount is 35.80 mm/month. Therefore, the target storage volume for dams, reservoirs, and other hydrological countermeasures is 87.6 million m<sup>3</sup>.

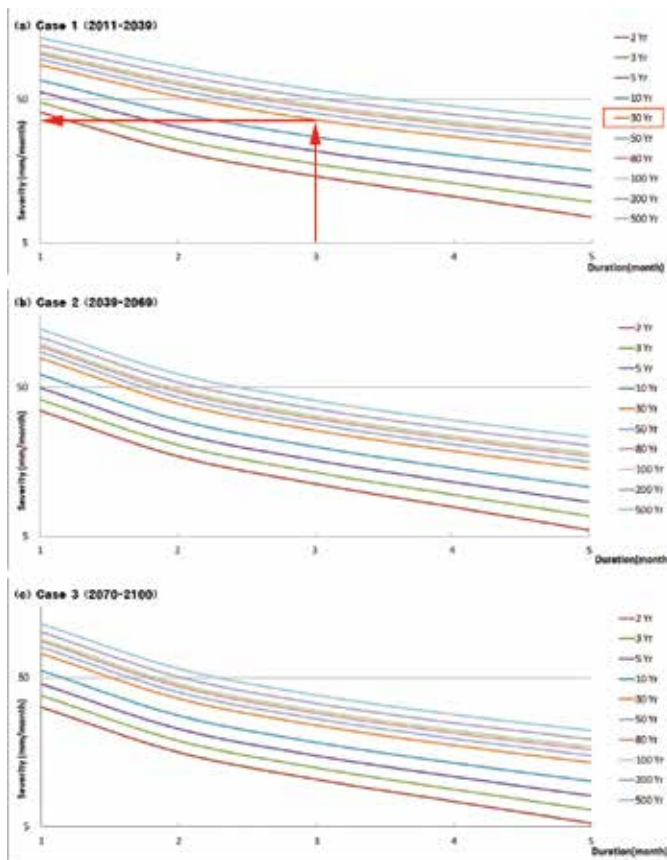


**Figure 9.** SDF curves for each case.

Brief steps to establish SDF curve on climate change are shown as follows:

- Step 1.** Collecting a hydrological, hydro-climatic, and drought data for target basin.
- Step 2.** Finding proper standardized truncation level for basin with observed data.

**Step 3.** Finding a proper distribution type with goodness-of-fit test.

**Step 4.** Selecting proper climate model.

**Step 5.** Constructing long-term hydrological model and conducting calibration and validation.

**Step 6.** Simulating streamflow for target periods.

**Step 7.** Extracting drought event based on the standardized truncation level.

**Step 8.** Bivariate frequency analysis with copula method.

**Step 9.** Estimating SDF curve for target periods.

## 5. Conclusions

This study briefly examines the establishing process for the SDF curves on climate change. The standardized truncation level was estimated with actual drought damage, and bivariate frequency analysis for drought duration and severity was estimated, and the SDF curves were also derived. Also, the SDF curves until 2100 years were derived based on the climate change models and scenarios, and long-term hydrological models are constructed and validated. The suggested method in this study can be used for water resources managements and planning as the quantitative indicator.

## Acknowledgements

This work was supported by the National Research Foundation of Korea (NRF) and by a grant funded by the Korean government (MEST; No. 2011-0028564).

## Author details

Jaewon Kwak<sup>1</sup>, Soojun Kim<sup>2\*</sup>, Duckhwan Kim<sup>3</sup> and Hungsoo Kim<sup>3</sup>

\*Address all correspondence to: soojun78@gmail.com

1 Forecast and Control Division, Nakdong River Flood Control Office, Busan, Korea

2 Columbia Water Center, Columbia University, New York, NY, USA

3 Department of Civil Engineering, Inha University, Incheon, Korea

## References

- [1] Wilhite, D. A. Drought as a natural hazard: concepts and definitions. In: Wilhite, D. A., editor. *Drought, A Global Assessment*. New York: Routledge; 2000.
- [2] Yoo, C., & Ryu, S. Analysis of drought return and duration characteristics at Seoul. *Journal of Korea Water Resources Association*. 2003;36(4):561–573.
- [3] Wilhite, D. A., & Glantz, M. H. Understanding the drought phenomenon: the role of definitions. *Water International*. 1985;10:111–120.
- [4] Wang, Q., Yan, D. H., Yuan, Y., & Wang, D. Y. Study on the quantification of drought in freshwater wetlands—a case study in Baiyangdian Wetland. *Wetland*. 2014;34(5): 1013–1025.
- [5] Vasiliades, L., Loukas, A., & Liberis, N. A water balance derived drought index for Pinios River Basin, Greece. *Water Resources Management*. 2011;25(4):1087–1101.
- [6] Fleig, A. K., Tallaksen, L. M., Hisdal, H., & Demuth, S. A global evaluation of stream-flow drought characteristics. *Hydrology and Earth System Sciences*. 2006;10(4):535–552.
- [7] Niu, J., Chen, J., & Sun, L. Exploration of drought evolution using numerical simulations over the Xijiang (West River) basin in South China. *Journal of Hydrology*. 2015;526:68–77.
- [8] Maity, R., Sharma, A., Nagesh Kumar, D., & Chanda, K. Characterizing drought using the reliability-resilience-vulnerability concept. *Journal of Hydrologic Engineering*. 2012;18(7):859–869.
- [9] Kousari, M. R., Dastorani, M. T., Niazi, Y., Soheili, E., Hayatzadeh, M., & Chezgi, J. Trend detection of drought in arid and semi-arid regions of Iran based on implementation of reconnaissance drought index (RDI) and application of non-parametrical statistical method. *Water resources management*. 2014;28(7):1857–1872.
- [10] Piechota, T. C., & Dracup, J. A. 1. Drought and regional hydrologic variation in the United States: associations with the El Niño-Southern oscillation. *Water Resources Research*. 1996;32(5):1359–1379.
- [11] Lavaysse, C., Vogt, J., & Pappenberger, F. Early warning of drought in Europe using the monthly ensemble system from ECMWF. *Hydrology and Earth System Sciences*. 2015;19(7):3273–3286.
- [12] Mishra, A. K., Desai, V. R., & Singh, V. P. Drought forecasting using a hybrid stochastic and neural network model. *Journal of Hydrologic Engineering*. 2007;12(6):626–638.
- [13] Akyuz, D. E., Bayazit, M., & Onoz, B. Markov chain models for hydrological drought characteristics. *Journal of Hydrometeorology*. 2012;13(1):298–309.



- [14] Szalai, S., Szinell, C. S., & Zoboki, J. Drought monitoring in Hungary: early warning systems for drought preparedness. In: Proceedings of an Expert Group Meeting; 5–7 Sep.; Lisbon, Portugal. 2000. pp. 5–7.
- [15] Bordi, I., & Sutera, A. Drought monitoring and forecasting at large scale. In: Bordi, A. Sutera, editor. *Methods and Tools for Drought Analysis and Management*. Netherlands: Springer; 2007. pp. 3–27.
- [16] Samra, J. S. Review and analysis of drought monitoring, declaration and impact management in India. In: Samra J. S., editor. *IWMI Working Paper 84, Drought Series Paper 2*, International Water Management Institute, Colombo, Sri Lanka; 2004.
- [17] Araghinejad, S. An approach for probabilistic hydrological drought forecasting. *Water Resources Management*. 2011;25(1):191–200.
- [18] Yuan, X., Wood, E. F., Chaney, N. W., Sheffield, J., Kam, J., Liang, M., & Guan, K. Probabilistic seasonal forecasting of African drought by dynamical models. *Journal of Hydrometeorology*. 2013;14(6):1706–1720.
- [19] Madadgar, S., & Moradkhani, H. A Bayesian framework for probabilistic seasonal drought forecasting. *Journal of Hydrometeorology*. 2013;14(6):1685–1705.
- [20] Yevjevich, V. M. An objective approach to definitions and investigations of continental hydrologic droughts. *Hydrology papers No. 23*, Colorado State University, Colorado: Fort Collins; 1967. pp. 23.
- [21] Cancelliere, A., & Salas, J. D. Drought length properties for periodic-stochastic hydrologic data. *Water Resources Research*. 2004;40(2):57–65.
- [22] Song, S., & Singh, V. P. Meta-elliptical copulas for drought frequency analysis of periodic hydrologic data. *Stochastic Environmental Research and Risk Assessment*. 2010;24(3):425–444.
- [23] Shiau, J. T. Fitting drought duration and severity with two-dimensional copulas. *Water resources management*. 2006;20(5):795–815.
- [24] Nelsen, R. B. *An introduction to copulas (Vol. 139)*. Springer Science & Business Media. Springer St. New York; 2013.
- [25] Mpelasoka, F., Hennessy, K., Jones, R., & Bates, B. Comparison of suitable drought indices for climate change impacts assessment over Australia: towards resource management. *International Journal of Climatology*. 2007;28(10):1283–1292.
- [26] Gianninia, A., & Biasuttia, M. A climate model-based review of drought in the Sahel: desertification, the re-greening and climate change. *Global and Planetary Change*. 2008;64(3–4):119–128.
- [27] Hirabayashi, Y., Shinjiro, K., Emori, S., Oki, T., & Kimoto, M. Global projections of changing risks of floods and droughts in a changing climate. *Hydrological Sciences*. 2008;53(4):754–772.

- [28] Elsner, M. M., Cuo, L., Voisin, N., Deems, J. S., Hamlet, A. F., Vano, J. A., Mickelson, K. E. B., Lee, S. Y., & Lettenmaier, D. P. Implications of 21st century climate change for the hydrology of Washington State. *Climatic Change*. 2010;102:225–260.
- [29] Wang, D., Hejazi, M., Cai, X., & Valocchi, A. J. Climate change impact on meteorological, agricultural, and hydrological drought in central Illinois. *Water Resources Research*. 2011;47; DOI: 10.1029/2010WR009845.
- [30] Kim, H., Park, J., Yoon, J., & Kim, S. Application of SAD curves in assessing climate-change impacts on spatio-temporal characteristics of extreme drought events. *KSCE Journal of Civil Engineering B*. 2010;30(6B):561–569.
- [31] Kim, S., Kim, B., Jun, H., & Kim, H. The evaluation of climate change impacts on the water scarcity of the Han River Basin in South Korea using high resolution RCM data. *Journal of Korea Water Resources Association*. 2010;43(3):295–308.
- [32] Kwak, J., Kim, D., Kim, S., Singh, V. P., & Kim, H. Hydrological drought analysis in namhan river basin, Korea. *Journal of Hydrologic Engineering*. 2013;19(8):05014001.
- [33] Kwak, J., Kim, S., Singh, V. P., Kim, H. S., Kim, D., Hong, S., & Lee, K. Impact of climate change on hydrological droughts in the upper Namhan River basin, Korea. *KSCE Journal of Civil Engineering*. 2015;19(2):376–384.
- [34] Heim Jr, R. R. A review of twentieth-century drought indices used in the United States. *Bulletin of the American Meteorological Society*. 2002;83(8):1149.
- [35] Dracup, J. A., Lee, K., & Paulson, E. G. On the statistical characteristics of drought events. *Water Resources Research*. 1980;16(2):289–297.
- [36] Loaiciga, H. A., & Leipnik, R. B. Stochastic renewal model of low-flow streamflow sequences. *Stochastic Hydrology and Hydraulics*. 1996;10(1):65–85.
- [37] Mishra, A. K., Desai, V. R., & Singh, V. P. Drought forecasting using a hybrid stochastic and neural network model. *Journal of Hydrologic Engineering*. 2007;12(6):626–638.
- [38] Rodriguez, J. C. Measuring financial contagion: a copula approach. *Journal of Empirical Finance*. 2007;14(3):401–423.
- [39] Consortium for Spatial Information. CGIAR-CSI [Internet]. 2014. Available from: <http://srtm.csi.cgiar.org/> [Accessed: Sep. 2015]
- [40] Wong, G., Lambert, M. F., & Metcalfe, A. V. Trivariate copulas for characterization of droughts. *ANZIAM Journal*. 2008;49:306–315.
- [41] Serinaldi, F., & Grimaldi, S. Fully nested 3-Copula: procedure and application on hydrological data. *Journal of Hydrologic Engineering*. 2007;12(4):420–430.
- [42] Serinaldi, F., Bonaccorso, B., Cancelliere, A., & Grimaldi, S. Probabilistic characterization of drought properties through Copulas. *Physics and Chemistry of the Earth*. 2009;34(10–12):596–605.

- [43] Zhang, L., & Singh, V. P. Gumbel–Hougaard Copula for trivariate rainfall frequency analysis. *Journal of Hydrologic Engineering*. 2007;12(4):409–419.
- [44] Horn, D. R. Characteristics and spatial variability of droughts in Idaho. *Journal of Irrigation and Drainage Engineering*. 1989;115(1):111–124.
- [45] Şen, Z. Probabilistic modelling of crossing in small samples and application of runs to hydrology. *Journal of Hydrology*. 1991;124(3–4):345–362.
- [46] Sharma, T. C., & Panu, U. S. Drought analysis of monthly hydrological sequences: a case study of Canadian rivers. *Hydrological Sciences Journal*. 2008;53(3):503–518.
- [47] Ministry of Land, Infrastructure and Transport. MOLIT [Internet]. 2013. Available from: <http://www.molit.go.kr/portal.do> [Accessed: Oct. 2015]
- [48] Ministry of Public Administration and Security. Annual disasters records 2001. Seoul, Korea: Ministry of Public Administration and Security; 2001.
- [49] Vogel, R. M., Hosking, J. R., Elphick, C. S., Roberts, D. L., & Reed, J. M. Goodness of fit of probability distributions for sightings as species approach extinction. *Bulletin of Mathematical Biology*. 2009;71(3):701–719.
- [50] El Adlouni, S., & Ouarda, T. B. Joint Bayesian model selection and parameter estimation of the generalized extreme value model with covariates using birth-death Markov chain Monte Carlo. *Water Resources Research*. 2009;45(6);DOI: 10.1029/2007WR006427
- [51] Saad, C., El Adlouni, S., St-Hilaire, A., & Gachon, P. A nested multivariate copula approach to hydrometeorological simulations of spring floods: the case of the Richelieu River (Québec, Canada) record flood. *Stochastic Environmental Research and Risk Assessment*. 2015;29(1):275–294.
- [52] Randall, D. A., Wood, R. A., Bony, S., Colman, R., Fichet, T., Fyfe, J., ... & Stouffer, R. J. Climate models and their evaluation. In *Climate Change 2007: the physical science basis*. In: Contribution of Working Group I to the Fourth Assessment Report of the IPCC. London, UK: Cambridge University Press; 2007.
- [53] Kyoung, M. Assessment of Climate Change Effect on Standardized Precipitation Index and Frequency Based Precipitation [thesis]. Incheon, Korea: INHA University; 2010. 165 p.
- [54] Kwon, Y., Kwon, W., & Boo, O. Future projections on the change of onset date and duration of natural seasons using SRES A1B data in South Korea. *Journal of Korean Geographic Society*. 2007;42(6):835–850.
- [55] Sugawara, M. Tank model. In: Singh, V. P., editor. *Computer models of watershed hydrology*. Water Resources Publications, Highlands Ranch, Colorado; 1995. pp. 165–214.



---

# **Drought Analysis and Water Resources Management Inspection in Euphrates–Tigris Basin**

---

Ata Amini, Soheila Zareie, Pezhman Taheri,  
Khamaruzaman Bin Wan Yusof and  
Muhammad Raza ul Mustafa

Additional information is available at the end of the chapter

<http://dx.doi.org/10.5772/63148>

---

## **Abstract**

Growing population, increasing basin development, and progressively declining water supplies are typical water resources issues in the Middle East. Drought is one of the most damaging climate-related hazards that affect more people than any other. For identifying drought-prone areas in the Euphrates–Tigris Basin, multifold aspects of drought and its features such as the frequency of drought occurrence and its spatial distribution were assessed. The long-term precipitation data were collected from different meteorological stations of Turkey and Iran, and standard precipitation index (SPI) was calculated. Due to the lack of raw data, the literature works on drought were used in Syria and Iraq to obtain a drought perception in these countries. Moreover, the policy of water resources management and the hydraulic works in these regions were considered. The results show significant changes in the precipitation in these regions over the past decades. The projects undertaken in the basin are not in line with the principles of integrated water resources management and intensify the drought and caused marshland demise in the downstream of the basin. The results of a comprehensive analysis of precipitation variation and water management in this research can alter the policy of water resources management in order to avoid drought in the basin.

**Keywords:** Euphrates, Rainfall, SPI, Tigris, *Water Resources*

## 1. Introduction

Water has played a vital role in the Euphrates–Tigris Basin (ETB), especially in Mesopotamia, which is the fertile land between the Euphrates and Tigris (ET) Rivers. Climate change together with increasing population makes the water resources an important issue in the region [1], which affects the social and economic conditions of this region. Very low precipitation caused a steep decline in agricultural productivity in the rain-fed ET drainage basins and displaced hundreds of thousands of people [2]. Climate change could seriously affect the water resources and lead to serious disputes among the countries that have territories in the ETB [3]. Bozkurt and Sen [1] investigated future climate change in the ETB and found that Turkey and Syria are most vulnerable to climate change, and downstream countries, especially Iraq, suffer more because they rely on the water released by the upstream countries. Middle East Region significantly suffers from decreasing water resources due to climate change [4]. The Middle East and North Africa (MENA) region represents 5% of the total world population, whereas contains only 0.9% of global water resources. The number of water-scarce countries in the Middle East and North Africa has risen from 3 in 1955 to 11 by 1990. Another seven countries, including Iran, are expected to join the list by 2025 [5]. ETB is in the midst of a water crisis and the worst drought in decades. At the current decline rate of water, the water supply in the basin will not be enough to avert such a widespread humanitarian crisis [6]. The recent drought that began from 2003 has further strained the limited water resources in the region [7]. Voss et al. [8] used Gravity Recovery and Climate Experiment (GRACE) satellite mission and [8] concluded an alarming rate of decrease of approximately  $-2.7$  cm/yr water height, equal to  $143.6$  km<sup>3</sup>, in the total water storage from 2003 to 2009. SPI<sup>1</sup> is an index for extract drought periods that considers precipitation only and the negative values of SPI indicate droughts. Karavitis et al. [9] used different scales of SPI for droughts in Greece and they declared that SPI has had high ability to announce drought. Paulo et al. [10] used SPI for several sites of Alentejo, Portugal, to find drought classes. A reported SPI in stations inside Syria, as a part of ETB, is presented by Skaf and Mathbout [11]. Their findings and results from literatures showed that the duration of most extreme drought in terms of intensity and areal extent in Syria corresponds to 1998–1999, 1972–1973, 2007–2008, and 1999–2000, respectively. Syria is one of the most economically affected countries by drought. Erian [12] showed that in Eastern Syria rainfall dropped to 30% of the annual average in 2008 and a main tributary of the River Euphrates dried up. Timimi and Jiboori [13] investigated the frequency of drought for the period of 1980–2010 in Iraq, based on SPI. Their results reveal that the country, in the past 30 years, faced frequent nonuniform drought periods in an irregular repetitive manner.

As severity of drought may have different effects in different regions and systems due to the underlying vulnerabilities, so the assessment of drought is a complex process [14]. The objectives of this study are to identify drought vulnerability at multiple time steps, so the effects of rainfall deficiency on water resources in the region and water resources management in ETB can be accessed. The drought vulnerability and water management information presented in

---

<sup>1</sup> Standardized Precipitation Index

this study can be applied in other sectors and used by water managers to ensure that they will act timely and effectively to tackle the drought-related losses in the regions.

## 2. Methodology

### 2.1. Study area

The Euphrates and Tigris, with 3000 and 1850 km lengths, respectively, are the most important rivers in the Middle East, which have been supporting agriculture in the ETB region since many centuries. Both rivers are fed by numerous tributaries, and the entire river system drains a vast mountainous region. They start from mountain ranges of today's Turkey and Kurdistan, and flow southeast through Iraq to the Persian Gulf. In the southern Iraq, both the rivers merge to feed the Mesopotamian marshlands, the land between the Euphrates and Tigris rivers. These marshlands used to be the largest wetland ecosystem in the western Eurasia and Middle East [15], which once covered over 15,000 km<sup>2</sup> of interconnected lakes, mudflats, and wetlands.

The headwater catchment generating the flow of ET is entirely located in the north and eastern parts of the ETB in the highlands of Turkey, Iraq, and Iran as a result of watershed's topography. The flow is regulated by the storage capacity of the limestone aquifers of the Taurus and Zagros mountains [16]. The annual precipitation in the upstream of ETB typically exceeds 1000 mm whereas in the south of Iraq it was found to be less than 100 mm. Most of this precipitation occurs as snow in winter and the water resources are mostly available in the form of snowmelt water during spring and winter [15]. As shown in **Figure 1**, the ETB spreads in the territories of Iraq (46%), Turkey (22%), Iran (19%), Syria (11%), Saudi Arabia (1.9%), and Kuwait (0.03%) [1]. Details of ET river systems are presented in **Table 1**.



**Figure 1.** The Euphrates–Tigris Basin and the riparian countries.

Country	River length (km)		Basin area (km <sup>2</sup> )	
	Euphrates	Tigris	Euphrates	Tigris
Iran	0	0	0	131,784
Turkey	1230	400	124,320	46,512
Syria	710	44	75,480	776
Iraq	1060	1418	177,600	209,304
Total	3000	1862	377400	387,600

**Table 1.** The Euphrates–Tigris characteristics.

## 2.2. Data

A challenge to conduct this research was the paucity of precipitation and water resources management data for the region. Inconsistent monitoring combined with a lack of data transparency and accessibility is a problem that plagues water managers in the ETB. Data shortage and inaccessibility result in an incomplete understanding of water availability and use in this area [8]. In this research, daily precipitation data were collected from Iran Meteorological Organization and Regional Water Companies located in the west and northwest of Iran, and inside or close to the ETB. Similarly, in Turkey daily precipitation data were collected from the climate stations located in the East of Turkey, which are operated by the Turkish State Meteorological Service. For Syria and Iraq, where availability of raw data for precipitation and water management was very limited, the data analyses presented in previous researches were considered.

## 2.3. Drought analysis

In this study, drought vulnerability in the regions of ETB, which are the main origins to supply water to the whole basin, was investigated. To check the quality of dataset, each daily total is compared with the climatological daily total maximum for the corresponding site. For this, stations with consistent and complete precipitation records were selected. Cumulative distribution of daily precipitation for each month was applied to obtain the monthly values. Missing data of the stations were completed by using the linear stochastic model called the Thomas-Fiering model. This model is based on the first-order Markov model and represents a set of 12 regression equations. The well-known Thomas-Fiering model equation is described as [17]

$$\frac{x_{i,j} - \bar{P}_j}{S_j} = \frac{x_{i,j-1} - \bar{P}_{j-1}}{S_{j-1}} + a_{ij} \sqrt{(1 - r_j^2)} \quad (1)$$

where  $X_{i,j}$  is the predicted rainfall for the  $j$ th month from the  $(j - 1)$ th month at time  $i$ ,  $P_j$  is the mean monthly rainfall during month  $j$ ,  $S_j$  is the standard deviation of monthly rainfall during



month  $j$ ,  $a_{ij}$  is the independent standard normal variable at time  $i$  in the  $j$ th month, and  $r_j$  is the serial correlation coefficient for rainfall from the  $(j - 1)$ th month to the  $j$ th month. Negative values obtained after applying Equation 1 were ignored. To identify the presence of drought or wet spells intensity for multiple time scales, several indices have been developed and adopted. The most well-known index is the SPI developed by McKee et al. [18]:

$$SPI = \frac{X_i - \bar{X}}{\sigma} \tag{2}$$

where  $X_i$  is the rainfall,  $\bar{X}$  is the arithmetic mean, and  $\sigma$  is the standard deviation of the series. The SPI provides a quick and handy approach to assign a single numeric value to the rainfall which can be compared across regions with markedly different climates and to reflect the impact of rainfall deficiency on the availability of various water sources [19]. The relative simplicity is a huge advantage of this index [20] and is among one of the most used indices by the researchers around the world. Therefore, its effectiveness in assessing the nature of the phenomenon has been tested in many climatic realities. Separate SPI value is calculated for a selection of time scales. McKee et al. [18] calculated the SPI for 3-, 6-, 12-, 24-, and 48 month time scales and defined the range for a “drought event” for any of the time steps and categorized the SPI to define various drought intensities (**Table 2**). In **Table 2**, negative and positive values of SPI represent rainfall less than and more than normal, respectively. For an equivalent normal distribution and adequate choice of fitted theoretical distribution of the actual data, the SPI can be considered as the value of standard deviations that the measured value would move away from the long-term mean.

Drought Class	SPI	Classification
3	>2.00	Extremely wet
2	1.50–1.99	Very wet
1	1.00–1.49	Moderately wet
0	-0.99	Near normal
-1	-1.00 to -1.49	Moderately dry
-2	-1.50 to -1.99	Severely dry
-3	-2.00	Extremely dry

**Table 2.** SPI drought categories.

To determine the area of influence of each individual station and utilized synthetic precipitation series in the study area, Thiessen polygons were employed. Since precipitation

is not distributed normally, a transformation is first applied so that the transformed precipitation values follow a normal distribution. Different statistical distributions are announced to model the time-series data. The gamma distribution to fit climatological data is the most well-known distribution [21] which is defined using its probability density function:

$$g(x) = \frac{1}{\beta^\alpha \Gamma(\alpha)} x^{\alpha-1} e^{-\frac{x}{\beta}} \quad \text{for } x > 0 \quad (3)$$

where  $\alpha > 0$  is the shape parameter,  $\beta > 0$  is the scale parameter, and  $x > 0$  is the amount of precipitation. Here, the gamma function is defined as  $\Gamma(\alpha)$ . To calculate the SPI value, the gamma stochastic distribution was transformed into the standard normal distribution. In this study, to compute the SPI for drought analysis, the Drought Indices Package (DIP) software presented by Morid et al. [22] was used. The package is capable of calculating and displaying SPI values at 3-, 6-, 12-, and 24-month time steps.

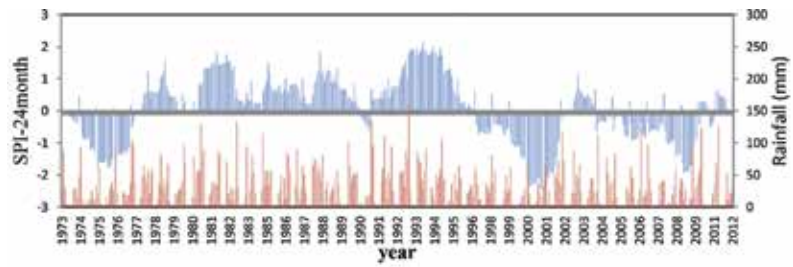
### 3. Results and discussion

Drought indices were analyzed at a regional scale in reference to the rainfall regime in the countries of ETB. **Figure 2** presents samples of calculated SPI values and the measured rainfalls for stations in Iran for the 24-month time scales.

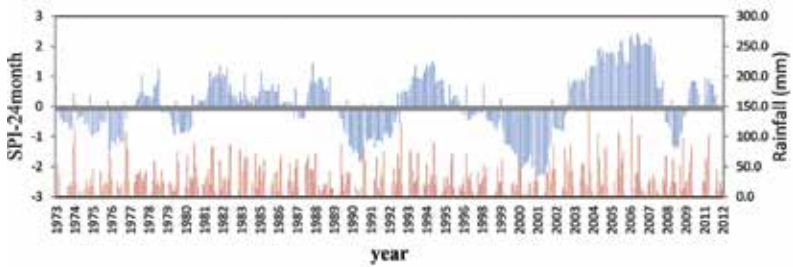
Apart from few stations such as the Khooshemehr station (**Figure 2a**), over the years of study, the calculated SPI indices indicated significant drying in many parts of ETB located inside Iran. There were both short-duration and long-duration droughts. Most of droughts were occurred during 1999–2014 in the stations (**Figure 2b–d**). Furthermore, the hyetographs shown in **Figure 2** indicated the considerable spatial and temporal changes in the precipitation total series of Iran, during the study period. Comparing the negative value of SPI in **Figure 2**, it could be concluded that the severity of drought in the Sanandaj station is more than the other stations considered in this study.

Biox et al. and Chen et al. [15, 23] showed that dams and reservoirs intensify the effect of drought on downstream community composition and structure. Therefore, it can be concluded that the severity of drought for these regions is attributed to the construction of dams or much withdrawal of water for irrigation in Sirvan watershed as a sub-basin of the Euphrates-Tigris basin. Consistent with the findings of this research, the drought occurrence in Iran is particularly more in its western and eastern parts, as reported by many researches [24, 25].

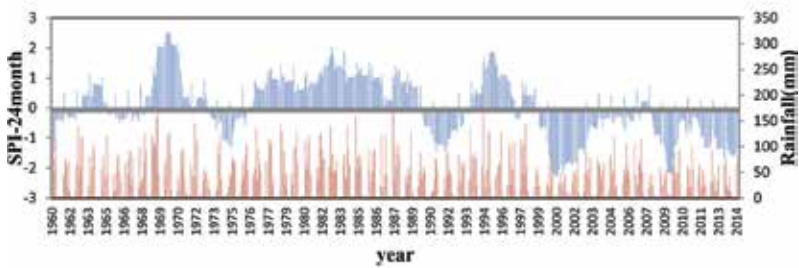
Turkey is a part of highlands of the ETB that receives much of the precipitation in form of snow in winter season. The samples of results for drought analysis using SPI and recorded rainfalls in the upper part of ETB, particularly in Turkey, are presented in **Figure 3**.



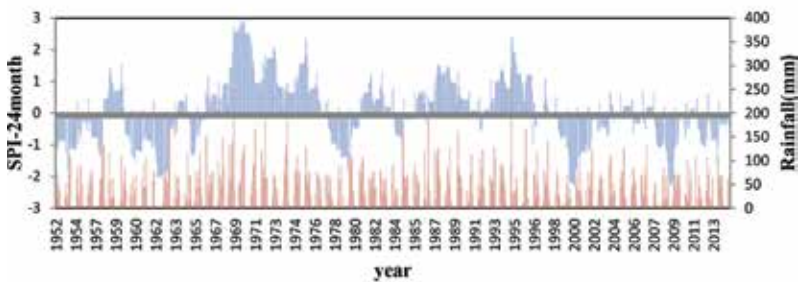
a. Khormazard station, W-Azerbaijan



b. Khooshemehr station, W-Azerbaijan



c. Sanandaj station, Kurdistan



d. Kermanshah station, Kermanshah

**Figure 2.** The 24-SPI index and monthly rainfall for stations in Iranian part of the ETB: (a) Khormazard station, W-Azerbaijan; (b) Khooshemehr station, W-Azerbaijan; (c) Sanandaj station, Kurdistan; and (d) Kermanshah station, Kermanshah.

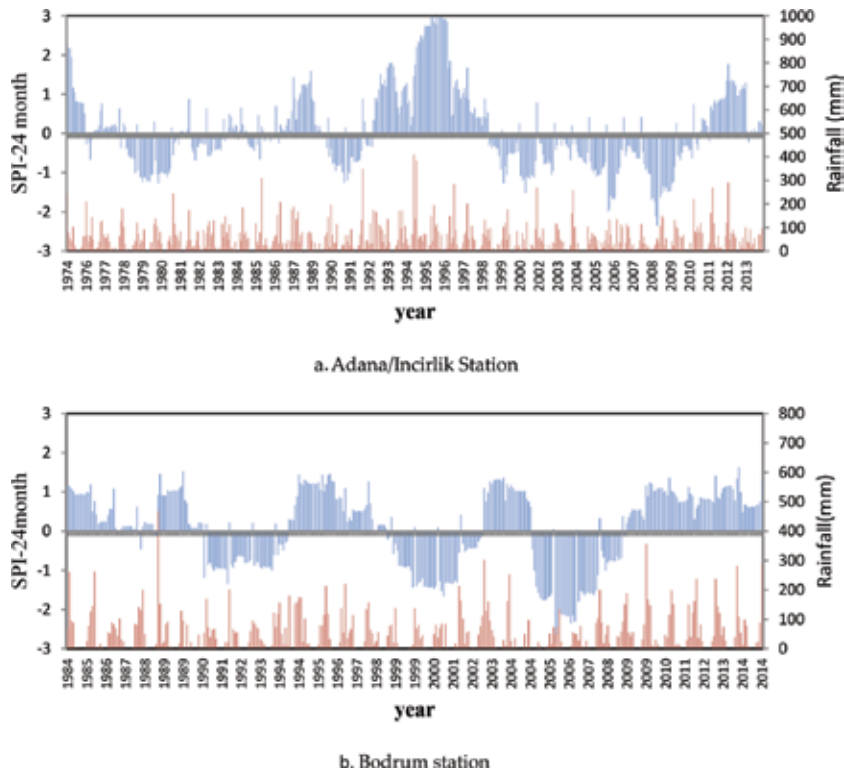


**Figure 3.** The 24-SPI index and monthly rainfall for stations in the Turkish part of the ETB: a. Adana/Incirlik station and b. Bodrum station.

In this research, the results of drought analysis for many stations in Turkey revealed that the regions of these stations experienced frequent moderate, severe, and extremely droughts for all years as shown in **Figure 3a**. However, in a few stations no drought was detected using SPI index (**Figure 3b**). Overall, a significant change in rainfall was determined in Turkey. These results are consistent with that reported by Bozkurt and Sen [1].

### 3.1. Water management

The ETB is associated with ancient civilization where irrigation schemes had been developed about the 5 millennium B.C. The headwater basin generating ET flows was entirely located in the north and eastern parts of the basin in the highlands of Turkey, Iraq, and Iran. Its hydrology and topography provide critical insight into understanding how hydraulic works affect the lower ETB, particularly the marshlands in south and middle of Iraq. Huge drainage and damming operations on the ET river systems in Iraq, Syria, Iran, and Turkey have diminished around 85% of the Mesopotamian marshlands, which originally covered an area of 20,000 km<sup>2</sup> [26]. The three rivers that feed the marshlands originate from riparian countries and all of these countries have extensive plans for control water resources to expand their irrigated agriculture. Construction and planning of mega structural water resources development

projects began in the early twentieth century in the region [27]. United Nation Environment Programme (UNEP)<sup>2</sup> in 2001 reported that the dams stores five times more than the Euphrates annual flow and twice that of the Tigris. **Table 3** shows the large dams according to the International Commission on Large Dams, ICOLD [28].

Country	Name	Nearest city	River	Year	Height (m)	Capacity (MCM)
Iran	Karoun 3	Eizeh	Karoun	2004	205	2970
	Dez	Andimeshk	Dez	1962	203	2856
	Karoun 1	Masjedsoleyman	Karoun	1976	200	3139
	Masjedsoleyman	Masjedsoleyman	Karoun	2001	177	230
	Gavoshan	Kamyaran	Gaveh Roud	–	136	550
	Karkheh	Andimeshk	Karkheh	2001	127	5575
	Vahdat	Sanandaj	Gheshlagh	–	80	224
	Eilam	Eilam	Baraftab and Chaviz	–	65	71
	Guilangharb	Guilangharb	Guilangharb	–	51	17
	Shahghasem	Yasouj	Parikedoun	1996	49	9
	Hana	Samirrom	Hana	1996	36	48
	Bane	Baneh	Banechay	–	20	4
	Chaghakhor	Boldaji	Aghbolagh	1992	13	42
Zrivar	Marivan	Zarivar	–	11	97	
Total						15,832
Turkey	Keban	Elazig	Firat	1975	210	31,000
	Karakaya	Diyarbakir	Firat	1987	173	9580
	Ataturk	Sanliurfa	Firat	1992	169	48,700
	Ozluce	Bingol	Peri	2000	144	1075
	Kralkizi	Diyarbakir	Maden	1997	126	1919
	Kuzgun	Erzurum	Serceme	1996	110	312
	Dicle	Diyarbakir	Dicle	1997	87	595
	Batman	Batman	Batman	1999	85	1175
	Erzincan	Erzincan	Goyne	1997	81	8
	Zemec	Van	Hosap	1988	80	104
	Kockopru	Van	Zilan	1992	74	86
	Kayalikoy	Kirkclareli	Kaya	1986	72	150
	Demirdoven	Erzurum	Timar	1996	67	34

<sup>2</sup> United Nation Environment Programme

Country	Name	Nearest city	River	Year	Height (m)	Capacity (MCM)
	Tercan	Erzincan	Tuzla	1988	65	178
	Birecik	Sanliurfa	Firat	2000	63	1220
	Sarimehmet	Van	Karasu	1991	62	134
	Sultansuyu	Malatya	Sultansaya	1992	60	53
	Mursal	Sivas	Nih	1992	59	15
	Surgu	Malatya	Surgu	1969	55	71
	Polat	Malatya	Findik	1990	54	12
	Goksu	Diyarbakir	Goksu	1991	52	62
	Kayacik	Karaburun		2002	50	117
	Hancagiz	Gaziantep	Nizip	1989	45	100
	Camgazi	Adiyaman	Doyran	1999	45	56
	Medik	Malatya	Tohma	1975	43	22
	Hacihidir	Sanliurfa	Sehir	1989	42	68
	K.Kalecik	Elazig	Kalecik	1974	39	13
	Gayt	Bingol	Gayt	1998	36	23
	Devegecidi	Diyarbakir	Devegecidi	1972	33	202
	Dumluca	Mardin	Bugur	1991	30	22
	Karkamis	Kahramanmaras	Firat	2000	29	157
	Cip	Elazig	Cip	1965	23	7
	Palandoken	Erzurum	Gedikcayiri	1997	19	1558
	Porsuk	Erzurum	Masat	1999	17	770
Total						99,598
<b>Syria</b>	Al Tabka	At Thawrah	Euphrates	-	-	11,200
Total						11,200
<b>Iraq</b>	Mosul	Mosul	Tigris	1983	131	12,500
	Derbendi Khan	Ba'qubah	Diyola river	1962	128	3000
	Dokan	-	Lesser Zab	1961	116	6800
	Haditha	Haditha	Euphrates	1984	57	8200
	Hamrin	Ba'qubah	Diyola river	1980	40	4000
	Dibbis	-	Lesser Zab	1965	15	3000
	Samarra-Tharthar	Samarra	Tigris	1954	-	72,800
Total						110,300

Table 3. Large dams in the ETB.

While the water resources development has been considered as one of the causes for damaging the marshland ecosystem [15] and intensifying the drought effects, it can be seen from the data in **Table 3** that the basin is now deeply regulated with cumulative storage capacity of riparian countries. Apart from the dams listed in **Table 3**, more than 20 dams are planned or are currently under construction in the basin. Further investigation shows that increased agricultural demand driven by land use policy and cropping pattern intensified the pressures on water resources in the ETB. In addition, the use of well water, mostly for agricultural needs, has rapidly increased in the ETB, causing a drop in the water level of the aquifers. Groundwater loss is found to be the major source of water reduction in the region. Voss et al. [8] reported a reduction in groundwater within last 12 years, equal to 1.73 cm/yr height.

The effect of manmade projects is greatest in the lower part of the basin in the marshlands in Iraq mainly in intensifying dust storm origins inside Iraq [29]. The marshlands have been desiccated through the combined actions of upstream damming in riparian countries as well as the development of extensive downstream drainage projects, in the past 30 years [3]. Without doubt Turkey is in the strongest position with regard to its potential control of a large part of the water resources of the ETB mainly due to the Southeast Anatolia Project (GAP). The project area neighbors with Syria in south and Iraq in southeast, which includes 22 dams and 19 hydropower plants and irrigation networks on the ETB.

It seems that there is a mismanagement of water resources in the region. As a few instances, the Tabqa dam in Syria planned to irrigate 640,000 ha of land. However, so far only 240,000 ha of land can be irrigated due to salinization and poor quality of land. Consistently, since 1990s large water management projects have been developed in Iran under a major policy to control surface water to serve other purposes such as irrigation and drinking. Thus, more than 20 dams have been constructed or are under construction in the Tigris Basin and an increasing amount of water is diverted from the rivers. The Karkheh is one of the largest dams in Iran with a reservoir capacity of 5.6 *Billion Cubic Meter* to irrigate 320,000 ha of land and produce 520 MW of hydroelectricity. Conversely, because of the water crisis and low water levels in Iran, the Karkheh dam irrigates one-third of the anticipated area and cannot produce even 1 kWh of energy in its lifetime. In Sirvan watershed, as a part of ETB inside Iran, more than 10 dams were constructed in the last decades without accomplishing the irrigation and drainage system. While Iran is facing a critical water shortage currently, huge amount of water is lost through evaporation from unusable dams and reservoirs.

In Iraq, because of inadequate leveling, lack of know-how, and poor water management practices, water is often poorly distributed. In the southern part of Iraq, diversion canals within the irrigation command area divert the ETB water from rivers to cultivated lands. Poor maintenance throughout the primary formal supply system caused water losses at all its stages of primary delivery. However, only about 30% of water supply available for irrigation annually actually reaches crops [30]. Overall, the irrigation system in Iraq is inefficiently managed.

More than 90% of water resources are used for agriculture. The on-farm water application rates in the region are high, and irrigation has a low efficiency. Keshavarz et al. [31] reported that overall irrigation efficiency in Iran ranges from 33 to 37%, which is lower than the average for both developing (45%) and developed (60%) countries. The most prominent causes of irriga-

tion inefficiency in the study areas include improper design of irrigation facilities, poor maintenance, careless operation, negligible water prices, and inadequate training of farmers.

## 4. Conclusions

In this research, drought and water resources managements were investigated in ETB. Moreover, the calculated SPI for Iran and Turkey and those reported for Syrian and Iraq confirmed that there are various dry periods, which affect these countries, especially during the past 15 years. Among these four countries, Turkey has less severity and frequency of drought than the other three countries, and Syria has the most. This problem will affect the stream flow strongly. Thus, the annual flow of the Euphrates and Tigris entering Iraq and groundwater sources in the riparian countries declined drastically. Drought has negative impact on health, the agricultural production, and economic condition of most people who live in ETB; and food scarce makes migration from these dry areas and expected to increase further in the future. Apart from deficiency of rainfall, the rules to control the amount of water in riparian countries of ET lead to a decrease in the water flow in the two rivers. It should be noted that each riparian country has the right to use, in an equitable and reasonable manner, the water of the international watercourses in its respective territory. Emphasis on acquired rights without considering the principles of integrated water resources managements to achieve the optimal use of water by the riparian countries is the major cause of water decline in the ETB. The ETB has to be considered as forming one single transboundary stream system, and should be managed accordingly. It seems that the impact of hydraulic works needs to be reassessed and mitigated by ensuring a minimal water flow to sustain life in the ETB, particularly in Mesopotamian marshlands. A portfolio of water and land resources should be drawn up and jointly evaluated. Such realities remind us that we need to act now to restore ETB ecosystems on a global scale.

## Acknowledgements

The authors are thankful of Ministry of Higher Education, Malaysia, and Universiti Teknologi Petronas for supporting this research under grants no. FRGS\_0153AB\_i61.

## Author details

Ata Amini<sup>1\*</sup>, Soheila Zareie<sup>2</sup>, Pezhman Taheri<sup>3</sup>, Khamaruzaman Bin Wan Yusof<sup>4</sup> and Muhammad Raza ul Mustafa<sup>4</sup>

\*Address all correspondence to: ata\_amini@yahoo.com



1 Agricultural and Natural Resources Research and Education Center of Kurdistan, AREO, Sanandaj, Iran

2 Water Resources Engineering, Water Engineering Department, University of Tabriz, Tabriz, Iran

3 Faculty of Civil Engineering, Fluvial and River Engineering Dynamics Group (FRiEnD), Universiti Teknologi MARA (UiTM), Malaysia

4 Department of Civil and Environmental Engineering, Faculty of Engineering, Universiti Teknologi PETRONAS (UTP), Malaysia

## References

- [1] Bozkurt, D. and Sen, O. L. Climate change impacts in the Euphrates–Tigris Basin based on different model and scenario simulations. *Journal of Hydrology*. 2013;480:149–161.
- [2] Trigo, R. M., Gouveia, C., Barriopedro, D. The intense 2007–2009 drought in the Fertile Crescent: Impact and associated atmospheric circulation. *Agricultural and Forest Meteorology*. 2010;150(9):1245–1257. DOI: 10.1016/j.agrformet.2010.05.006.
- [3] Ozdogan, M. Climate change impacts on snow water availability in the Euphrates–Tigris basin. *Hydrology and Earth System Sciences*. 2011; 15(9):2789–2803. DOI: 10.5194/hess-15-2789-2011.
- [4] Topcu, S., et al. Vulnerability of water resources under changing climate condition in Upper Mesopotamia. In: BHS 3rd International Conference, Newcastle, USA. 2010. DOI: 10.7558/bhs.2010.ic21.
- [5] World Bank Report. *From Scarcity to Security: Averting a Water Crisis in the Middle East and North Africa*, Washington, DC, USA; 1996. 32 pp.
- [6] Chenoweth, J. P., et al.. Impact of climate change on the water resources of the eastern Mediterranean and Middle East region: Modeled 21st century changes and implications. *Water Resources Research*. 2011;47(6). P: 1–18. DOI: 10.1029/2010WR010269.
- [7] U.S. Department of Agriculture (USDA), Foreign Agricultural Service. 2014. Middle East and Central Asia: Continued drought in 2009/2010 threatens greater food grain shortages. Available at: [http://www.pecad.fas.usda.gov/highlights/2008/09/mideast\\_cenasia\\_drought/](http://www.pecad.fas.usda.gov/highlights/2008/09/mideast_cenasia_drought/) [accessed 2014].
- [8] Voss, K. A., et al. Groundwater depletion in the Middle East from GRACE with implications for transboundary water management in the Tigris-Euphrates-Western Iran region. *Water Resources Research*. 2013;49(2):904–914. DOI: 10.1002/wrcr.20078.

- [9] Karavitis, C. A., et al. Application of the Standardized Precipitation Index (SPI) in Greece. *Water Resources Management*. 2011;3(3):787–805. DOI: 10.3390/w3030787.
- [10] Paulo, A. A., et al. Drought class transition analysis through Markov and Loglinear models, an approach to early warning. *Agricultural Water Management*. 2005;77(1–3): 59–81. DOI: 10.1016/j.agwat.2004.09.039.
- [11] Skaf, M. and Mathbout, S. Drought changes over last five decades in Syria, Economics of drought and drought preparedness in a climate change context. In: CIHEAM/FAO/ICARDA/GDAR/CEIGRAM / MARM; 2010. pp. 107–112. (Options Méditerranéennes: Série A. Séminaires Méditerranéens; n. 95).
- [12] Erian, W. Agriculture drought and land degradation risk in Arab region. The first Arab Regional Conference for Disaster Risk Reduction. 19–21 March 2011..
- [13] Timimi, Y. K. and Jiboori, M. H. Assessment of spatial and temporal drought in Iraq during the period 1980-2010. *International Journal of Energy and Environment*. 2013;4(2):291–302.
- [14] Vicente-Serrano, S. M., et al. Challenges for drought mitigation in Africa: the potential use of geospatial data and drought information systems. *Applied Geography*. 2012;34:471–486. DOI: 10.1016/j.apgeog.2012.02.001.
- [15] Chen, Z., Kavvas, M., Ohara, N., Anderson, M., and Yoon, J. Impact of water resources utilization on the hydrology of Mesopotamian marshlands. *Journal of Hydrologic Engineering*. 2011;16:1083–1092.
- [16] Issar, A. S. and Zohar, M. *Climate Change—Environment and History of the Near East*. 2nd Edition, ISBN 978-3-540-69851-7 Springer Berlin Heidelberg New York Springer; 2007. 290 pp.
- [17] Yurekli, K. and Kurunc, A. Performances of stochastic approaches in generating low streamflow data for drought analysis. *Journal of Spatial Hydrology*. 2005;5(1):20–31.
- [18] McKee, T. B., et al.. The Relationship of Drought Frequency and Duration to Time Scales. In: Eighth Conference on Applied Climatology; January 17–22; Anaheim, California. American Meteorological Society, Anaheim, CA 1993. p. 179–184
- [19] Yilmaz, L. Meteorological climate change effect of the Ataturk Dam in Turkey at Eastern Anatolia. *RMZ—Materials and Geoenvironment*. 2006;53(4):467–481.
- [20] Logan, K. E., et al. Assessing spatiotemporal variability of drought in the U.S. central plains. *Journal of Arid Environments*. 2010;74(2):247–255. DOI: 10.1016/j.jaridenv.2009.08.008.
- [21] Sonmez, F. K., et al. An analysis of spatial and temporal dimension of drought vulnerability in Turkey using the Standardized Precipitation Index. *Natural Hazards*. 2006;35(2):243–265. DOI: 10.1007/s11069-004-5704-7.

- [22] Morid, S., et al. Comparison of seven meteorological indices for drought monitoring in Iran. *International Journal of Climatology*. 2006;26:971–985.
- [23] Biox, D., et al. Response of community structure to sustained drought in Mediterranean rivers. *Journal of Hydrology*. 2010;383:135–146.
- [24] Khoshhal, J., Ghayoor, H. A, and Moradi, M. A survey on the impact of groundwater drought in Dehgolan Basin, Kurdistan Province. *Natural Geography Researches*. 2012;4(1):19–36.
- [25] Hosseinzadeh Talaei, P., et al. Hydrological drought in the west of Iran and possible. *Hydrological Processes*. 2014;28(3):764–773. DOI: 10.1002/hyp.9586.
- [26] Fitzpatrick, R. W.. Changes in soil and water characteristics of natural, drained and re-flooded soils in the Mesopotamian marshlands: Implications for land management planning. CSIRO Land and Water. CSIRO Land and Water. Client Report ,September, 2004.
- [27] Davis, D. W. and Hanbali, F.. Water Management in Iraq – Capability Restoration and Implications for Historic Marsh Restoration. In: Raymond Walton, M.ASCE, editor. *Impacts of Global Climate Change*; May 15–19, 2005; Anchorage, Alaska, United States. Anchorage, Alaska, United States: American Society of Civil Engineers; 2005. p. 1–9. DOI: 10.1061/40792(173)608.
- [28] FAO. 2016. AQUASTAT website. Food and Agriculture Organization of the United Nations (FAO). Website accessed on [2016/03/02].
- [29] Amini, A. The impacts of integrated water resources management on dust storms in Tigris–Euphrates basin. In: *First International Forum on Natural Airborne in Iran, Kermanshah*, 23–25 May, Kermanshah, Iran; 2012. p. 12.
- [30] United States Agency for International Development (USAID). *Agricultural Policy Dialogue Series No. 7, Irrigation Efficiency and Agricultural Competitiveness in Iraq*. Louis Berger Group, Inc.; Washington DC, US 2013.
- [31] Keshavarz, A., et al. Management of agricultural water consumption, drought, and supply of water for future demands. In: *Proceedings of the 7th International Conference on the Development of Dry Land*, Sept. 14–17, Tehran, Iran; 2003.



---

# Flood Lamination Strategies for Risk Reduction

---

Luca Franzi, Alessandro Pezzoli and Angelo Besana

Additional information is available at the end of the chapter

<http://dx.doi.org/10.5772/63553>

---

## Abstract

The purpose of 2007/60 UE Directive is namely the establishment of a framework for measures to reduce the risks of flood damage in Europe. In Italy, the Po Basin District Authority, with the contribution of the regional Authorities, published the hazard and risk maps, which are now in force and available for public participation. A common methodology to evaluate risks is now necessary, in order to set priorities for flood management and the financing of countermeasures (ReNDiS procedure). An analysis for the quantification of risk of flooding is presented in the chapter by means of the proportional index of risk (IRP). In particular, it is focused on the flood's lamination strategy, at the entrance of Turin, in terms of hazard and the risk reduction. The sensitivity analysis of the main variables that affect the results is presented and discussed. The benefits of the designed countermeasures are evaluated and quantified in terms of percentage risk reduction. The methodology proves to be a suitable means for decision-makers to compare flooding risks in the flood-prone areas, which are mapped by the 2007/60 UE Directive.

**Keywords:** flood directive, watershed basin management, risk, vulnerability, hazard

---

## 1. Introduction

In Italy, the overall risk of flooding is less severe than in many other European Union (EU) countries [1]; however, there are some areas where there are problematical situations which can be considered among the most important in Europe (**Figure 1**) and, in any case, floods represent the natural instability process more prevalent on the national territory. According to the latest report by the Institute for Environmental Protection and Research [2] on the hydrogeological instability, over 22% of the country is exposed to the danger of flooding: 4%

---

(12,186 km<sup>2</sup>) in areas at high hydraulic hazard,<sup>1</sup> 8.1% (24,358 km<sup>2</sup>) in medium hydraulic hazard areas and 10.4% (31,494 km<sup>2</sup>) in low hydraulic hazard areas. The total population at risk of floods is therefore to be over 16 million people (26.7% of the resident population) of which almost 2 million (3.3%) in areas of high hazard, almost 6 million (10%) in the areas of medium hazard and more than 8 million (13.3%) in low hazard areas.

This representation of the Italian situation is consistent with the conceptual framework of the Flood Directive 2007/60/EC on the assessment and management of flood risks proposed by the European Commission on 18/01/2006 and finally entered into force on 26 November 2007 [3]. *The Flood Directive* (FD) requires Member States to first carry out a preliminary flood-risk assessment by 2011 to identify the river basins and associated riparian areas at risk of flooding. Secondly, for such zones they would then need to draw up flood-risk maps and, thirdly, establish *Flood Risk Management Plans* (FRMP) focused on prevention, protection and preparedness by 2015.

The adoption of the FD means a major paradigm change in national policies to counteract the flooding, shifting the focus from the illusory idea of physical neutralization of the natural phenomena through the construction of defence systems to the most realistic target of reduction of their destructive potential on human societies by reducing the degree of exposure and vulnerability of people and activities. This new strategic vision therefore requires new cognitive instruments to measure the destructive potential of floods and then to assess the overall adequacy of intervention measures.

In Italy, in regard to implementation of the three steps indicated by the 2007/60/EC Directive (preliminary risk assessment, risk mapping and flood-risk management, plan implementation), it is possible to assert that the different river basin authorities have satisfied these requests (according to the act n.49/2010, the adoption of the flood management plan was due by December 2015) according to the guidelines given by the Ministry, which proposed homogeneous approaches to face the tasks [3]. On the other hand, the river basin authorities could already count on an important previous and common activity of delimitation and management of flood-risk areas, as required by the so-called 'post Sarno strategy'<sup>2</sup> but the approach taken by them for the risk assessment is mainly qualitative in nature and for this reason not entirely suited to an objective evaluation of the flood risk as required now.

Therefore, this chapter aims to provide a useful contribution of methodological and instrumental innovation in this regard. In particular, the strategy for flood lamination, consisting of a flood's lamination area on the Dora Riparia River, upstream of Turin's city, is presented in

---

1 In accordance to the Legislative Decree 23 February 2010, n. 49 ('Implementation of Directive 2007/60 / EC on the assessment and management of flood risks') are defined areas of high hydraulic hazard, the areas affected by frequent floods, namely with a return period between 20 and 50 years; medium hazard areas those with infrequent floods with return periods between 100 and 200 years; low hazard areas, those with low probability of floods, with return times over 500 years.

2 After the tragic landslide of Sarno that in May 1998 caused the deaths of 160 people, was first issued a Decree (180/1998), later converted in Law (267/1998, the Sarno law), which represents the cornerstone of the national strategy against hydrogeological risk in Italy. Strategy was based on four elements: the perimeter of the risk areas, the imposition of safeguard restrictions and use limitations, planning of structural interventions for risk reduction, the provision of warning systems and emergency plans to alert and protect people in areas still without the necessary structural interventions.

terms of hazard and the risk reduction. An analysis for the quantification of the risk of flooding is presented by means of the *Proportional Index of Risk* (IRP).

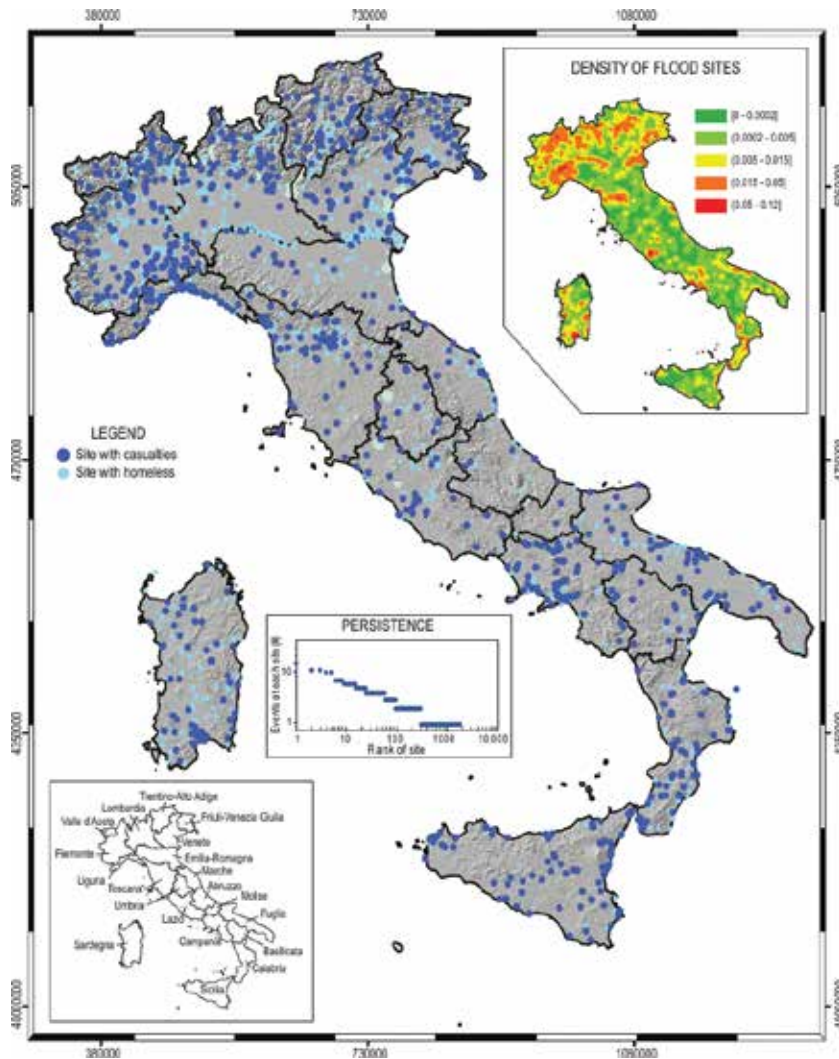


**Figure 1.** The map showing the location of 1836 sites affected by flood events with direct consequences to the population, in the period 590–2008. The upper-right corner shows the density of flood sites per square kilometre (Source: [4]).

## 2. The flood-risk management plans of the Po River Basin Authority

In the Po Basin district (about 71,000 km<sup>2</sup>), hazard and risk maps have been implemented according to the FD guidelines and are now in force. The institutional committee has recently adopted the FRMP.

Management plans define the objectives of the management of flood risk for areas in which a significant potential risk could exist, in order to reduce the possible negative flood consequences. The plans have to cover all aspects of the management of flood risk, with a particular focus to prevention, protection and preparedness, including flood forecasts and early warning systems, and take into account the characteristics of the river basin or sub-basins.

According to the 49/2010 Decree and the Ministry guidelines [3] specific definitions regarding flood risk have been adopted (**Table 1**).

Term	Definition	Source
Risk	“the combination of the probability of a flood event and of the potential adverse consequences for human health, the environment, cultural heritage and economic activity associated with a flood event”	Decree n.49/2010 2007/60 UE Flood Directive
Hazard	“the probability of occurrence, within a specific period of time in a given area, of a potentially damage natural process”	Decree n.49/2010
Exposure	“elements at risk, or receptors, that is, people, properties and goods that can be lost, human health, the environment, cultural heritage and economic activity”	2007/60 UE Flood Directive
Vulnerability	“the degree of a loss to a given element at risk, or set of such elements resulting from the occurrence of a flood with a given intensity”	[3]

**Table 1.** Definitions of the terms used in this chapter.

Flood and risk maps adopted by PBDA are not merely an information tool, but also a ‘*valuable basis for priority setting and further technical, financial and political decisions regarding flood risk management*’.

The approach followed for the risk mapping and representation can be qualitative or quantitative [5]. Limitations of a qualitative approach lay in the fact that qualitative assessment is generally based upon perceptions and opinions, as well as on judgements and consent, while quantitative risk assessment is based on numerical values and the use of computations and models to express the various components of risk. Poor resolution and ambiguity in hazard and exposure categorization are the main problems with the matrix approach, while, on the other hand, the lack of available dataset and the difficulty to quantify inputs (e.g. direct and indirect damages) are the main problems with quantitative models [6].

Which approach, qualitative or quantitative, is preferable is a subject of debate. In general, risk assessment can be regarded as a process of determining qualitative and quantitative aspects of risk related to a concrete situation and a recognized threat. The main purpose for flood-risk assessment is to gain a comprehensive understanding of flood risk, before identifying those mitigation measures that are likely to reduce such risk.

The availability of numerical models of risk, and therefore of quantitative estimations of risk, can facilitate the comparison of the benefits and the costs of the implementation of counter-



measures. In this frame, numerical models are a useful tool for decision-making, helping decision-makers to set the priorities in public financing, and guiding political decisions [7–9].

This true necessity is evident especially when the total amount of financial demand is higher than the available financial resources, regarding the uncertainty in the analysis of the flood risk and the associated management of the decisions' processes [10]. For instance, the recent *ReNDiS* project (*National Database of the projects for soil defence*, by ISPRA) by the Italian Government, which aims at setting priorities for financing the project for natural disaster countermeasures, shows that the demands for financing are over and by far higher than the available annual resources.<sup>3</sup> The collected projects are proposed by public administrations (Regions, Provinces and Municipalities) and refer to non-structural and structural countermeasures against natural hazards, including landslides, debris flows and floods. The geographic location and the state of implementation of the countermeasures is free for consultation for citizens, stakeholders, administrators and decision-makers (**Figure 2**).

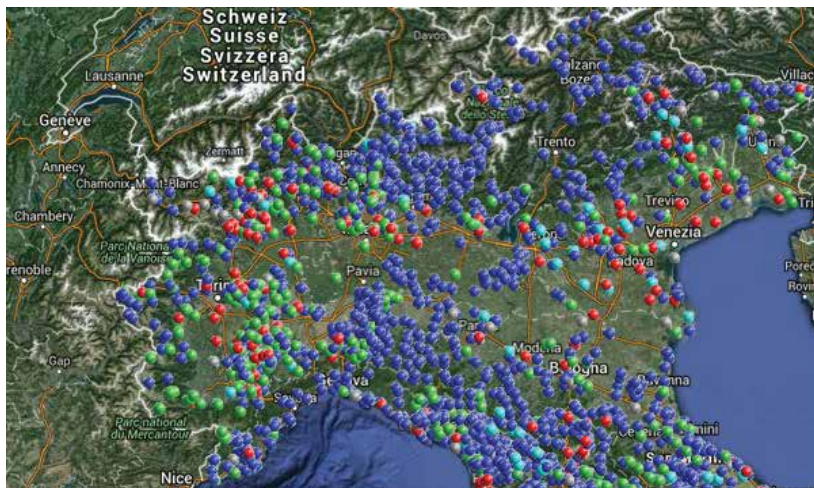


**Figure 2.** Sketch of the location of the projects for flood and landslide defence: blue indicates the finished work, green indicates the work in progress, red indicates work in the design, light blue indicates work that is no longer supported (Source: RENDIS database).

After the adoption of FRMP, with the recent act of the Prime Minister [11],<sup>4</sup> hazard and risk reduction criteria have become the prominent elements that guide the Ministry for financing

<sup>3</sup> RENDIS (Repertory of mitigation measures for National Soil Protection) consists of a repertory developed by ISPRA to share and publish collected data on the web. Through the interface ReNDiS-web, it is possible to view the actions that have been taken within a specific geographical area and query the database, obtaining the corresponding statistical reports on a range of features, or the typological and quantitative data. Currently, the ReNDIS data are limited to the most urgent measures to reduce landslide and flood risks funded by the Ministry of Environment. RENDIS is at address: <http://www.rendis.isprambiente.it/rendisweb/>

<sup>4</sup> D.P.C.M. 28 May 2015 – identification of the criteria and modalities for priority allocation of resources to the mitigation of hydrogeological risk.

the hydrogeological control countermeasures. In particular, according to the decree, some of the elements for the eligibility of financing are related to:

- the goods (if any) at high risk;
- people directly affected by flood;
- frequency of the event;
- reduction of the total number of endangered people; and
- reduction of risk.

As it can be seen, all these points are connected to the contents of the risk and hazard maps. Other elements are related to the environmental amelioration, time scheduling and state of design (preliminary, definitive, executive).

The recent 2015 Prime Minister's decree focuses on the concepts of risk, damage and hazard, with particular regard to their quantification.

The quantification of risk is not a simple task and methodologies depend greatly on the kind of available data. However, in Italy, a uniform methodology is needed, as required by the recent act of the Prime Minister.

In this research, the case of the hazard and risk reduction in Turin is described, with regard to the way on which flood risk due to Dora Riparia river inundation has been evaluated and computed. The effects of the implementation of designed countermeasure are revalidated through risk reduction computation.

### 3. Hazard and risk at Turin

Turin is a city and an important business and cultural centre in Northern Italy. Four major rivers pass through the city, that is, the Po and three of its tributaries, among which the Dora Riparia.

With the implementation of the hydrogeological asset plan (PAI) in 2001 and the recent flood directive, Dora Riparia flooding areas at Turin have been mapped, inundation areas have been reviewed in time, and are now available online. The flooding areas have been represented in the flood hazard maps, which cover the geographical areas, which could be flooded according to the following scenarios for different return periods (RPs):

- (L) floods with a low probability (RP = 500 years);
- (M) floods with a medium probability (for the Dora Riparia  $100 \leq RP \leq 200$  years);
- (H) floods with a high probability ( $20 \leq RP \leq 50$  years).

In FD hazard maps at Turin, flooding areas (**Figure 3**) were obtained by means of a hydraulic approach that is by

1. Implementing one-dimensional (1D) simulation model along the watercourse; for the lack of time and economic resources no 2D models have been used in endangered areas;
2. Considering the state of implementation of the countermeasures (levees, embankments, etc.);
3. Considering the effects of past floods, in particular the recent ones, (the most important recent flood event occurred in 2000 [12]).



**Figure 3.** Flood inundation areas in Turin (free map available on Regione Piemonte website<sup>5</sup>), for different flood scenarios.

By following the requirements of the FD (Act n.49/2010 of the Italian Government; [13]) risk has been mapped by referring to a qualitative approach, that is a matrix approach described herein (**Figures 4 and 5**):

- hazard has been ranked into three different categories (high, medium and low) according to the indication of the 2007/60 EU directive;
- exposure has been referred to the prevalent land use, based on Corinne land cover and ranked into four different categories; the criteria for gathering the different soil uses qualitatively took into account the value of the exposed goods;

<sup>5</sup> <http://www.regione.piemonte.it/difesa-suolo/cms/42-aggiornamento-delle-mappe-di-pericolosita-di-alluvione.html>

– risk has been ranked and mapped according to four categories R1, R2, R3 and R4, which are, respectively, low, medium, high and very high risk; the criteria for the determination of the risk category were debated and made uniform over the territory.

**Damage classes**

	D1	D2	D3	D4	
Hazard classes	L	R1	R1	R2	R2
M	R1	R2	R3	R4	
H	R1	R3	R4	R4	

**Figure 4.** Matrix method implemented by Regione Piemonte for risk classification. Hazard categories (L = low, M = medium, H = high) and exposure categories (increasing from D1 to D4).

Following this approach, by means of a geographic information system (GIS) implementation, qualitative maps have been published online (**Figure 5**).

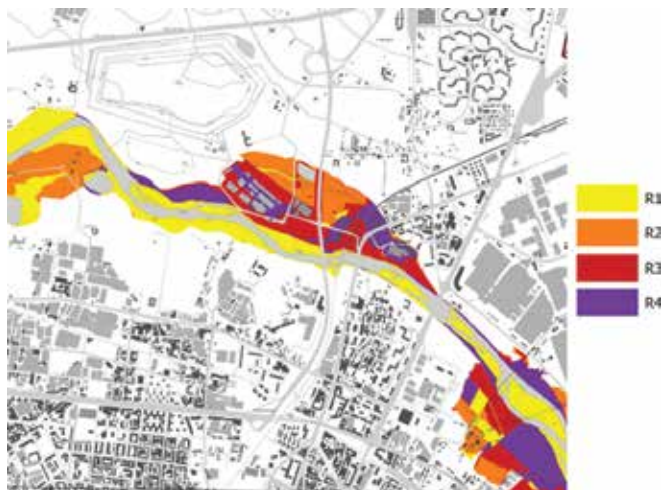


**Figure 5.** Map of risk in Turin. The map refers to the categorization of risk.<sup>6</sup>

As far as Dora Riparia is concerned, the analysis made in the feasibility study (*Studio di fattibilità della Dora Riparia*, indicated in the following as DRFS) showed the necessity to implement flood

<sup>6</sup> Maps can be downloaded at [http://osgis2.csi.it/direttiva\\_alluvioni/cartografia\\_direttivaalluvioni.html](http://osgis2.csi.it/direttiva_alluvioni/cartografia_direttivaalluvioni.html)

diversion areas (FDA) to reduce the impacts of the flooding on the city (**Figure 6**). As it is well known, a flood-diversion-area system consists of floodplain areas equipped with controlled gates. The gate opening creates depression waves that interfere with the flood wave to reduce peak flood discharges. The effects of the FDA control system have been simulated within the DRFS and consist of a reduction of the total endangered areas at Turin. The total cost for the FDA areas is more than 60 M€ and has been qualitatively indicated as a ‘high-priority’ intervention.

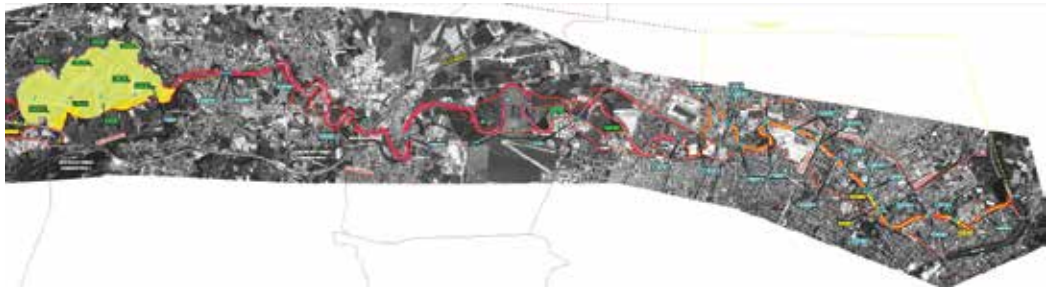


**Figure 6.** Dora Riparia watercourse (in red). Location (yellow) of the FDA and the city of Turin (right).

The choice of the type of the countermeasure, and, in particular, of the effectiveness of the FDA is not under discussion in this chapter. Such a type of structural countermeasure is the result of public confrontation and discussion, stakeholder’s involvement, etc., and is planned to be implemented together with other measures, structural and not-structural, such as public awareness, land use and regulatory plans.

A quantitative approach for evaluating the benefits of the implementation of the FDA countermeasures is described in the following chapter, based on an approach proposed in Regione Piemonte administration. The chief aim is quantifying numerically the risk and flood damages, by means of the available data and for application purposes. This implies the necessity of a robust approach, repeatable in different flood-prone areas of the watershed, in relatively short time.

#### **4. Methodology for flood-risk assessment and quantification**

As anticipated, the flood hazard in Turin has been mapped on the basis of the modelling results contained in DRFS. At now, the inundation areas have been mapped by referring to so-called ‘design conditions’, that is, by considering the effects of the implementation of the designed flood countermeasures. However, flood water levels have been calculated in the DRFS, either referring to the present conditions or referring to the design conditions, by means of a one-dimensional (1D) simulation model.

The chief aim in the activity described herein is to reach an overall quantification of risk and evaluating the benefits of the implementation of countermeasures at Turin, by optimizing the

present resources (economic, human, time). In this contest, the implementation of 2D hydraulic simulations or the updating of 1D models (already implemented in the DRFS) would have been too time consuming and resource spending.

The system adopted for flood inundation mapping and for the estimation of water depths in the flooded areas, that is, for hazard mapping, using the available one-dimensional hydraulic model results at cross sections, consists of the following steps [14–16]:

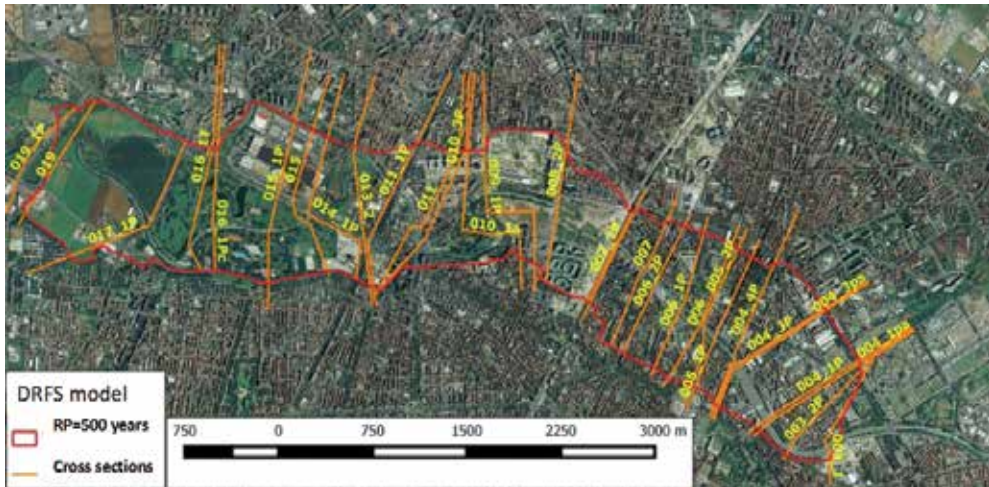


**Figure 7.** Map of the cross sections at which the flood levels have been computed in the DRFS.

- Water surface elevations are estimated using the hydraulic 1D model already implemented in the DRFS (**Figure 7**); the hydraulic model was executed for the design flow, calculated according to the guidelines of the FD; other hydraulic parameters are obtained by calibration.
- The water surface elevations at the cross sections of the hydraulic model are geo-referenced (mapped) on the digital terrain model, and a water surface (usually a triangular irregular network\_TIN\_format) is created; this step of procedure has been developed by means of *QGIS* and *GlobalMapper* software;
- The digital terrain model is subtracted from the water surface (TIN\_format) to obtain a water-depth map; the area with positive values in the water-depth map gives the flood inundation map; this step has been implemented by referring to DTM delivered by MATTM (Ministry of environment, soil and sea defence), which has a high spatial resolution (more than one point for square meter);
- the mean water depth at each receptor in the flooding area has been calculated, by referring the centroid of the receptor; all receptors contained in Regione Piemonte database have been considered, regardless of their prevalent use.

The described methodology was previously applied by Regione Piemonte to the Orco River, to the Dora Riparia River [13] and adopted by the Po Basin District Authority for flood mapping for the Orco River study case [17].

Hazard mapping is the basis for risk evaluation and quantification. The model that is here described (see also [13]) assumes that the quantitative risk for each  $i$ -th receptor can be calculated by the product of hazard, vulnerability and exposure:

$$R_i = H_i E_i V_i \tag{1}$$

where

$H$ : hazard,  $E$ : exposure;  $V$ : vulnerability.

Quantification of the three terms in Eq. (1) is a necessary step to quantify the total risk, as described subsequently. The procedure is the same as that described in [13]:

		EXPOSURE CLASSES			
		D1	D2	D3	D4
HAZARD CLASSES	L	R1	R1	R2	R2
	M	R1	R2	R3	R4
	H	R1	R3	R4	R4

**Figure 8.** Dora Riparia watercourse in Turin (blue line) and the zones indicated by OMI (estate market Observatory).

1. As far as the hazard is concerned, according to Maione [18], the term  $H_i$  can be calculated by referring to the mean occurrence probability per year of a flood, given by

$$H_i = \frac{1}{RP} \tag{2}$$

where  $RP$  is the return period. Inundation depth for each receptor in the flooding area is not directly considered in Eq. (2), by it is indirectly considered in  $E$  and  $V$  terms of Eq. (1), as it is described in the following paragraphs.

2. The exposure  $E_i$  for each receptor has been computed by multiplying the area  $A$  of the receptor for its economic value ' $e$ ' (expressed in €/m<sup>2</sup>) and for the total number ' $f$ ' of floors; the OMI (estate market observatory, free available online) dataset gives the mean economic value ' $e$ ' of the receptors, depending on the prevalent use (commercial, residential) and their location in the urbanized areas (OMI zones), which are considered homogeneous from the economic market point of view (see **Figure 8**).

For each homogeneous OMI zone and for each prevalent use, the OMI (free available online) dataset indicates maximum/mean/minimum economic values, which are regularly updated in time (see **Table 2**).

The total number of floors ' $f$ ' per building has been deduced by ISTAT data (free available online<sup>7</sup>). A mean value of four floors per building has been adopted in the applied model.

3. Vulnerability can be computed by means of a stage damage curve (SDC) as indicated by [19–20]. There is a wide variety of flood damage models in use internationally, differing substantially in their approaches and economic estimates. Comparison of different methods to evaluate vulnerability showed significant differences between the models that are clearly translated in different contests [20–21].

In the technical/engineering literature for natural hazards, physical vulnerability is generally defined on a scale ranging from 0 (no loss/damage) to 1 (total loss/damage). In the application to the study case, different SDC curves have been considered (see **Table 3**) and their application to the study case has been discussed. The depth-damage curve proposed by [22] has been adopted, in order to take into account either the content damage or the structural damage. Indirect damages have not been considered.

OMI ZONE	Minimum (€/m <sup>2</sup> )	Mean (€/m <sup>2</sup> )	Maximum (€/m <sup>2</sup> )
C8	1500	1850	2200
C9	1300	1600	1900
C10	1500	1850	2200
C16	2050	2425	2800
D9	1600	1925	2250
D10	1300	1575	1850
D11	1400	1750	2100
D13	1500	1825	2150
D14	1750	2150	2550

**Table 2.** Economic values (expressed per square meter) of the residential receptors in the flooding areas (Source: OMI market observatory, free available online).

<sup>7</sup> Data can be seen at the website <http://dati-censimentopopolazione.istat.it/>



<i>SDC model</i>	<i>Developer</i>	<i>Limitation to the study case application</i>	<i>Reference</i>
FLEMO	German Research Centre for Geosciences	Vulnerability can be computed for water depths by far lower than those of the study case	[23]
HAZUS-MH	FEMA	Typology of buildings (wooden-made) is different from Italian cases	[24]
Multi-Coloured Manual	Middlesex University	Typology of buildings	[25]
Rhine Atlas	Action Plan on Floods	The model shows the highest similarities. Vulnerability can be computed for water depths $h > 0$	[22]

**Table 3.** Discussion of the applicability of different SDC models to the study case.

The ICRP original curve has been changed in order to adapt it to present conditions of the buildings in the flooded areas in Turin. In particular, the adopted vulnerability curve takes into account the presence of basements, and therefore the curve starts from water depths lower than zero (**Figure 9**).

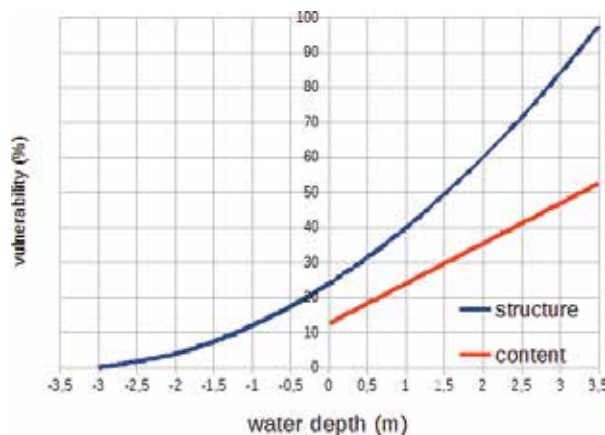


**Figure 9.** Vulnerability curve adopted in the implemented model.

For a given inundation scenario, that is, for a given return period  $RP$ , the vulnerability  $V_i$  and the exposure  $e_i$  of each receptors are computed.

The comprehensive estimation of the risk, for a given inundation scenario, can be easily obtained by assuming the superposing effects of inundation on each receptor. The *Proportional Index of Risk* [13] is therefore introduced, given by

$$IRP = \frac{\sum A_i f_i V_i e_i}{RP} \quad (3)$$

The term 'proportional' refers to the proportionality of the total economic exposure  $E_i$  with the area  $A_i$  of the receptor.

## 5. Results and discussion

The procedure is applied to the study case by referring to present hazard conditions and design hazard conditions.

DTM Source	Accuracy in elevation	Point density	Date of survey
Regione Piemonte	- ±0.30 m	One point per 25 square metres	2009
(MATTM) Ministry of environment, soil defence and sea	±0.05 m	One point per square metres	2011

**Table 4.** Main characteristics of the DTM tested in the implemented model.

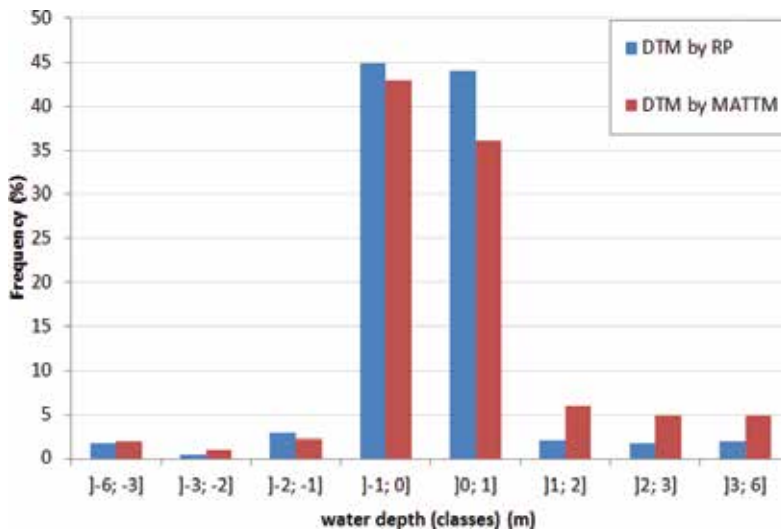


**Figure 10.** Frequency distribution of the water depths at the centroids of the receptors. Comparison of the results obtained using the two DTMs (Digital Terrain Model) described in **Table 4**.

A sensitivity analysis of the results has been carried out by considering and evaluating:

- the effects of DTM resolution on the results, in particular two DTMs, with a different resolution have been used: the DTM by MATTM and the DTM by Regione Piemonte (the main characteristics of the DTM are shown in **Table 4**); for each DTM, the total number of flooded receptors and the water depths at centroids of the receptors have been calculated, by following the described procedure:

The obtained results show that, notwithstanding the different characteristics and accuracy in altimetry of the two DTMs, the frequency distribution of the inundation depths at the centroids of the receptors is very similar (**Figure 10**). Differences in water depth calculation at the centroids of the receptors are of the same order of magnitude of the uncertainties which affect either the hydraulic model calculation (at cross sections, **Figure 7**) or the methodology applied to extend the computed 1D levels to the flooding areas.

- The effects of the choice on the OMI economic value ' $e_i$ '; in order to test the sensitivity of the model to OMI economic value, the benefits of the implemented countermeasures are calculated by

$$Benefits = \frac{IRP_{pres} - IRP_{des}}{IRP_{pres}} \quad (4)$$

where  $IRP_{pres}$  and  $IRP_{des}$  refer to the IRP indexes calculated by referring to present situation and design conditions, respectively, expressed in terms of percentage; it can be seen (**Figure 11**) that the benefits do not significantly vary with the choice of the OMI value regarding each OMI zone. In any case, the benefits are about 74%, in terms of IRP reduction. Obviously, in absolute terms, the benefits of the implementation of countermeasures vary in wide range for the minimum or medium or maximum OMI value, as shown in **Figure 11**.

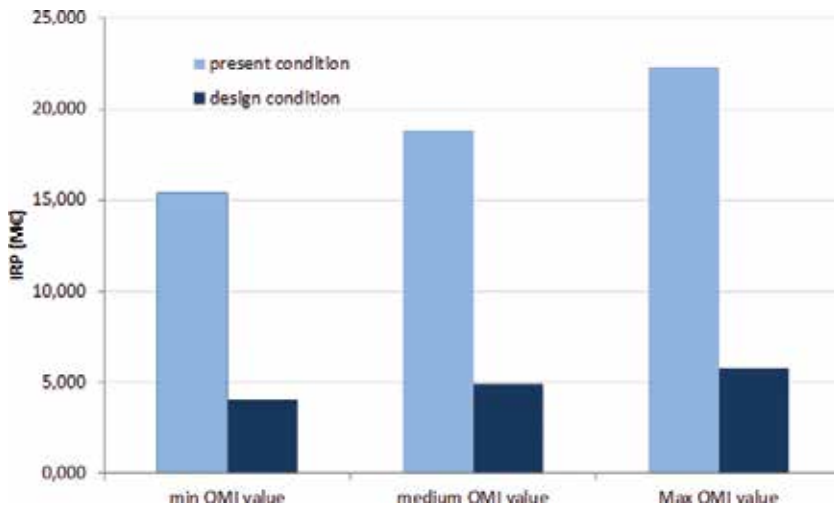


**Figure 11.** Effects on results of the choice of the OMI economic value.

- The effects of the implementation of countermeasures are not uniform, in terms of risk reduction. In **Figure 12**, the frequencies of receptors, which fall within the  $i$ -th IRP class intervals, have been calculated by referring to the present and to the design conditions

following the same procedure indicated in [13]. The effects and benefits of the implementation of the countermeasures are represented by

- the reduction of the total number of receptors falling in the flooding areas, that is, the total number of receptors for which IRP is higher than zero;
- the reduction of the total number of receptors for each  $i$ -th IRP class, that is, a reduction of risk for each IRP class.

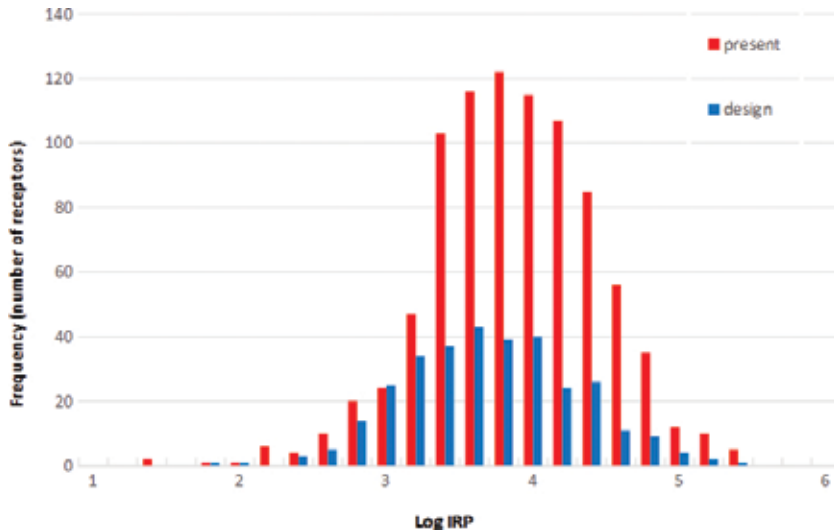


Figure 12. Frequency of receptors falling within the  $i$ -th class interval.

## 6. Conclusions

The effects of the implementation of the designed countermeasures at the Dora Riparia River in Turin have been quantified by applying a simple procedure as described in this chapter.

The procedure allows obtaining an overall indication of the benefits of a flood diversion area, located upstream Turin, by means of an index, called Proportional Index of Risk.

The model considers the three main components of risk, which are the vulnerability, the exposure and the hazard. Each component has been quantified by referring to the present conditions and to the design conditions. The procedure allows quantifying the benefits in terms of IRP percentage variation, that is, of risk variation. The results obtained in the Turin study case do not vary significantly when different DTMs are considered for hazard mapping and IRP calculation. In terms of IRP reduction, the effectiveness of the designed countermeasures is about 75%, regardless of the OMI value that has been considered.

On one hand, the application of more complex models to quantify risk and benefits, where indirect effects of flooding risk reduction (such as indirect costs due to recovery procedures

and civil protection) or indirect benefits (those on economy and stakeholder involvement) could also be considered, would have allowed a more in-depth understanding of the risk and benefits here described. On the other hand, probably the implementation of more complex models would have revealed to be too time consuming and resource spending. In this contest, the model reveals to be a simpler and easier method by optimizing the available data.

Consequently, the repeatability of the method to the different flood conditions mapped in the framework flood directive can allow a systematic understanding and quantification of the benefits of the design countermeasures.

In this frame, the IRP methodology can represent a simple means to quantify benefits, to rank the design countermeasures and, consequently, to set priorities in financial spending.

Adoption of methodologies, easy to be implemented, can reveal to be a substantial decision to implement administration procedure like the RENDIS procedure described in the text. The increasing demand, for efficient management of designed countermeasures' projects and for efficient allocation of financial spending, should address administration towards methods like the IRP, described in the chapter.

In more general terms, the identification and the use of numerical estimation tools of flood risk and damage have real usefulness well beyond the particular scope of the proposed case study here. In fact, this sort of indicators can be applied in

- policies of flood-risk prevention. The estimate of the damages caused by the potential floods to which a given area is exposed is a key decision-making factor for the choice of any preventive measures. In fact, objective measurements allow undertaking appropriate analysis to compare the cost of any preventive measures with corresponding benefits in terms of the expected damage reduction and, based on these, comparing alternative intervention policies. At a time when the financial resources available to national and regional governments are scarce, the objective justification of the huge costs that often require these policies is an important prerequisite to their implementation;
- policies of emergency management. This kind of estimations can be a support also in preparation, revision and updating of emergency management plans. The knowledge of entity and of spatial distribution of expected damage in fact represents the essential information for the provision of adequate emergency and warning systems of the population;
- damage compensation programmes. The quantification of the potential damage of floods is needed to predict the amounts and the receivers of possible compensatory measures of damages and victims;
- land-use planning. Spatial planning policies that take into account the existing flood-risk conditions and of the potential damages are more necessary than ever;
- insurance schemes. To fix the amounts of insurance against floods, the insurance and reinsurance companies must estimate, with the greatest reliability, the risk levels which the insured goods are exposed. In the event of disasters, if not well assessed, these risks may jeopardize financial coverage provided by the insurance and cause insolvency;

- precautionary choices of businesses and citizens. Even companies or individual citizens may be interested to know the damage that their properties are potentially exposed. Having this information can be useful, in fact, to evaluate the convenience to take out any insurance policies and to undertake individually or ask the competent authorities measures to protect against flooding.

## Author details

Luca Franzini<sup>1\*</sup>, Alessandro Pezzoli<sup>2</sup> and Angelo Besana<sup>2</sup>

\*Address all correspondence to: [luca.franzi@regione.piemonte.it](mailto:luca.franzi@regione.piemonte.it)

1 Regione Piemonte, Soil Defence Department, Italy

2 DIST Department, Politecnico di Torino and University of Turin, Italy

## References

- [1] European Environmental Agency (EEA). Water Resources in Europe in the Context of Vulnerability. Luxembourg: EEA; 2012. 96 p. DOI: 10.2800/65298
- [2] Istituto Superiore per la Protezione e la Ricerca Ambientale (ISPRA). Hydro-geologic hazards and risk indicators in Italy. Report 2015. 2015 ed. Rome: ISPRA-Settore editoria. 2015. 162 p. DOI: 978-88-448-0751-1.
- [3] MATTM-Ministry of environment, soil and sea defence. Indirizzi operativi per l'attuazione della direttiva 2007/60/ce relativa alla valutazione ed alla gestione dei rischi da alluvioni. 2013th ed. MATTM; 35 p. [www.minambiente.it](http://www.minambiente.it)
- [4] Salvati, P., Bianchi, C., Rossi, M., Guzzetti, F. Societal landslide and flood risk in Italy. *Natural Hazards and Earth Systems Sciences*. 2010;10:465–483. DOI: 10.5194/nhess-10-465, 2010
- [5] Vojinovic, Z., Abbott, M.B. Flood Risk and Social Justice: From Quantitative to Qualitative. *International water association ed.*; 2012. 600 p. DOI: 9781780400822
- [6] Merz, B., Thielen, A.H., Gocht, M. Flood risk mapping at the local scale: concepts and challenges. In: Begum, S. et al., editor. *Flood Risk Management in Europe*. London: Springer; 2007. p. 231–251.
- [7] Hunter, N.M, Bates, P.D., Nelz, S., Pender, G., Villanueva, I., Wright, N.G., Liang, D., Falconer, R.A., Lin, B., Waller, S., Crossley, A.J., Mason D.C. Benchmarking 2D hydraulic models for urban flooding. *Water Management*. 2008;161:13–30.

- [8] Apel, H., Aronica, G.T., Kreibich, H., Thielen, A.H. Flood risk analyses – how detailed do we need to be? *Natural Hazards*. 2009;49:79–98. DOI: 10.1007/s11069-008-9277-8
- [9] Ernst, J., Dewals B.J., Detrembleur, S., Archambeau, P., Erpicum, S., Piroton, M. Micro-scale flood risk analysis based on detailed 2D hydraulic modelling and high resolution geographic data. *Natural Hazards*. 2010;55:181–209. DOI: 10.1007/s11069-010-9520-y
- [10] Hall, J., Solomatine, D. A framework for uncertainty analysis in flood risk management decisions. *International Journal of River Basin Management*. 2008;6(2):85–98. DOI: 10.1080/15715124.2008.9635339
- [11] President of Council of Minister decree (28th May 2015) (DPCM). 2015. Rome: Istituto Poligrafico Zecca dello Stato. Available at: <http://www.minambiente.it/normative/dpcm-28-maggio-2015-individuazione-dei-criteri-e-delle-modalita-stabilire-le-priorita-di>
- [12] Environmental Protection Regional Agency (ARPA). Report of the flood event (13th-16th October, 2000). Turin: ARPA ed.; 2000.
- [13] Franzi, L., Bianco, G., Bruno, A., Fogliano S. Flood risk assessment and quantification in the Piedmont Region, Italy. In: Tiepolo, M., Ponte, E., Cristofori, E., editors. *Planning to cope with tropical and subtropical climate change*. Berlin: de Gruyter; 2016. DOI: 979-3-11-048078-8
- [14] Interagency Advisory Committee on Water Data (IACWD). Guidelines for determining flood flow frequency. In: *Bulletin 17B of the Hydrology Subcommittee*. Reston: Office of Water Data Coordination; 1982. Available at: [www.water.usgs.gov/osw/bulletin17b/dl\\_flow.pdf](http://www.water.usgs.gov/osw/bulletin17b/dl_flow.pdf)
- [15] Noman, N.S., Nelson, E.J., Zundel, A.K. Review of automated flood plain delineation from digital terrain models. *Journal of Water Resources Planning Management*. 2001;127:394-402.
- [16] Federal Emergency Management Agency (FEMA). Guidelines and specifications for flood hazard mapping partners \_Appendix C: guidance for riverine flooding analysis and mapping. 2003 ed. FEMA. Available at <http://www.fema.gov/media-library/assets/documents/13948>
- [17] Po River Basin District Authority (PBDA). Orco river hazard mapping. 2012. Available at: [www.adbpo.it/on-multi/ADBPO/Home/documento13535.html](http://www.adbpo.it/on-multi/ADBPO/Home/documento13535.html) (date of access 19.5.2016)
- [18] Maione, U., Moissello, U. *Statistics for hydrology*. 2nd edition, Pavia: Medea; 2015. DOI: 8866930830
- [19] Smith, D.I. Flood damage estimation – a review of urban stage-damage curves and loss functions. *Water SA*. 1994;20(3):231–238.
- [20] Jongman, B., Kreibich, H., Apel, H., Barredo, J.I., Bates, P.D., Feyen, L., Gericke, A., Neal, J., Aerts, J.C.J.H., Ward, P.J. Comparative flood damage model assessment:

towards a European approach. *Natural Hazard and Earth System Science*. 2012;12:3733–3752. DOI: 10.5194/nhess-12-3733-2012

- [21] Ciurean L.R., Dagmar Schroeter and Thomas Glade. Conceptual Frameworks of Vulnerability Assessments for Natural Disasters Reduction. In: prof. John Tiefenbacher ed., *Approaches to Disaster Management - Examining the Implications of Hazards, Emergencies and Disasters*. InTech. 2013. p.3-32. DOI: 10.5772/55538. Available at: <http://www.intechopen.com/books/approaches-to-disaster-management-examining-the-implications-of-hazards-emergencies-and-disasters/conceptual-frameworks-of-vulnerability-assessments-for-natural-disasters-reduction>
- [22] ICPR: International Commission for the Protection of the Rhine. *Action plan on flood defence*. Koblenz: International Commission for the Protection of the Rhine; 1998.
- [23] Kreibich, H., Thielen, A. Assessment of damage caused by high groundwater inundation. *Water Resources Research*. 2008;44:W09409. DOI: doi:10.1029/2007WR006621
- [24] Federal Emergency Management Agency (FEMA), HAZUS-MH MR4 Flood Model Technical Manual. Washington: Department of homeland security, FEMA, Mitigation Division editors. 2009. 569p.
- [25] Penning-Rowsell, E., Viavattene, C., Pardoe, J., Chatterton, J., Parker, D., Morris, J., editors. *The benefits of flood and coastal risk management: a handbook of assessment techniques*. Middlesex: Flood Hazard Research Centre; 2010.



# **Sustainable Land Use Planning in the River Basins**

---



---

# Sustainable Land Use Planning Model in Rural Basins

---

Ertuğrul Karas

Additional information is available at the end of the chapter

<http://dx.doi.org/10.5772/63714>

---

## Abstract

Soil erosion is a common problem that complicates watershed management in Turkey and around the world. The main objective of soil conservation work carried out in basins is to ensure sustainable watershed management. The first operation is to define the current situation in the basin. The initial and fundamental objective of erosion estimation based on existing data is generally deciding how to overcome the problem. However, the treatments carried out in most soil conservation studies are similar to each other. Any common, known, or defined methodology about erosion problems in watersheds has not been improved—until now. Considering this problem, the Sustainable Land Use Planning (SLUP) model was developed to determine soil conservation precautions, to set priorities for decision makers and to produce a common solution for rural watershed in Turkey. While the estimated average soil loss was determined to be  $7.66 \text{ t ha}^{-1}$  per year, some land use changes were proposed and land use management priorities were set in the direction of the model results to gain sustainable management in the Çelikli basin. At the end of the study, it was showed that the soil loss can be reduced about the rate of 91.2% applying the SLUP model.

**Keywords:** land use planning, soil erosion, soil conservation, SLUP model

---

## 1. Introduction

Soil is an indispensable resource for the continued existence of living organisms on Earth. Today, food security and the environmental sustainability of limited natural resource management have become more important. Population growth and complex situations in the use of natural resources have required skilled land use. As a result, soil erosion, which was an accepted part of the soil degradation process, is observed in various ways and degrees under the influence of factors such as climate, topography, and land use. The biggest change in natural resources in

the last 100 years has occurred as a result of changes in land use type and technological improvements. The major factors in accelerated soil degradation processes are improper land use, deforestation, soil erosion, overgrazing, vehicle off-roading, and inappropriate irrigation. The daily displacement of the upper layers of land due to heavy rains, accumulation of the carried soil, plant nutrients in storage structures, sedimentation, and processes such as eutrophication threatens the sustainability of natural resources. No matter the factors, soil degradation processes need to be correctly defined and must be established for the natural balance between living organisms. Today, the estimation of soil loss is one effort to reduce the effects that lead to soil degradation.

USLE, developed by Wischmeier and Smith [1], is globally the foremost and preferred popular model in predicting soil loss. The main objective of RUSLE and WEPP models, which were developed based on USLE, is to estimate soil loss from a given land. Research carried out at the parcel level, the contribution of many scientists [2–5], is maintained with the support of technology. Today, it is possible to achieve results in a very short time, to forecast the impact of alternative applications, and to analyze and evaluate the results with the help of computers that process data on the Geographic Information System (GIS) environment. With detailed analysis of each factor considered, the effectiveness of these model results is faster and easier. Environmental factors such as land use and soil characteristics can be easily obtained by means of this technique [6]. Thus, the identification of sensitive areas of erosion can offer unique opportunities for exposing priorities and providing measures to decision makers.

Numerous studies have been carried out over the last two decades using USLE-GIS integration in various part of the world [7–31]. So far, the efforts carried out on the estimation of soil loss have not yet adopted a common point in terms of analysis and evaluation. To keep soil loss under a defined threshold is the point of the alliance. In particular, these efforts have intensified in the last half century and have provided much more to the adoption of the concept of soil loss tolerance [1, 3, 32–47]. This is defined as the maximum permission level of soil loss from an area that will not cause any yield reducing. Soil loss tolerance values have been compared with rates of soil formation in many studies [48–65].

The first study interested in the SLUP model was applied in the Güvenc basin [66]. In this study, the areal distribution of soil erosion classes and soil conservation precautions was also obtained. According to the results, 64.68% of the basin had a non-existent or too low erosion degree, 9.18% had a low-moderate erosion degree, 7.53% had a moderate-high erosion degree, 4.33% had a high erosion degree, and 14.33% had a very high level erosion degree. It was shown that soil loss can be lowered from 16.30 to 1.44 t ha<sup>-1</sup>, reduced by approximately 91%, with the proposed approach across the entire basin.

Almost all of the soil conservation studies, carried out in the basins throughout the world up to now, have been focused on the estimation of soil loss. Despite some efforts, any approach that may be a solution offer to soil conservation measures to be taken in the basins has not been developed yet. This is considered as a major absence and requirement. The purpose of this study is to introduce the model called “Sustainable Land Use Management”, which was developed to ensure the most appropriate land use management plan by reducing soil loss in the basins considering the problems and requirements mentioned above.

## 2. Materials and methods

### 2.1. The study area

This study was conducted in a catchment known as Celikli, located in the Tokat region of north-east side of central Anatolia, Turkey (**Figure 1**). The basin is 1041.2 ha in area and has an average elevation of 1300 m above sea level. It is situated in the area transitioning from central Anatolia to the middle Black Sea region (latitude  $40^{\circ} 06' 31''$  N, longitude  $36^{\circ} 21' 40''$  E).

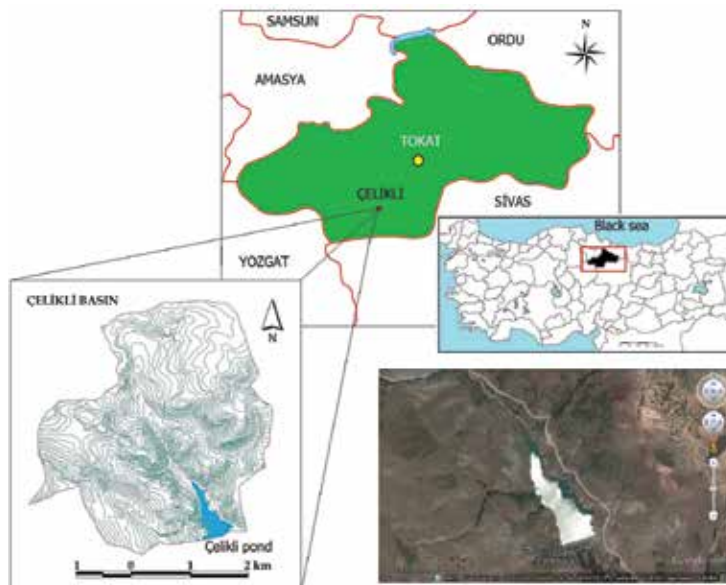


**Figure 1.** The location, topographic map and Google Earth view of the Çelikli basin.

The study area has semi-arid climatic conditions. The average annual temperature is  $8.1^{\circ}\text{C}$ , and the mean annual precipitation is 535.9 mm, 84.7% of which falls between October and May [67].

#### 2.1.1. Land use

Current land use for the basin was prepared by a detailed land investigation. The determined land use groups were given in **Table 1** and **Figure 1**. While dry farming areas occupy nearly 68% of the area, pasture and shrub land use have approximately 25 and 5.45%, respectively. Pasture land use, which is not appropriate for tillage due to insufficient soil depth, was left for native usage. In the last 60 years, most of the pastures and some forested areas were converted to agricultural land by ploughing. Consequently, native land use of the basin was considerably changed from pasture and forest to agriculture land use [67].

Land use	Area (ha)	Area (%)
Dry farming	706.9	67.88
Pasture	258.9	24.86
Shrub	56.7	5.45
Bare rock	8.5	0.82
Water surface	10.2	0.98
Total	1041.2	100.00

**Table 1.** Land use distribution of the basin.

Investigation of pasture composition was done to determine the coverage percentage, dry grass yield, and to describe the species of pasture plants on the selected 27 sample points in the basin. The analysis showed that the coverage rate was about 50% of this pasture area. Although some points are majority Graminea family, most have a mixed composition with Fabaceae, Labiatae, Convolvulaceae, Labiatae, and other species. Vegetation quality of pastures in the basin is generally determined as low [67].

Land Use Capability Class (LUCC) of the basin soils given in **Table 2** was also determined with the detailed investigations. LUCC is a classification process made considering soil, topography, climate, environment, crop cover and hydrological conditions. Limiting factors, such as soil properties and slope, are taken into account in favourableness of an area for determining of the most suitable management form such as agricultural, forestland, and pasture. In general, lands are classified as eight groups varying from 1 to 8. There are six different LUCC (II, III, IV, VI, VII, and VIII) in the basin except for I and V [67].

Land use capability classes	Area, (ha)	Area (%)
II	11.1	1.07
III	84.3	8.10
IV	52.1	5.00
VI	541.6	52.02
VII	333.4	32.02
VIII	8.5	0.82
Water surface	10.2	0.98
Total	1041.2	100.00

**Table 2.** Land use capability classes and areal distribution in the basin.

Around 84% of the basin soil is Class VI or VII. Classes II, III, and IV cover 14.07% of the basin and are available for agricultural aims. Although they have some restrictive factors, those areas can be used for agricultural production by carefully choosing plants, applying some special

conservation practices, and careful management techniques. About 84.86% of the basin soils (VI, VII, and VIII) are unsuitable for agricultural production, which are favourable mainly for grassland, forestland, or wildlife habitats in terms of LUCC.

When we look at the maps of land use and LUCC together in **Figure 2**, we can see that most of the basin soil is used for agricultural production (68%), although only 14% of the land is appropriate. The areas suitable for agricultural production (Classes II, III, and IV) are on the north-east side of the basin. Class VI is extensively used for agricultural aims. This current situation reveals that the area is unsuitable and unsustainable for basin management.

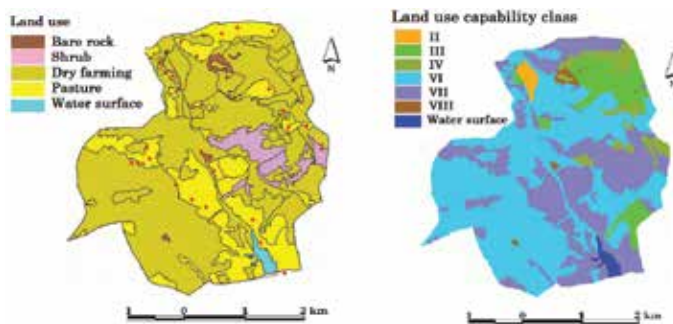


**Figure 2.** The maps of land use and land use capability class of the basin.

### 2.1.2. Soil sampling and analysis

Georeferenced soil samples were taken from top soil (0–0.3 m) and subsoil (0.3–0.6 m) in July 2002. In soil samples, organic matter [68], soil pH [69], lime ( $\text{CaCO}_3$ ) [68], electrical conductivity

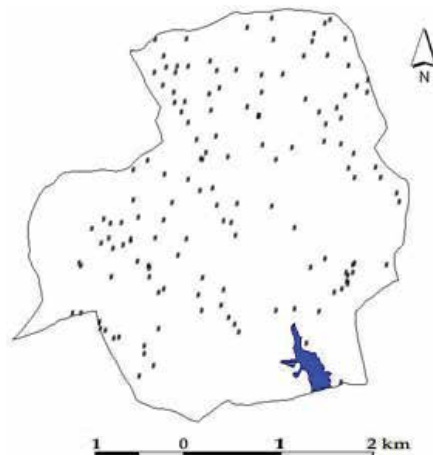


**Figure 3.** Soil sampling points in the basin.

(EC) [70], Cation exchange capacity [71], textural distribution [72], saturated hydraulic conductivity [73], and volumetric water content [74] were analyzed. Erodibility was calculated by a soil erodibility nomograph [75]. The sampling points are shown in **Figure 3**.

### 2.1.3. Soil map

Two satellite images (IRS-1C, with a  $5.8 \times 5.8$  m pixel size and LANDSAT-TM with  $30 \text{ m} \times 30 \text{ m}$  pixel size) were used to prepare a soil map of the basin, in addition to a cadastral map with a scale of 1/5000. The combined image of the basin obtained from these two images is given in **Figure 4**.

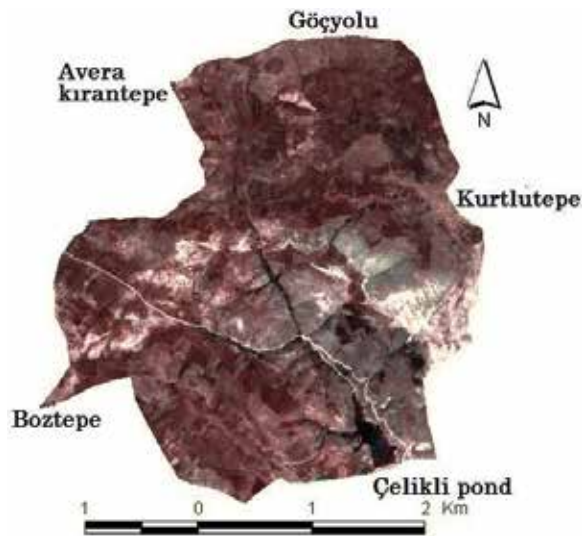


**Figure 4.** Satellite image of the basin.

The detailed soil map was prepared with a scale of 1/5000 and 9 soil series were identified. A description of soil profiles, environmental properties, and physical and chemical characteristics of the soil samples was taken from these profiles. The defined soil series in the basin is given in **Table 3**.

The soil series in the basin given in **Table 3** and **Figure 5** were classified according to the basis of soil taxonomy. Three ordos (Entisol, Mollisol, and Alfisol), three subordos (Orthent, Ustoll, and Ustalf), four big groups (Ustorthent, Haplustoll, Haplustalf, and Argiustoll), and three subgroups (Typicustorthent, Lithicustorthent, and Verticargiustoll) were determined using climatological and geological data [67]. Kevenli, Yelten, and Göçyolu are the soil series, which have the most widest in terms of area occupying 29.3, 28.33, and 13.59% of the total area, respectively. Although their average depths are changing from 24 to 67 cm, many soil properties are very close to each other such as exchangeable cations and texture distribution. Other six soil series (Yedikır, Yayla, Alıçlı, Uluyol, Kurtlutepeönü, and Akardere) in the basin include 30.76% of the total area varying from 1.60 to 10.52%



Soil series	Area (ha)	Area (%)
Kevenli	305.2	29.30
Yelten	295.0	28.33
Göçyolu	141.5	13.59
Yedikır	109.5	10.52
Yayla	69.8	6.70
Alıçlı	54.7	5.26
Uluyol	20.8	1.99
Kurtlutepeönü	18.0	1.72
Akardere	16.6	1.60
Water surface	10.2	1.98
Total	1041.2	100.00

Table 3. Soil series in the basin.

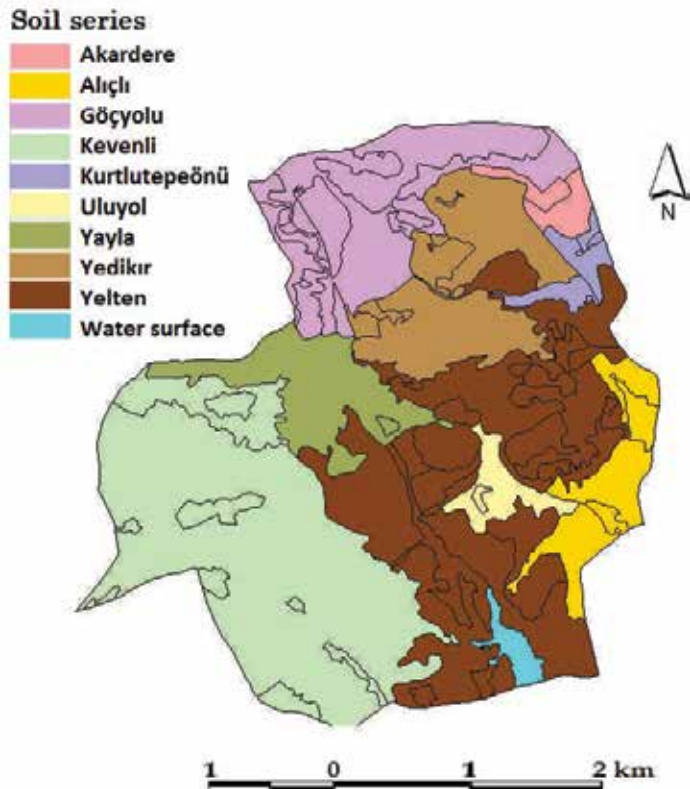


Figure 5. Soil series map of the basin.

Some physical and chemical properties of the soil series in the basin are given in the **Table 4**. Although the soil depths are between 24 and 90 cm, the basin soils have a generally shallow depth, low organic material, low lime content, and slightly alkaline character. Most of the soils have a silty clay loam (SCL) texture, and plant available water content for the mean depth (46 cm) is about 75 mm due to weak soil profile development.

Soil series	Depth cm	Salt %	pH	CaCO <sub>3</sub> %	Org. Matter %	%			Texture	Cation Exc. me/100g	Exchangable cations me/100g			
						Sand	Clay	Silt			Ca + Mg	K	Na	Total
Kevenli	67+	0.024	7.79	3.2	1.2	48.8	26.3	24.9	SCL	33.52	31.73	0.66	0.03	32.42
Yelten	31+	0.019	7.37	1.1	1.6	46.9	28.3	24.8	SCL	30.57	28.28	0.49	0.02	28.79
Göçyolu	24+	0.018	6.78	0.0	2.2	60.7	18.2	21.1	SL	26.95	26.14	0.51	0.01	26.66
Yedikır	66+	0.033	7.14	1.1	1.3	33.6	41.2	25.2	C	44.68	40.03	0.77	0.01	40.81
Yayla	51+	0.019	7.91	7.7	1.2	46.0	28.7	25.3	SCL	21.75	20.89	0.63	0.02	21.54
Alıçlı	51+	0.034	7.69	8.9	2.0	53.1	26.2	20.7	SCL	40.81	38.71	0.70	0.01	39.42
Uluyol	65+	0.017	7.89	12	0.9	59.5	21.9	18.6	SCL	21.58	20.28	0.47	0.01	20.76
Kurtlute peönü	67+	0.012	6.91	0.0	0.7	51.6	21.8	26.6	SCL	22.39	21.80	0.40	0.02	22.22
Akardere	90+	0.040	7.64	3.0	2.1	23.5	57.0	19.5	C	57.55	52.25	0.72	0.44	53.41
Mean	48.6	0.024	7.46	4.1	1.5	47.0	30.0	23.0	SCL					

**Table 4.** Some physical and chemical properties of soil series in the basin.

## 2.2. USLE model

Soil loss is estimated using the following equation in USLE [1]:

$$A = R \times K \times L \times S \times C \times P \quad (1)$$

where  $A$  is average annual soil erosion per unit area ( $\text{t ha}^{-1} \text{ year}^{-1}$ ),  $R$  is rainfall erosivity factor ( $\text{MJ mm ha}^{-1} \text{ h}^{-1} \text{ year}^{-1}$ ),  $K$  is soil erodibility factor ( $\text{t ha}^{-1} \text{ h ha}^{-1} \text{ MJ}^{-1} \text{ mm}^{-1}$ ),  $L$  is slope length factor,  $S$  is slope steepness factor,  $C$  is cover and management factor, and  $P$  is management practice factor.  $L$ ,  $S$ ,  $C$ , and  $P$  are all dimensionless.

### 2.2.1. Rainfall erosivity factor ( $R$ )

The rainfall erosivity factor ( $R$ ) shows the effect of rainfall impact on the amount and rate of runoff calculating the rainfall energy (EI) obtained from a maximum 30-min intensity ( $I_{30}$ ) having at least 12.7 mm of precipitation during a period of 15 min. The interval duration

between two storms must be at least 6 h [1]. After the calculation of the rainfall intensities, rainfall kinetic energy is calculated using the following equations [76]:

$$E_i = 0.019 + 0.0873 \log_{10} i \quad (2)$$

$i \leq 76 \text{ mm h}^{-1}$

$$E_i = 0.283i > 76 \text{ mm h}^{-1} \quad (3)$$

where  $E_i$  is the kinetic energy of 1 unit of rainfall ( $\text{MJ ha}^{-1} \text{ mm}^{-1}$ ) and  $i$  is the rainfall intensity ( $\text{mm h}^{-1}$ ).

The product of the total kinetic energy of rainfall ( $E$ ) and its peak 30-min intensity ( $I_{30}$ ):

$$R = E \times \left( \frac{i_{30}}{100} \right) \quad (4)$$

where  $R$  is the rainfall erosivity factor ( $\text{MJ ha}^{-1} \text{ cm h}^{-1}$ );  $I_{30}$  is the peak 30-min intensity of rainfall ( $\text{cm h}^{-1}$ ); and  $E$  is the total kinetic energy of rainfall ( $\text{J m}^{-2}$ ).

$R$  factor value for the whole basin was used as  $54.68 \text{ MJ ha}^{-1} \text{ cm h}^{-1}$ , taken from research carried out in the Tokat province from 1996 to 2005 [77].

### 2.2.2. Soil erodibility factor ( $K$ )

The soil erodibility indicates the erosion susceptibility of the soils, which is a function of soil texture, permeability and organic matter. It is explained using a soil erodibility monograph for farmland and construction sites mathematically [75].

The soil erodibility factor ( $K$ ) was determined for each soil sample based on analysis of soils in the laboratory. The equation referenced is as follows:

$$K = \left( (2.17 \times 10^{-4}) \times (M^{1.14}) \times (12 - a) + 3.25 \times (b - 2) + 2.5 \times (c - 3) \right) \times d \quad (5)$$

where  $M$  = (percentage of silt and fine sand)  $\times$  (100 - percentage of clay);  $a$  is the organic matter content (%),  $b$  is the soil structure (1–4),  $c$  is the permeability grade (1–6), and  $d$  is the coefficient of converting ( $d = 1.292$ ).

Soil samples collected from the predetermined points were marked using GPS. The  $K$  factor values of the soils were determined for each soil series from 142 samples; the  $K$  factors varied between 0.18 and 0.30. The basin  $K$  factor map is given in **Figure 6**.

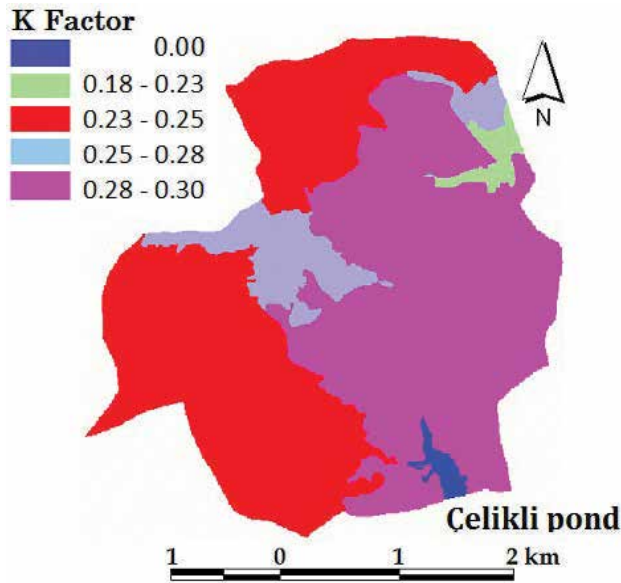


Figure 6. K factor map of the basin.

2.2.3. Slope length and steepness factor (LS)

Slope length and steepness (LS) factor reflects the impact of topography on soil erosion. With a unit plot of length 22.13 m, the USLE used the equation:

$$L = \left( \frac{\lambda}{22.13} \right)^m \tag{6}$$

where  $L$  is slope length factor,  $\lambda$  is slope length, and  $m$  is a coefficient that changes according to slope [if the slope ( $S$ ) >4%,  $m = 0.5$ , for  $S = 4\%$ ,  $m = 0.4$ , and if  $S \leq 0.3$  and  $m = 0.3$ ].

The equation used to calculate slope steepness factor ( $S$ ) in the USLE is given below:

$$S = \frac{0.43 + (0.30 \times s) + (0.043 \times s^2)}{6.574} \tag{7}$$

where  $S$  is slope steepness factor and  $s$  is slope (%).

Basin slope distribution and slope map are given in Table 5 and Figure 7, respectively.

Slope/land use		Agricultural		Pasture		Shrub		Bare rock	
%	Slope definition	ha	%	ha	%	ha	%	ha	%
0-2	Flat	32.9	4.66	5.3	2.03	0.0	0.00	0.0	0.00
2-6	Slight	320.9	45.40	55.2	21.3	3.1	5.49	3.6	41.9
6-12	Middle	266.0	37.60	97.3	37.5	20.9	36.8	3.2	37.5
12-20	Steep	72.6	10.20	71.5	27.6	26.0	46.4	1.0	12.0
20-30	Very steep	12.0	1.70	25.9	10.0	6.1	10.7	0.6	7.37
30-45	Rough	2.1	0.30	3.4	1.32	0.3	0.47	0.1	1.05
>45	Very rough	0.3	0.04	0.4	0.14	0.0	0.02	0.0	0.00
Total		706.9	100	258.9	100	56.7	100	8.5	100

Table 5. Slope distribution of the land use groups.

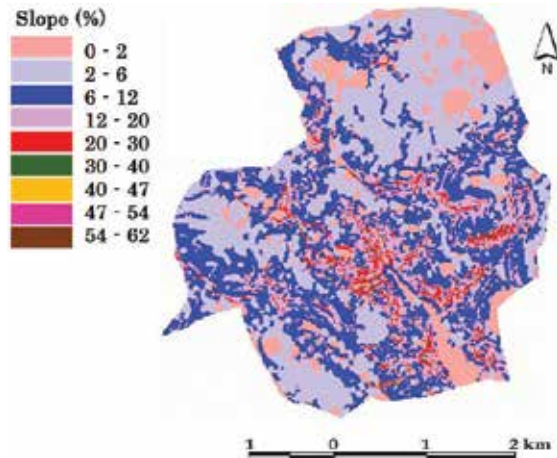


Figure 7. Slope map of the basin.

An equation was developed to compute length-slope factor:

$$LS = \left( \frac{A_s}{22.13} \right)^m \times \left( \frac{\sin \beta}{0.0896} \right)^n \quad (8)$$

The basin LS factor map was prepared using ArcView Spatial Analyst extension [78] and the digital elevation model (DEM), which was prepared with 10 m interval digitized contours from a 1/25,000 scale topographic map. The grid cell size for this study was chosen as 10 m for purposes of calculation. Therefore, a grid cell area was 100 m<sup>2</sup>. Flow accumulation and slope steepness values proposed by Moore and Burch [79] were used to calculate the LS factor as grid format. The equation given below calculates the combined LS factor for the basin.

$$LS = \left[ \left( \text{Flowaccumulation} \times \frac{\text{cell value}}{22.1} \right)^{0.4} \right] \times \left[ \left( \frac{\sin \text{slope}}{0.0896} \right)^{1.3} \right] \quad (9)$$

Basin LS factor values change between 0 and 39.91. The DEM and LS factor maps of the basin are given in **Figures 8** and **9**.

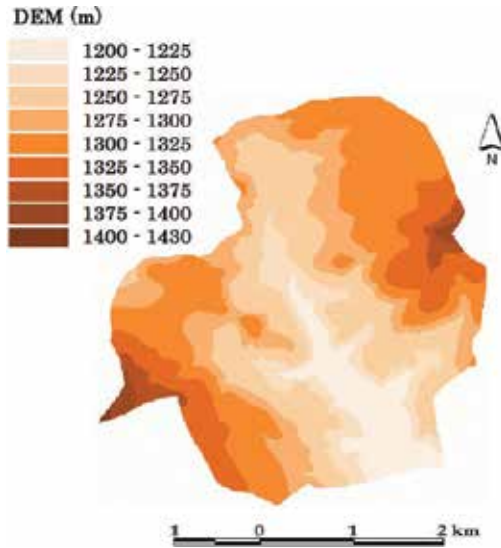


**Figure 8.** Digital Elevation Model (DEM) of the basin.

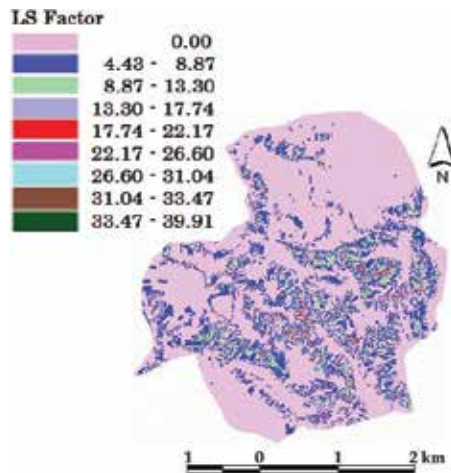


**Figure 9.** LS Factor map of the basin.

2.2.4. Cover and management factor (C)

C is the crop (cover) management factor, which is an indicator that shows the effectiveness of different crop management systems as comparatively for preventing of reducing of soil loss. It is a relative measurement of soil loss considering between a crop management system and continuously fallow and tilled land. Whereas the USLE was developed for use on agricultural fields, the proper C factor values are chosen for nonagricultural conditions.

For this study, C factor values were taken from the results of the USLE project [77] carried out at the basin for agricultural areas and based on data published in [80] for pasture and shrub. C factors for the basin are given in **Table 6** and **Figure 10**.

Land use	Quality	Changing interval	Selected value
Agriculture (dry)	Poor	0.10–10.40	0.25
Pasture	Poor	0.01–0.05	0.03
Shrub	Poor	0.003–0.40	0.038
Bare Rock	–	0.00	0.00
Water Surface	–	0.00	0.00

**Table 6.** C factor values used for the land use.

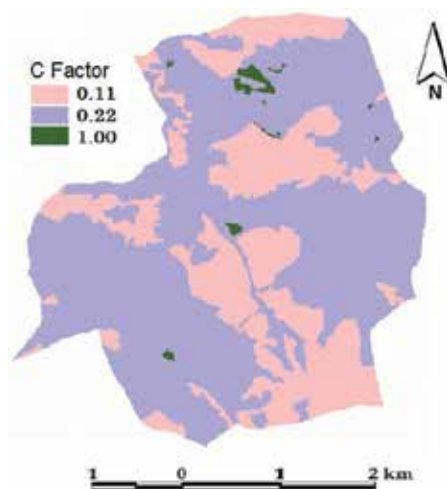


**Figure 10.** C factor map of the basin.

2.2.5. Management practice factor (P)

The effects of soil conservation practices that will reduce soil loss are determined by the management practice factor (P), which represents cropland practices such as contour farming, strip cropping by reducing runoff speed.

There were not any conservation measures for agricultural areas such as contour farming or strip cropping. For that reason, the  $P$  factor was accepted as 1.00 for the entire basin [67].

### 2.2.7. Soil loss tolerance

Soil loss tolerance ( $T$ ) is the permission level of soil loss that will not cause to reduce in productivity as economically [3, 75]. The amount of tolerance value ( $T$ ) that permitted must be equal to or less than the soil erosion rates [81]. Soil loss tolerance values were determined from according to rooting depth [37], and categorized into five classes, as shown in **Table 7**.

Rooting depth, cm	Soil loss tolerance ( $t\ ha^{-1}year^{-1}$ )	
	Renewable soil	Non-renewable soil
0–25	2.2	2.2
25–50	4.5	2.3
50–100	6.7	4.5
100–150	9.0	6.7
>150	11.2	11.2

**Table 7.** Implication of soil loss tolerance.

Soil depth and tolerance maps for the basin are in five groups changing from 2.2 to 11.2  $t\ ha^{-1}$ ; their depths are considered in **Figure 11**.

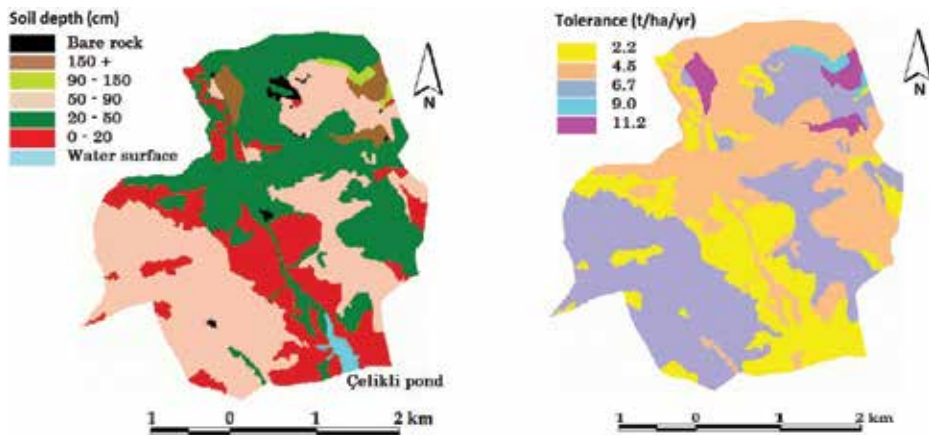


**Figure 11.** Soil depth map and soil loss tolerance map of the basin.

After calculation of the USLE, soil loss and tolerable soil loss rates can be compared to in terms of a specific management system considering their alternative to determine soil conservation measurements in farm planning.



2.2.8. Sustainable land use planning (SLUP) model

A method proposed by Karaş [82] was firstly applied in the Güvenç pond basin in Turkey. The described approach in **Table 8** was used for both the soil erosion rates and soil loss tolerance values. The presented table mainly includes all land use types. The principal idea of the table is to apply the required soil conservation precautions (SCP) for land use types according to existing soil erosion and present conditions using only one or a combination of as many precautions as possible. Applying all types of SCP has certain costs. Therefore, SCP practices were ordered from the cheapest to the most expensive. All of the SCP practices were compared to the soil loss tolerance (*T*) values. Customarily, unused (bare land) and agricultural areas are the most exposed to soil erosion. For example, the first and second SCP at the agricultural land use includes cultural methods, which contain practices such as conservation tillage, strip cropping, and contour farming. If soil erosion is still greater than the soil loss tolerance despite cultural precautions of the agricultural land use, third-degree SCP needs to be applied. Physical applications include terracing or the design and installation of a combined practice to remove settled solids and associated pollutants in all runoff of larger storms. However, if there are no possible events to prevent or reduce soil erosion to the level of *T* values using the first three SCP, the fourth-degree SCP, which includes changing land use type (natural transformation to pasture, rangeland, and forest), needs to be applied. If it is not possible to reduce soil erosion under a level of *T* values via the first four SCP practices, the fifth-degree SCP (including the fourth-degree precautions + physical structures) needs to be applied. Physical structures include graded stabilization structures, stream bed improvement, gabion threshold construction, and grassed waterways.

Erosion degree	The value of (A/T)	Erosion description	Proposed soil conservation precautions
1	≤1.0	None exists or too few	First-Degree Precautions (FDP) Consider cropping systems that will provide maximum protection for the soil. Use minimum tillage systems where possible. Soil management (increasing organic matter content, using soil stabilisers), crop rotation on agricultural areas, suitable tillage, minimum tillage, conservation tillage, mulching, mulch tillage, ridge tillage, strip tillage, fertilising, controlled grazing, pasture management) using suitable mechanisation tools for cultivation.
2	1.0 T – 2.0	Low – Moderate	Second-Degree Precautions (SDP) Use support practices, such as cross slope farming, that will cause the deposition of sediment to occur close to the source. (In addition to FDP applications, contour farming, inter cropping, mixed cropping, agro forestry and shrub establishment of agricultural areas, continued covering, and developing rangelands)

Erosion degree	The value of (A/T)	Erosion description	Proposed soil conservation precautions
3	2.0–4.0	Moderate–high	Third-Degree Precautions (TDP) Cultural Precautions + Physical Structures (In addition to SDP, strip cropping, cross slope, wind breaks, drainage, terracing on shrub land and rangeland) terracing, contour strips, installation of trench and holes for pasture management
4	4.0–6.0	High	Fourth-Degree Precautions (FoDP) Changing land use type (natural transformation to pasture, rangeland and forest)
5	>6.0	Very high or severe	Fifth-Degree Precautions (FiDP) Including FoDP + Physical structures Physical structures (graded stabilisation structures, stream bed improvement, construction of gabion threshold, grassed waterways, etc.) Proper forest management, Reforestation / afforestation, shifting cultivation, controlled cutting.

Descriptions: *A*—potential soil loss; *T*—soil loss tolerance value

**Table 8.** Soil conservation precautions according to land use and potential soil loss.

### 3. Results and discussion

#### 3.1. Soil loss

Potential Soil Loss (PSL) for the basin was estimated to be between 0 and 152.77 t ha<sup>-1</sup>, applying the USLE equation in the GIS environment. The PSL values for existing land use types were also obtained. The results show that the PSL is of 9.87 t ha<sup>-1</sup> for agricultural land use, 3.01 t ha<sup>-1</sup> for pasture, and 4.16 t ha<sup>-1</sup> for shrub. The mean calculated potential soil loss is 7.66 t ha<sup>-1</sup> for the entire basin. Detailed statistical results obtained for each land use type are given in **Table 10**.

Total soil loss for the general basin is about 7972.86.42 t year<sup>-1</sup>. While 87.51% of the total soil loss is lost from agricultural areas, pasture and shrub land use also contribute to the rate of 9.51 and 3.58%, respectively. When considered in terms of soil depth in the basin, mean soil loss tolerance values are around 4.5 t ha<sup>-1</sup>, which are accepted as the threshold level of the basin. This means that 89.79% of the total soil loss occurs over the threshold value.

According to the obtained results, agricultural lands are under a high potential soil loss risk. While the agricultural land use occupies 68% of the total area, 87.51% of total soil loss is sourced from this area. In the basin, the agricultural areas are mainly converted from forest and pasture, which are the native land use. Therefore, most of the soil loss is lost from this area. Furthermore, most of the agricultural land use areas are now class VI in terms of land use capability. Actually,

these areas should definitely not be ploughed. The soils in Class VI are generally unsuitable for agricultural production due to their severe limitations such as topographic soil conditions. These areas are generally appropriate for grassland, forestland, or wildlife habitat.

Although only 14% of the soils in the basin are appropriate for agricultural aims, 68% of the basin is used for the agricultural production. In agricultural land use, 31.37% of the area produces 72% of the total soil loss, which represents the soil loss over 11.2 t ha<sup>-1</sup> in **Table 9**.

Land use	Descriptive statistic	Soil loss (t ha <sup>-1</sup> year <sup>-1</sup> )						General
		0.0–2.2	2.2–4.5	4.5–6.7	6.7–9.0	9.0–11.2	>11.2	
Agriculture	Mean (t ha <sup>-1</sup> year <sup>-1</sup> )	0.52	3.31	5.55	8.00	10.06	22.69	9.87
	Cell number*	18,192	10,048	8361	6946	4971	22,172	70,690
	USLE(t ha <sup>-1</sup> year <sup>-1</sup> )	94.59	332.58	464.03	555.68	500.08	5030.82	6977.78
	Area (%)	25.73	14.21	11.83	9.83	7.03	31.37	100.00
Pasture	Mean	0.62	3.25	5.48	7.74	10.04	14.70	3.01
	Cell number	14,506	5274	2659	1584	854	1013	25,890
	USLE(t ha <sup>-1</sup> year <sup>-1</sup> )	89.93	171.00	145.71	122.60	85.74	148.91	763.89
	Area (%)	56.03	20.37	10.27	6.12	3.30	3.91	100.00
Shrub	Mean	0.90	3.32	5.55	7.64	10.01	14.32	4.16
	Cell number	1887	1475	1157	713	267	171	5670
	USLE(t ha <sup>-1</sup> year <sup>-1</sup> )	16.98	48.97	64.21	54.47	26.72	24.49	235.84
	Area (%)	33.28	26.01	20.41	12.57	4.71	3.02	100.00
Bare rock	Mean	0.0	–	–	–	–	–	0.00
	Cell number	850	–	–	–	–	–	850
	USLE(t ha <sup>-1</sup> year <sup>-1</sup> )	0.0	–	–	–	–	–	0.00
	Area (%)	100.00	–	–	–	–	–	100.00
Water surface	Mean	0.0	–	–	–	–	–	0.00
	Cell number	1030	–	–	–	–	–	1030
	USLE(t ha <sup>-1</sup> year <sup>-1</sup> )	0.0	–	–	–	–	–	0.00
	Area (%)	100.00	–	–	–	–	–	100.00
Basin general	Mean	0.58	3.29	5.54	7.77	10.05	22.28	7.66
Cell number	36,465	16,797	12,177	9243	6092	23356	104,130	
USLE(t ha <sup>-1</sup> year <sup>-1</sup> )	211.50	552.62	674.60	718.18	612.25	5203.71	7972.86	
Area (%)	35.02	16.13	11.69	8.88	5.85	22.43	100.00	

\*grid cell size 10 m × 10 m = 100 m<sup>2</sup>.

**Table 9.** Soil loss according to land use groups in the basin.

The calculated potential soil loss (PSL) using the USLE for the basin is given in **Figure 12**. PSL values were divided into the appointed soil loss tolerance ( $T$ ) values for each soil series to determine the soil erosion degree and the proposed soil conservation precautions on current land use, as explained in **Table 9**. The prepared erosion class map is given in **Figure 13**.

Erosion degree	$A/T$ rate	Description	Area (ha)	Area (%)
1	0–1	None exist or too few	548.4	52.67
2	1–2	Low–moderate	212.8	20.44
3	2–4	Moderate–high	172.0	16.51
4	4–6	High	63.9	6.13
5	>6	Severe	44.2	4.25
Total			101.3	100.00

**Table 10.** Areal distribution of soil erosion in Çelikli basin.

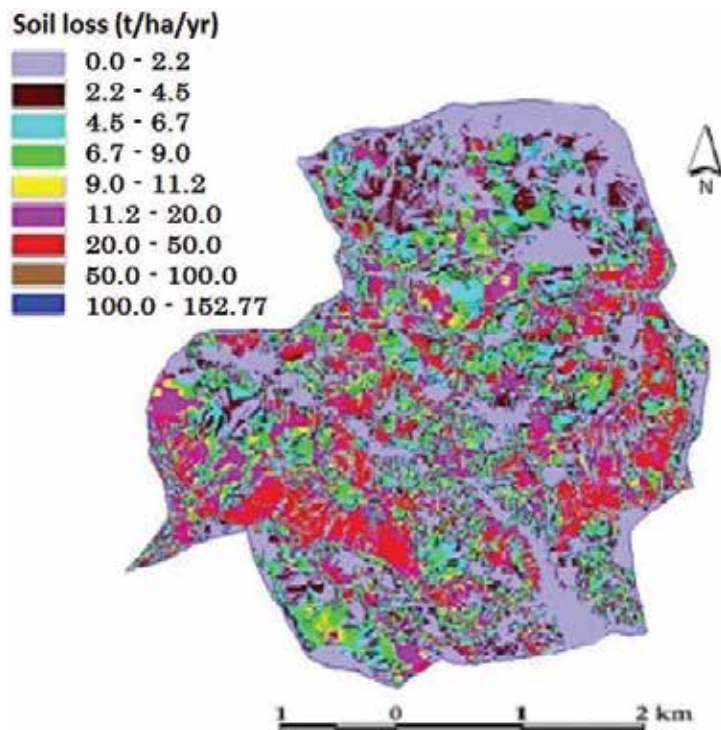


**Figure 12.** Soil loss map of the basin.

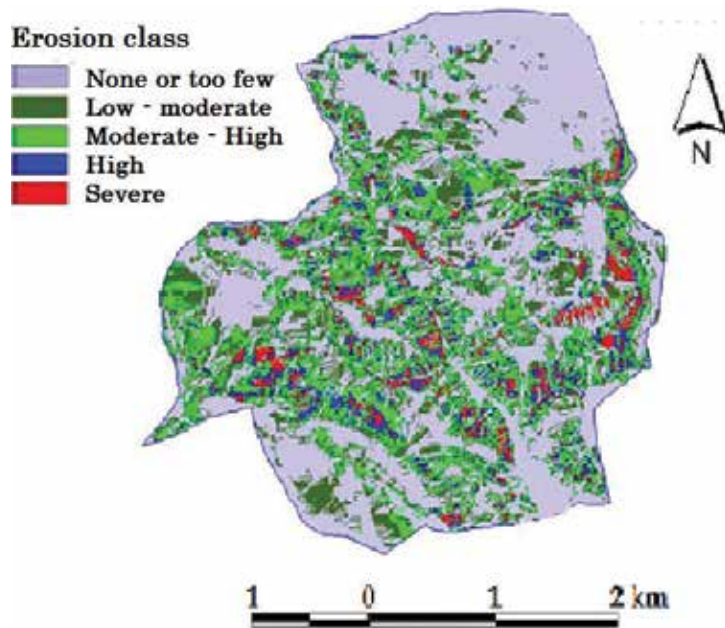


Figure 13. Erosion class map of the basin.

Areal distribution of soil erosion in Çelikli basin is given in **Table 10**. Currently, according to the results, soil loss in the 50% of basin has none exist or too few.

While pasture land use produces a total of 763.89 t of soil loss, only about 9.58% of total soil loss came from the pasture areas. Most of the pasture areas are around Çelikli pond and on the northern side of the basin. About 56.03% of soil loss in pasture land use is under  $2.2 \text{ t ha}^{-1}$ . Soil losses in 20.37% of the pasture areas are between 2.2 and  $4.5 \text{ t ha}^{-1}$ , which provides 171 t of loss.

Shrub area has 234.8 t of soil loss, which is the 2.95% of total loss. Shrub areas were formerly forested areas, and all of them now include brushwood from cutting down the forests for fuel during the last century. In these areas, the biggest soil loss is between 4.5 and  $6.7 \text{ t}$ , which is 27% of total soil loss.

### 3.2. Land use planning of the basin

The natural land usages of the basin are primarily pasture and forest. Areas in the basin under severe erosion risk are mainly agricultural, shrub, and pasture land uses, respectively. Actually, the pasture and forest were the native land use 100 years ago. As mechanization tools were developed, land conversions started to convert to meet agricultural aims and rural needs by cutting down trees for fuel and by cultivating the soil. In that basin, the carrying capacity for grazing was calculated by considering the number of animals. There were a total of 5000 animals in the basin, including 3000 native cows and 2000 sheep and goats, with a 258.9 ha pasture area [67]. In Turkey, a native cow and a sheep are accepted as 0.5 and 0.1 of a big cow

as a native unit (BBHB), respectively. Therefore, the grazed animal numbers were calculated as 1700 BBHB for the whole basin. When we calculate for the carrying capacity for each BBHB, the required pasture area is about 6.12 ha per head. Consequently, the needed area for pasture is about  $(1700 \times 6.12)$  10,404 ha. This result shows that the existing pasture area is not sufficient for grazing. The number of grazing animals is over the carrying capacity due to insufficient cover rate and forage yield. It is necessary to increase about 40 times the current pasture area for adequate grazing, or to expand it around 20 times by getting additional improvement measures (such as seedlings, fertilizing, controlled grazing) and applying some rain water harvesting techniques (such as constructing micro-basin water harvesting ridges, negarim type micro-basins, flood water harvesting pools, contour trenches, or bunds and terracing), and some planting measures (such as constructing consecutive brushes and trees as barriers for reducing surface runoff).

In agricultural areas, the wheat-fallow system is applied due to insufficient rainfall. The average wheat yield was determined as 1720 kg per ha for the selected 137 points. The average production cost for wheat is around 2960 kg ha<sup>-1</sup> in dry areas [83]. Thus, the net income for the Çelikli basin is under the production cost, which is not sustainable for dryland areas. The low productivity is not economical when compared with the obtained income considering soil loss. Moreover, the main source of soil erosion is agricultural fields, which occupy around 88% of total basin area. Currently, 78.34% of arable lands are not appropriate for agricultural usage by ploughing due to improper land use. Therefore, those areas should be converted to pasture land, as they were 100 years ago, for reducing soil loss and meeting the grazing capacity of the basin. This means the pasture areas will increase about 2.13 times, reaching 812.68 ha, which is 78% of the entire basin.

Shrub areas generally have low density coverage and are open to intensive rainfall conditions. Thus, to reduce soil loss they need conservation measures like being converted to forest by increasing the cover density.

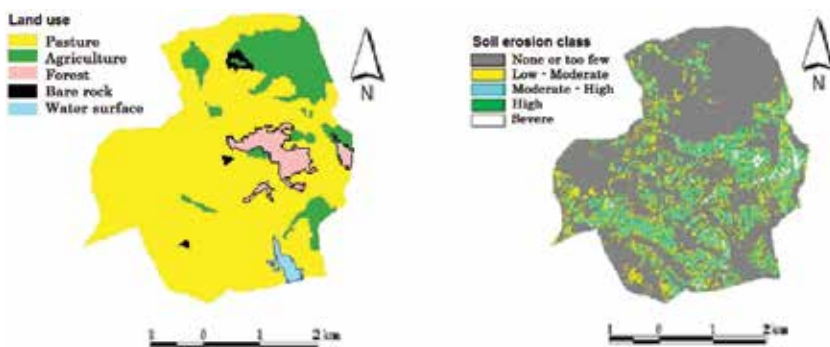


**Figure 14.** The proposed land use for sustainable management and soil erosion classes in the basin.

Currently, agricultural areas that have LUCC II, III, and IV are appropriate for arable land in the basin. They still unproductively use the wheat-fallow system for agricultural aims. Animal

production is a main income for the farmers living in the region. Some forage plants, such as vetch (*Vicia sativa*), forage pea (*Pisum sativum*), and sainfoin (*Onobrychis sativa*), can be grown under the dry conditions in the region. Agricultural production by ploughing risks soil erosion, causing movement of the soil and encouraging soil loss. When natural vegetation is removed for agricultural aims by ploughing, soil surface is exposed to intensive rainfall. Alternatively, the forage crops have the basic requirements for feeding the animals and are grown in the Çelikli province.

The research, carried out in the region, showed that sainfoin is one of the most favourable plants, which permanently covers the soil surface. Sainfoin is a perennial legumes-forage crop, which can be grown in poor soil and dry regions, where the rainfall is 300–400 mm per year for grazing animals. While it can obtain a harvest in dry regions in general, hay production can be changed between 2000 and 6000 kg per ha with a fertilization and maintenance. It is accepted as a rotation crop in arid regions and convenient for reducing soil erosion from the fields and ensuring nitrogen [84]. Sainfoin is advised to grow in areas that have low phosphorus soils [85]. It protects animals against bloat due to having tannins and it helps to increase protein absorption. It also keeps the soil in place thanks to main and side roots [86].

The land use proposed by the SLUP model was applied in the basin by considering the land use changes, the applications previously mentioned for agricultural, forest, and pasture land use. A final soil loss map of the basin and soil loss distribution is given in **Figure 14** and **Table 11**.

Agricultural land use in class VI was converted to pasture by reducing 79.13% of the total arable land. Current land use (wheat-fallow) was changed to permanent forage crops (sainfoin, *O. sativa*) applying no tillage or minimum tillage, strip cropping with contour farming, and using suitable mechanization tools for cultivation to reduce soil losses. The *C* factor was 0.25 for *O. sativa*. The *P* factor was 0.37 for strip cropping with contour farming. While the *P* factor was 1.0 with fall plough, the soil tillage method factor was 0.25 for no tillage farming. Therefore, the *P* factor was decreased from 1.00 to 0.0925. Soil losses on the agricultural land decreased from 9.87 to 0.24 t ha<sup>-1</sup>, and the reduction rate was approximately 97.56% considering those applications.

In pasture areas, first- and second-degree precautions were applied to reduce soil loss in addition to the installation of some permanent vegetation, such as buffer strips (e.g. Saltbush) situated in short intervals, including physical structures (such as terracing, contour strips, and installing trenches and holes) to intercept storm water runoff and minimize soil erosion. In pasture land use, overgrazing management and improvement studies (seeding, fertilizing) on poor areas are proposed for sustainable management. Pasture areas increased by converting them from agricultural land at a rate of 216% in the basin. The *C* factor for pasture area was selected as 0.025. Soil loss in pasture land use was decreased from 3.01 to 0.83 t ha<sup>-1</sup> by means of grazing management, improvement studies, and including some physical precautions.

Shrub land areas were another source of soil loss. This land was a forest before the trees were cut down. After planning, the shrub land was converted to its natural cover plant. The *C* factor was selected as 0.001 applying forest management. Therefore, soil loss in this land decreased

from 4.16 to 0.05 t ha<sup>-1</sup>. Overall, soil loss was lowered from 9.87 to 0.67 t ha<sup>-1</sup> with the SLUP model across the entire basin, reducing it by approximately 91.25%. After planning, land use changes are given in **Table 12**.

Land use	Descriptive statistic	Soil loss (t ha <sup>-1</sup> year <sup>-1</sup> )						General
		0.0–2.2	2.2–4.5	4.5–6.7	6.7–9.0	9.0–11.2	>11.2	
Agriculture (forage crop)	Mean (t ha <sup>-1</sup> year <sup>-1</sup> )	0.23	2.43	–	–	–	–	0.24
	Cell number*	14,713	37	–	–	–	–	14,750
	USLE (t ha <sup>-1</sup> year <sup>-1</sup> )	33.84	0.90	–	–	–	–	33.81
	Area (%)	99.75	0.25	–	–	–	–	100.00
Pasture	Mean	0.59	2.9	5.16	7.47	10.09	24.54	0.83
	Cell number	75,119	6403	148	77	23	59	81,830
	USLE (t ha <sup>-1</sup> year <sup>-1</sup> )	443.20	185.69	7.64	5.75	2.32	14.48	659.08
	Area (%)	91.59	8.02	0.19	0.10	0.03	0.07	100.00
Forest	Mean	0.05	–	–	–	–	–	0.05
	Cell number	5670	–	–	–	–	–	5670
	USLE (t ha <sup>-1</sup> year <sup>-1</sup> )	2.84	–	–	–	–	–	2.84
	Area (%)	100.00	–	–	–	–	–	100.00
Bare rock	Mean	0.0	–	–	–	–	–	0.00
	Cell number	850	–	–	–	–	–	850
	USLE (t ha <sup>-1</sup> year <sup>-1</sup> )	0.0	–	–	–	–	–	0.00
	Area (%)	100.00	–	–	–	–	–	100.00
Water surface	Mean	0.0	–	–	–	–	–	0.00
	Cell number	1030	–	–	–	–	–	1030
	USLE (t ha <sup>-1</sup> year <sup>-1</sup> )	0.0	–	–	–	–	–	0.00
	Area (%)	100.00	–	–	–	–	–	100.00
Basin general	Mean	0.49	2.90	5.16	7.47	10.09	24.54	0.67
	Cell number	97,382	6440	148	77	23	59	104,130
	USLE (t ha <sup>-1</sup> year <sup>-1</sup> )	479.88	186.59	7.64	5.75	2.32	14.48	696.66
	Area (%)	93.51	6.18	0.14	0.07	0.02	0.06	100.00

\*grid cell size 10 m × 10 m = 100 m<sup>2</sup>.

**Table 11.** Soil loss according to proposed land use groups in the basin.



Land use	Current land use (ha)	Proposed land use (ha)	Difference (ha)
Agriculture (wheat-fallow)	706.9	–	–706.9
Agriculture (forage crops)	–	147.5	+147.5
Pasture	258.9	818.3	+559.4
Shrub	56.7	–	–56.7
Forest	–	56.7	+56.7
Bare rock	8.5	8.5	–
Water surface	10.3	10.3	–
Total	1041.3	1041.3	

**Table 12.** Land use changing before and after planning in the basin.

## 4. Conclusion

Sustainable land use planning (SLUP) model was applied in a semi-arid basin, having different land use. Main problem in the basin had soil erosion due to land use problems such as improper land use, deforestation, and overgrazing. The grazing capacity for feeding animals is not sufficient due to poor vegetation and cover rate. It is necessary to increase the pasture area about 40 times for adequate grazing, or to expand it around 20 times by getting additional improvement measures and applying some rain water harvesting techniques and some planting measures. When it was evaluated the basin in terms of land use capability classes, some land use problems were determined. Although only 14.07% of the basin is available for cultivation, around 68% of the basin has been used for agricultural aims for years. The USLE and GIS were used to estimate soil loss in the basin. While the average soil loss was calculated as  $7.66 \text{ t ha}^{-1}$  for the entire basin, soil loss for agricultural, pasture, and shrub had  $9.87$ ,  $3.01$  and  $4.16 \text{ t ha}^{-1}$ , respectively, varying between 0 and  $152.77 \text{ t ha}^{-1}$  yearly. Total soil loss for the general basin is about  $7972.86 \text{ t}$  per year. While 87.52% of the total soil loss is lost from agricultural areas, pasture and shrub land use also contribute to the rate of 9.58 and 2.95%, respectively. When considered in terms of soil depth in the basin, mean soil loss tolerance values are around  $4.5 \text{ t per ha}$ , which are accepted as the threshold level of the basin. This means that 89.79% of the total soil loss occurs over the threshold value.

The land use proposed by the SLUP model was applied in the basin by considering the land use changes, the applications previously mentioned for agricultural, forest, and pasture land use. A final soil loss map of the basin and soil loss distribution was prepared. Agricultural land use in class VI was converted to pasture by reducing 79.13% of the total arable land. Current land use (wheat-fallow) was changed to permanent forage crops (sainfoin, *O. sativa*) applying no tillage or minimum tillage, strip cropping with contour farming, and using suitable mechanization tools for cultivation to reduce soil losses. While C factor was 0.25 for sainfoin, P factor was 0.37 for strip cropping with contour farming. While the P factor was 1.0 with fall plough, the soil tillage method factor was 0.25 for no tillage farming. Soil losses on the

agricultural land decreased from 9.87 to 0.24 t ha<sup>-1</sup>, and the reduction rate was approximately 97.56% considering those applications.

In pasture areas, first- and second-degree precautions were applied to reduce soil loss in addition to the installation of some permanent vegetation to intercept storm water runoff and minimize soil erosion. It was also applied an overgrazing management and improvement studies (seeding, fertilizing) on poor areas are proposed for sustainable management. Pasture areas were increased by converting them from agricultural land at a rate of 216% in the basin. The C factor for pasture area was selected as 0.025. Soil loss in pasture land use was decreased from 3.01 to 0.83 t ha<sup>-1</sup> by means of grazing management, improvement studies, and including some physical precautions.

Shrub land areas were another source of soil loss. This land was a forest before the trees were cut down. After planning, the shrub land was converted to its natural cover plant. The C factor was selected as 0.001 applying forest management. Therefore, soil loss in this land decreased from 4.16 to 0.05 t ha<sup>-1</sup>.

Overall, soil loss was lowered from 7.66 to 0.67 t ha<sup>-1</sup> with the SLUP model across the entire basin, reducing it by approximately 91.25%.

## Author details

Ertuğrul Karas

Address all correspondence to: ekaras@ogu.edu.tr

Department of Biosystem Engineering, Faculty of Agriculture, University of Osmangazi, Eskişehir, Turkey

## References

- [1] Wischmeier WH, Smith DD (1978) Predicting rainfall erosion losses: a guide to conservation farming, USDA Handbook: No. 537.
- [2] Koreleski K (2008) The influence of field factors on the intensity of water erosion exemplified by a mountain village (in Polish). *Infrastructure and Ecology of Rural Areas*, 3, 5–12.
- [3] Pretorius JR, Cooks J (1989) Soil loss tolerance limits: an environmental management tool. *Geojournal*, July 1989, 19(1), 67–75. doi:10.1007/BF00620551.
- [4] White AF (2002) Determining mineral weathering rates based on solid and solute weathering gradients and velocities: application to biotite weathering in saprolites. *Chemical Geology* 190, 69–89.

- [5] Williams JR, Dyke PT, Jones CA (1982) EPIC a model for assessing the effects of erosion on soil productivity. *Analysis of ecological systems: state of the art in ecological modelling*, pp. 553–572, Elsevier, Amsterdam.
- [6] Jain SK, Dolezal F (2000) Modeling soil erosion using EPIC supported by GIS, Bohemia, Czech Republic. *Journal of Environmental Hydrology*, 8, 1–11.
- [7] Arghinus C, Arghinus V (2011) The quantitative estimation of the soil erosion using USLE type ROMSEM model. Case-study—the Codrului Ridge and Piedmont (Romania). *Carpathian Journal of Earth and Environmental Sciences*, 6(2), 59–66.
- [8] Bathrellos GD, Skilodimou HD, Chousianitis KG (2010) Soil erosion assessment in Southern Evia Island using USLE and GIS. *Bulletin of the Geological Society of Greece*. In: *Proceedings of the 12th International Congress*, Patras, May, (3), 1572.
- [9] Bosco C, Rusco E, Montanarella L, Panagos P (2009) Soil erosion in the Alpine area: risk assessment and climate change. *Studi Trentini di Scienze Naturali*, 85, 117–123.
- [10] Cai C, Ding S, Shi Z (2000) Study of applying USLE and geographical information system IDRISI to predict soil erosion in small watershed. *Journal of Soil and Water Conservation*, 14, 19–24
- [11] Demczuk P (2009) Conform model USLE to automatic mapping intensity of soil erosion in the Bystrzanka Mountain Catchment (Flysh Carpathian) (in Polish). In: W. Bochenek and M. Kijowska (Eds.) *The integrated monitoring of the environment*, pp 239–244. Szymbark: IGiPZ PAN.
- [12] Devatha CP, Deshpande V, Renukprasad MS (2015) Estimation of Soil loss Using USLE Model for Kulhan Watershed, Chattisgarh—a case study. In: *International conference on water resources, coastal and ocean engineering*.
- [13] Drzewiecki W (2006) GIS and remote sensing data application to the assessment of land-use conditions (in Polish). *Geoinformatica Polonica*, 8, 7–22.
- [14] Elci S, Selcuk P (2014) Effects of basin activities and land use on water quality trends in Tahtali Basin, Turkey. *Environmental Earth Sciences* (2013)68, 1591–1598.
- [15] Erdogan EH, Erpul G, Bayramin İ (2007) Use of USLE/GIS methodology for predicting soil loss in a semiarid agricultural watershed. *Environmental Monitoring and Assessment*, August, 131(1), 153–161.
- [16] Fıstıkoglu O, Harmancıoglu NB (2002) Integration of GIS with USLE in assessment of soil erosion. *Water Resources Management*, 16, p.447.
- [17] Igwe CA, Akamigbo FOR, Mbagwu JSC (1999) Application of a SLEMSA and USLE erosion models for potential erosion hazard mapping in south-eastern Nigeria. *International Agrophysics*, 13, 41–48.
- [18] Irvem A, Topaloglu F, Uygur V (2007) Estimating spatial distribution of soil loss over Seyhan River Basin in Turkey. *Journal of Hydrology*, 336, 30.

- [19] Karaburun A (2010) Estimation of C factor for soil erosion modeling using NDVI in Buyukcekmece watershed. *Ozean Journal of Applied Sciences*, 3(1).
- [20] Karaş E (2005) Sustainable management of Küçükemalı and Güvenç basins according to water and sediment yield. PhD. Thesis. Ankara University, Graduate School of Natural and Applied Sciences, Department of Agricultural Structures and Irrigation, pp 236, Ankara (in Turkish).
- [21] Karaş E, Öztürk F (2013) Land use planning of Küçükemalı Pond Basin according to soil conservation measures. *Journal of Agricultural Faculty of Gaziosmanpasa University*, 2011, 28(2), 127–134, Tokat (in Turkish).
- [22] Koreleski K (2008) The influence of field factors on the intensity of water erosion exemplified by a mountain village (in Polish). *Infrastructure and Ecology of Rural Areas*, 3, 5–12.
- [23] Lastoria B, Misericocchi F, Lanciani A, Monacelli G (2008) An estimated erosion map for the Aterno-Pescara river basin. *European Water*, 21/22, 29–39.
- [24] Mellerowicz KT, Rees HW, Chow TL, Ghanem I (1994) Soil conservation planning at the watershed level using the Universal Soil Loss Equation with GIS and microcomputer technologies: a case study. *Journal of Soil and Water Conservation*, March-April, 49(2), 194–200.
- [25] Pacheco FAL, Varandas SGP, Sanches LF, Valle Junior RF (2014) Soil losses in rural watersheds with environmental land use conflicts. *Science of the Total Environment*, 1 July, 485–486, 110–120. doi:10.1016/j.scitotenv.2014.03.069.
- [26] Perović V, Životić L, Kadović R, Đorđević A, Jaramaz D, Mrvić V, Todorović M (2013) Spatial modelling of soil erosion potential in a mountainous watershed of South-eastern Serbia. *Environmental Earth Sciences*, January, 68(1), 115–128. doi:10.1007/s12665-012-1720-1.
- [27] Ştefanescu L, Constantin V, Surd V, Ozunu A, Vlad ŞN (2011) Assessment of soil erosion potential by the USLE method in Roşia montană mining area and associated natech events. *Carpathian Journal of Earth And Environmental Sciences*, 6(1), 35.
- [28] Wang X, Zhao X, Zhang Z, Yi L, Zuo L, Wen Q, Liu F, Xu J, Hu S, Liu B (2016) Assessment of soil erosion change and its relationships with land use/cover change in China from the end of the 1980s to 2010. *Catena*, February, 137, 256–268. doi:10.1016/j.catena.2015.10.004.
- [29] Yue-qing X, Jian P, Xiao-mei S (2009) Assessment of soil erosion using RUSLE and GIS: a case study of Maotiao River watershed, Guizhou Province, China. *Environmental Geology*, 56, 1643–1652. doi:10.1007/s10661-007-9894-9.
- [30] Zhu M (2015) Soil erosion assessment using USLE in the GIS environment: a case study in the Danjiangkou Reservoir Region, China. *Environmental Earth Science* 73, 7899–7908. doi:10.1007/s12665-014-3947-5.

- [31] Životić L, Perović V, Jaramaz D, Đorđević A, Petrović P, Todorović M (2012) Application of USLE, GIS, and remote sensing in the assessment of soil erosion rates in Southeastern Serbia. *Polish Journal of Environmental Studies*, 21(6), 1929–1935.
- [32] Bhattacharyya P, Bhatt VK, Mandal D (2008) Soil loss tolerance limits for planning of soil conservation measures in Shivalik–Himalayan region of India. *Catena*, 73(1), 117–124. doi:10.1016/j.catena.2007.10.001.
- [33] Johnson LC (1987) Soil loss tolerance fact or myth. *Journal of Soil and Water Conservation*, 42, 155–160.
- [34] Jones OR, Eck HV, Smith SJ, Coleman GA, Hauser VL (1985) Runoff, soil, and nutrient losses from rangeland and dry-farmed cropland in the southern high plains. *Journal of Soil and Water Conservation*, January/February, vol. 40(1), 161–164.
- [35] Mandal D, Sharda VN, Tripathi KP (2010) Relative efficacy of two biophysical approaches to assess soil loss tolerance for Doon Valley soils of India. *Journal of Soil and Water Conservation*, January/February, 65(1), 42–49.
- [36] Mannering JV (1981) The use of soil loss tolerances as a strategy for soil conservation. In: Morgan, R.P.C. (Eds.) *Soil conservation. Problems and prospects*, pp 337–350. John Wiley, Chichester.
- [37] McCormack DE, Young KK, Kimberlin LW (1981) Technical and societal implications of soil loss tolerance. In: R.P.C. Morgan (ed.) *Soil conservation, problems and prospects*. John Wiley and Sons, New York, NY.
- [38] Pierce FJ, Larson WE, Dowdy RH (1984) Soil loss tolerance: maintenance of long-term soil productivity. *Journal of Soil and Water Conservation*, 39, 136–138.
- [39] Schertz DL (1983) The basis for soil loss tolerances. *Journal of Soil and Water Conservation*, 38(1), 10–14
- [40] Skidmore EL (1982) Soil loss tolerance. In: *Determinants of soil loss tolerance*, pp 87–93. ASA Spec. Publ. 45. ASA, Madison, WI.
- [41] Smith RM, Stamey WL (1964) How to establish erosion tolerances. *Journal of Soil and Water Conservation*, May-June, 19(3).
- [42] Smith RM, Stamey WL (1965) Determining the range of tolerable erosion. *Soil Science*, 100, 414–424.
- [43] Sparovek G, DeMaria IC (2003) Multiperspective analysis of erosion tolerance. *Scientia Agricola*, Abr/Jun, 60(2), 409–416, doi:10.1590/S0103-90162003000200029.
- [44] Sparovek G, De Yong VLQ (1997) Definition of tolerable soil erosion values. *Revista Brasileira de Ciência do Solo*, 21, 467–471.
- [45] Sparovek G, Schnug E (2001) Temporal erosion-induced soil degradation and yield loss. *Soil Science Society of America Journal*, 65, 1479–1486.

- [46] Sparovek G, Weill MM, Ranieri SBL, Schnug E, Silva EF (1997) The life-time concept as a tool for erosion tolerance definition. *Sci. Agric. Piracicaba*, 54 (Numero Especial), 130–135.
- [47] Verheijen FGA, Jones RJA, Rickson RJ, Smith CJ (2009) Tolerable versus actual soil erosion rates in Europe. *Earth-Science Reviews*, 94(1–4), May, 23–38. doi:10.1016/j.earscirev.2009.02.003.
- [48] Alewell C, Egli M, Meusburger K (2014) An attempt to estimate tolerable soil erosion rates by matching soil formation with denudation in Alpine grasslands. *Journal of Soils and Sediments* (H. Special issue: soil formation and weathering in time and space), 15(6), 1383–1399. doi:10.1007/s11368-014-0920-6.
- [49] Anderson SP (2005) Glaciers show direct linkage between erosion rate and chemical weathering fluxes. *Geomorphology*, 67, 147–157. doi:10.1016/j.geomorph.2004.07.010.
- [50] Bouchard M, Jolicoeur S (2000) Chemical weathering studies in relation to geomorphological research in southeastern Canada. *Geomorphology* 32, 213–238. doi:10.1016/S0169-555X(99)00098-7.
- [51] Friend JA (1992) Achieving soil sustainability. *Journal of Soil and Water Conservation*, 47, 156–157.
- [52] Fujisaka S (1994) Learning from six reasons why farmers do not adopt innovations intended to improve sustainability of upland Agriculture. *Agricultural Systems*, Edinburgh, 46, 409–425.
- [53] Green EG, Dietrich WE, Banfield JF (2006) Quantification of chemical weathering rates across an actively eroding hillslope. *Earth and Planetary Science Letters*, 242, 155–169.
- [54] Heimsath AM, Chappell J, Dietrich WE, Nishiizumi K, Finkel RC (2002) Late Quaternary erosion in southeastern Australia: a field example using cosmogenic nuclides. *Quaternary International*, 83–85, 169–185.
- [55] Heimsath AM, Dietrich WE, Nishiizumi K, Finkel RC (1997) The soil production function and landscape equilibrium. *Nature*, 388, 358–361.
- [56] Heimsath AM, Dietrich WE, Nishiizumi K, Finkel RC (1999) Cosmogenic nuclides, topography, and the spatial variation of soil depth. *Geomorphology*, 27, 151–172.
- [57] Heimsath AM, Dietrich WE, Nishiizumi K, Finkel RC (2001) Stochastic processes of soil production and transport: erosion rates, topographic variation and cosmogenic nuclide in the Oregon coast range. *Earth Surface Processes and Landforms*, 26, 531–552.
- [58] Kliment'ev AI, Tikhonov VE (2001) Ecohydrological analysis of soil loss tolerance in agrolandscapes. *Soil Erosion*, 34(6), 673–682.
- [59] Miklos AAW (1992) *Biodynamique d'une couverture pédologique dans da region de Botucatu (Bresil-SP)*. Ph D Thesis, Université de Paris. Paris, France, 1995.

- [60] Minasny B, McBratney AB (2001) A rudimentary mechanistic model for soil formation and landscape development II. A two-dimensional model incorporating chemical weathering. *Geoderma*, 103, 161–179.
- [61] Owens LB, Watson JP (1979) Rates of weathering and soil formation on granite in Rhodesia. *Soil Science Society of America Journal*, 43(1), 160–166. doi:10.2136/sssaj1979.03615995004300010031x.
- [62] Peter BS, Donald MF, Thomas WG, Katherine M, Susan LB (2004) Rate of weathering rind formation on Costa Rican basalt. *Geochimica ET Cosmochimica Acta*, 68(7), 1453–1472. doi:10.1016/j.gca.2003.09.007.
- [63] Small EE, Anderson RS, Hancock GS (1999) Estimates of the rate of regolith production using <sup>10</sup>Be and <sup>26</sup>Al from an alpine hillslope. *Geomorphology*, 27(12), 131–150.
- [64] Wakatsuki T, Rasyidin A (1992) Rates of weathering and soil formation. *Geoderma*, 52, 251–264. doi:10.1080/00380768.1993.10416984.
- [65] White AF (2002) Determining mineral weathering rates based on solid and solute weathering gradients and velocities: application to biotite weathering in saprolites. *Chemical Geology*, 190, 69–89.
- [66] Karaş E, Oğuz İ (2015) A new approach to determine land use planning and soil conservation measures based on soil erosion classification. *Carpathian Journal of Earth and Environmental Sciences*, 10(2).
- [67] Oğuz İ, Karaş E, Susam T, Tetik A, Noyan ÖF, Akar Ö (2006) Tokat—Artova Çelikli havzasında toprak bozulmasının belirlenerek, sürdürülebilir bir tarım için havzanın planlanması, Tarım ve Köyişleri Bakanlığı, Tarımsal Araştırmalar Genel Müdürlüğü, TAGEM–BB–TOPRAKSU–2006/19, Enstitü Yayın No: 230, Teknik Yayın No: 45, 116 s. Tokat (in Turkish).
- [68] Nelson DW, Sommers LE (1982) Total carbon, organic carbon, and organic matter. In: *Methods of soil analysis, part 2, 2nd ed.*, ed. A. L., pp 539–579. Madison: ASA and SSSA.
- [69] McLean EO (1982) Soil pH and lime requirement. In: *Methods of soil analysis, part 2, 2nd ed.*, ed. A. L., pp 199–224. Madison: ASA and SSSA.
- [70] Richards LA (1954) *Diagnosis and improvement saline and alkali soils (USDA Agricultural Handbook No. 60)*. Washington, D.C.: U.S. Government Printing Office.
- [71] Rhoades JD (1982) Cation exchange capacity. In: *Methods of soil analysis, part 2, 2nd ed.*, ed. A.L., pp 149–157. Madison: ASA and SSSA.
- [72] Gee GW, Bauder JW (1986) Particle size analysis. In: *Methods of soil analysis, part 1, 2nd ed.*, ed. A. Klute, pp 383–411. Madison: ASA.
- [73] Black CA (1965) *Methods of soil analysis, part 2: Chemical and microbiological properties*. Madison: ASA.

- [74] Klute A (1986) Water retention: laboratory methods. In: Black, C.A., ed. Methods of soil analysis. I. Physical and mineralogical methods. Madison: American Society of Agronomy, Soil Science Society of America, pp 635–662.
- [75] Wischmeier WH, Johnson CB, Cross BV (1971) A soil erodibility monograph for farmland and construction sites. *Journal of Soil and Water Conservation*, 26, 189–193.
- [76] Foster GR, McCool DK, Renard KG, Moldenhauer WC (1981) Conversion of the universal soil loss equation to SI metric units. *Journal of Soil and Water Conservation*, 36(6), 355–359.
- [77] Oğuz İ (1997) K, R, C and P factors of USLE equation in Koluvial soil group at Tokat province. Research Report, 102, 69–79, Ankara (in Turkish).
- [78] ESRI (2003) GIS standards and interoperability. *ArcNews*, ESRI, Spring, 25(1),.
- [79] Moore I, Burch G (1986) Physical basis of the length-slope factor in the universal soil loss equation. *Soil Science Society of America Journal*, 50, 1294–1298.
- [80] Çanga MR (1995) Soil and water conservation. University of Ankara, Faculty of Agriculture, Publication no. 1386, p 118. Ankara. (in Turkish).
- [81] Stamey WL, Smith RM (1964) A conservation definition of erosion tolerance. *Soil Science*, 97(3), 183–186.
- [82] Karaş E (2007) Application of SWAT, USLE and RUSLE on Güvenç basin. *Soil and Water Resources Research Institute of Eskişehir*, Research report: TAGEM-BB-TOP-RAKSU-2007/43. p 123. Eskişehir (in Turkish).
- [83] Altıntaş G (2014) Production inputs and costs of some agricultural productions grown in Tokat, Amasya, Yozgat and Sivas provinces. *Agricultural Research Institute of Tokat*, No: 261-P23. Tokat (in Turkish).
- [84] Elçi Ş, Ekiz H, Sancak C (1996) Problems of sainfoin production in Turkey. The third congress of forage crops, June 16–18, Erzurum (in Turkish).
- [85] Miller DA, Hoveland CS (1995) Other temperate legumes. In: R. F. Barnes, D. A. Miller and C. J. Nelson (ed.) 5th ed. *Forages: an introduction to grassland agriculture*. p. 276. Iowa State Univ. Press, Ames.
- [86] Anonymous (2015b) *Onobrychis*. <https://en.wikipedia.org/wiki/Onobrychis>. Accessed 08 November 2015.



---

# Modelling Agri-Environmental Measures for Minimizing Soil Erosion While Protecting Valuable Agricultural Land

---

Matjaž Glavan, Polona Ojsteršek Zorčič and  
Marina Pintar

Additional information is available at the end of the chapter

<http://dx.doi.org/10.5772/63380>

---

## Abstract

Erosion processes in river basins and the consequent transport of sediment and sediment-bound pollutants to reservoirs cause hydromorphological changes and eutrophication, as well as the loss of reservoir storage capacity. This chapter deals with the optimal selection and implementation of agri-environmental measures in river basins to reduce sediment yield and load. The main aim of this was to contribute to more efficient river basin management by minimizing soil erosion, while protecting valuable agricultural land. This includes implementing measures at the most critical source areas, where they are most effective and necessary. The river Ledava basin was selected as the study area. It covers an area of 105 km<sup>2</sup> in northeast Slovenia and southeast Austria. The results of monitoring the river Ledava discharge reveal that the average annual concentration of sediment in the water body exceeded the recommended value of 25 mg/l by 46.7%. Using the Soil and Water Assessment Tool (SWAT), we were able to determine critical source areas and simulate the effects of eight different agri-environmental scenarios on sediment yield reduction. The results show that critical source areas comprise 12% of the river basin. Most of the scenarios reduced sediment load in the river Ledava where steeper slopes in the sub-basin prevail and where high average annual sediment transport from hydrologic response units (HRUs) has been identified. The impact of the scenarios on the average annual sediment load (ton/year) in the river was lower than for the sediment yield (ton/ha) at the HRU level.

**Keywords:** erosion, sediment, agriculture, SWAT, agri-environmental measures

## 1. Introduction

Soil erosion has a significant impact regarding the degradation of valuable agricultural land, where a combination of rainfall, soil type, slope properties, and land management can result in extensive loss of soil and associated nutrients [1, 2]. At the same time, erosion processes in the river basin and the transport of sediment and sediment-bound pollutants cause hydromorphological changes and eutrophication of surface water [3, 4]. Although erosion is a natural process, the rate of soil loss is site specific and can significantly increase with inappropriate land management (e.g., removal of vegetation cover, overgrazing, fire, mineralization of organic matter, and compaction through mechanization) and climate change [5]. According to the Food and Agriculture Organization of the United Nations (FAO), erosion resulting from human activities is 100–700 times faster than the natural rate (0.1–1.0 ton/ha/year) [6]. Theoretically, soil erosion should be maintained at a rate that is equal to or below the natural rate at which new soil forms [5]. However, this balance is difficult to achieve because of differences in soil, slopes, land cover, and climate that are site dependent. Due to the Soil Strategy for England [7], estimated erosion rates in England and Wales range between 1 and 20 ton/ha/year for most agricultural fields. The mean soil loss rate in the European Union's erosion-prone land (agricultural land, forests, and semi-natural areas) has been found to be 2.46 ton/ha/year, resulting in a total soil loss of 970 Mt annually [8]. In Slovenia, about 4 ton/ha of soil are lost on average every year [9].

In order to mitigate the on-site and off-site effects of erosion processes, several control measures have been designed around the world. Measures adapted to specific farming systems to improve the environment are termed agri-environmental measures (AEM), adopted as the instrument of the Common Agricultural Policy. The introduction of the Water Framework Directive (WFD, 2000/60/EC) has increased interest in soil conservation, mainly because of the impact of runoff and associated sediment and pollutants on water quality [1]. Policy interventions (Good Agricultural and Environmental Condition, GAEC) over the last decade in Europe have reduced the soil loss rate by 9.5% on average and by 20% for arable land [8]. Many other studies report the positive effect of measures (rotation, conservation tillage, cover crops, contour farming, vegetative filter strips, terracing, etc.) on soil loss reduction at the field scale [1, 10–15] or the river basin scale [16–21]. As the performance of measures is highly dependent on local circumstances (e.g., soil type, slope, crop and climate), combining different measures can lead to a greater reduction of soil loss and sediment yield [16, 19, 22].

AEM can, however, also produce negative socioeconomic effects [20], because to achieve the water quality target under the WFD, the extent of arable land should be reduced from 77.2 to 46%, pasture increased from 4 to 15% and afforestation from 10 to 21%. Similar negative economic effects were reported by [23].

To avoid negative economic effects and to achieve the maximum possible benefit, the allocation of selected measures should focus on areas where they are most effective and necessary. The optimal locations for AEM are areas that contribute disproportionately high sediment and nutrient loads, which are often referred to as critical source areas (CSAs). These areas have a particular type of soil, land use, land management, and slope and represent an overlap with areas prone to generating high volumes of runoff and erosion [24]. The use of river basin

models, such as the Soil and Water Assessment Tool (SWAT) [25], can help in identifying CSAs and prioritizing areas for the cost-effective implementation of AEM [26–28].

Many studies worldwide have used SWAT to evaluate the impact of land-use scenarios and mitigation measures on water quality and sediment yield reduction [16, 17, 19, 29–32]. The assessment of AEM using SWAT can ensure the most cost-effective allocation of measures, minimizing sediment yield, while protecting valuable agricultural land.

This chapter deals with the optimal selection and implementation of AEM in a river basin, in order to reduce sediment yields from land surfaces and sediment loads in the river. The main aim of this study was to contribute to more efficient river basin management by minimizing soil erosion while protecting valuable agricultural land. This includes the identification of CSA, where AEM are most effective and necessary.

## 2. Materials and methods

### 2.1. Study site

The river Ledava basin was selected for the study. It covers an area of 105 km<sup>2</sup> in northeast Slovenia and southeast Austria (**Figure 1**). Some 33.7 km<sup>2</sup> lies in Austria and 71.6 km<sup>2</sup> in Slovenia. The highest elevation on the Austrian side is 598 m above sea level, in Gleichenberger Kogel, and on the Slovenian side, 418 m above sea level at the Sotinski breg. Over a third of the basin comprises arable land (37.8%), followed by forests (36.7%), meadows (12.1%), orchards (3.4%), and other land use (10%). The otherwise homogenous hilly landscape is steeper in the upper part of the river basin. Inclinations between 0–11, 11–24, 24–35, 35–50, and over 50% represent, respectively, 35.5, 37.0, 16.1, 7.9, and 3.5% of the study area. Poorly adhering tertiary and quaternary sediments, the topographical properties and the exchange of soils with low and high permeability increase the possibility of landslides and erosion processes. Landslides in this area are small in extent but numerous, with the majority (48.9%) occurring on inclinations at or above 9° or 15.4% [33, 34].

The basin area consists of higher and steeper terrain in the headwaters of the river Ledava in Austria, as a result of stiffer geological composition of phyllite carboniferous slates and basaltic tuff of volcanic origin, and homogeneous hills in Slovenia, dominated by tertiary marlstone and claystone. The bottom of the valley is covered with alluvial clay and sandy clay sediments. Almost a third (27.07%) of the area's soil consists of pseudogley district brown soils and district brown soils on Pliocene sediments, which are washed out and not very fertile. Because the soil in the river valley is relatively impermeable, the density of the river channels network (**Figure 1**) is considerably higher (1.77–2.35 km/km<sup>2</sup>) than the average in Slovenia (1.33 km/km<sup>2</sup>). The river Ledava (Limbach in German) is a left tributary of the Mura River and originates in the village Pichl, Steiermark, (in the Kapfenstein municipality) at an altitude of 430 m. The length of the river to the mouth of the reservoir is 17.4 km, 8 km of which runs through Austria. The ecomorphological situation [35] of the headwater part of the river's network channels is evaluated as sustainably managed. In its central section, the river is channelized along agricultural areas, with fortified banks managed as grassland and with occasional shrub cover.

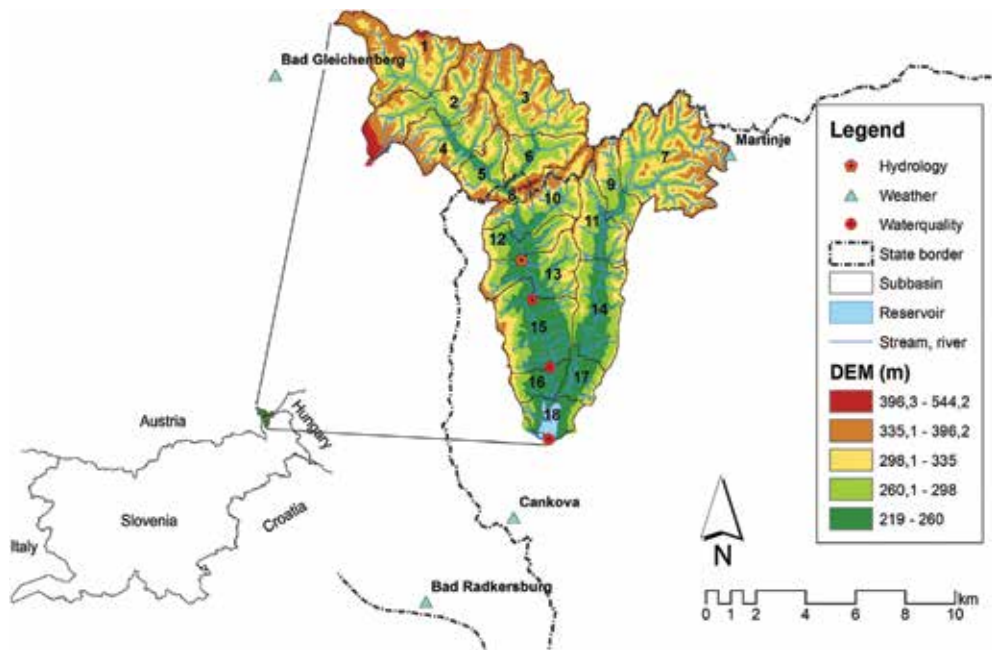


**Figure 1.** The river Ledava basin study site.

The river Ledava basin area has a continental climate, with average annual precipitation between 800 and 900 mm, falling mainly in the summer as showers and thunderstorms. The highest average temperatures (2003–2014) were measured in July (21°C) and the lowest in January (-0.1°C). The hydrological regime of the river is characterized by a rain–snow mixture, with the highest flows in early spring and late autumn. Low flows in the summer are the result of higher temperatures, higher evapotranspiration, and rainfall interception by vegetation. The maximum average monthly river flows (1993–2013) were measured between December and March (-0.47 to 0.42 m<sup>3</sup>/s), with the highest river flow recorded in August 2005 (29.3 m<sup>3</sup>/s). Due to the rapid hydrological response in the basin, the river Ledava flooded regularly. In order to protect the city of Murska Sobota and the cultivated land along the river, the Ledavsko jezero reservoir was built in 1977.

The results of simultaneous monitoring from June 2013 to May 2014 on the Ledava river and the Ledavsko reservoir reveal that the average annual concentration of sediment in both water bodies exceeded the recommended value (Fish Directive, 2006/44/EC) of 25 mg/l by 46.7% in the river and by 73.3% in the reservoir.

## 2.2. Model description

We selected the SWAT to evaluate the effects of different AEM on sediment yield and to evaluate CSAs in the river Ledava basin. SWAT is a physically based, spatially distributed basin scale model developed by the Agricultural Research Service (ARS) of the US Department of Agriculture (USDA) [36]. The main objective of the model development was to support river

basin managers in evaluating the effects of alternative management decisions concerning water resources and nonpoint-source pollution in large river basins over a longer time span [25]. In SWAT, a river basin is divided into sub-basins based on topography and river networks. Sub-basins are further divided into hydrologic response units (HRUs), based on unique land cover, soil, slope, and management practice combinations. Processes such as surface runoff and sediment yield are simulated for each HRU, and the contributions of each HRU are then aggregated for the sub-basin by a weighted average. Water is then routed to the outlet of the river basin. For this study, we used the SWAT 2012 model version, ArcGIS 10.0 software and the ArSWAT 2012.10\_0.15 interface.

Erosion and sediment yields were estimated for each HRU using the modified universal soil loss equation (MUSLE). Whereas USLE uses rainfall as an indicator of erosive energy, MUSLE uses the amount of runoff to simulate erosion and sediment yields. This increases the prediction accuracy of the model, eliminates the need for a delivery ratio, and provides an estimation of single storm sediment yield [37]. MUSLE is represented by Eq. (1):

$$sed = 11.8 \times (Q_{surf} \times q_{peak} \times area_{hru})^{0.56} \times K_{USLE} \times C_{USLE} \times P_{USLE} \times LS_{USLE} \times CFRG \quad (1)$$

where *sed* is the sediment yield on a given day (metric tons),  $Q_{surf}$  is the surface runoff volume (mm H<sub>2</sub>O/ha),  $q_{peak}$  is the peak runoff rate (m<sup>3</sup>/s),  $area_{hru}$  is the area of the HRU (ha),  $K_{USLE}$  is the USLE soil erodibility factor [(0.013 ton/m<sup>2</sup>/h)/(m<sup>3</sup>-ton/cm)],  $C_{USLE}$  is the USLE cover and management factor,  $P_{USLE}$  is the USLE support practice factor,  $LS_{USLE}$  is the USLE topographic factor, and *CFRG* is the coarse fragment factor.

Each of these factors can be adjusted to represent the adoption of AEM such as slope terracing, contour farming, field crop strip sowing, and residue management. Overland flow routings in SWAT model are controlled by curve number (CN) and coefficient of Manning's roughness (*n*). AEM can be represented by modifications of CN and *n* values affecting decrease in surface runoff by increasing infiltration (e.g., contour farming, slope terracing, and field crop strip sowing) and flow rate decrease by runoff interception (e.g., crop residue management, and field crop strip sowing), respectively, [38]. The effectiveness of vegetated filter strips (*VFS*) varies for different forms of sediments and nutrients. A single *VFS* is for modelling of concentrated flow split into two segments. In segment one, 90% of the *VFS* area obtains the least flow and segment two with 10% of area obtaining the major runoff (25–75%). Three parameters can be modified in the SWAT model to adapt modelled *VFS* design. The first one is drainage of the spatial area-to-*VFS* area ratio (*DAFSratio*), the second is percentage of the field drained by the most heavily loaded 10% of the *VFS* (*DFcon*), and the third is percentage of the flow through the most heavily loaded 10% of the *VFS* that is fully channelized (*CFfrac*) [28]. AEM can be simulated for specific dates and by explicitly defining the appropriate management parameters for each HRU.

### 2.3. Database and data analysis

Recently available geographical information system (GIS) maps for topography, land use, and soils for Slovenia and Austria were used to represent the area (**Table 1**). The stream network was defined based on a predefined stream network obtained from the Environment Agency of the Republic of Slovenia (ARSO). The topographic information was used for automatic delineation of the river basin. Land use and soil maps were superimposed over the basin.

Data type	Scale	Source	Data description
<b>Topography (DEM raster)</b>	Slovenia: 25 m Austria: 1 m	The Surveying and Mapping Authority of the Republic of Slovenia, GIS-Steiermark, and GIS-Burgenland	Elevation, overland and channel slopes, lengths
<b>Soils</b>	Slovenia: 1:25000 Austria: 1 km Raster	Ministry of Agriculture, Forestry and Food of the Republic of Slovenia; Biotechnical Faculty (University of Ljubljana) Austrian Research Centre for Forests	Spatial soil variability, soil types, and properties
<b>Land use</b>	Slovenia: 1 m Raster (Graphical Units of Agricultural Land) Austria: 1:5000	Slovenia: Ministry of Agriculture, Forestry and Food of the Republic of Slovenia Austria: GIS Steiermark, GIS Burgenland, and Municipalities (St. Anna am Aigen, Kapfenstein, Neuhaus am Klausenbach)	Land use, Land cover classification, and spatial representation
<b>Land management information</b>	/	Chamber of Agriculture and Forestry of Slovenia-Agricultural advisory service in Cankova	Crop rotations (harvesting, planting, management), fertilizer application (rates and time)
<b>Weather</b>	Slovenia 3 and Austria 2 stations	Environment Agency of the Republic of Slovenia (ARSO), Zentralanstalt für Meteorologie und Geodynamik (ZAMG), Austria	Daily precipitation, Temperature (max., min.), relative humidity, wind, solar radiation from 2003-2014
<b>River discharge</b>	1 Point	Environment Agency of the Republic of Slovenia	Daily flow data (m <sup>3</sup> /s) from 2003 to 2014
<b>Waste water treatment plants</b>	Slovenia: 3 Austria: 2	Environment Agency of the Republic of Slovenia; Land Steiermark-Amt der Steiermärkischen Landesregierung	Average daily discharge of orgP, sediment and orgN
<b>Water quality</b>	Two monitoring stations (Pertoča and Ledavsko jezero)	Bi-weekly monitoring	TSS, NO <sub>3</sub> <sup>-</sup> , NO <sub>2</sub> <sup>-</sup> , PO <sub>4</sub> <sup>2-</sup> TP, TN, temperature, dissolved O <sub>2</sub> (2013-2014)

**Table 1.** Model input data sources for the river Ledava sub-basin.

Data for 11 years (2003–2014) of daily observed precipitation, the temperature from five stations and the relative humidity, wind speed, and solar radiation data from two stations

were obtained from the ARSO and Zentralanstalt für Meteorologie und Geodynamik (ZAMG) in Austria. In order to better understand the endpoint and transport of sediment and nutrients, data for typical management practices such as crop growth, fertilizer application, and tillage operations for different land use were gathered from the Chamber of Agriculture and Forestry of Slovenia—Agricultural Advisory Service, in Cankova.

Because the water quality data provided by ARSO were insufficient, bi-weekly water quality monitoring was carried out for 1 year (2013–2014). Concentrations of total suspended sediments (mg/l) were measured bi-weekly, from June 2013 to May 2014, at the sampling point of Pertoča (46°46′26,52" N 16°2′24,64" E), located on the river Ledava about 1.5 km upstream of the Ledavsko jezero reservoir. In total, 94 samples were taken and analyzed at the National Laboratory of Health, Environment and Food and Erico d.o.o.

## 2.4. Model setup and evaluation

For this study, the SWAT model was built up by dividing the river Ledava basin into 18 sub-basins (**Figure 1**) and 5758 HRUs. A warm-up period of 3 years (2003–2005) was used to initialize the model. For the calibration, data from 2006 to 2010 were used for flow calibration and from 2011 to 2013 for validation. For sediment calibration, data from 2013 to 2014 was used. Due to the small amount of measured sediment data over 1 year (June 2013–June 2014), validation for sediment was not performed.

The first step in the calibration and validation process in SWAT is to determine the most sensitive parameters for a given basin. Sensitivity analysis is helpful for identifying and ranking parameters that have a significant impact on specific model outputs, such as streamflow or sediment [39]. For the sensitivity analysis and calibration, special software called SWAT-CUP is used, which offers semi-automatic or combined manual/automatic calibration. Among the algorithms included in SWAT-CUP, the most efficient to calibrate a project is Sequential Uncertainty Fitting (SUFI-2), the use of which has been found to require fewer simulations to complete a calibration/uncertainty project [40] and is highly recommended for the calibration of SWAT models [25].

In this study, sensitivity analysis was performed using measured data for the river Ledava. The analysis was carried out for average daily flow and sediments. We used the default lower and upper bound parameter values for all parameters [37]. **Table 2** illustrates the parameters that have the greatest impact on the model when they are changed. The sensitivity analyses demonstrate the great importance of the parameters that are associated with surface runoff and snow (SFTMP, SMTM, TIMP, SOL\_AWC, SURLAG, and CN2) and channel routing (CH\_BNK\_BD, CH\_COV, SPEXP, and SPCON).

The most sensitive parameters were used to perform model calibration. Calibration is a process to better parameterize a model to a given set of local conditions, thereby reducing prediction uncertainty. During calibration, parameters are varied within an acceptable range until a satisfactory correlation is achieved between measured and simulated data [18, 25]. In this study, calibration of the model was performed for flow and sediment on a daily and monthly basis.

	Parameters	Definition	Process	Range	Sensitivity rank
<b>Stream flow</b>	CN2.mgt	SCS runoff curve number for moisture condition 2	Runoff	35-98	1
	SURLAG.bsn	Surface runoff lag time	Runoff	0-12	2
	SOL_AWC(...).sol	Available water capacity of the soil layer	Soil	0-0.3	3
	TIMP.bsn	Snow pack temperature lag factor	Snow	0.01-1	4
	SFTMP.bsn	Snowfall temperature	Snow	-5 to 5	5
	SMTMP.bsn	Snow melt base temperature	Snow	-5 to 5	6
<b>Sediment</b>	SPCON.bsn	Calculating maximum amount of sediment reentrained	Channel	0-0.01	1
	SPEXP.bsn	Calculating sediment reentrained in channel sediment routing	Channel	1-1.5	2
	CH_COV1.rte	Channel cover factor	Channel	-0.001 to 1	3
	CH_BNK_BD.rte	Bulk density of channel bank sediment	Channel	1.1-1.9	4

**Table 2.** Parameters identified during sensitive analysis to be sensitive to changes.

The model performance for river flow and sediment base simulation was tested with graphical comparison and with the help of objective functions commonly used in hydrological studies, such as the Pearson coefficient of correlation ( $R^2$ ), Nash–Sutcliffe simulation efficiency ( $E_{NS}$ ), and Percent bias ( $PBIAS$ ) [41]. Several authors [20, 36, 42] provide further discussions regarding the strengths and weaknesses of using  $R^2$ ,  $E_{NS}$ , and  $PBIAS$ .

## 2.5. Scenarios for AEM

In order to achieve “good ecological potential” in accordance with the Water Framework Directive (2000/60/EC) and Fish Directive (2006/44/EC), management measures have to be undertaken. Choosing measures often present a problem, because their effectiveness will depend on the type and source of pollution, as well as on the size and characteristics of the drainage area. At the same time, measures should be cost-effective, with minimum implementation and maintenance costs, with long-term effectiveness and without requiring major interventions in the area.

Based on a literature review [43], a list of 13 erosion AEM was proposed (cover crops, crop rotation management, conservation tillage, strip cropping, residue management, grassland conversion, vegetative filter strips, grassed waterways, riparian buffer strips, terracing, sedimentation basins, bank erosion protection, and check dams). Due to the heterogeneous characteristics of the study area, climatic conditions, ways of implementing the measures, different methods of measurement, capabilities of the model, and statements in relevant literature, we considered a set of measures as guidelines for the selection of scenarios. For the final selection of measures, we took into consideration the following five criteria:



1. Land use, crop production management, and technologies;
2. Landscape characteristic (soil type, slope, and farmland area);
3. AEM already implemented in the river basin;
4. Model requirements;
5. Data availability.

Scenario/parameters	Used value	Default value	Range
<b>S1-Vegetative filter strip on 0-11% slope</b>			
VFSRATIO	60	10	0-300
VFSCON	0.5	0.5	0.25-0.75
VFSSCH	0	90	0-100
<b>S2-Vegetative filter strip on 11-24% slope</b>			
VFSRATIO	40	10	0-300
VFSCON	0.5	0.5	0.25-0.75
VFSSCH	0	90	0-100
<b>S3-Vegetative filter strip on 0-24% slope</b>			
VFSRATIO	60, 40	10	0-300
VFSCON	0.5	0.5	0.25-0.75
VFSSCH	0	90	0-100
<b>S4-Conservation tillage</b>			
EFTMIX	0.3	Equipment based	0-1
DEPTIL 150 (field cultivator)	150	Equipment based	0-750
DEPTIL 220 (field cultivator)	220	Equipment based	0-750
BIOMIX	0.4	0.2	0.2
OV_N	0.21	0.14	0.17-0.47
<b>S5-Strip cropping or contour planting on 11-24% slope</b>			
CN2	-3 units	HRU based	0-100
USLE_P	0.80	1	-1 to 1
<b>S6-Terraces on 11-24% slope</b>			
CN2	-6 units	HRU based	0-100
USLE_P	0.16	1	0-1
TERR_SL	15	20	0-100
<b>S7-No cover crops in winter</b>			
Winter cover crop has been removed from rotation			
<b>S8-Cover crops every year</b>			
After harvest in fall winter cover crops (red clover) was applied. In spring leftover was plough into a ground as green manure			

**Table 3.** Parameters and values used in the scenario simulations for the river Ledava basin.

From the 13 measures, we excluded those for which effectiveness increases in line with an increasing area of implementation (grassed waterways and sedimentation pools). Such measures are unsuitable for the study area, due to its scattered land parcel structure. Because of the important proportion of agricultural land on slopes >11%, we chose terraces, although they are not typical for this landscape and are rarely used. According to data from 2014 on the implementation of AEM in the Rural Development Program (RDP) under the EU Common Agricultural Policy (CAP) obtained from the Agency of the Republic of Slovenia for Agricultural Markets and Rural Development, three measures have also been implemented in the area to improve soil fertility and reduce soil erosion. These are cover crops, crop rotation management, and winterkill cover crop. We also selected vegetative filter strips, because the literature review indicates that these are among the most commonly used measures to reduce the effects of diffuse pollution. Five different measures were finally selected, from which eight modelling scenarios were built (**Table 3**).

We simulated measures for areas that are the most sensitive to erosion, such as arable land and drained arable land on slopes from 0 to 11% and from 11 to 24%. The aim of the scenarios was to find the most effective measure or combination of measures to effectively reduce soil erosion, sediment transport into the river and sediment flow into the downstream lake. Given the fact that orchards represent only 2.46% and vineyards 0.82% of the basin area, we decided to simulate the measures only for the arable land. This comprises the most critical areas in terms of soil erosion and covers 38.02% of the basin area. The current average arable land management practice in the basin involves a 7-year crop rotation.

### 3. Results and discussion

#### 3.1. Calibration and validation

##### 3.1.1. Hydrology calibration and validation

Objective functions show that the simulated total flow is within the acceptable range (**Table 4**; **Figure 2**). To achieve acceptable calibration and validation results, a list of model parameters was changed from default to final values (**Table 5**). **Table 4** lists the calibration and validation values for the model performance for flow. Values >0.5 for the coefficient of determination ( $R^2$ ) are considered acceptable, while negative PBIAS values indicate a small overestimation of the simulated values. Nash–Sutcliffe efficiency ( $E_{NS}$ ) on monthly and daily time steps are in the acceptable range [41]; however, the  $E_{NS}$  coefficient is very sensitive to values that stand out from the average [42]. SWAT simulated the streamflow trends very well, as simulated streamflow values do not exceed the measured streamflow data by more than 15% [41]. Comparing simulations run under different time steps shows that this element is important for understanding model performance [44]. Results show that on daily and yearly time steps, model simulations for streamflow are between good and very good in terms of correlating with measured values. The model simulations are weaker for monthly time steps. However, as our results will be presented as a yearly average, we can state that our model is calibrated

sufficiently to be used for further scenario simulations. After the base model calibration was completed, the parameters remained fixed for further use in scenario modelling.

Objective function	Calibration (2005-2010)			Validation (2011-2013)
	Year	Month	Day	Day
$E_{NS}$	0.99	0.49	0.57	0.50
PBIAS	-5.29	-5.20	-5.30	14.08
$R^2$	0.70	0.62	0.57	0.53

**Table 4.** Statistical values for the annual, monthly and daily time step calibration for river flows of the river Ledava (2006-2010).

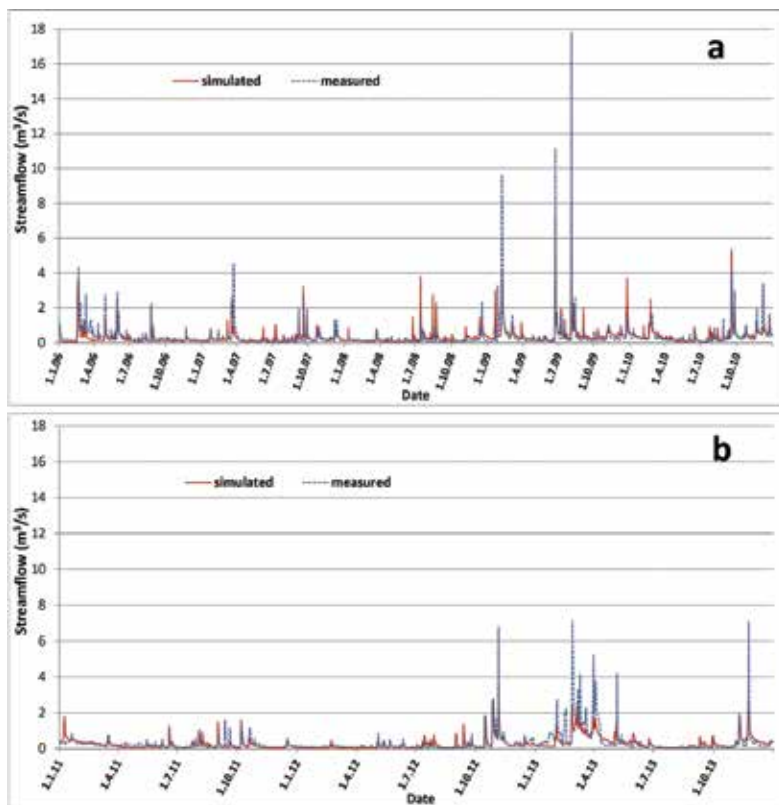


**Figure 2.** A comparison of simulated and measured values for river flow ( $m^3/s$ ) in the river Ledava for (a) calibration period (2006–2010) and (b) validation period (2011–2013).

Parameters		Range	Default	Final
<b>River flow</b>				
ALPHA_BF	Baseflow alpha factor	0-1	0.048	0.5972
CANMX	Maximum canopy storage	0-100	0	-0.2017
CN2	SCS runoff curve number for moisture condition 2	35-98	Default	-0.0753
ESCO	Soil evaporation compensation factor	0-1	0.95	0.88
GW_DELAY	Groundwater delay	0-500	31	90.35
GW_REVAP	Groundwater "revap" coefficient	0.02-0.2	0.02	0.158
GWQMN	Threshold depth of water in the shallow aquifer required for return flow to occur	0-5000	1000	1400
SFTMP	Snowfall temperature	-5 to 5	1	1.66
SMFMN	Minimum melt rate for snow during the year (occurs on winter solstice)	0-10	4.5	1.397
SMFMX	Maximum melt rate for snow during year (occurs on summer solstice)	0-10	4.5	6.46
SMTMP	Snow melt base temperature	-5 to 5	0.5	1.5933
SNOCOVMX	Minimum snow water content that corresponds to 100% snow cover	0-500	1	3.9767
SOL_AWC	Available water capacity of the soil layer	0-1	default	0.1917
SOL_K	Saturated hydraulic conductivity (mm/h)	0-2000	default	0.1883
SURLAG	Surface runoff lag time	0.01-24	4	0.2617
TIMP	Snow pack temperature lag factor	0-1	1	0.1321
<b>Sediment</b>				
ADJ_PKR	Peak rate adjustment factor for sediment routing in the sub-basin (tributary channels)	0.5-2	1	1.815
PRF_BSN	Peak rate adjustment factor for sediment routing in the main channel	0-2	1	2
SPCON	Linear parameter for calculating the maximum amount of sediment that can be reentrained during channel sediment routing	0.0001-0.01	0.0001	0.001197
SPEXP	Exponent parameter for calculating sediment reentrained in channel sediment routing	1-1.5	1	1.4
CH_COV1	Channel erodibility factor	-0.05 to 30	0	5.4
CH_COV2	Channel cover factor	-0.001 to 30	0	5.4
CH_ERODMO	Channel erodibility factor. Jan-Dec	0-1	0	0.3

**Table 5.** The parameters, range (min. and max. value), default and final values used in the model for the flow and sediment calibration and validation of the river Ledava basin.

Due to the smaller volume of data covered, the performance results for the model validation period are often lower than for the calibration period [25]. Nevertheless, the results of the validation in this study are in line with the calibration results.  $E_{NS}$  values during calibration (0.57) and validation (0.50) indicate a good agreement between measured and simulated values, as demonstrated by the coefficient of determination ( $R^2 > 0.5$ ). Only the *PBIAS* results vary between calibration and validation values. For calibration of the model, simulated values were overestimated, whereas for validation, the values were slightly underestimated. The *PBIAS* for validation is in the range of good to very good related to the calibration results.

### 3.1.2. Sediment calibration

Objective functions for a daily and monthly time step sediment calibration (**Table 6; Figure 3**) show that the model is acceptable for predicting sediment. Statistics significantly improve when only one outlier value is not included in the calculation. Due to the limited amount of data for sediment, with only 1 year of measurements, validation was not carried out. Sediment load was calculated as the product of the measured concentrations of sediment (mg/l) and the average daily and monthly flows (m<sup>3</sup>/s). The coefficient of determination ( $R^2$ ) indicates a moderate to strong positive agreement for daily and monthly time steps. The Nash–Sutcliff coefficient ( $E_{NS}$ ) only exceeds 0.5 for monthly time steps when the outlier value (17. 2. 2014 amounted to 259.8 ton/day) is excluded. *PBIAS* describes the 18% deviation of the results for a daily time step, which is in the range for very good model performance [41]. The performance in simulation of trends with  $E_{NS}$  values (ranging from 0.26 to 0.11 for monthly and daily time steps, respectively) reveals that the simulation was unsatisfactory. However, this is because the efficiency coefficient is sensitive to extreme values and yields sub-optimal results when the dataset contains outliers [41]. The performance for  $R^2$  and  $E_{NS}$  improves to a satisfactory level for daily time steps following the removal of outlier values. A better prediction of  $E_{NS}$  could be expected with a larger number of data samples over longer period of time [45].

Objective function	Sediment load (ton/day)			
	Monthly		Daily	
	All values	No outlier value	All values	No outlier value
$E_{NS}$	0.26	0.57	0.11	0.38
<i>PBIAS</i>	36.55	-14.09	53.04	17.69
$R^2$	0.37	0.64	0.22	0.39

**Table 6.** Objective functions for daily and monthly values of sediment concentration (mg/l) and sediment load (ton/day) in the river Ledava at the Pertoča observation station (June 2013 to March 2014).

**Figure 3** shows the impact of one outlier value on the model statistical performance results for sediment. This value is a result of heavy precipitation (an average daily rainfall of 17.14 mm from the previous day to midnight at the nearby meteorological station at Cankova). This was a local storm with a local effect on sediment load. The impact of the outlier value is also evident

from the difference in the coefficients of  $E_{NSr}$ ,  $R^2$  and  $PBIAS$ . In all cases, the results were substantially improved when the outlier value was removed from the dataset, which is understandable considering the effect of this value on the average.

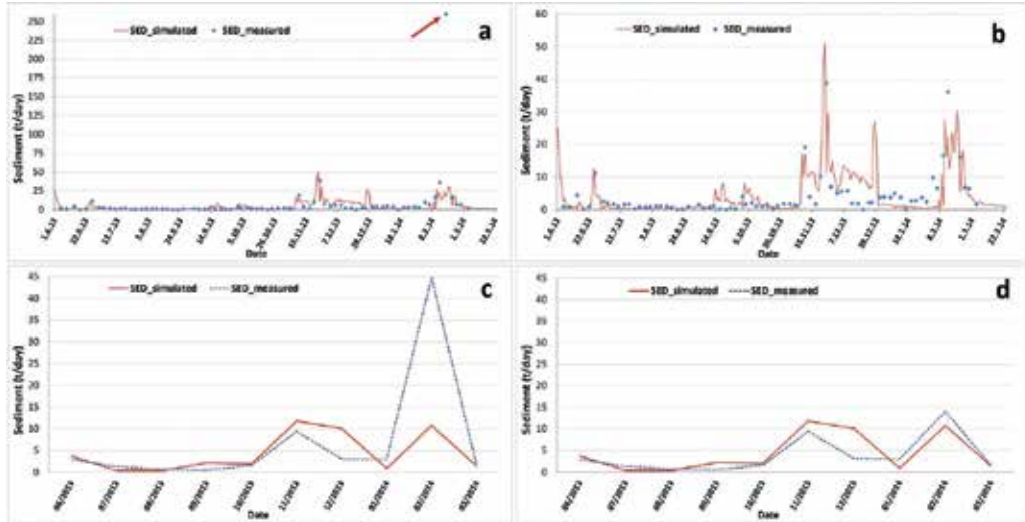


**Figure 3.** A comparison of the simulated and the calculated average daily (a, b) and monthly (c, d) sediment load (ton/day) in the river Ledava (Pertoča) between June 2013 and March 2014, with (a, c) and without (b, d) one outlier value.

### 3.2. Base scenario

Through analysis of the base scenario, we determined the CSAs, that is, where the source and transport areas that are connected to water bodies coincide. HRUs, where the annual average sediment yield exceeded 0.5 ton/ha, were considered to be CSAs (**Figure 4**). It turns out that CSAs represent only 12.2% of the entire river Ledava basin, whereas the most intense erosion occurs on arable land and encompasses 88.2% of all CSAs. These areas have unstable geology and soil types susceptible to soil erosion and for that reason are strongly subject to the action of weather forces [34]. The spatial variability of sediment yield is influenced by many factors, particularly land use, management practice, slope, and soil characteristics. The impact of land management and its graphical representations greatly depend on the accuracy of the spatial and attribute data used in the modelling process. The average annual sediment yield at the HRU level was divided into five classes (**Figure 4**).

The average annual sediment yield (0.28 ton/ha) in the river basin calculated with SWAT coincides with earlier calculations for this area based on land use and slope recalculations [34, 46]. The source of sediment in this river basin is spatially heterogeneous and on average amounts to between 0.3 and 0.9 ton/ha/year. This study shows that in certain HRUs, sediment yield can reach up to 4.10 ton/ha/year (**Table 7**; **Figure 4**). This value can be exceeded during periods of heavy rainfall, such as in 2009 when the highest value in the river reached 18.17 ton/ha. The most critical areas, with a sediment yield of 0.5 ton/ha, comprise an area of 1260 ha or

11.97%. They can be found on slopes between 11 and 24 and over 50%, and on all types of agricultural land. These areas contribute 60.9% of all the sediment transported from the HRUs into the river. The highest amount of sediment is transported from arable fields with drainage systems (0.60 ton/ha/year), other arable fields (0.40 ton/ha/year), and vineyards (0.37 ton/ha/year). Among the most erodible soil types are heavy gley and pseudogley soils. Sub-basins (1, 2, 4 and 5) with a maximum transport of sediment at the HRU level are located in Austria, where the area is characterized by intensive agricultural land, heavy soils, and steep topography. Soils with a high proportion of clay and without vegetation cover and steep topography are more erodible [5, 9, 34, 30].

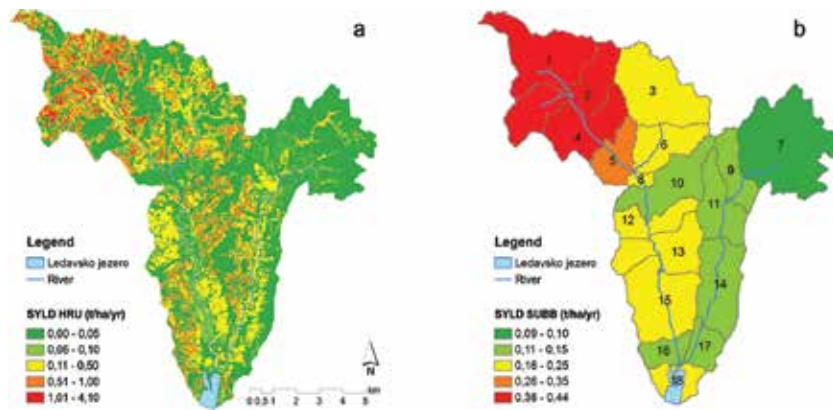


**Figure 4.** Average annual sediment yield (ton/ha/year) on the HRU level (a) and the sub-basin level (b).

Erosion class (ton/ha)	Area (ha)	Area from total (%)	Average sediment yield (ton/ha)
1.01-4.10	355.06	3.37	1.72
0.51-1.00	905.32	8.60	0.69
0.11-0.50	2245.50	21.33	0.23
0.06-0.10	855.62	8.13	0.08
0.00-0.05	6163.80	58.56	0.01
Sum/average	10,525.31	100.00	0.28

**Table 7.** Average annual values of sediment yield (ton/ha) at the HRU level presented with five classes (2006-2013).

### 3.3. Scenario evaluation

Evaluation of the measures used in the scenarios is dependent on achieving set goals and benchmarks. In the context of this research, the main objective was to reduce soil erosion and improve river water quality, which can be achieved by mitigating sediment yield and transport into the river Ledava.

New scenarios did not have any important impact on the predicted average annual flow in the river Ledava. The main reason lies in the configuration of the model parameters, because the modelling runoff curve CN was set at a uniform value for the entire river basin area. Among other things, the vegetation buffer zone in SWAT does not affect the surface runoff [37]. The small impact of measures used in the study on the river flow has also been confirmed in other studies [47, 48]. Whereas scenario S2 increased the simulated average flow rate, scenario S8 is the only one that decreased it. The review of average monthly values shows that scenarios S1, S2, S4, S5, and S6 reduce the river flow between May and October. This was influenced by increased evapotranspiration and intercepted precipitation by the vegetation canopy during the growing season [14]. Low flow rates between October and April result from the growth of cover crops on agricultural land (S8), which influences soil water retention. At the same time, cover crops can improve soil properties and can increase organic carbon content, soil stability, and the infiltration rate [49].

The sediment reduction efficiency of scenarios was estimated by comparing the simulation results of the base scenario with AEM scenarios (**Tables 8 and 9**). The efficiency ( $r$ ) of the scenario was calculated according to [29] as follows:

$$r = \left( \frac{y_{base} - y_{scenario}}{y_{base}} \right) \times 100 \quad (2)$$

where  $y_{base}$  represents the base scenario sediment transport (SYLD in tonnes/ha/year) and  $y_{scenario}$  represents sediment transport (SYLD in tonnes/ha/year) according to the simulation results of the agri-environmental scenarios. The calculation is presented as a percentage change.

Sediment transport from the HRU is reduced in all cases, except for scenario S7 (**Table 8; Figure 5**). It is apparent that the sediment yield (ton/ha/year) reduction at the level of the HRU is most affected by vegetative filter strips (S2: 43.4% and S3: 56.1%) and terraces (S6: 42.4%), followed by conservation tillage (S4: 20.3%), contour tillage (S5: 18.9%), and cover crops (S8: 11.9%). A combination of vegetative filter strips (S3) on slopes up to 11% (S1) and from 11 to 24% (S2) is much more effective than any other measure. A very similar impact on sediment yield reduction at HRU level can be observed between scenarios S2 and S6, although they greatly differ in terms of financial and labor input. All the scenarios were most effective in the sub-basin dominated by agriculture land with slopes of up to 24%.

Most of the scenarios reduced sediment load in the river Ledava where steeper slopes in the sub-basin prevail and where high average annual sediment transport from the HRU was identified (**Table 9**). The impact of the scenarios on the average annual sediment load (ton/year) in the river was lower than at the HRU level. In this regard, scenarios S3 and S6 were also more effective than other measures (S4, S5, and S8): A highly similar order in the impact of the scenarios on sediment load in the river was achieved, although with less variation from the baseline scenario. Scenario S3 was the most efficient at reducing sediment load, followed by S2 and S6. Unlike S6, vegetative filter strips were more efficient in the lowland basin, with a smaller transport of sediment from the HRU. The importance of cover crops is observed in



the S7 scenario, where cover crops were removed from rotation. Overall, negative changes appeared in comparison with the baseline scenario impacting on increase in the sediment yield at HRU level and sediment load in the river Ledava at the outlet of sub-basins.

Sub-basin	Area Ha	Sediment yield (ton/ha/year) Base	Scenarios percentage change in sediment yield (%)							
			S1	S2	S3	S4	S5	S6	S7	S8
1	917.25	<b>0.42</b>	8.64	32.35	40.90	14.65	14.07	32.15	-8.59	8.98
2	827.44	<b>0.44</b>	12.84	41.75	54.59	19.56	18.09	41.34	-11.15	11.62
3	970.18	0.18	9.25	32.35	41.60	16.42	15.09	31.66	-8.23	8.16
4	650.81	<b>0.37</b>	9.86	43.79	53.65	19.37	18.72	43.01	-10.49	11.67
5	368.31	<b>0.28</b>	15.24	48.29	63.52	21.31	20.44	46.67	-12.58	13.69
6	480.25	0.20	16.40	50.93	67.34	24.81	22.77	49.24	-14.11	13.75
7	1414.75	0.09	10.55	41.09	51.64	22.97	19.26	39.44	<b>-22.26</b>	10.15
8	64.69	0.16	14.92	40.27	55.18	19.41	16.75	37.85	-18.13	13.13
9	351.44	0.10	<b>28.65</b>	53.43	<b>82.09</b>	29.67	23.74	50.34	<b>-19.47</b>	<b>18.61</b>
10	652.25	0.14	17.14	54.47	71.61	27.64	24.57	52.44	-17.07	14.15
11	507.63	0.12	<b>23.37</b>	<b>55.92</b>	<b>79.30</b>	<b>30.80</b>	<b>25.33</b>	<b>53.81</b>	<b>-21.20</b>	<b>16.69</b>
12	352.75	0.15	<b>21.60</b>	54.82	76.42	<b>30.22</b>	24.92	53.07	<b>-19.11</b>	15.10
13	603.69	0.16	20.16	54.16	74.32	<b>30.10</b>	24.51	52.28	-16.83	<b>16.87</b>
14	704.31	0.13	20.11	<b>57.10</b>	77.21	28.83	<b>25.78</b>	<b>54.65</b>	<b>-24.15</b>	15.37
15	879.56	<b>0.22</b>	20.06	<b>64.42</b>	<b>84.48</b>	<b>31.55</b>	<b>28.62</b>	<b>61.95</b>	-13.09	<b>16.46</b>
16	232.81	0.14	<b>21.42</b>	52.92	74.34	26.95	24.64	51.72	-9.42	16.08
17	255.25	0.11	<b>25.49</b>	<b>59.91</b>	<b>85.40</b>	<b>31.44</b>	<b>27.98</b>	<b>57.17</b>	-12.89	<b>18.75</b>
18	291.94	0.15	20.80	<b>57.13</b>	<b>77.93</b>	28.44	<b>26.55</b>	<b>54.99</b>	-11.18	14.80
Average	<b>105.31</b>	<b>0.28</b>	<b>12.78</b>	<b>43.36</b>	<b>56.13</b>	<b>20.33</b>	<b>18.94</b>	<b>42.41</b>	<b>-11.53</b>	<b>11.91</b>

The five largest changes in the scenarios are shown in bold.

**Table 8.** The impact of the agri-environmental scenarios (S) on the average annual sediment yield in the sub-basin level expressed as a percentage (%) change to the baseline scenario (2006-2013) for the river Ledava basin.

In sub-basins 1, 2, and 4, where erosion processes are most prominent, the simulated implementation of terraces on slopes between 11 and 24% decreased the amount of sediment in the river by 51, 51.4, and 54.1% (**Table 8**). By contrast, the effect of terraces on reducing the sediment transport from the HRUs (**Table 8**) was the largest in sub-basin 15 (62%), where average annual sediment transport was 0.76 ton/ha. The average annual sediment transport from the HRUs in sub-basins 11, 14, and 17 was relatively small (0.11–0.13 ton/ha), where the maximum amounts of sediment were transported from areas with slopes between 11 and 24%

(from 0.40 to 0.49 ton/ha/year). On average, scenarios S5 and S8 had the smallest impact on sediment load reduction in the river (**Table 9**). Results show that the effect of inferior non-construction measures, such as conservation tillage (S4) or contour or strip cropping (S5), achieve a smaller reduction effect than terraces (S6) or vegetation buffer zones (S1–3) [36]. Scenarios S7 and S8 show the importance of winter cover crops on soil erosion processes and sediment yield transport at the HRU level, as well as on simulated sediment load and concentration in the river Ledava.

Sub-basin	Scenario impact on sediment load at outflow								
	ton/year	Percentage (%) change from base							
	Base	S1	S2	S3	S4	S5	S6	S7	S8
1	569.16	13.06	30.36	39.92	27.07	23.69	51.40	-35.18	28.28
2	1013.30	10.88	30.00	36.45	25.63	23.32	50.97	-26.86	21.39
3	191.80	7.51	36.73	40.13	21.74	20.64	43.28	-17.48	10.55
4	1452.34	9.68	28.44	33.82	24.01	22.29	54.14	1.10	19.91
5	1259.76	-5.00	10.73	13.09	7.17	5.30	34.56	0.19	1.03
6	386.23	11.43	43.39	47.39	39.40	36.79	59.75	-41.70	30.03
7	29.42	25.77	15.54	30.29	32.15	21.09	43.06	-32.27	15.92
8	1270.28	10.30	-8.19	-11.79	-16.76	-13.90	16.07	0.13	-8.03
9	60.61	15.39	11.40	20.75	25.19	16.47	33.04	-23.26	14.43
10	1481.55	9.60	-6.31	-8.13	-11.47	-8.91	19.19	-0.83	-5.26
11	127.04	24.66	21.52	34.91	29.34	19.99	41.40	-25.39	15.86
12	1628.80	9.40	-5.46	-6.69	-8.79	-6.77	20.26	-2.53	-4.49
13	1771.26	9.14	-3.35	-3.93	-4.62	-3.26	22.28	-2.55	-2.45
14	222.31	22.58	20.04	33.23	29.94	21.06	43.80	-26.77	17.37
15	1969.03	9.53	-0.71	0.00	-1.87	-0.53	24.72	-5.41	-0.49
16	2160.74	12.36	4.70	5.03	4.87	6.13	28.41	-17.14	6.09
17	269.69	20.33	18.10	29.06	30.25	22.48	44.17	-86.39	20.23
18	2597.44	12.56	6.79	8.47	7.93	8.17	30.47	-24.68	7.73
Average	<b>933.14</b>	<b>12.74</b>	<b>14.32</b>	<b>19.20</b>	<b>14.70</b>	<b>12.11</b>	<b>36.91</b>	<b>-20.04</b>	<b>10.71</b>

The five largest changes in the scenario are shown in bold.

**Table 9.** The impact of the scenarios on the average annual sediment load (ton/year) at the outlets from the sub-basins and at the inflow into sub-basins 18, expressed as a percentage (%) change from the baseline scenario (2006-2013).

We conclude that the reduction in sediment transported at the sub-basin level was an effect of the proper placement of modelled AEM in CSAs where soil erosion and the sediment transport are highly evident, and also an effect of a higher proportion of forest, which may reduce

excessive runoff [50]. The differences between the effect of terraces on the sediment transport at HRU level and the sediment yield in the river at the outlet from a sub-basin have also been reported in previous studies [20]. These situations, where AEM are more effective at the HRU level than at the sub-basin outlet or whole-basin outlet, are due to morphology of the terrain and soil properties [51–53].

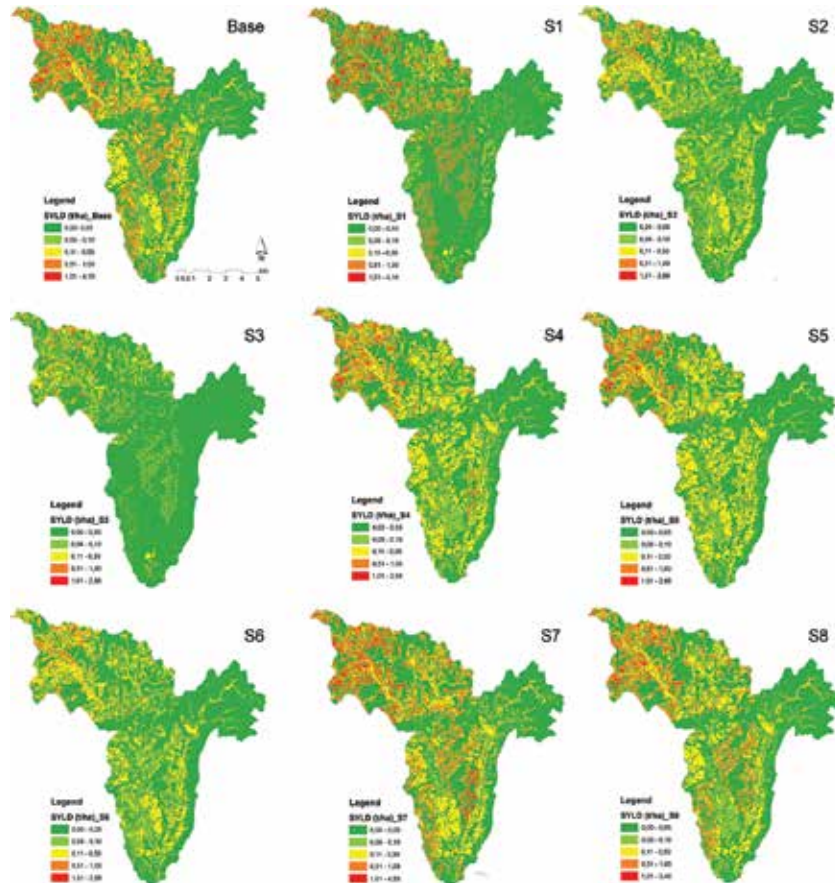


**Figure 5.** Changes in the average annual amount of sediment transported with surface runoff from HRUs as modelled by scenarios for the river Ledava basin.

#### 4. Conclusions

According to the agricultural, environmental, and water policies in member states of the EU-28, AEM should be implemented according to need, the willingness of farmers to adopt the measures, existing management practice and the natural conditions in the relevant region. This study reveals the measures that are relevant to address the protection of agricultural soil in

the selected river Ledava basin study area. The fact that the measures are more effective when they are introduced at a smaller scale (HRU level) and are necessary only in the CSAs, is important in terms of protecting valuable agricultural land in situ.

The main uncertainties in our research are connected with obtaining data and its comparability between two countries. The precision of all spatial layers varied greatly, as not one layer was at the same scale for the two countries. Wherever possible, we upscaled or downscaled the layers. To overcome this issue, countries in future should establish a common data protocol for transboundary river basins. One of the everlasting problems is state monitoring of water quality sampling. Monitoring is spatially rare, with wide time steps between sampling. There are frequent changes to the spatial position of the sampling point, river flow and water quality sampling points are often in different places, and in certain cases monitoring stops after few years. To overcome this, we carried out 1-year sampling of sediment concentrations at several points along the river. However, this required our own financial and working power resources, which are limited. We recommend that the relevant state environmental agency responsible for surface water measurements should pay more attention to the location of monitoring points and should ensure long-term, regular, and comparable time series. Calibration of the model results for soil erosion and sediment transport was done only with comparison to measured values in the river streamflow. Although we had three general maps representing erosion rates at a different spatial scale to previous studies [8, 9], actual soil erosion was never measured in the area. We propose a series of on-site field measurements of soil erosion at different slope, land usage, and soil types to evaluate the results of this and other similar studies.

One of the important factors for the effectiveness of AEM is climate change. Climate change already dictates differing land use, crop types, management, and production technology. This is already affecting the processes of mass transfer from catchment areas into water bodies, and we can expect that these processes will escalate in the future. These effects can only be determined with additional modelling of climate change impact. For example, currently foreseen AEM have been found to be less effective under future climate change scenarios, however not to the extent of being unnecessary.

The criteria for individual parameters that define the AEM in the model are necessary in order to assess, evaluate, and select alternatives with regard to the objectives of the decision-maker. Therefore, it is necessary to supplement the missing limit values for the water quality parameters, in particular those related to soil erosion, sediment yield, and sediment loads in surface water bodies.

The results show that CSAs occupy 12.2% of the river basin. Most of the scenarios predict reduced sediment in the river Ledava where steeper slopes in the sub-basin prevail and where high average annual sediment transport from the HRUs is identified. The impact of the scenarios on the average annual sediment load (ton/year) in the river was lower than at the HRU level. An extremely similar order in the impact of the scenarios on total sediment load in the river was achieved, although with less change from the baseline scenario. Overall, negative changes and or reductions appeared according to the baseline scenario in the sediment yield at HRU level and sediment in the river Ledava at the outlet of the sub-basin. This study enables us to better understand the processes of selecting environmentally effective

measures and their contribution to the long-term improvement of the surface water bodies' ecological status in accordance with the Water Framework Directive. This also opens up the potential for selecting cost-effective and socioeconomically friendly solutions addressing the rural development programs of EU member states under the Common Agricultural Policy.

## Acknowledgements

This work was funded by the SPIRIT Slovenia, Public Agency of the Republic of Slovenia for the Promotion of Entrepreneurship, Innovation, Development, Investment and Tourism, and Savaprojekt Ltd.

## Author details

Matjaž Glavan<sup>1</sup>, Polona Ojsteršek Zorčič<sup>2</sup> and Marina Pintar<sup>1</sup>

\*Address all correspondence to: [matjaz.glavan@bf.uni-lj.si](mailto:matjaz.glavan@bf.uni-lj.si)

1 Agronomy Department, Chair for Agrometeorology, Agricultural Land Management, Economics and Rural Development, Biotechnical Faculty, University of Ljubljana, Ljubljana, Slovenia

2 SAVAPROJEKT Ltd., Krško, Slovenia

## References

- [1] Posthumus H, Deeks LK, Fenn I, Rickson RJ. Soil Conservation in two English catchments: linking soil management with policies. *Land Degrad Dev.* 2011 Jan–Feb;22(1): 97–110.
- [2] Walling DE, Collins AL, Jones PA, Leeks GJL, Old G. Establishing fine-grained sediment budgets for the Pang and Lambourn LOCAR catchments, UK. *J Hydrol.* 2006 Oct 30;330(1–2):126–41.
- [3] Rickson RJ. Can control of soil erosion mitigate water pollution by sediments? *Sci Total Environ.* 2014 Jan 15;468:1187–97.
- [4] Annandale GW. Reservoir Sedimentation. *Encyclopedia of Hydrological Sciences.* Chichester, UK; John Wiley & Sons, Ltd; 2006.
- [5] Morgan RPC. Soil erosion and conservation. Malden; Oxford; Carlton: Blackwell Publishing; 2005.

- [6] Roose E. *Land Husbandry: Components and Strategy*. Rome: FAO; 1996.
- [7] DEFRA. *Safeguarding Our Soils: A Strategy for England*. London: Department for Environment, Food & Rural Affairs; 2009. Available from: [https://www.gov.uk/government/uploads/system/uploads/attachment\\_data/file/69261/pb13297-soil-strategy-090910.pdf](https://www.gov.uk/government/uploads/system/uploads/attachment_data/file/69261/pb13297-soil-strategy-090910.pdf)
- [8] Panagos P, Meusburger K, Van Liedekerke M, Alewell C, Hiederer R, Montanarella L. Assessing soil erosion in Europe based on data collected through a European network. *Soil Sci Plant Nutr*. 2014 Jan 2;60(1):15–29.
- [9] Komac B, Zorn M, Fridl J. Soil erosion on agricultural land in Slovenia – measurements of rill erosion in the Besnica valley = Erozijska prsti na kmetijskih zemljiščih v Sloveniji – meritve zlebične erozije v dolini Besnice. *Acta Geogr Slov*. 2005(45):53–86.
- [10] Wei W, Chen LD, Zhang HD, Yang L, Yu Y, Chen J. Effects of crop rotation and rainfall on water erosion on a gentle slope in the hilly loess area, China. *Catena*. 2014 Dec; 123:205–14.
- [11] Espejo-Perez AJ, Rodriguez-Lizana A, Ordonez R, Giraldez JV. Soil loss and runoff reduction in olive-tree dry-farming with cover crops. *Soil Sci Soc Am J*. 2013 Nov–Dec; 77(6):2140–8.
- [12] Stevens CJ, Quinton JN, Bailey AP, Deasy C, Silgram M, Jackson DR. The effects of minimal tillage, contour cultivation and in-field vegetative barriers on soil erosion and phosphorus loss. *Soil Tillage Res*. 2009 Dec;106(1):145–51.
- [13] Yang Q, Meng FR, Zhao ZY, Chow TL, Benoy G, Rees HW, et al. Assessing the impacts of flow diversion terraces on stream water and sediment yields at a watershed level using SWAT model. *Agr Ecosyst Environ*. 2009 Jul;132(1–2):23–31.
- [14] Zhang JH, Frielinghaus M, Tian G, Lobb DA. Ridge and contour tillage effects on soil erosion from steep hill slopes in the Sichuan Basin, China. *J Soil Water Conserv*. 2004 Nov–Dec;59(6):277–84.
- [15] Posthumus H, De Graaff J. Cost-benefit analysis of bench terraces, a case study in Peru. *Land Degrad Dev*. 2005 Jan–Feb;16(1):1–11.
- [16] Strauch M, Volk M. SWAT plant growth modification for improved modeling of perennial vegetation in the tropics. *Ecol Model*. [Article]. 2013 Nov;269:98–112.
- [17] Kaini P, Artita K, Nicklow JW. Optimizing structural best management practices using SWAT and genetic algorithm to improve water quality goals. *Water Resour Manag*. 2012 May;26(7):1827–45.
- [18] Glavan M, Pintar M. Modelling of surface water quality by catchment model SWAT. In: Kumarasamy M, editor. *Studies on Water Management Issues*. Rijeka, Croatia: InTech; 2012a.

- [19] Lam QD, Schmalz B, Fohrer N. The impact of agricultural Best Management Practices on water quality in a North German lowland catchment. *Environ Monit Assess.* 2011 Dec;183(1–4):351–79.
- [20] Tuppad P, Kannan N, Srinivasan R, Rossi CG, Arnold JG. Simulation of agricultural management alternatives for watershed protection. *Water Resour Manag.* 2010 Sep; 24(12):3115–44.
- [21] Volk M, Liersch S, Schmidt G. Towards the implementation of the European Water Framework Directive? Lessons learned from water quality simulations in an agricultural watershed. *Land Use Policy.* 2009 Jul;26(3):580–8.
- [22] Bosch NS. The influence of impoundments on riverine nutrient transport: An evaluation using the Soil and Water Assessment Tool. *J Hydrol.* 2008 Jun 20;355(1–4):131–47.
- [23] Posthumus H, Deeks LK, Rickson RJ, Quinton JN. Costs and benefits of erosion control measures in the UK. *Soil Use Manag.* 2015 Oct;31:16–33.
- [24] Pionke HB, Gburek WJ, Sharpley AN. Critical source area controls on water quality in an agricultural watershed located in the Chesapeake Basin. *Ecol Eng.* 2000 Apr;14(4): 325–335.
- [25] Arnold JG, Moriasi DN, Gassman PW, Abbaspour KC, White MJ, Srinivasan R, et al. Swat: model use, calibration, and validation. *Trans ASABE.* 2012 Jul–Aug;55(4):1491–508.
- [26] Panagopoulos Y, Makropoulos C, Mimikou M. Diffuse surface water pollution: driving factors for different geoclimatic regions. *Water Resour Manag.* 2011 Nov 1;25(14):3635–60.
- [27] Ghebremichael LT, Veith TL, Watzin MC. Determination of critical source areas for phosphorus loss: Lake Champlain basin, Vermont. *Trans ASABE.* 2010 Sep–Oct;53(5): 1595–604.
- [28] White WJ, Morris LA, Pinho AR, Jackson CR, West LT. Sediment retention by forested filter strips in the Piedmont of Georgia. *J Soil Water Conserv.* 2007 Nov–Dec;62(6):453–63.
- [29] Arabi M, Frankenberger JR, Enge BA, Arnold JG. Representation of agricultural conservation practices with SWAT. *Hydrol Process.* 2008 Jul 30;22(16):3042–55.
- [30] Glavan M, White SM, Holman IP. Water quality targets and maintenance of valued landscape character—experience in the Axe catchment, UK. *J Environ Manag.* 2012 Jul 30;103:142–53.
- [31] Ullrich A, Volk M. Application of the Soil and Water Assessment Tool (SWAT) to predict the impact of alternative management practices on water quality and quantity. *Agric Water Manag.* 2009;96(8):1207–17.

- [32] Rousseau AN, Savary S, Hallema DW, Gumiere SJ, Foulon E. Modeling the effects of agricultural BMPs on sediments, nutrients, and water quality of the Beaurivage River watershed (Quebec, Canada). *Can Water Resour J.* 2013;38(2):99–120.
- [33] Natek K. Endangerment and regenerative capacities of the surface in northeast Slovenia, defined on the basis of surface regeneration in Haloze after the storms of July 1989. Possibilities of regional and spatial development of Spodnje Podravje and Prlekija Region. Conference proceedings. Ljubljana, Slovenia: Association of the Geographical Societies of Slovenia, VB & S; 1996.
- [34] Komac B, Zorn M. Landslides in the Pomurje region. Pomurje Region – Sustainable regional development along the Mura River. Conference proceedings. Ljubljana, Slovenia: Association of the Geographical Societies of Slovenia, Littera picta; 2009.
- [35] Šajn-Slak A, Smolar-Žvanut N, Vrhovšek D, Krivograd-Klemencič A. = Ecohydrological research and conceptual solutions for ecoremediation in the upper catchment area of the Ledava river. International conference on ecoremediation. Maribor, Slovenia; University of Maribor, Faculty of Philosophy, International Centre for Ecoremediation; 2008.
- [36] Gassman PW, Reyes MR, Green CH, Arnold JG. The soil and water assessment tool: historical development, applications, and future research directions. *Trans ASABE.* 2007 Jul–Aug;50(4):1211–50.
- [37] Neitsch SL, Arnold JG, Kiniry JR, Williams JR. Soil and water assessment tool theoretical documentation—Version 2005. Texas, Temple: Agricultural Experiment Station, Blackland Research Center, Agricultural Research Service, Grassland, Soil and Water Research Laboratory; 2005.
- [38] Xie H, Chen L, Shen ZY. Assessment of agricultural best management practices using models: current issues and future perspectives. *Water.* 2015 Mar;7(3):1088–108.
- [39] van Griensven A, Meixner T, Grunwald S, Bishop T, Diluzio A, Srinivasan R. A global sensitivity analysis tool for the parameters of multi-variable catchment models. *J Hydrol.* 2006 Jun 15;324(1–4):10–23.
- [40] Abbaspour KC, Yang J, Maximov I, Siber R, Bogner K, Mieleitner J, et al. Modelling hydrology and water quality in the pre-alpine/alpine Thur watershed using SWAT. *J Hydrol.* 2007 Feb 15;333(2–4):413–30.
- [41] Moriasi DN, Arnold JG, Van Liew MW, Bingner RL, Harmel RD, Veith TL. Model evaluation guidelines for systematic quantification of accuracy in watershed simulations. *Trans ASABE.* 2007 May–Jun;50(3):885–900.
- [42] Krause P, Boyle DP, Båse F. Comparison of different efficiency criteria for hydrological model assessment. *Adv Geosci.* 2005;5:89–97.
- [43] Ojstršek Zorčič P. Selection and Implementation of Ecoremediation Measures in the Reservoir Watershed. Ljubljana: University of Ljubljana; 2015.



- [44] Glavan M, White S, Holman IP. Evaluation of river water quality simulations at a daily time step—experience with SWAT in the axe catchment, UK. *Clean Soil Air Water*. 2011 Jan;39(1):43–54.
- [45] Van Liew MW, Arnold JG, Garbrecht JD. Hydrologic simulation on agricultural watersheds: choosing between two models. *Trans ASAE*. 2003 Nov–Dec;46(6):1539–51.
- [46] Zorn M, Mikos M. Soil erosion measurements in a forest in Slovenian Istria. *Journal of the Association of Surveyors of Slovenia*. 2010 Sep; 68(7/8): 361–366, 379–392
- [47] Bracmort KS, Arabi M, Frankenberger JR, Engel BA, Arnold JG. Modeling long-term water quality impact of structural BMPs. *Trans ASABE*. 2006 Mar–Apr;49(2):367–74.
- [48] Cho J, Lowrance RR, Bosch DD, Strickland TC, Her Y, Vellidis G. Effect of watershed subdivision and filter width on SWAT simulation of a coastal plain watershed1. *J Am Water Resour Assoc*. 2010 Jun;46(3):586–602.
- [49] Dabney SM, Moore MT, Locke MA. Integrated management of in-field, edge-of-field, and after-field buffers. *J Am Water Resour Assoc*. 2006 Feb;42(1):15–24.
- [50] Norris JE. *Slope Stability and Erosion Control Ecotechnological Solutions*. Dordrecht: Springer; 2008.
- [51] Verstraeten G, Poesen J, Gillijns K, Govers G. The use of riparian vegetated filter strips to reduce river sediment loads: an overestimated control measure? *Hydrol Process*. 2006 Dec 30;20(20):4259–67.
- [52] Chiang LC, Chaubey I, Hong NM, Lin YP, Huang T. Implementation of BMP strategies for adaptation to climate change and land use change in a pasture-dominated watershed. *Int J Environ Res Pub Health*. 2012 Oct;9(10):3654–84.
- [53] Bohanec M. *Decisions and modeling*. Ljubljana, Slovenia: DMFA - založništvo; 2012.



---

# River Engineering and River Basin Development

---



---

# Riverine-Based Aquifers and Riparian Exchange: A Conceptual Discussion

---

Modreck Gomo and Joe Magner

Additional information is available at the end of the chapter

<http://dx.doi.org/10.5772/63277>

---

## Abstract

This chapter presents a conceptual discussion of the aquifers that typically occur along river channels and the riparian exchange of water as influenced by valley and channel type and management. Definitions of alluvial and bedrock river channel, based on literature, are provided while highlighting their general attributes and exchange options. Conceptual aquifer models occurring along alluvial and bedrock river channels are then described and presented with respect to groundwater-surface exchanges and solute fate and transport. There is theoretical reasoning to suggest that channel aquifers and concordant riparian zones can be conceptualized and classified based on valley type and the nature of the river channel hosting the aquifer. The information presented in the conceptual models can be used during desktop studies to strategically plan the optimal management for aquifer and riparian protection and restoration activities subject to anthropogenic risk. Riparian zone management is needed more so today, because basin land use in many parts of the world has advanced to the point of creating both water quantity and quality disequilibrium.

**Keywords:** Alluvial aquifer, alluvial river channel, bedrock river channel, groundwater-surface exchange, riparian management, ecosystem services

---

## 1. Introduction

Considerable studies exist on the geomorphologic processes governing the formation and functioning of alluvial and bedrock river channels [1–4]. However, very little effort has been devoted to the conceptual description of the influence that these river channels can have on the nature of aquifers that could develop along them given human demands related to food and water insecurity. There are several valley and channel type classifications that have been

---

developed from a geomorphic perspective [5, 6]. We will use the Rosgen system throughout this chapter to link groundwater-surface water exchange to systems observed in nature.

“Alluvial aquifer” is a common term that is often used in reference to aquifers that generally comprise unconsolidated sediments from previous channel deposits, both current and historic (glacial past) [7–10]. However, this is also done without mention to type of the river channel hosting the aquifer. In nature, alluvial aquifers can occur along both the alluvial and bedrock river channels but with different characteristics and implications for groundwater-surface water exchange. The type of valley hosting the river channel can therefore have some influence on the development of the nature and characteristics of the aquifer system. Typically, Rosgen valley VIII encompasses the flat sand and gravel-rich sediment found with fluvial transport. In glaciated regions, Rosgen valley type IX is common; these flat valleys can have deep deposits and provide opportunities for irrigated agriculture. Besides alluvial aquifers, other riparian eco-hydrologic systems can also develop along the river channel including more lacustrine sediments: Rosgen valley type X and large deltas Rosgen type XI [6]. Slower velocities drop out fine sand and silt where there is a change in energy gradient and oxbow ponds, and wetlands can form. The lacustrine and delta valley types offer more residence time for nutrient attenuation and trapping; thus the groundwater-surface water exchanges are highly influenced by heterogeneity of the well-sorted sediments.

Riverine channel aquifers are a worldwide important source of groundwater; they are often targeted to supply water for agriculture and domestic purposes [11–16]. By nature, riverine channel aquifers exist because of regional groundwater discharge. The riverine ecosystem synthesis [17] defined the importance of a cross-sectional view of river basins across scale. Riverine aquifers play an important role on the chemical and physical functional processes that support human and aquatic life. Specifically, wetland systems form critical water storage, biotic habitat and pollutant attenuation. In order to develop appropriate investigation and management methodology that can ensure sustainable utilization of the water resources, a good conceptual understanding of such aquifers and potential implications for groundwater-surface water exchange is essential because the groundwater discharge sustains the ecosystem services present in a riparian zone.

This chapter is therefore aimed at improving the conceptual understanding of the aquifers that can occur along a river channel as influenced by the regional geology, valley type, channel type and the concordant ecosystem services that may be at risk if land use is not properly managed.

## **2. River channels**

River channels can be generally classified into bedrock and alluvial channels [1, 3, 18–20]. Bedrock channels occur and flow directly through the underlying bedrock, assuming a rock material that allows fluid flow. Alluvial channels are formed in sediments previously deposited in fluvial or glaciofluvial flows and naturally pass fluids through primary pores depending on the hydraulic conductivity [21]. In nature, it is possible that along river channels, alternations could occur between alluvial and bedrock channel types as influenced by

heterogeneity of the Earth processes. Such alternations could be in the form of mixed bedrock-alluvial [4, 22–24] and separately as an alluvial reach with specific bedrock outcrops between alluvial reaches [19, 26]. Examples of igneous bedrock outcropping occur in central Minnesota and along the Minnesota Wisconsin border in north-central USA. These systems can often have unique biotic features because of the bedrock position. Conceptual representations of bedrock and alluvial are shown in **Figures 1** and **2**. **Figure 3** shows a photo of mixed bedrock-alluvial channels taken from [27]. All of the examples shown would fit a Rosgen valley type V and/or VI depending on the geology and mountain terrain.

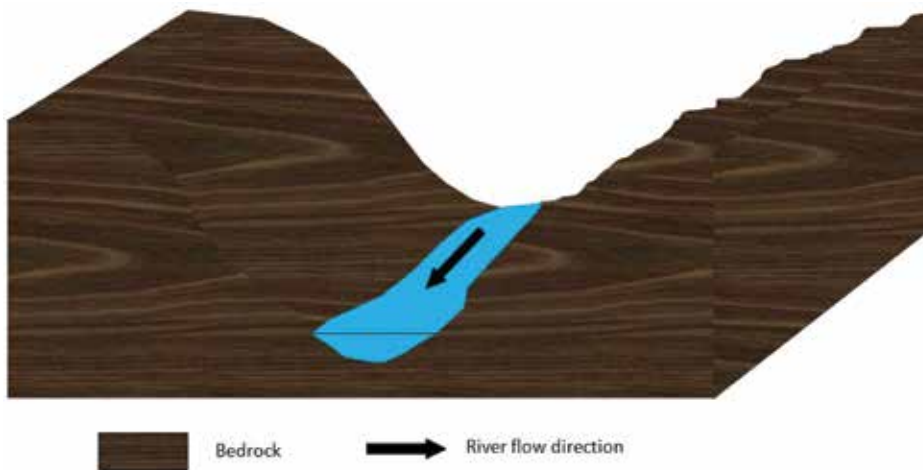


**Figure 1.** Conceptual representation of bedrock river channel (modified from [21]).

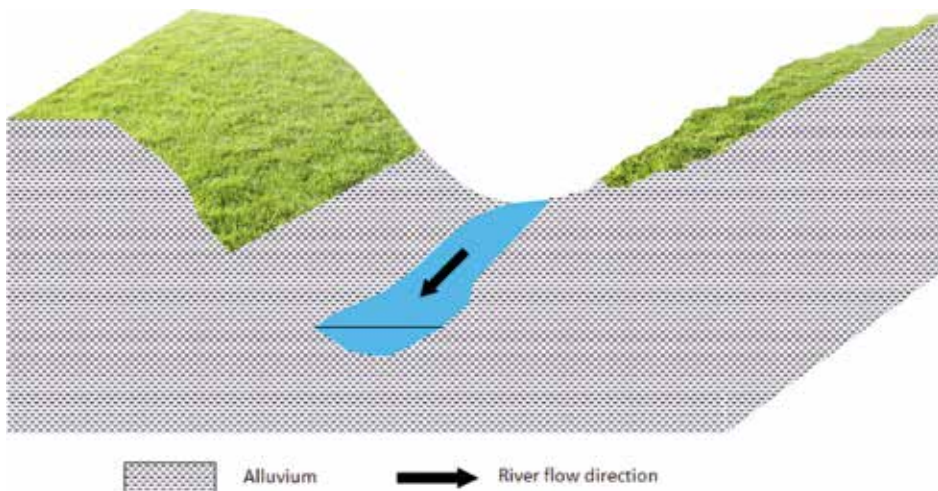


**Figure 2.** Conceptual representation of an alluvial river channel (modified from [21]).



**Figure 3.** Photo of a mixed bedrock-alluvial channel (taken from [27]).

A key distinction between the figures above is directly related to hydraulic conductivity. **Figure 1**, where the channel is set in bedrock, is primarily unidirectional; little, if any, bank storage of high-stage water can occur unless the properties of the rock allow for fluid flow. In contrast to **Figure 1**, the channel shown in **Figure 2** is multi-directional; groundwater can resurge and flood water can be stored in the alluvium. The channel in **Figure 3** can provide a limited amount of bank storage, but only high stages and only under sustained high stage.

### 3. Conceptual models of river channel aquifers

#### 3.1. Bedrock river channel aquifers

A bedrock river channel can potentially host different types of aquifer systems; however, hydrogeological characterization will require differing approaches, tools and techniques. Aquifers that could be formed in concert with bedrock channels will mainly consist of (a) alluvial cover, (b) fractured/weathered bedrock, (c) porous-bedrock aquifer, (d) alluvial cover overlying fractured/weathered bedrock aquifer, (e) alluvial cover overlying porous-bedrock aquifer and (f) all alluvial sediment. In all these examples, the valley type will be defined by the regional geology; steep mountainous systems will have little to no groundwater exchange except where alpine terraces and deltas form.



### 3.1.1. Alluvial cover aquifer

This can occur on a mixed bedrock-alluvial river channel. In this instance, the bedrock is an aquitard while the overlying alluvial covers have sufficient porosity and permeability to respectively store and allow movement of groundwater (**Figure 4**). Depending on the river stage elevation, there could be direct or indirect hydraulic exchanges between the groundwater in the alluvial cover aquifer and surface water in the river.

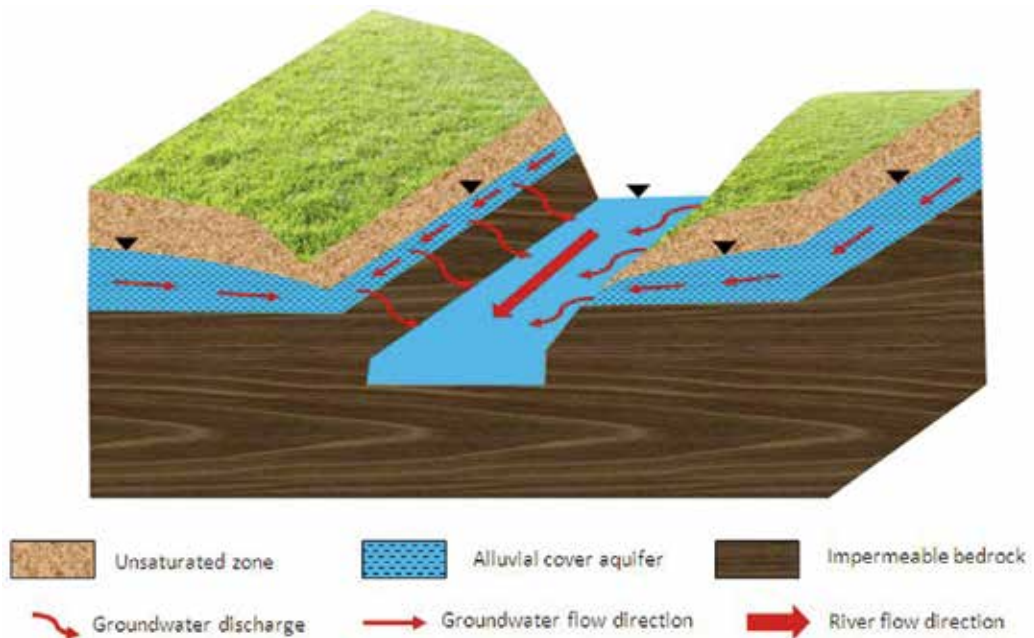


**Figure 4.** Conceptual representation of an alluvial cover aquifer on a mixed bedrock-alluvial river channel.

However, by definition a bedrock river channel must be cut into bedrock and flow through the bedrock, which implies that the river stage will always be within the impermeable bedrock. When the river stage is within the bedrock, it can therefore not be in direct hydraulic contact with top alluvial cover aquifer. The most likely form of groundwater-surface water exchange would occur as groundwater discharge at the contact plane between alluvial cover and impermeable bedrock (assuming the hydraulic gradient in the alluvial cover aquifer is towards the river).

Under the conditions assumed in **Figure 4**, the river will gain water from the alluvial cover aquifer; thus, it represents a groundwater sink. However, when groundwater is being abstracted from a well drilled into the alluvial cover aquifer, the cone of depression cannot extend beyond the river; thus, the river could act as an impermeable/no flow hydraulic boundary. A schematic showing how the river channel of an alluvial cover aquifer acts as a no flow boundary to the cone of depression created by a pumping well drilled into the aquifer is presented in **Figure 5**.

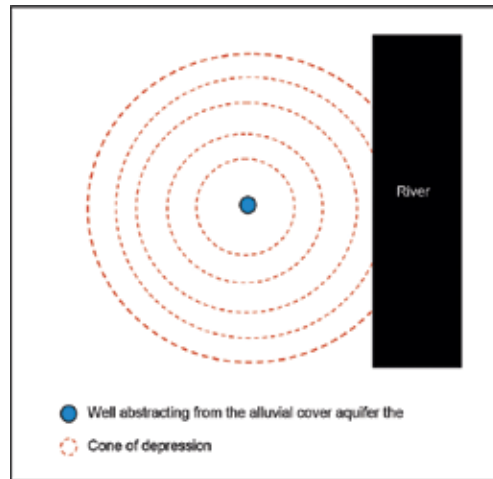


**Figure 5.** Schematic showing how the river channel of an alluvial cover aquifer acts as a no flow boundary to the cone of depression created by a pumping well drilled into the aquifer.

Abstracting groundwater from the alluvial cover aquifer would therefore not draw water from the river or cause the ingression of river water into the aquifer because the two are not hydraulically connected. This however does not mean that abstraction from such an aquifer cannot negatively affect the river. Indirectly, abstraction from the alluvial aquifer will effectively reduce the discharge into river, which could also impact negatively on the functioning of the riparian and river ecosystems. A flatter valley type is required such as a Rosgen IX formed in glaciofluvial sediments. An example of this system can be found in flat outwash plains of central Minnesota (USA) near adjacent to the Mississippi River.

### 3.1.2. Alluvial cover and bedrock aquifer

It is possible that the bedrock underlying the alluvial cover aquifer can have sufficient properties to allow storage and movement of water, thus making it also an aquifer. This could occur in form of (1) porous-bedrock aquifer (**Figure 6**), (2) fractured/weathered bedrock aquifer (**Figure 7**) or both. When the bedrock is also an aquifer, the groundwater resource would then occur and flow in both the alluvial cover and underlying bedrock aquifer. Since the river flows only through the bedrock, only the bedrock aquifer can be in hydraulic contact with the river water thereby presenting the opportunity for direct groundwater-surface water exchanges. Porous bedrock most often consists of weakly cemented sandstone. Finer-grained or compacted sandstones will allow a limited amount of groundwater movement, but not enough to be considered a viable aquifer. Nevertheless, fine-grained bedrock can weather and develop fracture networks allowing for secondary porosity. If the sedimentary rock is carbon based, the bedrock can enlarge by dissolution. Carbonate bedrock aquifers can be extensively developed with cave networks with rapid pipe-like hydraulic conductivity; these systems are referred to as karst and exist in selected locations throughout the world [28]. More commonly, carbonate aquifers have smaller fractures (1–10 cm) that function similar to porous media flow.

Typical Rosgen valley types found in these systems are VI (fault-controlled valleys) and VII (dissected fluvial slopes); these systems can be observed in Pennsylvania, USA.

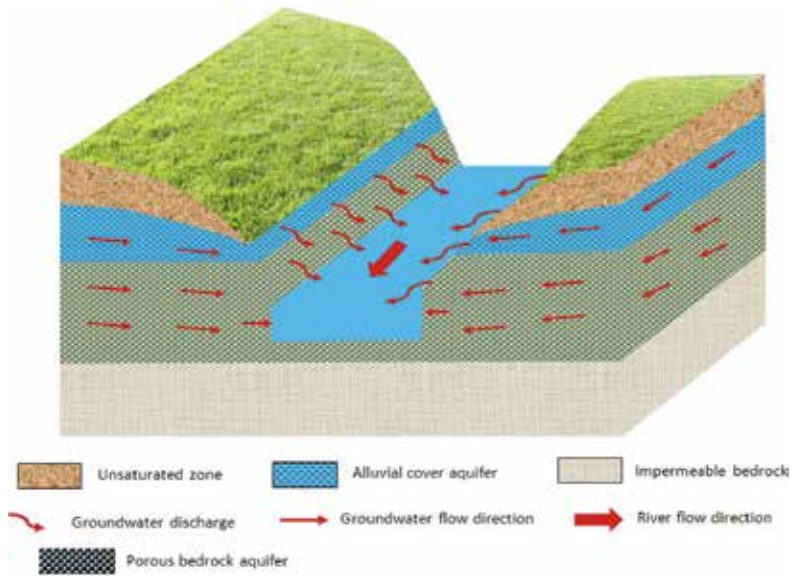


Figure 6. Conceptual representation of alluvial cover and porous-bedrock aquifers on a bedrock river channel type.

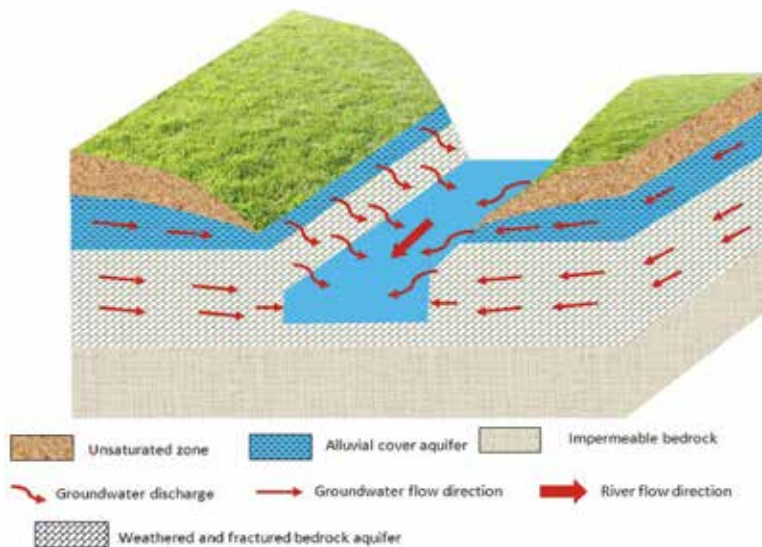


Figure 7. Conceptual representation of an alluvial cover and fractured-bedrock aquifers on a bedrock river channel type.

Depending on the permeability of the formation separating the alluvial cover and bedrock aquifer, the two could behave as hydraulically connected or separate systems. The aquifers will behave as hydraulically connected systems when the separating geological formation is permeable to allow vertical exchanges between the aquifer systems. In this situation, abstracting from a well drilled into the alluvial cover aquifer could also draw water from the deep bedrock aquifer through vertical leakage and potential draw from the river. The bedrock aquifer can also receive its recharge through the overlying alluvial cover aquifer. Ref. [29] observed deep fractured bedrock aquifer that derived 80–100% of its recharge during stressed (pumping) conditions through vertical and horizontal flow from the overlying deposits.

When the geological formation between the alluvial cover and bedrock aquifers is at least semi-impermeable, the two aquifers will hydraulically behave as separate systems. Because of the impermeable confinement, the bedrock aquifer will not receive recharge from the overlying alluvial cover aquifer and water held in the alluvial material will move laterally toward the river and resurge as a spring. In this scenario, abstracting from one aquifer would also not directly affect the other aquifer, since they are not hydraulically connected; however, abstraction from the bedrock aquifer could create a gradient and draw water from the river because of the hydraulic connectivity. Depending on connectivity between the river and the aquifer, river base-flow could be adverse and drive failure of ecosystem services. When abstracting from the bedrock aquifer system, the river potentially represents a recharging hydraulic boundary; this is more common when aquitards or semi-impermeable layers limit upland recharge. This is because when the cone of depression of a high-capacity well expands into the river, the river acts as a source of water for the aquifer (recharge boundary). Due to this groundwater-surface water exchange effect, direct transfer of pollutants can occur between the river and bedrock aquifer, which could negatively affect the water quality. Investigation of groundwater-surface water exchanges is therefore an important issue in this channel aquifer model.

### 3.2. Alluvial river channel

#### 3.2.1. Alluvial aquifer

In an alluvial aquifer channel, typically a Rosgen VIII broad flat valley type, groundwater occurs and flows in the alluvium deposits (**Figure 8**). The river almost always flows within the sediments; thus, it is generally in hydraulic contact with the alluvial aquifer thereby presenting the opportunity for direct groundwater-surface interaction between the two reservoirs. The aquifer can therefore be recharged from the river or resurge into the river. Groundwater abstraction from the alluvial aquifer can draw water from the river if the cone of depression expands to the river. Pollution can also be transported from one resource to the other during the exchanges. In a Rosgen type XI (delta valley type), the valley slope may result in a losing river channel if the regional water table has dropped below the alluvial bed. An example of this type of riverine system can be found along the eastern front of the Rocky Mountains in Montana (USA) where snow-melt drops down from higher elevations into the delta in May/June but fails to fully flow east because of the drier climatic regime. Groundwater-surface water

exchange is an important facet of this aquifer model; one that demands extensive evaluation before anthropogenic development.

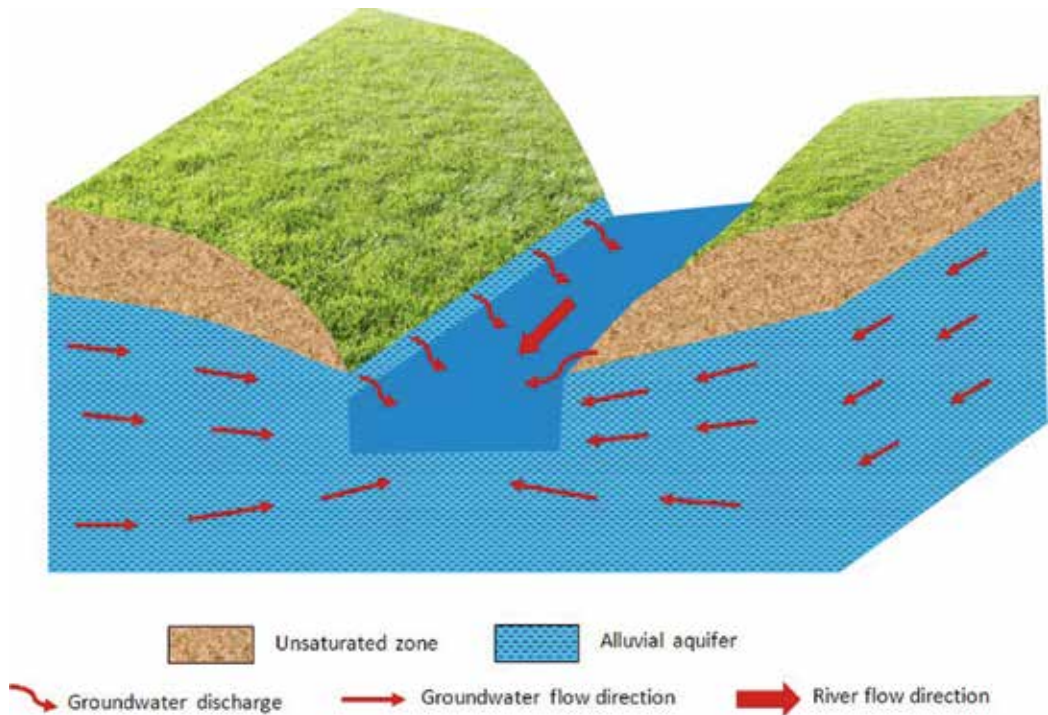


**Figure 8.** Conceptual representation of an alluvial aquifer on an alluvial river channel.

## 4. Conclusions

We have presented conceptual models of aquifers that could occur on river channels as influenced by the valley and stream type. A classification that conceptually splits channel aquifers based on the river and valley type has been presented to illustrate possible management concerns. The classification would split aquifers that can occur along a bedrock river channel into (a) alluvial cover aquifer, (b) fractured/weathered bedrock, (c) porous-bedrock aquifer, (d) alluvial cover overlying fractured/weathered bedrock aquifer, (e) alluvial cover overlying porous-bedrock aquifer and (f) alluvial.

The information presented in the conceptual models can be used during desktop studies to strategically plan the optimal management for aquifer and riparian protection and restoration activities subject to anthropogenic risk.

## Author details

Modreck Gomo<sup>1</sup> and Joe Magner<sup>2\*</sup>

\*Address all correspondence to: magne027@umn.edu

1 University of the Free State, Bloemfontein, South Africa

2 University of Minnesota, St. Paul, MN, USA

## References

- [1] Richards KS. *Rivers: Form and Process in Alluvial Channels*. London: Methuen; 1982. 361 p.
- [2] Vigilar GG, Diplas P. Stable channels with mobile bed: Model verification and graphical solution. *Journal of Hydraulic Engineering*. 1998;124:1097–1108.
- [3] Turowski MJ, Hovius N, Wilson A, Horng M. Hydraulic geometry, river sediment and the definition of bedrock channels. *Geomorphology*. 2008;99:26–38.
- [4] Turowski JM. Semi-alluvial channels and sediment-flux-driven bedrock erosion. In: Church M, Biron PM, Roy AG, editors. *Gravel-Bed Rivers: Processes, Tools, Environments*. Chichester: John Wiley & Sons; 2012. p. 401–416. DOI: 10.1002/9781119952497.ch2
- [5] Brooks KN, Ffolliott PF, Magner JA. *Hydrology and the Management of Watersheds*. 4th ed. Hoboken: Wiley-Blackwell; 2013. 533 p.
- [6] Rosgen DL. *The River Field Book*. Ft Collins CO: Wildland Hydrology; 2015.
- [7] Kelly WR. Heterogeneities in ground-water geochemistry in a sand aquifer beneath an irrigated field. *Journal of Hydrology*. 1997;198:154–176. DOI:10.1016/S0022-1694(96)03316-1
- [8] Weng PH, Coudrain-Ribstein A, Talbi A, Bendjoudi, H. Groundwater circulations between alluvial aquifer and underlying Senonian Chalk in the Seine Valley. *Physics and Chemistry of the Earth, Part B: Hydrology, Oceans and Atmosphere*. 1999;24(1–2): 151–154. DOI:10.1016/S1464-1909(98)00027-6
- [9] Klingbeil R, Kleineidam S, Asprien U, Aigner T, Teutsch G. Relating lithofacies to hydrofacies: Outcrop-based hydrogeological characterization of quaternary gravel deposits. *Sedimentary Geology*. 1999;129:299–310. DOI:10.1016/S0037-0738(99)00067-6

- [10] Mansell MG, Hussey SW. An investigation of flows and losses within the alluvial sands of ephemeral rivers in Zimbabwe. *Journal of Hydrology*. 2005;314:192–203. DOI: 10.1016/j.jhydrol.2005.03.015
- [11] Ackerman DJ. Hydrology of the Mississippi River Valley alluvial aquifer, south-central United States— A preliminary assessment of the regional flow system. U.S. Geological Survey Professional Paper 1416-D; 1996. 56 p.
- [12] Rebouças A. Groundwater resources in South America. *Episodes*. 1999. 3:22:232–237.
- [13] Czarniecki BJ, Phillip D, Hays DP, McKee WP. The Mississippi River Valley Alluvial Aquifer in Arkansas: A Sustainable Water Resource? U.S. Geological Survey. 2002; Fact Sheet 041-02A.
- [14] Seely M, Henderson J, Heyns P, Jacobson P, Nakale T, Nantanga K, Schachtschneider K. Ephemeral and endorheic river systems: Relevance and management challenges. In: Turton A Ashton and P Cloete, editors. *Rivers, Sovereignty and Development: Hydropolitical Drivers in the Okavango River Basin Transboundary*. Pretoria: African Water Issues Research Unit – Geneva: Green Cross International; 2003. p. 187–212.
- [15] Zaisheng H. Alluvial aquifers in the North China Plain. In: Cherry, de Marsily G, editors. *Aquifer Systems Management*. London – Taylor & Francis; 2007. p. 118–126.
- [16] Wagner W. *Groundwater in the Arab Middle East*. Heidelberg: Springer-Verlag; 2011. p 330.
- [17] Thorp JH, Thoms MC, DeLong MD. The riverine ecosystem synthesis: Biocomplexity in river networks across space and time. *River Research and Applications*. 2006;22:123–147.
- [18] Ashley GM, Renwick WH, Haag GH. Channel form and processes in bedrock and alluvial reaches of the Raritan River. *New Jersey Geology*. 1988;16:436–439.
- [19] Miller JR. Development of anastomosing channels in south-central Indiana. *Geomorphology*. 1991;4:221–222.
- [20] Tooth S, McCarthy ST, Brandt D, Hancox PJ, Morris R. Geological controls on the formation of alluvial meanders and floodplain wetlands: The example of the Klip River, Eastern Free State in South Africa. *Earth Surface Processes and Landforms*. 2002;27:797–815.
- [21] Charlton R. *Fundamentals of Fluvial Geomorphology*. Oxford: Taylor & Francis Group; 2008.
- [22] Mitchell DK. Stream power and incision of five mixed alluvial-bedrock streams, northern New Mexico. *New Mexico Geology*. 2000;22:83–84.
- [23] McCarthy TS, Tooth S. Incised meanders along the mixed bedrock–alluvial Orange River, Northern Cape Province, South Africa. *Zeitschrift für Geomorphologie*. 2003;48:3:273–292.

- [24] Tooth S and McCarthy TS. Anabranching in mixed bedrock-alluvial rivers: the example of the Orange River above Augrabies Falls, Northern Cape Province, South Africa. *Geomorphology*. 2004;57:235–262.
- [25] Montgomery DR, Abbe TB, Buffington JM, Peterson NP, Schmidt KM, and J.D. Stock. Distribution of bedrock and alluvial channels in forested mountain drainage basins. *Nature*. 1986;381:587–589.
- [26] Van Niekerk AW, Heritage GL, Broadhurst LW, Moon BP. Bedrock anastomosing channel systems: Morphology and dynamics of the Sabie River, Mpumalanga Province, South Africa. In: Miller AJ, Gupta A, editors. *Varieties of Fluvial Form*. Chichester: Wiley; 1999. p. 33–51.
- [27] Keen-Zebert A. *Spatial Variation of Alluvial and Bedrock Channel Type in the Upper Guadalupe River, Texas* [thesis]. San Marcos: Texas State University; 2007.
- [28] Beck BF. *Applied Karst Geology*. Rotterdam: A A Balkema; 1993.
- [29] Emery JM, Cook GW. A determination of the nature of recharge to a bedrock fracture system. In: *Proceedings of National Water Well Association, Eastern Regional Groundwater Conference*; July 1984; Worthington, Ohio. National Water Association; 1984. p. 62–77.



---

# Monitoring of Surface Water Status in the Lower Danube Basin

---

Igor Cretescu, Zsófia Kovács and  
Sorin Mihai Cimpeanu

Additional information is available at the end of the chapter

<http://dx.doi.org/10.5772/64399>

---

## Abstract

Water pollution demands emergency actions for better water resource management to respect the concept of sustainable development. The aim of the Water Framework Directive, as long-term water policy of the European Union, is to assure the good quality of surface waters. Each state from Europe has to identify all the river basins lying within their national territory and to assign them to individual river basin districts. In this respect, an effective integrated system and monitoring technology, analysing, interpreting data and utilizing the results to make decisions related to the water resources protection, were developed. The main objectives are focused on the expansion of monitoring activities and obtaining more detailed information on the state of surface waters. Specific recommended equipment which enables to perform the analysis of recommended water quality parameters should be placed on the monitoring stations of the Lower Danube Basin. Respectively, this lack of equipment provides a challenge in the development of effective methodologies for collection and analysis of water quality data. The main priority was the development of an integrated water catchment area management strategy and to build up the online continuous monitoring system. Some of the technical goals for continuous water monitoring were reached in Hungary and Romania and are presented here.

**Keywords:** surface water monitoring, water quality, early water system, water management

## 1. Introduction

The main objective of humanity is to find solution for environmental issues especially the ones related to water pollution which demands emergency actions for a sustainable development of the society. Protection and management of water resources are the key elements of sustainable development. The Water Framework Directive (WFD 2000/60/EC) was created as the long-term water policy of the European Union (EU) [1]. The aim of the WFD is that the quality of surface waters achieve good ecological and chemical status by 2015 (2021, 2027). All countries from Danube riverbanks should have an inventory of all the river basins lying within their national territory and should assign them to individual river basin districts.

The most international river basin in the world is the Danube River Basin which covers more than 800,000 km<sup>2</sup> and covers 10% of European territory including 19 countries. The Danube River is divided into three 'reaches'. The Upper Danube stretches from the Danube's source in Germany to the 'Porta Hungarica' east of Vienna. The middle Danube then flows until the dam namely 'Portile de Fier' (Iron Gates) in Romania. The Lower Danube then runs into the Black Sea. Taking into consideration the huge dimensions of the Danube catchment area and the number of the countries with different specific conditions, transboundary river basin management requires a special attention [2–4]. In 1994, the Danube River Protection Convention was signed by the main stakeholder countries from the region with the goal to enhance transboundary cooperation to protect the river and its basin. The EU and 14 countries from the Danube Basin are contracting parties of the International Commission for the Danube River (ICPDR). The Commission works to manage the waters of the Danube Basin sustainably [2]. The preparation of the Danube River Basin District Management Plan (DRBMP) was the most important task in the implementation of the Water Framework Directive [4]. To reach the set goals, the first DRBMP was prepared in 2009, and it is reviewed every 6 years. The first review was made in 2015, when activities were investigated which had negative effects on the quality of Danube Basin waters, and the Commission also evaluated the current status of water bodies and the effects of interventions. Based on the results, Danube countries have prepared action plans together to be implemented in the upcoming period. The examination of important pressures in the Danube River Basin (DRB) is the crucial elements of the plan. In this respect, the development of an effective integrated system consisting of monitoring technology, data analysis, interpretation and result utilization system is essential to make decisions to protect water resources. Nowadays, due to the advanced progress of science and technology, new measurement and communication techniques were developed, leading to real-time decision-making tools. In this chapter, our attention is focused especially on the aspects related to integrated river basin monitoring. The main objectives are focused on the expansion of monitoring activities and obtaining more detailed information on the status of surface water [2].

### 1.1. Danube River Basin status-monitoring process

The main hazards to water quality in the Danube River Basin are the following: nutrient pollution, hazardous substances, hydro-morphological alterations and organic pollution.

There are many anthropogenic sources which affect the water quality of the Danube catchment area [4]. Overlooking the state of waters, economical water utilization analysis, monitoring system planning and designation and joint program measures were all planned, so that the objectives of the Water Framework Directive could be reached [4]. Monitoring programmes provide appropriate information about the status of the Danube Basin; the subprogrammes are in harmony with the implementation schedule of the WFD. The goal of the TransNational Monitoring Network (TNMN) system is to provide a comprehensive picture about pollution events, the long-term changes in water quality, and main pollution loads of the Danube basin. It provides the comparability of data, that is, uniformity of data acquisition and exchange. Every year TNMN prepares an annual report from the measurement data of national laboratories, which include sampling location, measurement parameter list and the processing of measurement results. The requirements of the WFD have to be met both by the Danube River Protection Convention and the TNMN (revised) surface water surveillance monitoring programmes. Meanwhile, Joint Danube Survey (JDS) contains investigative monitoring results.

Investigative monitoring is mainly a national task, but to fulfil the goals of the basin level, JDS was established, which is repeated every 6 years. Surveys performed by JDS in 2001, 2007 and 2013 gave a snapshot from the whole length of the Danube and the significant tributaries. The goal of the JDS is to fill missing information from the monitoring networks of the Danube River Basin, to harmonize monitoring methods already used, to evaluate the effects of novel chemical compounds or elements in various matrices and to test new devices and methods. JDS programmes enhance the reliability of data and information provided by the TNMN system.

#### *1.1.1. TransNational Monitoring Network*

The TNMN of the ICPDR monitors water quality of the Danube River Basin regularly. The TNMN is able to act as the basis of an integrated water quality measurement network in the whole catchment, and it not only provides data of water quality and pollution trends but also helps in harmonizing water quality assessment and evaluation methods in the affected area. The laboratories in the network are allowed to use analytical methods of their choice as long as these meet certain pre-agreed criteria, and enable the analysis of physical-chemical quality elements and priority substances. A system-wide quality control programme (performed yearly) was established to ensure that data have high quality across the basin. Data are stored in a database established by ICPDR. National laboratories provide data to information managers, who collect, check and convert the data into a data exchange file format (DEFF file), which are then sent to the data centre for final checking and processing. When the ICPDR gives its approval, these data are sent to the website of the project [4]. Measurement points for water quality assessment within the TNMN are presented in **Figure 1** [5]. Shown in **Figure 1**, there are 114 surveillance monitoring stations, where water quality components are analysed and 12 measurements per year are reported in TNMN yearbook [6].

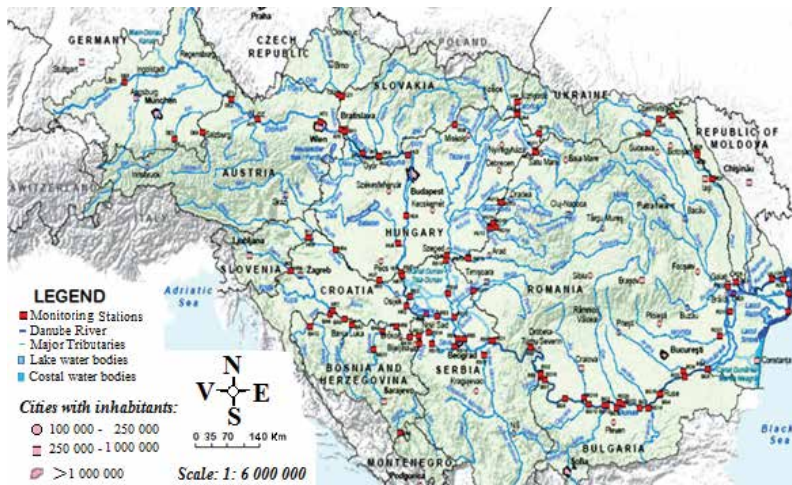


**Figure 1.** The map of surveillance monitoring stations in the Danube Basin (TNMN) (adapted from [6]).

### 1.1.2. Joint Danube Survey

Annual water quality evaluation has been complemented by JDSs to provide a picture of the ecological status of the Danube. They obtain biological and microbiological, chemical, hydro-morphological and toxicological data. They are the world's largest river research expedition, with the goal to give comprehensive and reliable data and information from the whole length of the Danube and its several tributaries, about both water quality and causes of pollution. The other tasks of JDS are to provide information about parameters which are not present in the continuous monitoring plan, to help the work of ICPDR and to call attention to water quality management. The first Joint Danube Survey was in 2001. A total of 140 various parameters (chemical, biological, microbiological) were measured on the entire length of the river, thereby providing a considerable amount of data [3, 4]. The survey is supposed to be repeated every 6 years, thus another snapshot was made in 2007 and 2013 about the status of the Danube and its tributaries. The surveys have shown that the quality of water in the Danube River Basin show an improving tendency, but it showed also that special problems have to be tackled at several tributaries and near large cities in the lower section. JDS improves available databases, and thus helps evaluation of water quality [3].

## 1.2. Water quality of Danube River Basin

TNMN, which gives national data, and the three JDS surveys provide information for the status assessment of the Danube River Basin. The upstream water pollution has negative consequences on the downstream protected areas, especially on the Danube Delta Nature Reservation. At the same time, riparian localities that use water from the Danube for anthropic activities are influenced. Around 65% of the whole length of the Danube is at risk of nutrient pollution, this makes it a challenge which needs urgent attention, especially, that it connects freshwater and marine habitats. The development of novel solutions and nutrient management strategies

are needed to reduce the N and P content of the DRB [7]. Agglomeration, agriculture and industry are the main sources of nutrients. There are two kinds of pollution sources: diffuse and point sources.

The measurement results of TNMN between 2001 and 2009, and the JDS1 (2001) and JDS2 (2007) results were processed from the viewpoint of nutrient pollution [8]. The measured parameters are N-ammonium, N-nitrite, N-nitrate, P-orthophosphate and two total forms total nitrogen and total phosphorous, and all of them show that there is an improving tendency of nutrient load.

Regular laboratory measurements taken in the TNMN system show larger concentration values than JDS expedition measurement results. From the evaluation of the TNMN between the 2001 and 2009 timeframe, it can be seen that there is a minimal decrease in the concentrations nearing the lower river section, but in the Lower Danube section itself in the case of  $\text{NO}_3\text{-N}$  and  $\text{PO}_4\text{-P}$  concentrations there is a more frequent occurrence of extreme values [8]. From the evaluations prepared by Hamcevic et al, 2015, it can be also seen that there are more extreme values in the Lower Danube region, meaning that local effects are more extreme. This highlights the importance of continuous monitoring and its *raison d'être*. Urban, municipal and industrial run-off can contain heavy metals, which cause harm to water ecosystems when their concentration becomes larger than the tolerance limits [9]. A number of surface water bodies in the Danube River Basin District have not reached good chemical quality status (2013/39/EU), as they were heavily affected by priority substances (heavy metals, pesticides, industrial pollutants, other pollutants). The goal of heavy metal monitoring is to measure its effect on the Danube Delta. The 2008/105/EC directive prescribes concentration limit values for 33 priority and 8 other pollutants. The modifying directive 2013/39/EU broadened the list with 12 new substances. On the Danube and its tributaries in respect of Annual Average Environmental Quality Standards (AA-EQS) and Maximum Allowable Concentration Environmental Quality Standards (MAC-EQS), the critical pollutants are cadmium, mercury, lead and copper [9]. From the analysis prepared by Mr. László Ferenc, 2015, it can be seen that in the timeframe of 2008–2011, dissolved cadmium load decreased, while dissolved lead, mercury and copper load increased. From the viewpoint of heavy metals, tributaries have significant loads. Tributaries are the most affected from the viewpoint of heavy metals (e.g. tributaries: cadmium, 33; lead, 25; mercury, 33; and nickel, 15) [4], so they do not accomplish the goals set by WFD.

These surveys support future strategies and the elaboration of action plans, and they also help in the selection of location and measured indicator parameters of continuous monitoring systems.

### **1.3. Some aspects concerning the progress of transboundary monitoring in the Tisa Basin**

It is known that the basin of the Tisa River brings a high hydrological contribution to the water balance of the Danube Basin. However, special attention is needed on the Tisa Basin due to the environmental issues associated with the pollution generated by accidents within the mining industrial areas located in the basin. In this way, it was necessary to prepare a strategy for the management of the emergent problems related to transboundary pollution accidents.

This strategy envisaged to set up the measures for the elimination or diminishing of dangerous substances, in line with the overall trend of the environmental issue and of European legislation, based on a variety of approaches correlating with the different particular cases. Therefore, in the European Member States, the Integrated Pollution Prevention and Control Directive (IPPC) and the Dangerous Substances Directive were implemented. Other directives such as the Urban Wastewater Treatment Directive and other environmental management tools, such as the Best Available Techniques (BAT) for industrial sectors and Best Environmental Practices for Agriculture, played an essential role in the diminishing of environmental impact of hazardous substances in the Tisa River Basin [10, 11].

#### 1.4. The Danube Accident Emergency Water System

In the frame of the International Commission for the Protection of the Danube River (ICPDR), some measures for accident prevention have been considered for the Danube and Tisa countries. The Danube Accident Emergency Water System (DAEWS), which during transboundary pollution accidents is able to alert stakeholder countries, was also established by the ICPDR.

Particularly, decision-making tools are very useful for a better management of surface waters, including the Danube Basin, where an Accident Emergency Warning System (AEWS) was implemented. This AEWS represents a mode of putting in practice the decisions from the Helsinki Transboundary Convention of 1992 and the Sofia International Danube Protection Convention of 1994 [5].

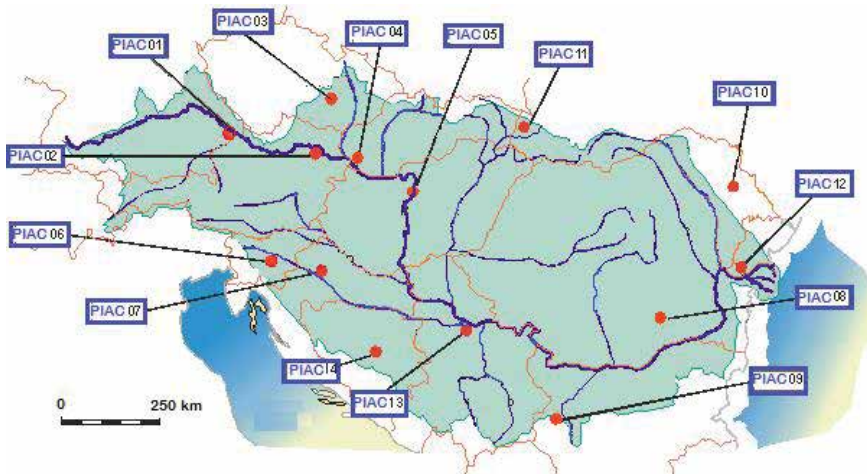


**Figure 2.** Implementation of the Accident Emergency Warning System (AEWS) within the Danube River Basin adapted from [12].

When a risk of transboundary water pollution is detected by the AEWS, a warning message is transmitted to the countries belonging to the affected river, via through a Principal International Alert Center (PIAC) located in each country (see **Figure 2**). These structures play an

important role in the decision process concerning the action measures for public protection. PIAC includes a non-stop communication unit for warning messages, an expert unit for impact assessment and a decision making to determine a situation for which an international warning should be launched [12].

This system will make timely and effective damage prevention and mitigation possible, which can be the results of transboundary pollution disasters, for which we have seen examples in the last two decades [4].

### **1.5. Areas of use of real-time preventive water monitoring systems**

The most important tool of water quality protection and quick detection of pollutants is the periodical measurement or monitoring of water pollutant concentration. Because of this the laboratories of national authorities perform national and international, so-called, cross-border water quality measurements. These information are used in the preparation of annual TNMN reports, also, countries prepare their water management plans based on data provided by the authorities. Based on the applied long-term and expedition-like monitoring activities, we think that the currently available equipment park and informatics services make it possible to apply a real-time preventive warning monitoring system on the Danube Basin. There are operating automatic water quality monitoring stations on the Danube water basin, but in this chapter, we show you a cost-effective method with a modular solution, which can be used effectively

- in the areas where based on the results of traditional monitoring, there is a large number of extreme results
- in areas where actions are implemented, to check the results of the action
- at critical emission locations (ARS points)
- on tributaries.

The forecasting monitoring system which we introduce here is suitable for the prompt detection of pollutants, and for alarm duties, as it is operating continuously, as only real-time monitoring can ensure forecasting and detection of pollutants.

The methodology of such a cost-effective system was elaborated for the largest tributary of the Danube, the Tisza [11]. The adaptation and application of the forecasting continuous early warning-monitoring system in the Lower Danube region could influence effectively the improvement of the quality of the Black Sea, the reduction of eutrophication by timely interventions.

## **2. Water-monitoring network methodology**

In the Lower Danube Basin, the main priority is to build a water quality network system of water catchments areas, which involves specific analytical equipments designed for water quality parameters selected for each particular station. The following aspects should be considered to support the above-mentioned objectives:

- Most important background information of the catchment area. Description of river basin (or catchment area)
- Application of adequate international standard methods
- Assessment of existing monitoring systems
- WFD typology of water bodies (high-, mid-, lowland altitude)
- Identification of pollution sources (hot spots; diffuse sources)
- Determination of pollutants (physical-chemical, biological parameters)
- State of tributaries
- Assignment of sampling sites and water sampling methods
- Power supply/power consumption
- Optimization of operational and maintenance cost.

The Early Warning System (EWS) is a key tool in surface water management, with a different mechanism. Overall, the two components—early warning function and effect-based monitoring of water analysis—form a cost-effective integrated system, which could perform sampling, analysis and toxicity testing of surface waters [11].

It should be noted that EWS contributes to the evaluation of different scenarios and to solving specific issues. To assure accurate analysis of the scenarios, the elements of the EWS should be in conformity with European regulations. Compatibility between the elements of the EWS, including information systems and databases from each country should be assured when considering implementation and information communication within EU countries.

Implementing the EWS on the Lower Danube water basin substitutes the lack in the monitoring system of surface water bodies, as related to the following aspects [11]:

- Limited timelines and insufficient frequency for realistic evaluation of the quality progress of water streams.
- Lack in appropriate details regarding the water quality parameters for pollutant modelling.

### **2.1. Special installation aspect**

When installing an EWS, several aspects should be taken into consideration [11]. Special installation aspects: overall, two objectives are envisaged when the online monitoring station is installed on a water body. One objective is the monitoring of water surface quality according to the WFD (measurement locations are set in the national monitoring network), while the other objective is to provide early warning of accidental pollution (e.g. early detection of pollutant generated by different types of pollution sources).

Particular installation aspects: In the case of online monitoring systems used for early warning detection, there are several recommendations:



- The early warning detection system has to be near the potential polluting sources, which allows rapid detection of pollution phenomena.
- Installation of such systems should allow sampling from low water levels; in the same time, the measuring systems should be anchored against high water flows and floods; for the systems that are located on the riverside, it is necessary to provide the feeding systems with technological water for analysis purposes. In these cases, specific sampling pumps with autonomous power supply (not connected to the electricity network) should be considered. Long sampling lines should be avoided, as the dwelling time of the sample within the pipe should not be more than 10–20 s. For this reason, sampling pipes shorter than 30–50 m are usually recommended.
- Generally speaking, the installation layout should ensure easy access to the system to perform regular maintenance. In the case of floating systems, these should be easily accessible by boats.
- Power supply should be provided from different sources, for example, electrical networks, solar cells, batteries etc. When a source is not available, it could be replaced by another one.
- In terms of communication technology for sending measurement data, several alternatives can be considered: GSM signals, telephone line, WIFI, etc. Data are collected and processed via a server that is connected to the Internet, being accessible by a user having necessary access rights.
- Moreover, the system should be equipped with specific defence elements against any sabotage act, such as alarms, camera connected to the Internet, etc. For example, the changes in the Global Positioning System (GPS) coordinates of the floating unit or in the integrity structure can trigger sound effects or SMS alarms.

## 2.2. Determination of the measuring parameters

Determination of the measuring parameters at the sampling site should be performed by taking into consideration the following aspects [11]:

- The measurement range, the type and concentration of the pollutant. In contrast to predictable scenarios, in the case of complex environments with frequent changes in the different parameters due to the pollution phenomena, measurement of conductivity (or of other easily measurable parameters) for process monitoring is often recommended, due to its simplicity.
- The potential polluting sources of the water catchment area are also important in establishing the measuring parameters. For example, the measurement of pH only, instead of both chemical oxygen demand (COD) and pH could be performed in the waters with low pH, such as those associated with whey pollution emitted from a cheese factory, due to low pH. The change in the pH could indicate the presence of pollution.
- When several methods are available for a measured parameter, a low-cost alternative should be considered, even if there is a loss of accuracy. This is the case, for example, when we

compare a chemical analyser versus a standard method. In some cases, there are non-standard methods that could perform better for online measurement because of easy maintenance, low operating costs and simple design, but at the cost of a weaker correlation with the laboratory results. For example, when measuring COD with standard dichromate method, the results are closer to laboratory results than in the case of using UV absorption. However, the investment and operating costs associated with the use of UV absorption are lower than in the case of the analyser working with the dichromate method. In addition, the measurement frequency can increase from one measurement per hour of the dichromate method to one measurement per minute in the other case, at a similar accuracy.

- Measuring summarized parameters (TOC: total organic carbon; COD: chemical oxygen demand; BOI: biological oxygen demand; TN: total nitrogen; TP: total phosphorous; PAH: polyaromatic hydrocarbon; phenol index) or online measurement of toxicity appears to be essential in the case of early warning detection systems.
- Also, all automatic water samplers should be integrated for better diagnosis of the pollution.

Modular expandable systems are currently being proposed for use at particular sites, where specific parameters have to be monitored. Appropriate integration of different units (including those related to different manufacturers) is supposed to increase the efficiency of the overall monitoring system. For different devices, suitable connection systems should be provided. Also, the system should be modular, so when a device needs replacement, the spare item should be easily placed into the unified signalling system, precalibrated in line with metrological standards. Several more aspects are presented in literature data in Water Quality Early Warning System on Transboundary Watercourses of Tisza River Basin, 2014 [11].

### 3. Monitoring of water quality aspects

Online water analysis advantages:

- Indication of short-term and long-term changes in water quality as a basis for water management measures
- Early detection of incidents and illegal discharges
- Assessment of hazard potential arising from discharges
- Clues to identity of water pollution offenders
- Sampling platform
- Prevention: continuous monitoring of water bodies has a deterrent effect that helps prevent illegal discharges or other water pollution
- Continuous data collection for decision making
- Others: for example, verification of success of water conservation measures.

A new analytical monitoring concept is required, as at a single point, pollution peaks can usually be detected for 0.5–2 h, some of which occur at night and in the weekend. Therefore measurement intervals should be on an hourly basis if possible, operating 24/7.

The main priority is to develop integrated water catchment area management plans, and to establish the network of online continuous monitoring system of the water catchment area. Online monitoring systems indicate long and short-term changes of water quality parameters, the data obtained this way can be used to establish a basis for water management measures and activities.

### 3.1. Water quality parameters (WFD)

To determine the parameters which should be measured by the online monitoring stations to be installed on surface waters the Water Framework Directive should be referred to [1]. Based on an ecological approach, the Water Framework Directive divides hydro-chemical attributes into two groups: the background physical-chemical parameters supporting the ecological status and the specific pollutants typical of the particular water catchment area.

The reduction of dangerous substances from point sources can basically be achieved by regulatory actions. The 2008/105/EC directive [13] contained environmental quality regulations and water pollution immission limits. This was modified by the 2013/39/EU directive, in respect to priority substances (12 new substances in the list).

The parameters characterizing the chemical status of the water body are divided into three main groups, according to **Table 1**.

General physical-chemical parameters	Nutrition indicators	Priority hazardous substances (by "33+8" list and the list of "other hazardous substances")
Water temperature, pH, electrical conductivity, dissolved oxygen, total suspended solids, COD <sub>p</sub> , COD <sub>k</sub> , TOC, BOD <sub>5</sub> , total dissolved solid (TDS), total water hardness, dissolved iron, dissolved manganese, calcium, magnesium, sodium, potassium, alkalinity, chlorine, sulphate	Ammonium, nitrate, total nitrogen, orthophosphate, total phosphorus, chlorophyll-a	"33" list organic: Polyaromatic hydrocarbon (PAH) compounds: naphthalene, anthracene, fluoranthene(VI), halogenated polyaromatic hydrocarbons: benzo(a)pyrene 1,2,4-trichlorobenzenes, pentachlorobenzene, hexachlorobenzene, pesticides: alachlor, atrazine, chlorfenvinphos, chlorpyrifos, endosulfan (alpha-endosulfan), hexachloro-cyclohexane, gamma lindane isomer "Other hazardous substances" organic: DDT compounds, aldrin, dieldrin, carbon-tetrachloride, tetrachloro-ethylene "33" list (heavy metals): cadmium, lead, mercury, nickel "Other hazardous materials" (heavy metals): total chrome, arsenic, zinc, copper

**Table 1.** The parameters characterizing the chemical status of the water body [1, 13, 23].

These essential quality parameters for water pollution assessment are used in different ways. It is imposing that in all of the cases the set value is lower than the limited values specified in environmental legislation in each country in strong correlation with the European legislation [14]. In order to have a better evaluation, the usage of a global water quality index should be taken into consideration according to literature data [15]. The methodology for determining these water quality parameters is also presented in detail in technical literature, but some particular achievements of authors, with application in the water quality monitoring will be presented in the following paragraphs.


#### 4. Overview of applicable low cost surface water monitoring technology and methodology



The range of devices suitable for continuous on-line monitoring, which are shown in this chapter were developed in Hungary and utilized on the stream Veszprémi-Séd in 2013, and the river Ipel in 2015. The development of a heavy metal monitoring device has taken place in Romania, which was used for quality measurements on the Bahlui River. By unifying these systems and connecting them to expert systems on national levels an effective water management system could be established on the Lower Danube Basin.

The versatile character of the mobile water quality station is accomplished by the modular structure of the station, being designed to work in extreme weather conditions. Further requirements for the monitoring stations without human intervention are related to continuously and reliably ensuring the operation of equipment, the maintenance of devices and the optimal consumption of reagents. The initial investment costs are moderate, but the operating and maintenance costs are significant. The station can be moved easily, and therefore, it can be relocated within hours if necessary. It allows operation for long periods, with low maintenance and in isolated places.

##### 4.1. Types of monitoring stations and signals for EWS systems

In **Table 2** are presented the most recommended types of monitoring stations [11].

Type of monitoring station	Measureable parameters	Technical characteristics
Multi-parameter system built in buoy 	Multi-parameters selected from the following: water temperature, pH, redox-potential, conductivity, DO, turbidity, chlorophyll-a, blue algae, SAC254, PAH, parameters measureable with ion-selective electrodes (ammonium, chloride, nitrate)	Energy supply: solar cell and battery. Sensors with low energy demand

Type of monitoring station	Measureable parameters	Technical characteristics
Simple multi-parameter measurement system built in device case installed on the riverbank	Water temperature, pH, redox-potential, conductivity, DO, turbidity, chlorophyll-a, blue algae, SAC254, PAH, oil pollution, parameters measureable with ion-selective electrodes	Energy supply: solar cell and battery. Central unit with the measurement system installed on buoy. An automatic sampler with low energy demand is considered
Measurement system installed into small-sized mobile container 	Water temperature, pH, redox potential, conductivity, dissolved oxygen, turbidity, chlorophyll-a, blue algae, SAC254, PAH, oil pollution, parameters measureable with ion-selective electrodes	Energy supply: solar cell and battery. Versatile system, which can be easily relocated to critical locations, according to the necessity. Central unit with the measurement system installed on buoy. An automatic sampler with low energy demand is considered
Complex measurement system installed into a brick building or large container 	Water temperature, pH, redox potential, conductivity, dissolved oxygen, turbidity, chlorophyll-a, blue algae, SAC254, PAH, oil pollution, parameters measureable with ion-selective electrodes Complex measurements carried out by chemical analysers: TOC, COD, toxicity, heavy metal analyser, online gas-chromatograph, special analysers suitable for measuring individual parameters	Higher energy demand than the above ones. Energy supply by electric power supply connected to the following electricity sources: solar cells with large solar panels and fuel cell Complex measurement system installed into a brick building or large container. The connection of pure technological water may also be necessary
Automatic samplers	This system allows connecting an automatic sampler which takes water sample and stores it cooled in standard circumstances in case limit values are exceeded or on operator's remote instruction	

**Table 2.** The recommended types of monitoring stations.

The advances of flow techniques for analysis of persistent pollutants (organic pollutants as pesticide, drugs, dyes, etc. or inorganic pollutants as heavy metal ions) from surface waters [16] are presented in detail in a book chapter, vol. 3, edited by C. Zaharia.

A more comprehensive presentation about organic pollutant detection using flow injection analysis techniques could be found in our review [17]. Also, for total content of organic (measured as COD by flow analysis with chemiluminescence detection), a new pulsed xenon flash lamp photoreactor was developed together with Warmya and Mazurya University from Olsztyn, Poland [18].

For detection of heavy metal ions, new electrochemical sensors were developed according to our review [19]. Among the electrochemical techniques, potentiometry and voltammetry are the most suitable for monitoring of heavy metal ions in surface waters. Therefore, special solid-contact ion-selective electrode for copper(II) detection in water samples were developed as potentiometric sensors, together with the University of Barcelona, Spain [20]. Among the monitored heavy metals, mercury plays an important role due to its toxicity, bioaccumulation and hard biodegradability. The methodologies for mercury analyses in water samples are complex, need expensive equipment and require qualified operators. Taking into consideration all the above aspects, our attention was focused on a voltammetric technique suitable for mercury detection and quantification of their concentration in water samples involving the experiences of our colleagues from the oldest university in Iasi and in Romania [21].

The signal types for EWS systems are presented in **Table 3**.

Water quality signals	Signals concerning the measurement system	Safety signals	False alarm
- Signal (normal) when a warning is sent in SMS (text or voice message) or e-mail when a specified limit value is exceeded - Signal of sampling when in predefined situations the sample is stored with the help of the installed cooled sampler, and the operator takes the water sample to the laboratory (e.g. hourly sampling, 24-hour average sample, sampling is always done and if problem occurs, it keeps the sample and gives a signal). If the sample is stored, the type of dish concerning the physical-chemical parameters to be determined must be specified (e.g. glass or plastic)	- Signal for failure of measuring device - Signal for erroneous sampling (e.g. no water sample, pump problem) - Battery level is low - Signal for running out/replacing reagent - Signal for calibration	- Signal for opening door - Signal for changing GPS coordinates - Signal for power supply problems	- Operating problem (contamination of probe-head sensor, blocking of sampling tube, failure of measurement system)

**Table 3.** Signal types for EWS systems [11].

#### 4.2. Methodology for EWS

When considering the equipment and technology from different countries, EWS approach could be changed according to several aspects such as [11]:

- Automated simulation of different pollution scenarios. Different kinds of warning procedures, including SMS, e-mails, etc. and different responsibility levels; the person in charge will receive warning messages to perform the corresponding management tasks according to the procedure.
- Integration of each national EWS within international warning systems:
- Existence of some alarm centres as Principal Industrial Alarm Centre (PIAC) and Accident Emergency Water System (AEWS).
- Complementary data (e.g. weather, precipitation) and their integration into the system are necessary when precipitation is expected; also the pollution front could be estimated according to the distance of the location from the pollution source.

The Early Warning System has user friendly features, and its logical structure is presented in **Figure 3**.

The development of an expert system for monitoring of surface water in the *Lower Danube Basin* was an imperative for a better management of water resources, taking into account the higher degree of pollution in this area, which was caused by the anthropogenic activities (industry and agriculture) from the riverine countries. Therefore, the specialists from the Technical University of Iasi (Romania), Technical University of Chisinau (Republic of Moldova) and University of Pannonia from Veszprém (Hungary) brought their contribution to the development of such an advanced monitoring expert system [22].

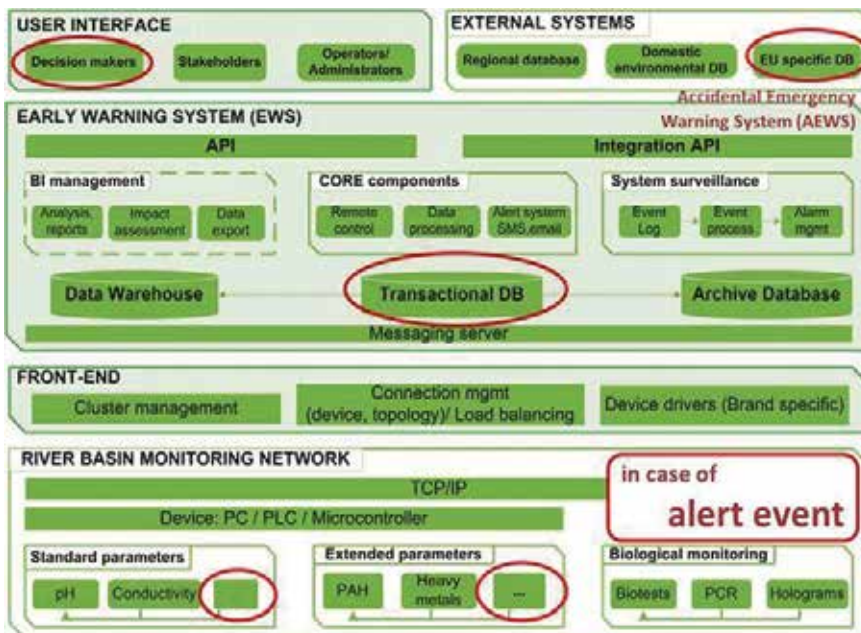


**Figure 3.** Logical architecture of Early Warning System [11].

## 5. Conclusion

According to the objective stipulated in the Water Framework Directive (WFD), good chemical and ecological status/or potential has to be ensured and achieved for all surface water bodies. Monitoring results serve the validation of the pressure analysis. An overview of the impacts on water status is required to initiate measures. In this context, the issues addressed in this manuscript could be of real interest for specialists. Implementing the Early Warning System (EWS) on the Lower Danube water basin would significantly improve our abilities to detect any kind of accidents related to surface water bodies.

In the 'Overview of applicable low cost surface water monitoring technology and monitoring methodology' section, some technical achievements for continuous water monitoring made in Hungary (mobile water quality stations, water monitoring buoy, robotic analyser ship, continuous monitoring and EWS methodology) and Romania (flow techniques for analysis of persistent pollutants and water quality expert system) are described. Also, some aspects concerning the development of a monitoring expert system designed for the surface waters in the context of sustainable management of water resources in Romania, Hungary and Moldavia are welcome in order to assure the complementarity with above mentioned technical achievements. Harmonizing these systems ensure the adaptation on the Lower Danube Basin. Moreover, in the previous papers of the authors, more details on the monitoring of water quality and the dispersion of common pollutants are presented; finally, the evolution of water quality indicators is predicted by using mathematical models.

In the light of WFD, the specialists from Technical University of Iasi (Romania), Technical University of Chisinau (Republic of Moldavia) and University of Pannonia from Veszprém (Hungary) brought their contribution to the development of an expert system for monitoring of surface water in the context of sustainable management of water resources in the *Lower Danube Basin*.

## Author details

Igor Cretescu<sup>1</sup>, Zsófia Kovács<sup>2</sup> and Sorin Mihai Cimpeanu<sup>3</sup>

\*Address all correspondence to: icre@tuiasi.ro

1 Environmental Engineering and Management Department, "Gheorghe Asachi" Technical University of Iasi, Iași, Romania

2 Institute of Environmental Engineering, University of Pannonia, Veszprém, Hungary

3 University of Agronomical Sciences and Veterinary Medicine, Bucharest, Romania



## References

- [1] EU Water Framework Directive (WFD). Directive 2000/60/EC of the European Parliament and of the Council establishing a framework for the Community action in the field of water policy [Internet]. 23 October 2000. Available from: [http://ec.europa.eu/environment/water/water-framework/index\\_en.html](http://ec.europa.eu/environment/water/water-framework/index_en.html)
- [2] ICPDR. The Danube River Basin District Management Plan, Part A-Basin-wide overview, update 2015, ICPDR-International Commission for the Protection of the Danube [Internet]. 16 December 2015. Available from: <https://www.icpdr.org/main/management-plans-danube-river-basin-published>.
- [3] Liška I., Wagner F., Sengl M., Deutsch K., Slobodník J. Joint Danube Survey 3. In: 4 Chapter monitoring networks and status assessment. ICPDR – International Commission for the Protection of the Danube River; 2011 update 2015.
- [4] Liška I. The Danube river basin, managing an international river basin towards water quality protection: the Danube case. In: *The Handbook of Environmental Chemistry*. 9 July 2015th ed. Springer-Verlag, Berlin, Heidelberg; 2015. Vol. 39, pp. 1–20. DOI: 10.1007/698\_2015\_388
- [5] ICPDR. International Commission for the Protection of the Danube River [Internet]. Available from: <http://www.icpdr.org>
- [6] Mrafkova L., Slovak, Hydrometeorological Institute, Bratislava in cooperation with the Monitoring and Assessment Expert Group of the ICPDR. In: I. Liska, editor. ICPDR Secretariat, 2015. *Water Quality in the Danube River Basin-2013, TNMN-Yearbook 2013*. <https://www.icpdr.org/main/publications/tnmn-yearbooks>: ICPDR – International Commission for the Protection of the Danube River, Overall coordination and preparation of the TNMN Yearbook and database in 2015; 2015.
- [7] Popovici M. The Danube River Basin, Nutrient Management in the Danube River Basin. In: *The Handbook of Environmental Chemistry*. 19 December 2014th ed. Springer-Verlag, Berlin, Heidelberg; 2014. Vol. 39, pp. 23–38. DOI: 10.1007/698\_2014\_311
- [8] Hamchevici C., Udrea I. The Danube River Basin, Pollution nutrients in the Danube Basin. In: *The Handbook of Environmental Chemistry*. 9 July 2015th ed. Springer-Verlag, Berlin, Heidelberg; 2015. pp. 39–60. DOI: 10.1007/698\_2015\_388
- [9] Ferenc László. The Danube River Basin, Pollution by Metals in the Danube River Basin. In: *The Handbook of Environmental Chemistry*. 9 July 2015th ed. Springer-Verlag, Berlin, Heidelberg; 2015. pp. 85–94. DOI: 10.1007/698\_2015\_388
- [10] ICPDR. Journey to a Balanced Tisza Basin. An Introduction to the Integrated Tisza River Basin Management Plan [Internet]. 2011. Available from: [https://www.icpdr.org/main/sites/default/files/Tisa\\_04082011.pdf](https://www.icpdr.org/main/sites/default/files/Tisa_04082011.pdf)
- [11] VRIC Nonprofit Ltd., Environmental Institute s.r.o. Initial study – water quality early warning system on transboundary watercourses of Tisza river basin, Chapter 1–4.

[http://www.danubewaterquality.eu/uploads/mod\\_files/WQM-EWS\\_part-1-4\\_EN\\_v2.0\\_.pdf](http://www.danubewaterquality.eu/uploads/mod_files/WQM-EWS_part-1-4_EN_v2.0_.pdf): Danube Region Strategy PA4; 2014.

- [12] ICPDR. International Operations Manual for PIACs of the Danube AEWS, International Operations Manual for Principal International Alert Centres of the Danube Accident Emergency Warning system [Internet]. 2014. Available from: <https://www.icpdr.org/main/activities-projects/aews-accident-emergency-warning-system>
- [13] The European Parliament and of the Council. 2008/105/EC; Directive 2008/105/EC of the European Parliament and the Council on environmental quality standards in the field of water policy, amending and subsequently repealing Council Directives 82/176/EEC, 83/513/EEC, 84/156/EEC, 84/491/EEC, 86/280/EEC and amending Directive 2000/60/EC. Official Journal of the European Union – EUR-Lex. 2008 (24 December 2008).
- [14] Benchea R.E., Cretescu I., Macoveanu M. Monitoring of water quality indicators for improving water resources management of Bahlui River. *Environmental Engineering and Management Journal*. 2011;10(3):357–366.
- [15] Breabăn I.G., Paiu M., Cojocaru P., Cretescu I. Studies upon the groundwater quality index of the aquifer from Barlad middle basin. In: *International Multidisciplinary Scientific GeoConference, 13th SGEM GeoConference on Water Resources. Forest, Marine and Ocean Ecosystems, SGEM2013 Conference Proceedings*; 2013; Albena, Bulgaria. 2013. pp. 317–324. ISBN 978-619-7105-02-5/ISSN 1314-2704.
- [16] Cretescu I., Benchea R.E. Chapter 8: Advances of flow techniques for analysis of persistent pollutants from surface waters, in *Current Topics*. In: C. Zaharia, editor. *Concepts and Research Priorities in Environmental Chemistry. “Alexandru Ioan Cuza”*, Iasi ed. Iasi, Romania. 2012. pp. 173–192. DOI: ISBN general: 978-973-703-797-8, ISBN volume: 978-973-703-798-5
- [17] Benchea R.E., van Staden J., Cretescu I., Macoveanu M. Flow injection analysis for the determination of organic pollutants in surface waters. In: *The Annals of the “Dunarea de Jos” University of Galati, Mathematics, physics, chemistry, informatics, III(XXXII), Fasc. II*; 2009; 2009. pp. 38–50.
- [18] Benchea R.E., Cretescu I., Kalinowski S., Koronkiewicz S. A novel pulsed xenon flashlamp photoreactor and its potential applications in flow analysis with chemiluminescence detection. *Analytical Methods*. 2013;5:3650–3656.
- [19] Tutulea M.D., Cretescu I., Sibiescu D., Stan C.S. Electrochemical sensors for heavy metal ions detection from aqueous solutions. *Environmental Engineering and Management Journal*. 2012;11(2):463–470.
- [20] Tutulea M.D., Wilson D., Valle M.D., Schreiner C.M., Cretescu I. A solid-contact ion selective electrode for copper(II) using a succinimide derivative as ionophore. *Sensors*. 2013;13(4):4367–4377.

- [21] Verestiuc P.C., Cretescu I., Tucaliuc O.M., Breabăn I.G., Nemtoi G. Voltammetric studies on mercury behavior in different aqueous solutions for further development of a warning system designed for environmental monitoring. *Journal of Electrochemical Science and Engineering*. 2014;4(4):177–186. DOI: 10.5599/jese.2014.0068
- [22] Cretescu I., Craciun I., Benchea R.E., Kovács Z., Iavorschi A., Sontea V., Macoveanu M. Development of an expert system for surface water quality monitoring in the context of sustainable management of water resources. *Environmental Engineering and Management Journal*. 2013;12(8):1721–1734.
- [23] The European Parliament and the Council. Directive 2013/39/EU of the European Parliament and of the Council of 12 August 2013 amending Directives 2000/60/EC and 2008/105/EC as regards priority substances in the field of water policy Text with EEA relevance. *Official Journal of the European Union – EUR-Lex*. 2013 (24 August 2013).



---

# Turbulence Diffusion Mechanism in Submerged Vegetation Flows

---

Michio Sanjou

Additional information is available at the end of the chapter

<http://dx.doi.org/10.5772/63207>

---

## Abstract

Many aquatic plants are often observed, and the submerged canopy flow appears in natural rivers. Complex flow patterns such as Karman vortex and related coherent motions are formed behind vegetation. In particular, mass and momentum transfers and the vertical mixing process are promoted significantly between the within-canopy layer and over-canopy layer. Therefore, it is very important for river ecosystem to reveal turbulent diffusion in submerged vegetated open-channel flows. The present study conducted simultaneously PIV and laser-induced fluorescence (LIF) measurements using a pair of high-speed cameras to analyze the contribution of coherent vortex to the turbulent diffusion property.

**Keywords:** vegetation flows, turbulence, diffusion process

---

## 1. Introduction

Aquatic vegetation elements yield a complex current structure which consists of the within-canopy layer and the over-canopy layer. Streamwise velocity reduces within canopy in a submerged vegetation flows in which the water depth is larger than the vegetation height, and a relevant shear instability is generated in the vertical direction. This induces coherent turbulence events such as ejection and sweep; near a boundary zone includes the vegetation edge between the within-canopy and the over-canopy. It is therefore very important for preservation of an aquatic habitat and a river environment to reveal transport mechanisms of heat, mass, sediment concentration, and momentum in the vegetation edge. This chapter focused on fundamental hydrodynamic characteristics and related turbulent diffusion properties in the

---

vegetated open-channel flows, because the ejections and the sweeps may have significant relationship with the convection and diffusion of nutrition and suspended sediments.

Case	$H$ (cm)	$h$ (cm)	$U_m$ (cm/s)	$Fr$	$Re$ ( $\times 10^4$ )
1	5.0	5.0	10.0	0.14	0.5
2	6.25			0.13	0.63
3	7.5			0.12	0.75
4	10.0			0.10	1.0
5	12.5			0.09	1.25
6	15.0			0.08	1.5
7	20.0			0.07	2.0

**Table 1.** Hydraulic condition varying relative water depth.

A turbulence structure in these canopy flows has been studied intensively in the meteorology. Raupach and Thom [1] have revealed velocity profiles and generation properties of turbulence energy by measurements of air tunnel with a roughness wall. Gao et al. [2] have conducted field measurements in deciduous forest and reported that the sweep and ejection motions influence heat transport significantly. Raupach et al. [3] have pointed out an analogy between the canopy-flow property and mixing-layer zone.

In contrast, river environmental problems arouse public interest recently, and thus, turbulence structure, mass, and momentum transport and their diffusion property of the vegetated open-channels have been highlighted. Nepf et al. [4] have proposed a diffusion model of dye concentration on the basis of random walk model, and they applied to the wake region behind an emergent plant model. Furthermore, Nepf [5] has revealed the relation between the turbulence. Sections 2 and 3 introduce turbulence structure in submerged vegetation flows and turbulent diffusion properties, respectively, on the basis of measurement results.

## 2. Turbulence structure in submerged vegetated flows

Hydrodynamic properties in vegetated canopy rivers, in which velocity distributions are largely changed in the vertical direction, are required to be revealed in hydraulic engineering. Specifically, the submergence depth, that is, the ratio of the water depth  $H$  to the vegetation height  $h$ , governs such hydrodynamics and coherent turbulent events significantly. There exists an outer layer in which the log-law layer is formed under high submergence condition, whereas, in the low submergence, the flow is directly influenced by the vegetation elements. Therefore, our research group conducted turbulence measurements in vegetated canopy open-channel flows by changing the relative submergence, and consequently, mean-flow properties, turbulence structure, and coherent motions were revealed as mentioned below.

## 2.1. Experimental method and hydrodynamic condition

The laboratory experiments were conducted in 10 m long and 40 cm wide tilting flume as shown in **Figure 1**. The plant models were composed of non-flexible strip plates and attached vertically on the bottom. The present plant model 50 mm height, 8 mm width, and 1 mm thickness.  $H$  is the water depth, and  $h$  is the vegetation height.  $L_v$  and  $B_v$  are the streamwise and spanwise spacings between neighboring elements, respectively.  $x$ ,  $y$ , and  $z$  are the streamwise, vertical and spanwise coordinates. The vertical origin,  $y=0$ , was chosen as the channel bed. The mean velocity components in each direction are defined as  $U$ ,  $V$ , and  $W$ , the turbulent components are  $u$ ,  $v$ , and  $w$ , respectively. For measurements of two components instantaneous velocity, that is,  $\tilde{u}(t) \equiv U + u(t)$  and  $\tilde{v}(t) \equiv V + v(t)$ , within and above the canopy vegetation, a laser light sheet (LLS) was projected into the water vertically from the free-surface side. The LLS thickness is 2 mm thick, and it was generated by 2 W Ar-ion laser. The LLS was located at 7 m downstream from the inflow section. The illuminated images were taken by a CMOS camera (1000 × 1000 pixels) with 200 Hz frame rate and 60 s sampling time. The instantaneous velocity components in the vertical two-dimensional plane could be obtained by PIV algorithm. **Table 1** shows hydraulic cases. Seven kinds of hydraulic conditions were chosen by changing the relative submergence depth, that is,  $H/h = 1.0, 1.25, 1.5, 2.0, 2.5, 3.0, 4.0$ , and the bulk mean velocity was constant for these cases, that is,  $U_m = 10$  cm/s.

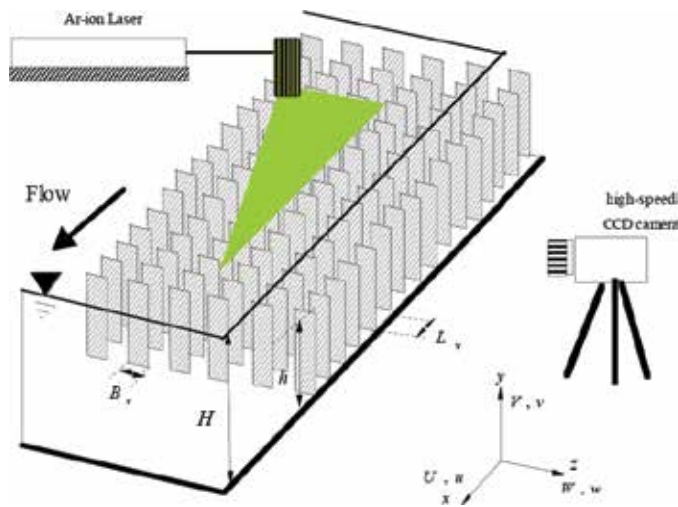


**Figure 1.** Experimental setup for PIV measurement in vegetated flume.

## 2.2. Mean flow structure

The whole depth region could be classified into two or three sublayers on the basis of the vertical profiles of mean streamwise velocity and Reynolds stress (see Poggi et al. [6]; Ghisalberti and Nepf [7]). Our research divides the vegetated open-channel flow into three sublayers as shown in **Figure 2**. The lowest layer within the canopy is termed the “wake zone (emergent

zone),” as defined by Nepf and Vivoni [8] and Ghisalberti and Nepf [7]. They defined the penetration depth  $h_p$  of momentum transfer, which is the upper limit of the wake zone and defined as the elevation of 10% of the maximum Reynolds stress. In the wake zone, the horizontal momentum transfer is dominated by stem wakes, and the vertical momentum transport is comparatively smaller than horizontal one. A middle sublayer includes the vegetation edge and is termed the “mixing-layer zone,” which is characterized by the lower limit of  $h_p$  and the upper limit of  $h_{log}$ , which is defined later. The velocity profile has one inflection point near the canopy edge, and thus, the velocity fluctuations evolve to form large-scale coherent motions of sweeps and ejections, as pointed out by Raupach et al. [3]. The streamwise velocity profile obeys well the following log-law of rough boundary layers in a free surface layer termed the “log-law zone”:

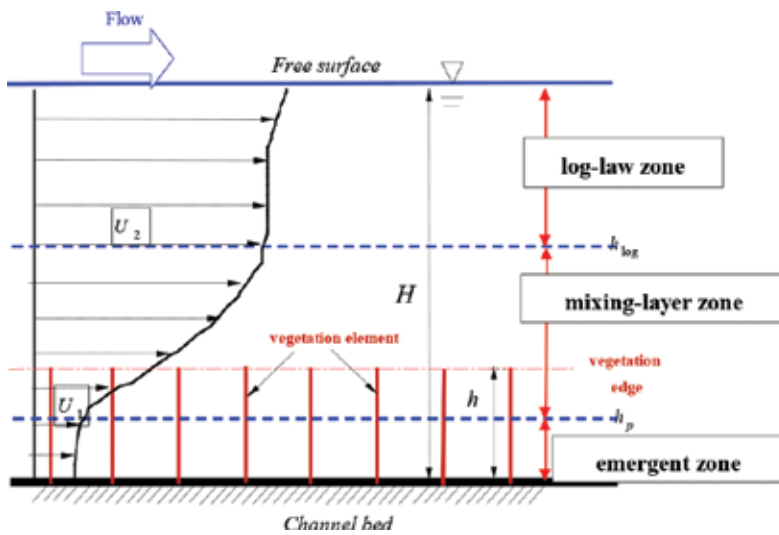


Figure 2. Classification of vertical layers in submerged vegetation flow.

$$\frac{U}{U_*} = \frac{1}{\kappa} \log \left( \frac{y-d}{y_0} \right) \tag{1}$$

in which,  $d$  and  $y_0$  are the zero-plane displacement thickness and the roughness height, respectively. The von Karman constant  $\kappa$  was used as the standard value in the open-channel flows, that is,  $\kappa=0.412$  (Nezu and Nakagawa [9]). Figure 3 shows the non-dimensional time-averaged velocity profiles for all submergence depth patterns. The results are normalized by the velocity at the vegetation edge,  $U_h$  layer is given by the following equation. A large velocity gradient  $\partial U / \partial y$  is observed at the canopy edge, and in contrast,  $\partial U / \partial y$  becomes smaller near the flume bed within-canopy. This is common tendency for all cases, irrespective of the submergence depth  $H/h$ . The velocity profiles



observed in the log-law zone, that is,  $y \geq h_{\log}$ , is recognized to coincide well with Eq. (1) in the large submergence depth of  $H/h = 2.5, 3.0$  and  $4.0$  as indicated in **Figure 4**.

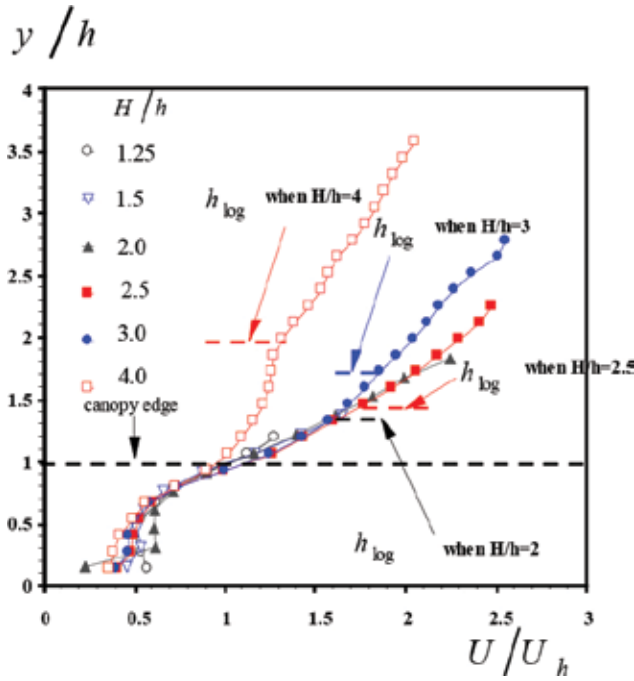


**Figure 3.** Streamwise velocity profile normalized by outer variables.

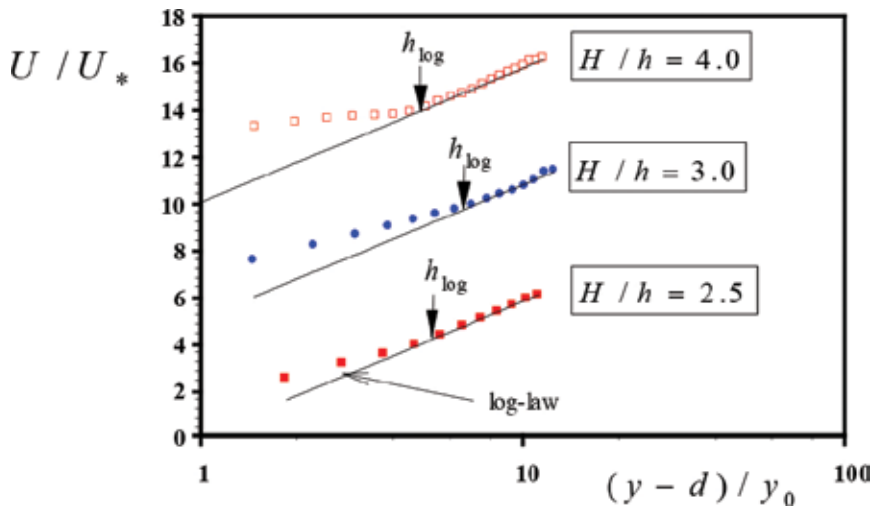


**Figure 4.** Examination of log-law over the canopy.

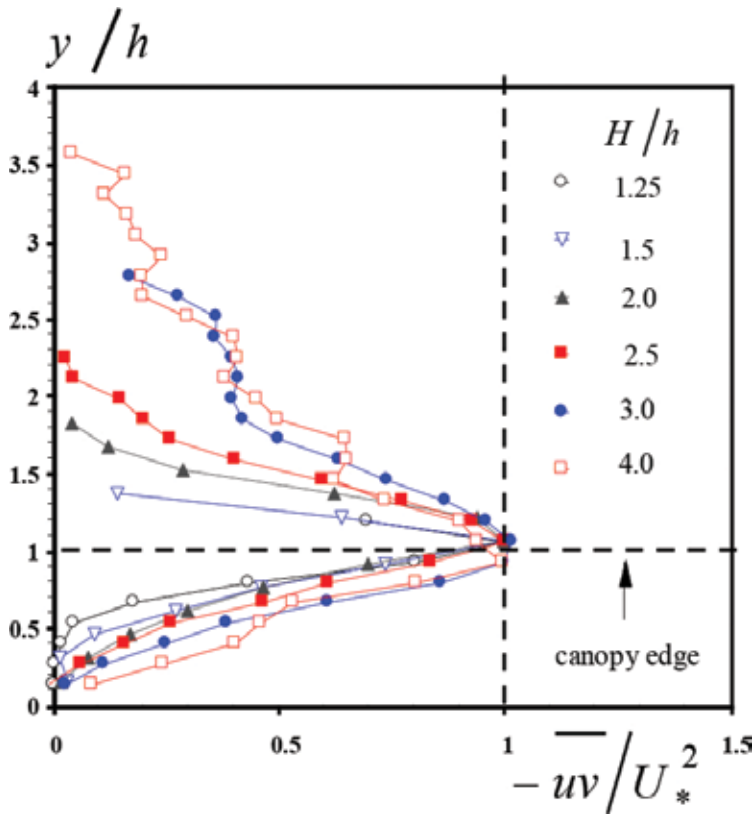
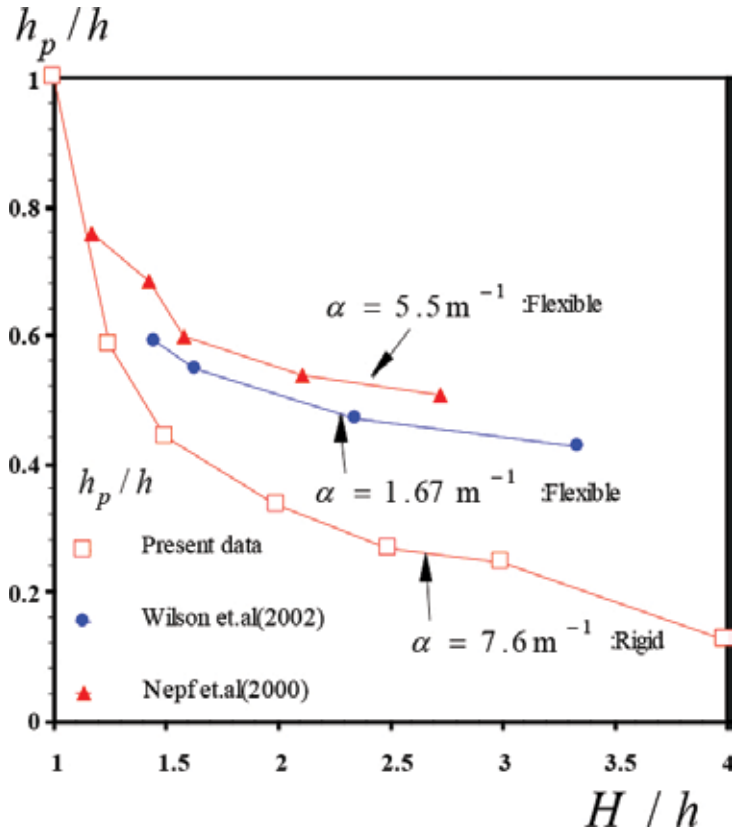


Figure 5. Reynolds stress profile.

Figure 5 shows the vertical profiles of Reynolds stress  $-\overline{uv}$  normalized by the friction velocity  $U_*$ . The friction velocity could be evaluated as a peak value of  $-\overline{uv}$ . This result implies that  $-\overline{uv}$  becomes larger within the canopy with an increase of the submergence depth. This suggests that the downward momentum transfer toward the within-canopy of  $y < h$  is promoted more significantly as  $H/h$  increases. Figure 6 shows the relationship between the penetration depth  $h_p$  and the submergence, in which previous other researchers' data in flexible canopy flows. The present result indicates that the penetration depth decreases with an increases of  $H/h$  in the same manner as pointed out by Nepf et al. [4] and Wilson et al. [10].  $h_p$  becomes smaller in the present rigid canopy than in the flexible ones for the wide range of the submergence depth. This may be because the oscillations of flexible vegetations depressed the momentum transfer. The mean flow profile of mixing layer is given by the following equation.

$$\frac{U - \bar{U}}{\Delta U} = \frac{1}{2} \tanh\left(\frac{y - \bar{y}}{2\theta}\right) \tag{2}$$

in which,  $\bar{U} = 1/2(U_1 + U_2)$ ,  $\Delta U = U_2 - U_1$ ,  $\bar{y} = (h_{\log} + h_p)/2$ , and  $\theta$  is the momentum thickness.  $U_1$  is the constant velocity of the low-speed zone in mixing layer and corresponded to the velocity at  $y = h_p$  in the present canopy-flow model (**Figure 2**).



**Figure 6.** Relationship between the penetration depth and the relative depth.

$U_2$  is the constant velocity of the high-speed zone and assumed to be equal to the velocity at  $y = h_{\log}$ . **Figure 7** compares the mean flow profiles of the present canopy flow with the tangent hyperbolic curve of Eq. (2). In all cases, the present data are almost coincident with the Eq. (2) in the mixing-layer zone of  $h_p < y < h_{\log}$ . It is found that the width of the mixing-layer zone, that is,  $\delta = h_{\log} - h_p$ , becomes larger with an increase of  $H/h$ . In contrast, in the shallow submerged cases,  $H/h = 1.25$  and  $1.5$ , the discrepancies between the measured data and Eq. (2) are comparatively large, and consequently, the analogy between the canopy shear layer and the mixing layer becomes smaller.

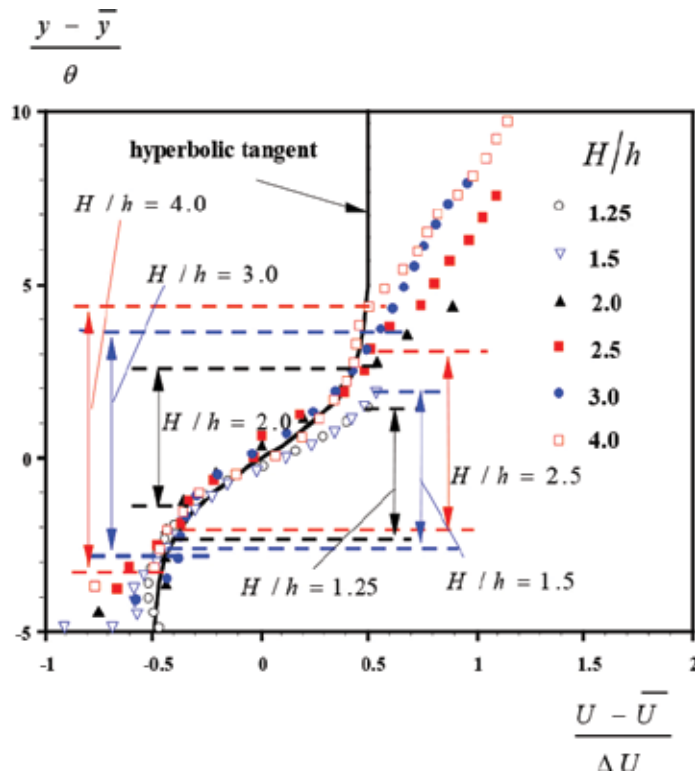


Figure 7. Examination of analogy with mixing layer.

### 2.3. Space–time analysis

Contours of space–time correlation between the streamwise velocity components,  $C_{uu}$ , are shown in Figure 8.  $C_{uu}$  is defined by as follows:

$$C_{uu} \equiv \frac{(\tilde{u}_0 - U_0) \times (\tilde{u}_{0+\Delta} - U_{0+\Delta})}{u_0' \times u_{0+\Delta}'} \quad (3)$$

in which, the subscript 0 denotes a reference point,  $(x_0, y_0, z_0, t)$  and  $0 + \Delta$  denotes a movable point  $(x_0 + \Delta x, y_0 + \Delta y, z_0 + \Delta z, t + \tau)$ .  $u' \equiv \sqrt{u^2}$  is the turbulence intensity, and the over-bar means the time-averaged operator. A large correlation-value zone is found to be transported downstream with an increase of the time lag  $\tau$ , and thus an existence of mean coherent motions was recognized in Figure 8.

In the result of  $\tau = 1.2s$ , a trajectory line of the maximum correlation position was also shown at every 0.3 s. The vertical movement of the coherent motion is much smaller than the longitudinal one, and the coherent lump structure is moved in parallel to the horizontal canopy

plane. The convection velocity of mean eddies was evaluated from the distance between the maximum two-point correlation positions.

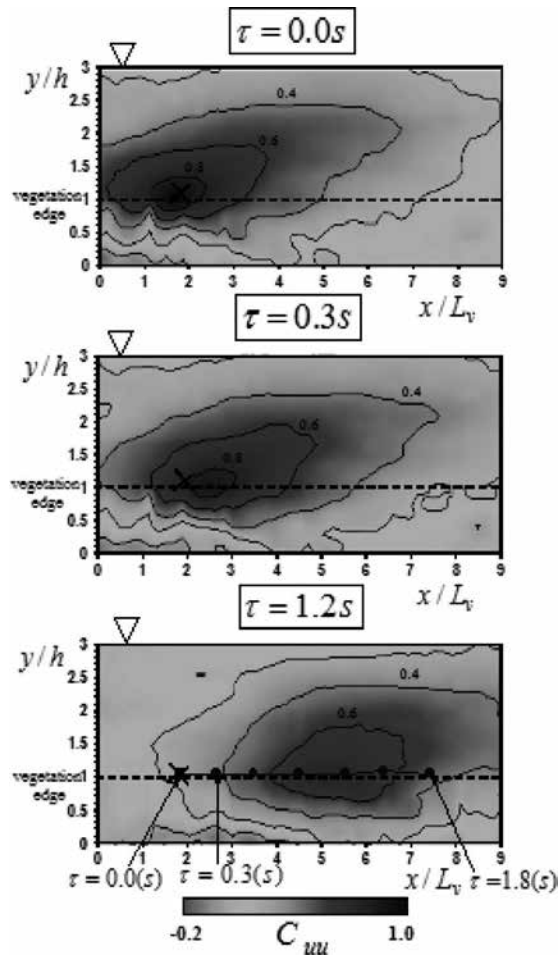


Figure 8. Space–time correlation property.

#### 2.4. Visualization of coherent structure

Figure 9 shows time variation of the distributions of the instantaneous Reynolds stress  $-uv$ . In contrast, Figure 10 shows the time series of the instantaneous velocity vectors, in which the contours of the streamwise velocity fluctuations  $u(x, y, t)$  were also included. The time  $t$  indicated in Figure 9 corresponds to that of Figure 10 in order to compare the both figures each other. At  $t=0$  s, a large distribution of  $-uv$  is observed locally, which is indicated by a dashed circle “A” in Figure 9. Figure 10 suggests that the instantaneous velocity fluctuations are negative,  $u < 0$ , and thus, the upward vectors of the low-speed fluid are observed in the circle “A.” That is to say, this zone forms a lump structure of the ejection motions. At  $t=0.36$

s, the ejection lump is convected downstream, and it is followed by the other local distribution of the dashed circle “B,” which consists of a downward high-speed fluid, ( $u > 0$  and  $v < 0$ ), that is, a lump structure of the sweep motions. At  $t = 0.96$  s, the ejections and sweeps are transported downstream. These results suggest that the local distributions of the high Reynolds stress correspond well to these lump structures of coherent motions. It was found from all digital frames that the sweeps and ejections seem to appear alternatively and periodically.

Periods of the sweeps and ejections,  $T_s$  and  $T_e$ , together with the period  $T_M$  of mixing layers are shown in **Figure 11**.  $T_M$  is a generation period of coherent eddies in pure mixing layer which is proposed theoretically by Ho and Huerre [11], as follows;

$$T_M = \frac{\theta}{0.032U} \tag{4}$$

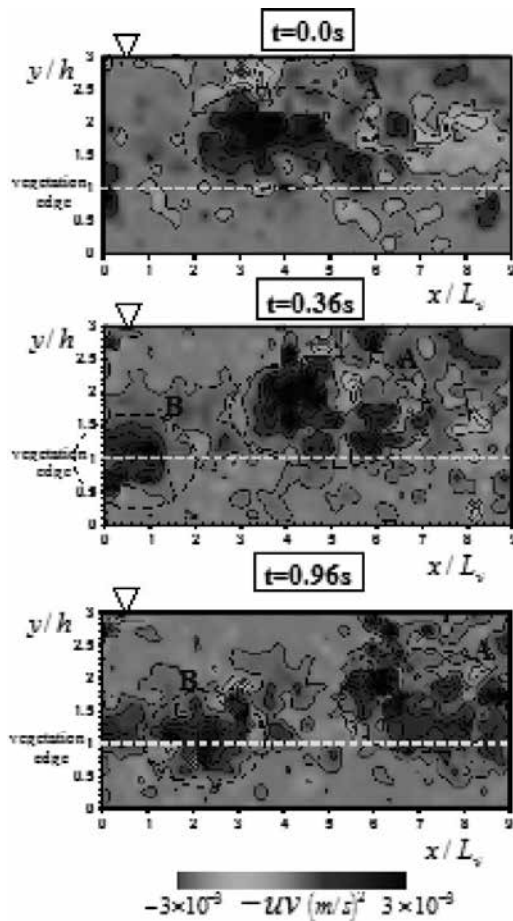


Figure 9. Instantaneous Reynolds stress.

$T_S$  is almost same as  $T_E$  for all submergence cases, and they become larger with an increase of  $H/h$ , and this tendency is also observed in the theoretical value  $T_M$ . It is, therefore, found that the coherent motion of aquatic canopy flows resemble well that of mixing-layer flows, as pointed out for terrestrial canopy flows (see Raupach et al. [3]).

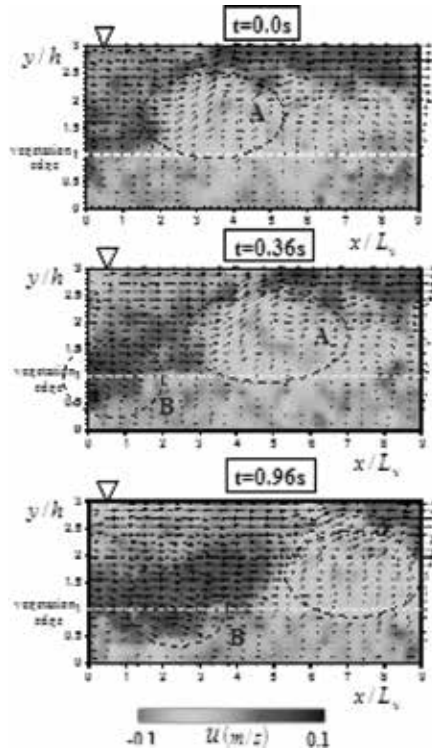


Figure 10. Instantaneous velocity vectors.

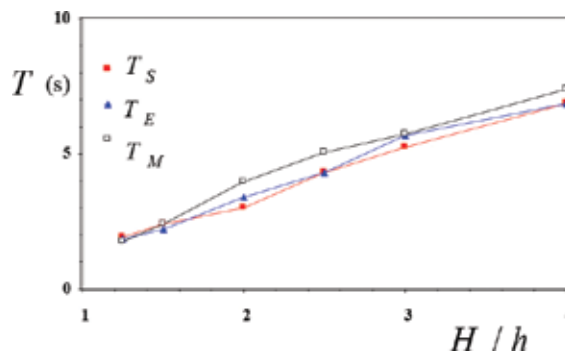
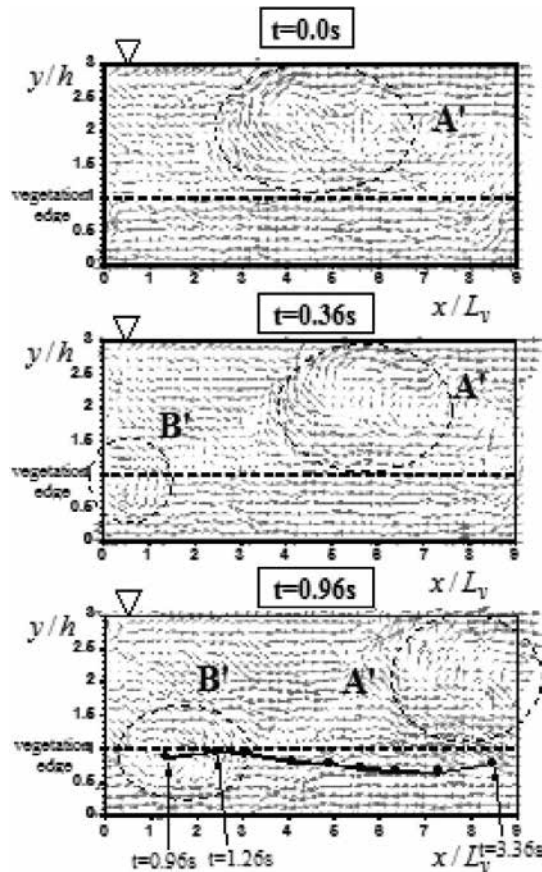


Figure 11. Periodicities of coherent events.

### 2.5. Detection of spanwise vortices

PIV measurements in turbulent boundary layers conducted by Adrian et al. [12] allow us to understand a packet structure of hairpin vortices. **Figure 12** shows same time-series of the instantaneous velocity vectors subtracted by a vortex convection velocity  $U_c$  near the vegetation edge. The convection velocity was evaluated from the space–time correlation analysis as mentioned before. **Figure 13** shows the distributions of the instantaneous vorticity  $\Omega(x, y, t)$  at the same time as used in **Figure 12**. The time of these figures correspond to that of **Figures 9 and 10**. A vortex-like velocity-vector distribution appears in the ejection lump (the dashed circle of “A”) at  $t=0$  s, and this lump is coincident with a large positive vorticity zone observed in **Figure 13**. This vortex-like structure is convected downstream at  $t=0.36$  s, and at the same time, vortex-like structure is also observed in the upstream region, which corresponds to the sweep zone of the dashed circle of “B.” This sweep zone has a large positive vorticity as shown in **Figure 13**.



**Figure 12.** Instantaneous velocity vectors.



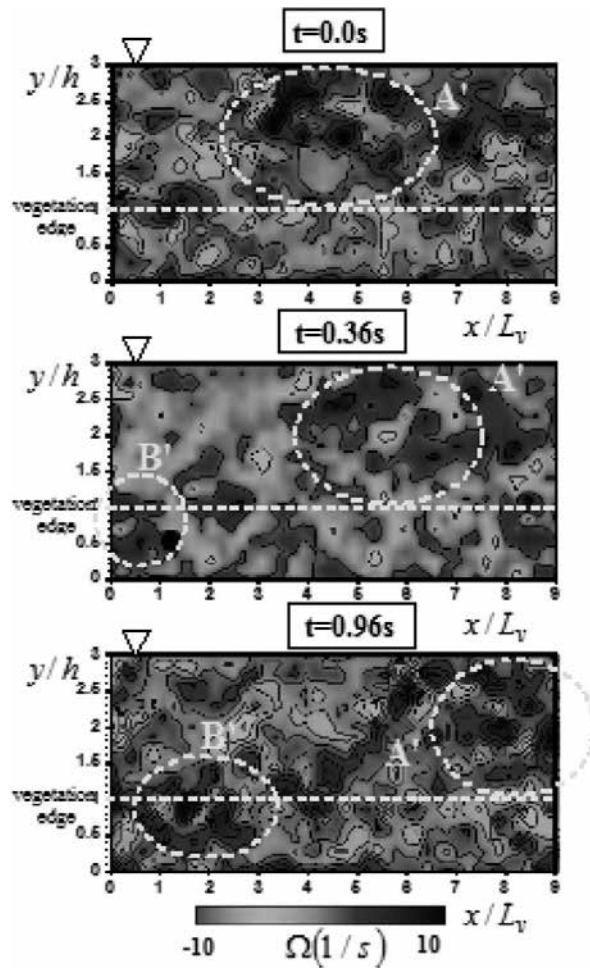


**Figure 13.** Instantaneous vorticity distribution subtracted by eddy convection velocity.

Consequently, the ejections and sweeps form the organized coherent eddies. These coherent eddies are convected downstream at  $t=0.96$  s. A trajectory line of core position of the coherent eddy “B” is also indicated at every 0.3 s in **Figure 12**. The vortex core was defined as the maximum position of the instantaneous vorticity  $\Omega$ . The eddy observed near the vegetation edge at  $t=0.96$  s. is transported into the within-canopy by the surrounding downward vectors, and this eddy exists within-canopy at  $t=3.36$  s.

A length scale of the coherent eddy was evaluated accurately from the present PIV measured data in the following ways:

$$L_x \equiv \int_0^\infty \frac{\overline{u(x_0, y_0, t_0)u(x_0 + x, y_0, t_0)}}{\overline{u'(x_0, y_0)u'(x_0 + x, y_0)}} dx \quad (5)$$

$$L_y \equiv \int_0^\infty \frac{\overline{u(x_0, y_0, t_0)u(x_0, y_0 + y, t_0)}}{u'(x_0, y_0)u'(x_0, y_0 + y)} dy \tag{6}$$

, in which  $L_x$  and  $L_y$  are the length scales for the streamwise and vertical directions.  $L_x$  is larger than  $L_y$  for all depth, and thus, it is found that oval-like vortices are generated near the vegetation edge. Both  $L_x$  and  $L_y$  are larger with an increase of  $H/h$ , and this suggests that large-scale vortices develop in the large submergence depth. In such a large submerged condition, the vertical length scale  $L_y$  has the same order of magnitude as the vegetation height, that is,  $L_y \cong h$ , as and indicated in **Figure 14**. Raupach et al. [3] reported the same tendency in the terrestrial canopies.

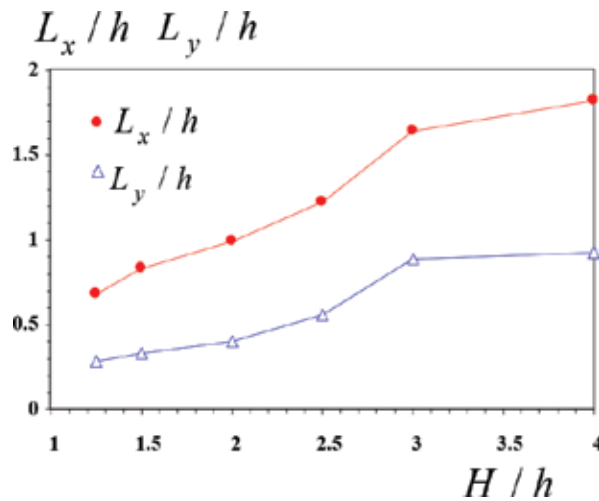


**Figure 14.** Relationship between the integral scales.

### 3. Turbulent diffusion in submerged vegetated canopy open-channel flows

Environmental problems in river basin have been recently highlighted as public interest, and thus, many researchers tried to reveal mass and momentum transfers associated with the wind waves, turbulence diffusion, and coherent vortex. Komori et al. [13] have revealed that wind waves promote gas transfer beneath air–water interface. There exists experimental works focused on the diffusion process in the vegetated canopies. Nepf et al. [4] have proposed a diffusion model of dye concentration on the basis of random walk model, and they applied it to the wake region behind an emergent plant model.

Furthermore, Nepf [5] has revealed the relation between the turbulence diffusion and the transport mechanism of dye concentration. However, there are many uncertainties about

turbulent diffusion mechanism, because it is hard to measure the velocity fluctuations and the concentration simultaneously. In consideration of this subject, our group tried to conduct some simultaneous measurements of PIV and the laser-induced fluorescence (LIF) using a pair of high-speed cameras, and evaluated the relation between the turbulent diffusion property and the coherent motions reasonably.

### 3.1. Experimental method

A schematic depiction of the turbulent diffusion in vegetated open-channel flows is shown in **Figure 15**. The shear instability occurs due to the velocity inflection point between the within-canopy and the over-canopy in the submergence condition as mentioned above. This instability causes the sweeps and ejections near the canopy edge, and these coherent motions have significant effects on mass and momentum exchanges between the within- and over-canopies. Concentration of sediment and nutrition are comparably large near the bottom bed in natural rivers, and these convection and diffusion processes are related significantly with activities of aquatic ecosystem. It is thus important to reveal the diffusion properties of turbulence in vegetated open-channel flows in order to promote such an environmental subject intensively.

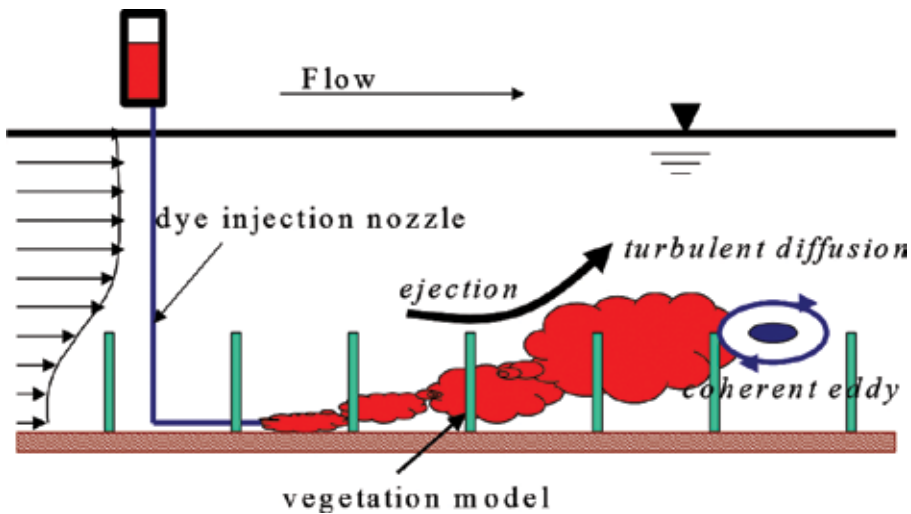


**Figure 15.** Sketch of developing vortices and turbulent diffusion.

The PIV-LIF measurement is introduced in this section. The contribution of turbulence structure to the diffusion process of the dye concentration is investigated by injecting dye near the flume bottom. Experiments were conducted in a 10 m long and 40 cm wide glass-wall flume. **Figure 16** shows the experimental setup and coordinate system.  $\tilde{c} = C + c$  is the instantaneous dye concentration, which is defined in the same manner as velocity components, that is, the Reynolds decomposition.  $H$  is the water depth, and  $h$  is the vegetation height. A vegetation element was made of  $h = 50$  mm non-flexible acrylic plate and 8 mm cubic base, in same manner as **Figure 1**.

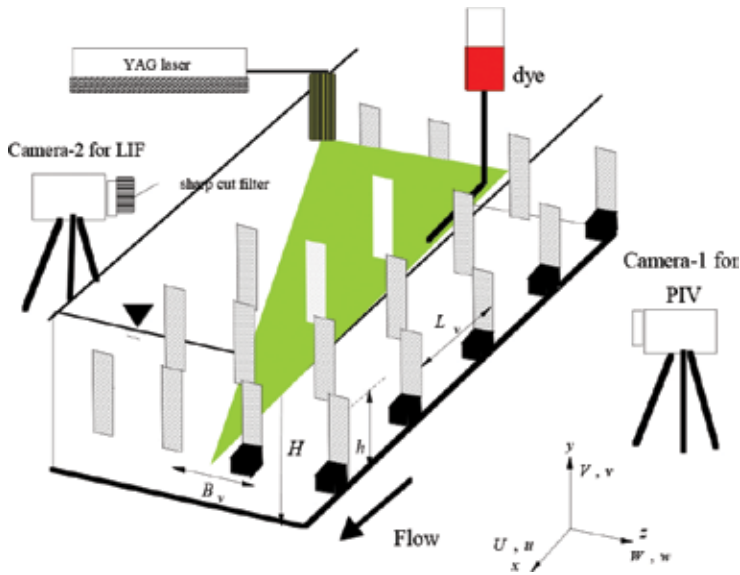


**Figure 16.** Experimental setup for PIV/LIF simultaneous measurement.

These vegetation models were placed vertically on the flume bed with a square grid allocation of  $L_v = B_v = 24$  mm, in which  $L_v$  and  $B_v$  are streamwise and spanwise spacings between the neighboring plants, respectively. Dye (Rhodamine-B), the concentration of which was 0.1 g/l, was injected through a small stainless tube into the flow near the flume bed. The streamwise origin,  $x=0$ , and the vertical origin,  $y=0$ , were chosen as a tip of the injection nozzle and on the flume bed, respectively. The spanwise position of the injection nozzle was at the centerline of the non-wake region between the vegetation elements, which corresponds to the position of the laser light sheet (LLS) as mentioned later. The injection velocity of dye was controlled as coincident with the streamwise flow velocity at the same elevation. Two sets of high-speed CMOS cameras ( $1000 \times 1000$  pixels) were placed at both sides of the flume. One camera was used to PIV measurements, and the other was used to the LIF measurements. These cameras could be controlled simultaneously by using trigger signals of a pulse generator. 2 W YAG laser light sheet (LLS) was projected into the non-wake region, and the illuminated plane was taken by two sets of cameras with 200 Hz frame rate and 45 s sampling time. The time series of the instantaneous velocities ( $\tilde{u}$ ,  $\tilde{v}$ ) were obtained by the PIV algorithm. The reflection wavelength of the tracer particles is 537 nm (laser beam), In contrast, a fluorescence of dye induced by laser becomes a 580 nm wavelength. Therefore, it was possible that only the images of dye were taken by one CMOS camera using a sharp cutoff filter. The instantaneous distribution of the dye concentration was calculated from brightness values of the LIF images.

**Table 2** shows the hydraulic condition.  $U_m$  is the bulk mean velocity,  $Re \equiv U_m H / \nu$  is the Reynolds number, and  $Fr \equiv U_m / \sqrt{gH}$  is the Froude number. In this study, the emergent case ( $H/h = 0.9$ ) was also conducted in order to consider the effects of the submergence depth on

turbulent diffusion. The bulk mean velocity of the emergent vegetation case was the same as that of the within-canopy zone measured in the submerged case.  $\lambda$  is the vegetation density.

Case	$H/h$	$U_m$ (cm/s)	$H$ (cm)	$Re$	$Fr$	$h$ (cm)	$\lambda$
Submerged	3.0	10.0	15	15,000	0.08	5.0	0.39
Emergent	0.9	4.2	4.5	1890	0.06		

Table 2. Hydraulic condition for PIV/LIF experiments.

### 3.2. Basic characteristics of flow structure

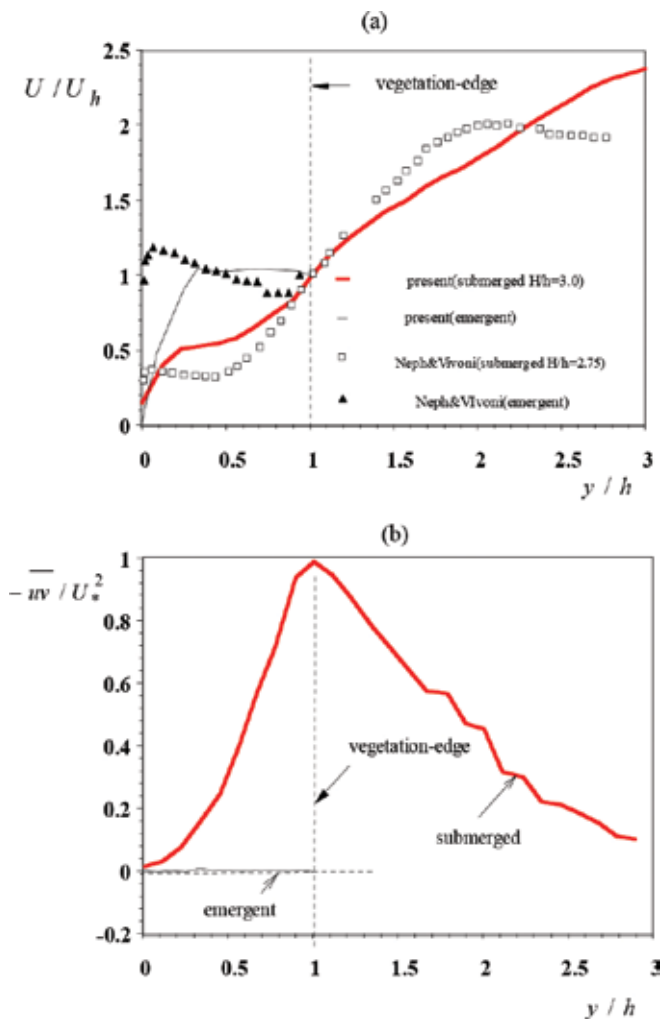
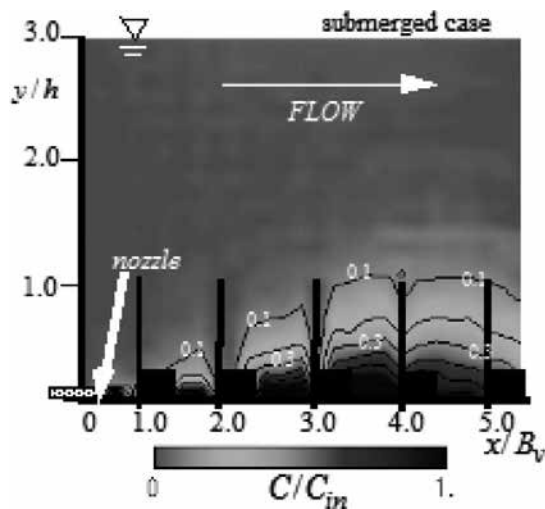


Figure 17. Vertical profiles of time-averaged velocity and Reynolds stress. (a) Mean velocity, (b) Reynolds stress.

**Figure 17a, b** shows the vertical profiles of time-averaged primary velocity  $U(y)$  and Reynolds stress  $-\overline{uv}$ , respectively. The value of  $U$  was normalized by the velocity at the vegetation edge,  $U_h$ . The friction velocity  $U_*$  is defined as the value of  $-\overline{uv}$  at the vegetation edge,  $y/h = 1$ . In the submerged case, the velocity profile  $U(y)$  seems to resemble a mixing-layer type, in which the velocity difference is seen remarkably between the within-canopy and the over-canopy. Consequently, a typical shear layer is formed between them and coherent motions such as sweeps and ejections are generated near the canopy edge. Although there are some discrepancies between the present data and Nepf and Vivoni's data, the same tendency is obtained in both data. Nepf and Vivoni suggested that the velocity dip phenomenon appears near the free surface, at  $y/h = 2$ . This may be because secondary currents are generated due to the small aspect ratio of their flume experiments. Reynolds stress  $-\overline{uv}$  is recognized to have maximum at  $y/h = 1$ , and this implies that the momentum exchanges are promoted significantly by the velocity shear shown in **Figure 17a**.

In the emergent case,  $U(y)$  is almost constant except for the near-bed region in both of the present data and Nepf and Vivoni's data.  $-\overline{uv}$  becomes negligibly small in comparison with the submerged case. It is considered that the vertical momentum transport is negligibly small in the emergent vegetation.



**Figure 18.** Distribution of time-averaged dye concentration.

### 3.3. Time-averaged dye concentration

The distribution of time-averaged concentration  $C(x, y)$  is shown in **Figure 18** in which the contour values are normalized by the time-averaged concentration at the nozzle tip  $C_{in}$ . The dye concentration is observed to be transported in the streamwise direction, associated with the vertical diffusion. **Figure 19a** shows the vertical profile of  $C/C_{bed}$ , in which  $C_{bed}$  is the time-averaged concentration at the first measurement point very near the flume bed,  $y/h = 0.06$ .

These profiles can be described well by the following exponential function at every longitudinal position.

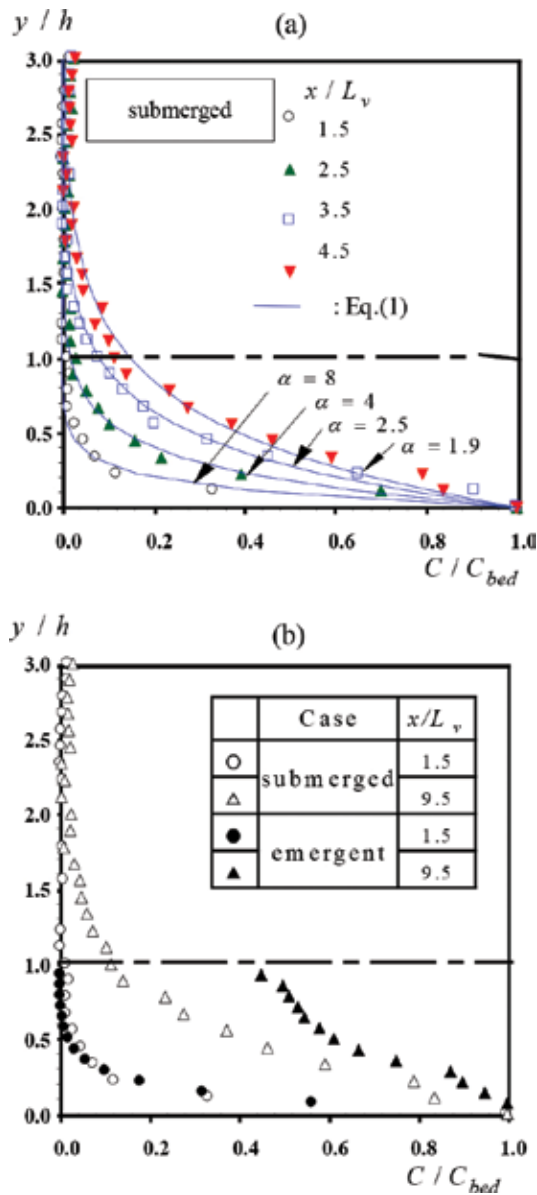


**Figure 19.** Vertical profiles of time-averaged concentration. (a) For submerged cases, (b) comparison of submerged and emergent cases.

**Figure 19b** shows some comparisons between the submerged and the emergent cases. The concentration is larger within the canopy at  $x/L_v=9.5$  in the emergent case than in the

submerged case. This implies that the streamwise exchanges are conducted more significantly in emergent than submerged vegetation. **Figure 20** shows the streamwise variation of the diffusion width  $\delta$ . It is defined as the elevation at which  $C = 1/2 C_{bed}$  (a half-value width).  $\delta$  increases more linearly in the emergent than in the submerged cases. In contrast, in the submerged case,  $\delta$  increases mildly at  $x/L_v > 4$  and attains constant downstream of  $x/L_v > 7$ .

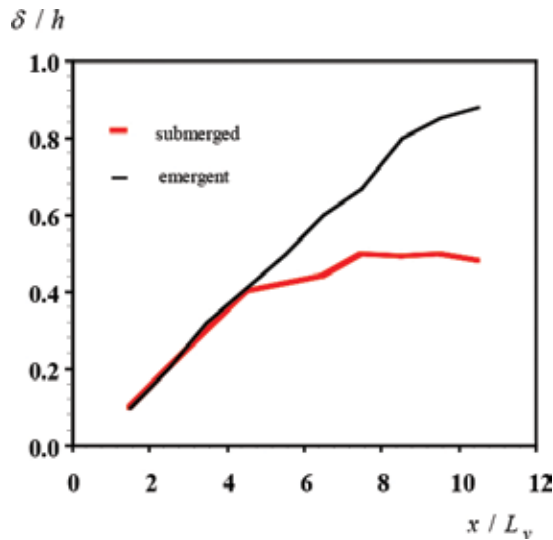


Figure 20. Longitudinal variation of diffusion width.

### 3.4. Evaluation of turbulent diffusivity

Reynolds stress and the correlation  $\overline{vc}$  between the velocity and concentration are connected to be the following forms by the gradient diffusion model.

$$-\overline{uv} = \nu_t \partial U / \partial y \tag{7}$$

$$-\overline{vc} = K_y \partial C / \partial y \tag{8}$$

in which  $\nu_t$  is the eddy viscosity, and  $K_y$  is the turbulent diffusivity in the vertical direction. **Figure 21** shows the vertical profiles of  $\nu_t$  and  $K_y$  evaluated from Eqs. (7) and (8).  $K_y$  increases from the within-canopy to the canopy-edge zone, and decreases in the free surface region of  $y/h > 2$ . It has a peak value over the canopy of  $1 < y/h < 2$ . The profile of  $K_y$  resembles that of  $\nu_t$ . Therefore, it is considered that  $K_y$  is nearly equal to  $\nu_t$  in the vegetation-edge zone because the turbulent Schmidt number  $S_c \equiv \nu_t / K_y$  becomes almost one.



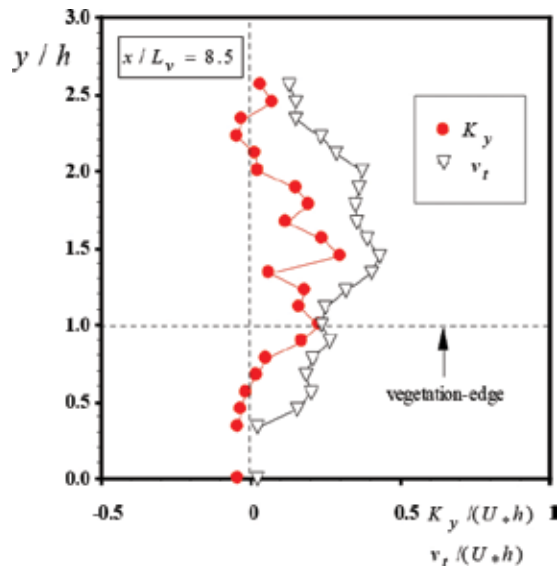


Figure 21. Vertical profiles of turbulence diffusivity and eddy viscosity.

#### 4. Conclusions

The Section 2 explained the PIV turbulence measurements and their results in the vegetated open-channel flows. Particularly, mean-flow properties, turbulence structure, and coherent motions were revealed as follows;

1. In the larger submergence depth condition, the momentum transfer of Reynolds stress toward the within canopy layer is promoted significantly. Consequently, the penetration depth is evaluated reasonably from the Reynolds stress distributions. On the basis of mean velocity profiles and the eddy periodicity, it was found that there is a significant analogy between the canopy shear layer and the mixing shear layer.
2. The coherent eddy has a significant relation with generations of the sweeps and the ejections, and the trajectory of the vortex core is driven by these coherent motions. The length scales of coherent eddies were evaluated from PIV images, and it was found that the large-scale eddies appear in large submergence depth.

The Section 3 introduced PIV and LIF simultaneous measurement technique with two sets of high-speed cameras, which could evaluate the relation between the turbulent diffusion property and coherent motions. The main findings obtained here are as follows;

1. Two components of the instantaneous velocity vectors and the dye concentration were measured simultaneously using the combination of PIV and LIF methods. The dye concentration is lifted up to the over-canopy by the ejection motions, and returned to the within-canopy by the sweep motion.

2. The contribution of the sweep motion to the transport of the dye concentration is larger than that of the ejection motions near the vegetation edge, and it was found from the simultaneous measurements of the velocity and concentration that the turbulent diffusivity is in the same order of magnitude as the eddy viscosity.

## Author details

Michio Sanjou

Address all correspondence to: michio.sanjou@water.kuciv.kyoto-u.ac.jp

Department of Civil and Earth Resources Engineering, Kyoto University, Kyoto, Japan

## References

- [1] Raupach, M. R. and Thom, A. S.: Turbulence in and above plant canopies. *Ann. Rev. Fluid Mech.* 1981;13:97–129.
- [2] Gao, W., Shaw, R. H. and Pawu, K. T.: Observation of organized structure in turbulent flow within and above a forest canopy turbulent in and above plant canopies. *Bound. Layer Meteorol.* 1989; 47: 349–377.
- [3] Raupach, M. R., Finnigan, J. J. and Brunet, Y.: Coherent eddies and turbulence in vegetation canopies: the mixing-layer analogy. *Bound. Layer Meteorol.* 1996; 78: 351–382.
- [4] Nepf, H. M., Sullivan, J. A. and Zavistoski, R. A.: A model for diffusion within emergent vegetation. *Linnol. Oceanogr.* 1997; 42(8): 1735–1745.
- [5] Nepf, H. M.: Drag, Turbulence, and diffusion in flow through emergent vegetation. *Water Resour. Res.* 1999; 35: 479–489.
- [6] Poggi, D., Porpotato, A. and Ridolfi, L.: The effect of vegetation density on canopy sub-layer turbulence. *Bound. Layer Meteorol.* 2004; 111: 565–587.
- [7] Ghisalberti, M. and Nepf, H.: The structure of the shear layer in flows over rigid and flexible canopies. *Environ. Fluid Mech.* 2006; 6: 277–301.
- [8] Nepf, H. M. and Vivoni, E. R.: Flow structure in depth-limited vegetated flow. *J. Geophys. Res.* 2000; 105: 28547–28557.
- [9] Nezu, I. and Nakagawa, H.: Turbulence in open-channel. *IAHR Monogr. Balkema.* 1993.

- [10] Wilson, C. A. M. E, Stoesser, T., Bates, P. D. and Batemann Pinzen, A.: Open channel flow through different forms of submerged flexible vegetation. *J. Hydraul. Eng.* 2003; 129: 847–853.
- [11] Ho, C. M. and Huerre, P.: Perturbed free shear layers. *Ann. Rev. Fluid Mech.* 1985; 16: 365–424.
- [12] Adrian, R. J., Meinhart, C. D., Tomkins, C. D.: Vortex organization in the outer region of the turbulent boundary layer. *J. Fluid Mech.* 2000; 422: 1–54.
- [13] Komori, S., Nagaosa, R. and Murakami, Y.: Turbulence structure and mass transfer across a sheared air–water interface in wind driven turbulence. *J. Fluid Mech.* 1983; 249: 161–183.



---

# River Ecosystems Management and Conservation

---



---

# **Selected Structural Features of the Riverine Plants, *Trapa natans* (Lythraceae) and *Justicia americana* (Acanthaceae)**

---

James L. Seago Jr., Willow B. Eyres and  
Matthew Volny

Additional information is available at the end of the chapter

<http://dx.doi.org/10.5772/63709>

---

## **Abstract**

Aquatic, stoloniferous plantlets with floating leaves and nodal, adventitious roots of *Trapa natans* and emergent, stoloniferous, rooted plants of *Justicia americana* from the Oswego River, New York, USA, were investigated to determine root and shoot structures. These riverine eudicots have typical root anatomy with aerenchyma, endodermis, and exodermis. Both species contain stem tissues with endodermis which encircles one stele in *T. natans* and polysteles in *J. americana*. The aquatic stolon of *T. natans* has circumferentially spaced primary xylem with primary phloem. Erect stems of *J. americana* normally lack an endodermis in aerial portions above the water line. Extensive collenchyma is a conspicuous feature under the epidermis in stems of both species. Large stolon cortical cavities are characteristic of *T. natans*, but they are not found in the hypocotyls; in *J. americana* aerenchyma lacunae occur throughout ground tissue. The peduncle of *T. natans* has a stele with a ring of vascular tissue of primary xylem with phloem exterior to the xylem, surrounded by endodermis and air cavities, and pith aerenchyma. Leaves of both species do not contain barrier layers. Petioles of *T. natans* usually contain subepidermal collenchyma and aerenchyma with enlarged lacunae in inflated bladders.

**Keywords:** anatomy, *Justicia americana*, *Trapa natans*

---

## 1. Introduction

The Oswego River is a short (<40 km), north flowing river, whose tributaries connect many of the Finger Lakes of central New York state to Lake Ontario. The river is considered part of a canal system that links Lake Ontario to the famous Erie Canal, which stretches from east to west across New York state; consequently, over the last 188 years, it has been the scene of much river traffic. Its flow has been altered with dredging, dams, and locks to control the ship channel, to produce electricity, and to be part of the canal system. In recent decades, one invasive plant, the infamous water chestnut, *Trapa natans* L., has become a familiar sight in the river and a considerable nuisance to users of the river. It has floating (except with fruit-anchored young stages) stoloniferous ramets with rosettes of rhombic-shaped leaves [1]. The long ignored native water willow, *Justicia americana* (L.) Vahl., is an important shore-line stabilizer and is a stolon- and root-anchored, emergent, linear-leaved [1], sometimes growing in close proximity to the water chestnut.



**Figures 1–9.** *Trapa natans* and *Justicia americana* in habitat settings. 1. Species together at dock in Minetto, New York, June. 2. *Trapa*, view in Oswego River, looking north, early July, 1500 m south of Minetto Dam. 3. *Trapa* at river's edge in June. 4. *Justicia* along river's shore, south of Minetto Dam in early July. 5. *Justicia* along river's shore, south of Minetto Dam, in June. 6. *Trapa*, as in **Figure 2**, in early August. 7. *Trapa* setting, as in **Figure 2**, in early October. 8. *Trapa* setting, as in **Figure 2**, in early November. 9. *Justicia* remnants, as in **Figure 4**, in early November. Abbreviations for all microscopic figures: aer, aerenchyma; cav, cavities; cl, collenchyma; cor, cortex; e, endodermis; f, phloem fiber; st, stele; sx, secondary xylem; v, leaf veins; x, primary xylem; \*, periderm; t, trichomes.

Water chestnut is native to the warm temperate regions of Eurasia and North Africa. It has been of greater interest and study than water willow because of its invasiveness; there is some disagreement as to which decade *Trapa natans* first entered North America and became



established. Naylor [2] stated that water chestnut was first recorded in North America near Concord, Massachusetts in 1859, whereas Hummel and Findlay [3] claimed that it was first introduced in 1875, and Pemberton [4] stated that it was in 1884 in Sanders Lake, Schenectady, east central New York, not far from the Oswego River of central New York. Its presence in ponds near Schenectady, New York, was also noted in Britton and Brown [5], and other aspects of its occurrence and control were noted in the 1930s [6, 7]. Arber [8] believed that *Trapa natans* was on its way to extinction, at least in Europe, and in 1974, Ogden [9] mapped its occurrence in New York State only along the Hudson and Mohawk Rivers, east of the Oswego River, but including Schenectady. Its overall growth characteristics have been described by many researchers, especially Groth et al. [10].

Water willow is a native plant [1, 11, 12] that may play roles in shoreline stabilization [13, 14] and in providing breeding habitats [15]. In recent decades, both species have occurred together in the Oswego River, New York, especially in the section south (upriver) of the Minetto Dam that is a small reservoir. In photographs of this section of the Oswego River from the late 1800s, the invasive water chestnut was not observed during summers, and the occurrence of water willow could not be determined [Carl Allen, Minetto, NY, personal communication]. Currently, *Justicia americana* does not appear extensive enough to be important for fish habitat [15, 16]. The senior author's personal observations of the Oswego River before the mid 1980s did not reveal water chestnut or water willow, which might have been disrupted or blocked by boulders installed at various times [Carl Allen, personal communication], including in the 1990s, to reinforce the shore line upriver from the nearby dam after the Minetto Bridge was razed and replaced.

This research was begun as part of the senior author's long-term studies on the development and structure of the root cortex of flowering plants. Prior to this study, roots of these native and invasive riverine plants have been little studied although aspects of the growth and structure of water chestnut had been noted early [8, 17, 18]. In general, relatively few dicotyledons have been examined except, for example, the brief descriptions of Justin and Armstrong [19], Smirnoff and Crawford [20], Perumalla et al. [21], Peterson and Perumalla [22], and Metcalfe and Chalk [23, 24], and the distributions, drawings, and brief descriptions of New York aquatic and wetland plants, including both *Trapa natans* (not then reported in the Oswego River region) and *Justicia americana* (found in the Oswego River), by Ogden [9]; persons (Oswego County Soil and Water Conservation District, personal communication to JLS) involved with river conservation (water levels, shoreline maintenance, etc.) could provide only limited detail about the history of these plants in the Oswego River. Altogether, there is a paucity of reliable information on the shoots and roots of these two species [8, 9, 17, 18, 23–27], especially as structural characteristics may relate to habitat function [13, 27, 28]. It seemed especially troubling that, while Sculthorpe [28] had long ago described some aspects of the adventitious and lateral roots of *T. natans*, recent ecological studies [29, 30] had referred to these as feathery leaves. Sculthorpe [28] had also noted the induced nature of the "floats" or inflated petioles of the rhombic leaves. The presence of characteristic leaf trichomes has also been noted in *Trapa natans* by Metcalf and Chalk [25]. Since we had become aware over the last two decades that there had been an increasing population of both floating and emergent

plants along the shores of the reservoir upriver from the lock and dam across the Oswego River in Minetto, Oswego County, New York, we decided to examine the two prominent species, *Trapa natans* (Lythraceae) and *Justicia americana* (Acanthaceae), where they occur together at a small dock (**Figure 1**) and separately (**Figures 1–9**) within 100–1500 m upriver of a hydroelectric dam with lock in Minetto, Oswego County, New York. Here, we present selected developmental and structural observations on root and shoot tissues to illustrate the kinds of anatomical adaptations of native and invasive eudicot species to their riverine habitats.

## 2. Study of *Trapa natans* and *Justicia americana*

### 2.1. Plants and study location



**Figures 10–15.** *Trapa natans* and *Justicia americana*, closeups. 10. *Trapa* seedling with hypocotyl and adventitious roots, nodes with undeveloped leaves. 11. *Trapa* section of stolon with nodes and adventitious roots. 12. *Trapa* rhombic leaves, petioles with bladders, peduncle with young fruits. 13. *Justicia* multiple stolons along shoreline river bottom. 14. *Justicia* an erect shoot with piece of stolon and adventitious roots. 15. *Justicia* single stolon with individual roots.

We studied plants of *Trapa natans* and *Justicia americana*, which grow in the calm, shore-line, or near-shore waters of the Oswego River south (upstream) of the Minetto Dam in Minetto, Oswego County, New York, USA. Here, the Oswego River is a slightly widened reservoir south of a hydroelectric facility, lock/dam, and bridge with a deeper, flowing channel in the middle and eastern sides of the river and the calmer water on the western sides. Hundreds of plants were examined over 15 years.

### 2.1.1. *Trapa natans* L. (Lythraceae)

Plants were studied from early June through September (2000–2015; see **Figures 1–3**). In some years, ramets grew so prolifically that they pushed up against each other (**Figure 6**). By late October each year, the plants had died and started to disappear (**Figures 7 and 8**). In mid-October 2010, when the plants were already dying, and again in August 2011, after fruits had been produced, the plants were sprayed with Rodeo and large swaths died in the 2011 spraying, but successfully reappeared in 2012 and 2013. Adventitious roots, hypocotyls, stems (the term, stolon, is used instead of rhizome because these stems are not embedded in the rocky substrate of river bed), pedicels, and leaves (petioles and lamina of rhombic leaves) of plantlets were harvested from anchored, floating, rosette plantlets or ramets within 10 m of shore, their branching ramets, clusters of nodal adventitious roots, mature leaves, and peduncles of flowers and fruits (**Figures 3 and 10–12**). The axes of *T. natans* from which specimens were taken varied greatly in dimensions. Roots were mostly 10–65 mm long and less than 1 mm in diameter (**Figure 11**), except for the first adventitious roots arising from the cotyledonary nodes (**Figure 10**), which were much longer and often descended into the substrate river bottom. Stolons harvested were 3–4 mm in diameter, except near the water surface, where they were 5–6 mm. Petioles were proximally and distally 3–4 mm in diameter and 7–10 mm in the bladder (**Figure 12**). Peduncles were expanded from the tip of the stolons to 7–10 mm in diameter but were very irregular (**Figure 12**).

### 2.1.2. *Justicia americana* L. (Acanthaceae)

Plants were studied from June to November within 2 m of the shoreline over the 15 years of study (**Figures 4, 5 and 9**). *Justicia americana* plants are anchored in the substrate (sand, gravel, rocks, and boulders). Adventitious roots, stolons (sectioned more than 20 cm from their tips), erect stems (submerged portions sectioned within 10 cm of their base and emergent within 20–40 cm of their tips), and some leaf bases were harvested from the sampled stem sections (**Figures 13–15**). Of the plants we sampled, adventitious roots varied greatly in length from a few cm to 30+ cm and in diameter from 0.5 to 1.0 mm. The erect shoots were usually 70–100 cm long, submerged portions 6–8 mm in diameter and aerals varied widely from 2 to 8 mm in diameter. Stolons were 8–12 mm in diameter.

### 2.1.3. Specimen preparations

For root apical characteristics, root tips from roots of varying lengths were harvested, fixed in FAA or FPA, and processed into paraplast wax by standard techniques; most sectioned material was stained with safranin and fast green FCF [31–33]. For root, stem, pedicel, and leaf structure, hand-cut sections were made and examined either without or with staining; the staining consisted of berberine (BER), berberine–aniline blue (BAB), berberine–toluidine blue O (BTBO), fluorol yellow (FY), sudan red 7B, phloroglucinol HCl, or toluidine blue O (TBO) [34]. Most bright-field observations were done with a Nikon Labophot microscope (SUNY at Oswego), and epifluorescence and differential interference contrast (DIC) observations were done on a Zeiss Axiophot epifluorescence microscope (University of Waterloo, Ontario).

Bright-field, epifluorescence, and laser confocal (LCF) images, including tile scans, were done on a Zeiss LSM700 (SUNY at Oswego).

## 2.2. Results

*Trapa natans* and *J. americana* grow in close proximity only at a shore-line, disturbed dock (2000–2015; **Figure 1**). In early June, the plants of *T. natans* are sparse and small (**Figures 1** and **10**) with plants arising from fruits lodged or anchored in the river bottom and with one main axis and one-two branches. In June highly branched plants of *T. natans*, in plantlets or ramets, extensively cover the near-shore, calm waters (**Figures 2** and **3**), and by mid July, they have both horizontal-oriented and vertical-oriented leaves crowded against each other (**Figure 6**); later, all vegetative portions decay and disappear by changes in water levels that disrupt the dying plants (**Figures 7** and **8**). The stands of *J. americana* arise vegetatively from overwintering rhizomes and become extensive along the shoreline by late June and early July (**Figures 4** and **5**). At first, stems elongate from the previous year's stolons with detectable old roots, and each stolon adds new shoots with new roots at nodes; new stems are added in the summer along the muddy river bottom (**Figures 5** and **13–15**), and the erect leafy stems gradually died back in October and early November (**Figure 9**).

### 2.2.1. *Trapa natans*

The embedded fruits of *T. natans* anchor germinated plants in the river bottom, the single hypocotyls (typically 4–8 cm long from each fruit; **Figure 10**) elongate without primary root emergence; there was no primary root in any of the hundreds of plants examined. The epicotyl elongates into the first internode (**Figure 10**), and a stolon with reduced leaves grows to the water surface. Only when the stolon reaches the surface does a typical rosette of rhombic leaves result (**Figure 3**). Beyond the cotyledonary node (**Figure 10**), adventitious roots soon emerge along the stolon at each node (**Figures 10** and **11**) up to the rosette of rhombic, floating leaves where internode elongation is extremely reduced (**Figures 3** and **12**). The adventitious roots from the cotyledonary node grow horizontally or grow down into the substrate (**Figure 10**). At the other nodes, adventitious roots form asymmetrically and grow outward (**Figure 11**), but there is no observable difference between water roots and other roots, as described by Sculthorpe [28]; roots that emerge horizontally tend to grow horizontally, and roots that emerge vertically tend to grow in that orientation. Of specimens we examined, most adventitious roots measure 10–65 mm long and produce numerous lateral roots to their tips as they age (**Figure 11**), but there are much longer roots from some nodes, especially the cotyledonary node (**Figure 10**). Flowers and later fruits with short peduncles occur among the leaves at the water surface (**Figure 12**).

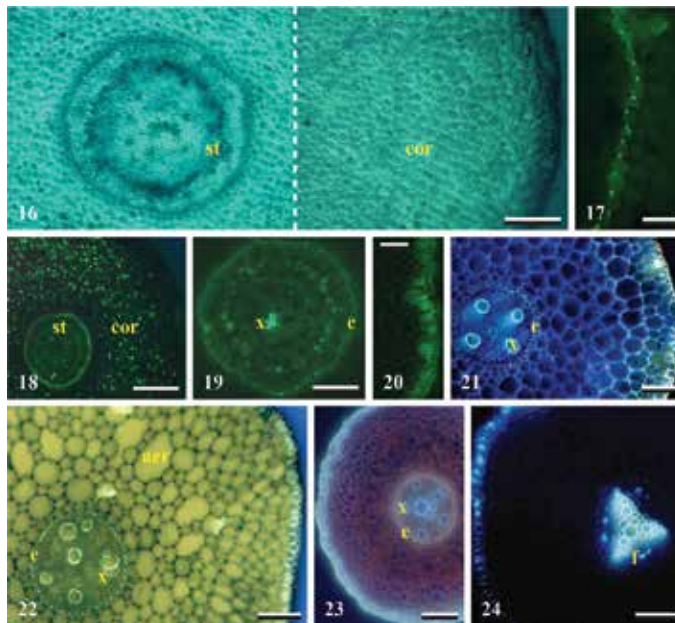
### 2.2.2. Hypocotyl

The hypocotyl has an unusual structure (**Figure 16**); delimited by an endodermis (**Figure 17**), its stele has a little, unevenly distributed, tracheary tissue near its center that takes various forms (**Figures 16**, **18**, and **19**). The tracheary cells are surrounded by rings of extensive immature tissues which never become well differentiated into more xylem or into phloem

(Figures 16, 18, and 19); a ring of endodermis, which has Casparian bands (Figure 17), followed during development by suberin lamellae, prominent on the outer tangential walls (Figure 19) surrounds the stele. There is little to no air space in the stele or cortex of the hypocotyl (Figure 16). The hypocotyl is often green in the outer cortex, and there is no distinct exodermis, but the epidermis has fluorescent cell walls and the cell layer under it shows some fluorescence (Figure 20).

### 2.2.3. Roots

The stele of roots is typically tetrarch (Figures 21 and 22), but hexarchy and pentarchy occur in large roots (Figure 23) and triarchy in some roots (Figure 24). Central metaxylem vessel elements with a discontinuity of mature xylem elements between protoxylem and metaxylem are common (Figures 22 and 23).

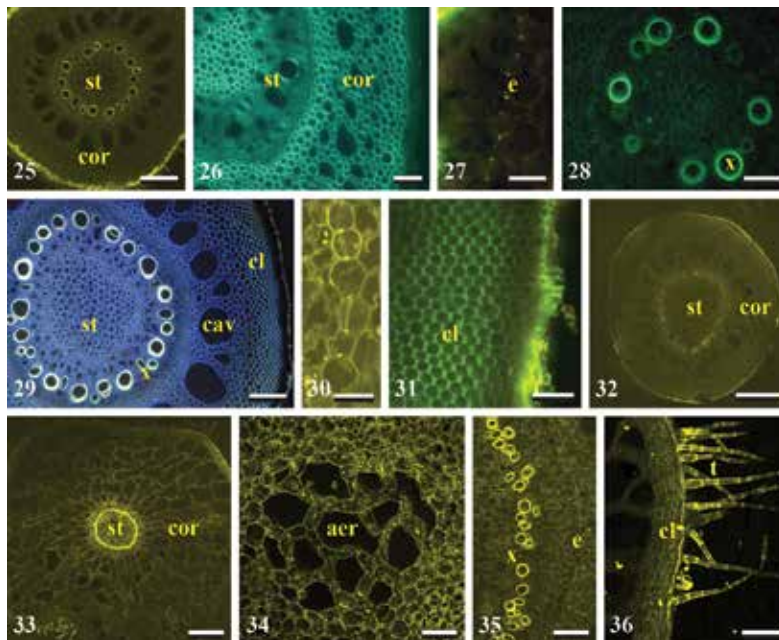


**Figures 16–24.** *Trapa natans* hypocotyl and adventitious roots, all transverse sections. 16. Hypocotylar/transition region section in DIC, scale bar = 150  $\mu\text{m}$ . 17. Hypocotyl endodermis with Casparian bands stained with BTBO, scale bar = 70  $\mu\text{m}$ . 18. Hypocotyl with endodermis delimited stele and cortex berberine stained, scale bar = 200  $\mu\text{m}$ . 19. Hypocotyl stele with few tracheary elements, BTBO, scale bar = 100  $\mu\text{m}$ . 20. Hypocotyl epidermis and hypodermis (exodermis), scale bar = 70  $\mu\text{m}$ . 21. Adventitious root 10 cm long, tetrarch stele, endodermis with Casparian bands, BAB, scale bar = 60  $\mu\text{m}$ . 22. Adventitious root, 7 cm long, protoxylem and metaxylem, phloem, endodermis with Casparian bands, aerenchyma, exodermis, BAB, scale bar = 100  $\mu\text{m}$ . 23. Adventitious root, pentarch stele, metaxylem, protophloem between points of protoxylem, endodermis with Casparian bands and suberin lamellae, exodermis, autofluorescence, scale bar = 150  $\mu\text{m}$ . 24. Adventitious root, triarch stele with limited secondary xylem and phloem fibers, BAB, scale bar = 150  $\mu\text{m}$ .

The root cortex of *Trapa natans* is characterized by aerenchyma in its middle by both schizogeny and expansigeny (Figures 22 and 23; for terminology see [32], but it often has asymmetrically

larger lacunae in the inner cortex in some anchored, substrate roots. Typically, the endodermis has only Casparian bands (**Figure 21**) in both substrate-bound roots from the cotyledonary node and roots growing only in water from the stolons under floating plantlets. Anchored roots may have faint evidence of extra wall material or suberin lamellae in the endodermis (**Figure 23**). There is usually a biseriate hypodermis with an outer, uniseriate exodermis of Casparian bands (**Figures 21 and 22**) and suberin lamellae (**Figure 23**). The epidermis may be lost. Limited secondary growth with phloem fibers may occur (**Figure 24**).

#### 2.2.4. Stolons



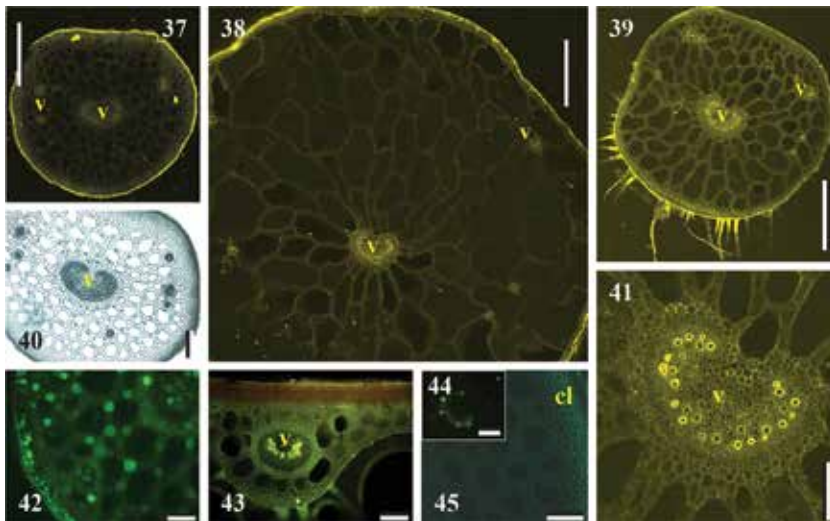
**Figures 25–36.** *Trapa natans* stolons and peduncles, all transverse sections. 25. Overview of stolon transverse section TS from epidermis to pith, LCF, scale bar = 500  $\mu\text{m}$ . 26. First internode above hypocotyl, DIC, scale bar = 200  $\mu\text{m}$ . 27. First internode, endodermis with Casparian bands, BTBO, scale bar = 70  $\mu\text{m}$ . 28. First internode stele with 6–10 vessel elements and pith, BAB, scale bar = 120  $\mu\text{m}$ . 29. Stolon, typical stele with numerous vessel elements in xylem, cortex with cavities, BAB, scale bar = 250  $\mu\text{m}$ . 30. Endodermis with Casparian bands in stolon, LCF, scale bar = 50  $\mu\text{m}$ . 31. Stolon, collenchyma underlying hypodermis, remnant exodermis, and early periderm, BAB, scale bar = 120  $\mu\text{m}$ . 32. Distal stolon with stele and included aerenchyma, LCF, scale bar = 1200  $\mu\text{m}$ . 33. Peduncle with ring of tightly packed xylem cells, trichomes in lower left, LCF, scale bar = 1000  $\mu\text{m}$ . 34. Peduncle with aerenchyma in pith, LCF, scale bar = 100  $\mu\text{m}$ . 35. Peduncle stele tightly packed xylem, endodermis with Casparian bands, LCF, scale bar = 70  $\mu\text{m}$ . 36. Peduncle multicellular trichomes, collenchyma, LCF, scale bar = 200  $\mu\text{m}$ .

Growth of the epicotyl into a stolon produces stem tissue, which possesses a central core of vascular tissue (overview in **Figure 25**). In the first internode (**Figures 26 and 27**), beyond the hypocotyl, there are usually only 9–11 vessel elements in a ring surrounding a non-aerenchymatous pith (**Figure 28**) with limited phloem; there are lysigenous cavities near the xylem elements that appear to be protoxylem lacunae (**Figure 26**). The endodermis has Casparian

bands (Figure 27) but never appears to develop suberin lamellae. The cortex of the first internode is characterized by large lacunae, developed mostly by schizogeny with expansigeny, and a multiseriate hypodermis with a uniseriate exodermis, comprising Casparian bands and suberin lamellae. The boundary between hypodermis and mid cortex has collenchyma (Figure 26). The epidermis may be often lacking.

The stolon axis beyond the first internode until the distal stolon has a fairly large central cylinder or stele in which there are 15–25 vessels in a ring (Figure 29), varying with size of the stolon, outside a large pith; except for protoxylem lacunae in the stele, there is normally no pith aerenchyma throughout most of the length of the stolon. The stele is encircled by an endodermis with Casparian bands (Figure 30). There are usually 20 large cavities in the middle of the cortex (Figure 29), and there is a wide collenchyma region under a hypodermis and remnant epidermis (Figure 31). An initial periderm-like zone develops in many stolons (Figure 31). Only the distal stolon, where it leads into peduncle, contains pith aerenchyma, as well as cortical cavities (Figure 32).

#### 2.2.5. Peduncles



**Figures 37–45.** *Trapa natans* leaves—petioles and lamina, transverse sections. 37. Proximal petiole, note aerenchyma lacunae, veins, LCF scale bar = 1000  $\mu\text{m}$ . 38. Petiole bladder, note large aerenchyma lacunae, veins, LCF, scale bar = 1000  $\mu\text{m}$ . 39. Distal petiole, note aerenchyma lacunae and trichomes, veins, LCF scale bar = 1000  $\mu\text{m}$ . 40. Proximal petiole, aerenchyma, vein, TBO, scale bar = 350  $\mu\text{m}$ . 41. Distal petiole vein without endodermis, aerenchyma, LCF, scale bar = 200  $\mu\text{m}$ . 42. Proximal petiole, vein and epidermis, aerenchyma, BAB, scale bar = 80  $\mu\text{m}$ . 43. Leaf lamina, note vein and air spaces, aerenchyma, autofluorescence, scale bar = 400  $\mu\text{m}$ . 44. Petiole vein, BTBO, scale bar = 150  $\mu\text{m}$ . 45. Proximal petiole, epidermis and collenchyma, BAB, scale bar = 120  $\mu\text{m}$ .

Peduncles to flowers and one-seeded drupes are larger than stolons and are characterized by a central core of vascular tissue and pith (Figure 33), but the pith has large schizo-expansigenous cavities (Figure 34). There is a conspicuous ring of xylem cells with intervening individual

parenchyma cells between most tracheids (**Figure 35**); small, inconspicuous phloem elements lie in a ring between the xylem and an endodermis. The endodermis has tangentially elongated cells and long Casparian bands (**Figure 35**). Various sized lacunae occur in the inner cortex and a collenchyma ring underlies the epidermis, but its cells are not as thick-walled as in other stems. Clusters of multicellular trichomes extend from epidermal cells, usually with a thick cuticle (**Figure 36**).

### 2.2.6. Leaves

At the nodes in early growth, initially, there are extremely reduced leaves with <1 mm long buds (**Figure 10**; reduced, submersed leaves found above the first few nodes were not studied here; see [28]) and later multiple adventitious roots along the axis under water (**Figure 11**). Leaf petioles are comprised of a longer proximal petiole, inflated mid-petiole bladder, and shorter distal petiole (**Figure 12**); a main vein or vascular bundle and two to eight smaller lateral veins are characteristic (**Figures 37–40**), but branches of the veins occur. The bladder (**Figure 38**) contains more and longer cells and larger lacunae than cells and lacunae in the proximal (**Figures 37 and 40**) and distal (**Figures 39 and 41**), non-inflated portions of the petiole. The aerenchyma arises by schizogeny and expansigeny (**Figures 42 and 43**). There is no endodermis or exodermis (**Figures 41, 43, and 44**).

The rhombic leaf lamina has palmate venation with none of the veins containing barrier layers, although a bundle sheath surrounds some veins, especially the mid-vein. Palisade parenchyma is typical and often contains crystals at its base, but spongy mesophyll has a more characteristic lacunar appearance than typical leaf spongy mesophyll (**Figure 43**). Collenchyma under the epidermis is usually present in petioles and even the leaf blade (**Figures 37–40, 43, and 45**). The cuticle on the surfaces, especially lower epidermis, is thick (**Figures 37–39**). Multicellular epidermal trichomes are common on the epidermis of petioles and blades beneath major veins (**Figures 39 and 43**).

## 2.3. *Justicia americana*

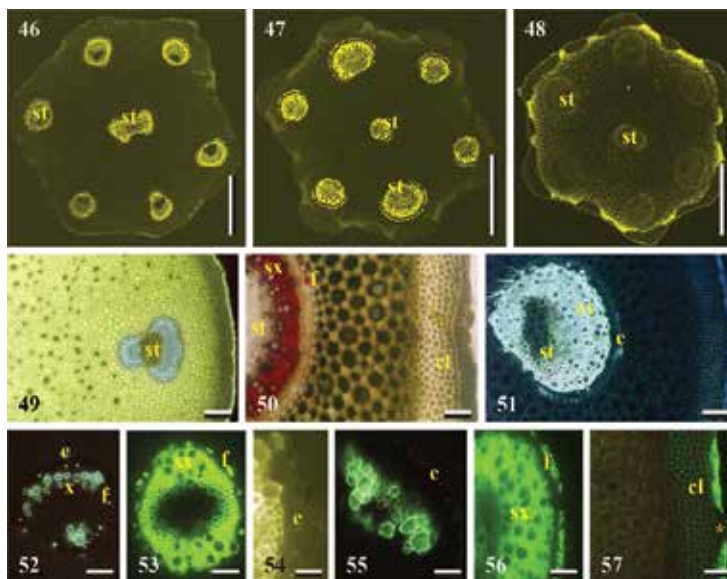
In its habitat setting along the shore, *J. americana* overwinters via its underwater stolons, sensu Sculthorpe [28], which run above the shallow river bottom at the shore, and buds which elongate in late spring (**Figures 13–15**) to produce at first a few shoots (**Figures 13 and 15**) and later many stolon branches and upright, erect shoots (**Figures 13 and 14**). These stolons may grow between the boulders (**Figures 13–15**) that had been placed along the shoreline during the 1990s. Stolons initially form a few adventitious roots per node at about the second or third visible node and later produce clusters of roots at the nodes nearest the base of the erect shoots (**Figure 15**). The depth of water varies every year, but 10–50 cm of erect shoots is under the surface of the water at various times during a season.

### 2.3.1. Stems

The stems of *Justicia americana* include the submerged (**Figure 46**) and aerial portions of the vertical erect stems (**Figures 47—3rd internode, 48—5th internode**) and stolons (**Figure 49**).



They have six large, peripheral steles (a mushroom shape for each stele in stolons, **Figure 49**) and one or two central bundles with a pith in each stele of their hexangular stems, a polystelic situation. The ground tissue, in which the peripheral steles and central stele(s) of the stems is embedded, is extensive; the peripheral parenchyma and collenchyma can be termed cortex. The steles develop secondary xylem (**Figures 50, 51, and 53**) and even show indications that stolons persist for two years with more secondary xylem. Phloem cells and fibers are present as a more or less thin arc around the outer portions on the six peripheral bundles (**Figures 50–53**) and, after typical early primary growth (**Figure 52**), the central bundle has xylem with surrounding small patches of primary phloem and fibers (**Figure 53**). Primary growth shows the position of protoxylem toward the inside of each group of xylem cells, as well as the presence of early phloem fibers and endodermis (**Figures 52 and 53**).

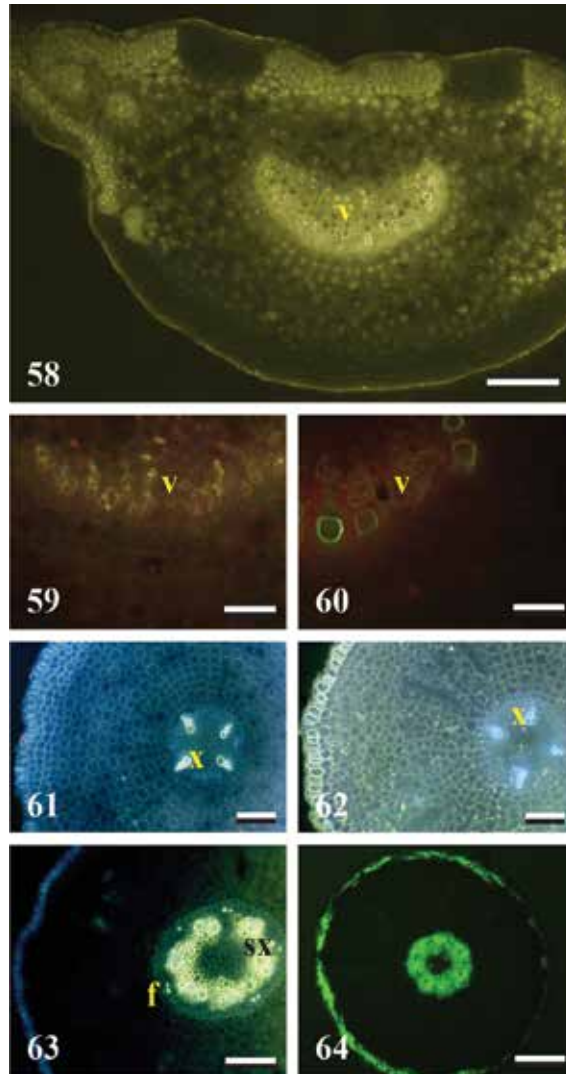


**Figures 46–57.** *Justicia americana* erect stems and stolons. 46. Submerged erect stem, hexagonal stem, 1 central-doubled, and 6 peripheral steles, LCF, scale bar = 2000  $\mu\text{m}$ . 47. Erect aerial stem third internode, LCF, scale bar = 1000  $\mu\text{m}$ . 48. Erect aerial stem fifth internode, LCF, scale bar = 1000  $\mu\text{m}$ . 49. Stolon, one mushroom-shaped stele, aerenchyma, exodermis near right edge, BAB, scale bar = 150  $\mu\text{m}$ . 50. Stolon, phlorogucinol-stained to show phloem fiber, periderm, scale bar = 100  $\mu\text{m}$ . 51. Stolon, peripheral stele, xylem, few phloem fibers, endodermis, BTBO, scale bar = 120  $\mu\text{m}$ . 52. Stolon, young stele, primary xylem, phloem fibers already present, BTBO, scale bar = 110  $\mu\text{m}$ . 53. Submerged erect stem, central stele, endodermis, BER, scale bar = 100  $\mu\text{m}$ . 54. Aerial stem with endodermis, BTBO, scale bar = 70  $\mu\text{m}$ . 55. Young aerial stem with endodermis, BTBO, scale bar = 100  $\mu\text{m}$ . 56. Aerial stem without endodermis, phloem fibers, BTBO, scale bar = 100  $\mu\text{m}$ . 57. Stolon, collenchyma, BER, scale bar = 200  $\mu\text{m}$ .

Submerged aerial stems usually contain endodermis (**Figure 54**), and aerial portions at the third internode usually do not (**Figure 55**), but early year high waters often have endodermis around each stele (**Figure 56**). Ground tissue from the cortex to the central region contains schizogenous–expansigenous lacunae, and thus, stems have aerenchyma (**Figure 49**). There are an extensive collenchyma band under the epidermis and a hypodermis between the

epidermis and the collenchyma that shows exodermal traits (**Figures 50, 51 and 57**). Accompanying secondary growth in the steles via a vascular cambium is limited cork cambium growth in the outer layer of cortex that produces a few layers of cork cells (**Figures 50 and 57**).

### 2.3.2. Leaves



**Figures 58–64.** *Justicia americana* leaves and adventitious roots. 58. Leaf lamina, mid vein, BAB, scale bar = 200  $\mu\text{m}$ . 59. Submerged leaf lamina, vein, no endodermis, BAB, scale bar = 50  $\mu\text{m}$ . 60. Aerial leaf lamina, vein, no endodermis, BAB, scale bar = 50  $\mu\text{m}$ . 61. Short adventitious root, tetrarch, BAB, scale bar = 100  $\mu\text{m}$ . 62. Short adventitious root, tetrarch, schizo-lysigenous aerenchyma, exodermis, FY, scale bar = 100  $\mu\text{m}$ . 63. Long adventitious root, secondary xylem, and phloem fibers, BAB, scale bar = 100  $\mu\text{m}$ . 64. Long adventitious root, secondary growth, remnant exodermis, initial periderm, BAB, scale bar = 200  $\mu\text{m}$ .

Leaves of *J. americana* are structured like mesophytic leaves, except that they have cellulosic thickened cell walls under the epidermis that could be termed collenchyma (**Figure 58**). Whether submerged (**Figure 59**) or aerial (**Figure 60**), veins do not have any barrier layers in their lamina or petioles, and their air spaces are similar.

### 2.3.3. Roots

The stele typically has three to five protoxylem and protophloem strands or poles (usually tetrarch; **Figures 61** and **62**) and a pith, but metaxylem may rarely occupy the stele center. In older roots, there is limited secondary growth; secondary xylem (**Figures 63** and **64**) is accompanied by phloem fiber formation (**Figure 63**). The cortex is delimited by an endodermis with Casparian bands only (**Figure 61**). The mid-cortex is characterized by radial lacunae which are primarily produced by schizogeny in the mid to out cortex, but some cell deaths occur; therefore, it is termed schizo-lysigenous aerenchyma (**Figure 62**). The biseriate hypodermis has a uniseriate exodermis with Casparian bands and thick suberin lamellae (**Figures 62** and **63**) and in older roots a periderm may start to form (**Figure 64**).

## 3. Discussion

We have provided anatomical characteristics of two important riverine plants, the infamous, invasive *Trapa natans*, and the native *Justicia americana* that contribute to our understanding for the reasons these species are successful in their respective habitats.

In appearance, the ramets of *T. natans* most closely resemble the drawings in Crow and Hellquist [[1], p. 209] who accurately depicted multiple, anchoring, adventitious roots arising from the cotyledonary node above the extension of the hypocotyl out of the fruit/seed. *Trapa natans* has structural traits which allow it to be well-adapted to its anchored, floating habitat in quiet parts of rivers. *Justicia americana* is equally well adapted to its shoreline habitats by its tough stolons with adventitious roots and upright stems on the shoreline.

Unlike Arber [8] and Menegus et al. [27], we never found evidence of an elongated primary root, seminal roots, or even an aborted primary root outside of the seed/fruit in hundreds of plants, which were connected to the fruits by their stolons, in *T. natans*. Rather, the hypocotyl elongates vertically from the fruit/seed, and the first roots are adventitious roots from the cotyledonary node, arising outside the seed/fruit; there never is a primary root. The variable xylem patterns in the hypocotylar region are a manifestation of a transition from root to stem. Except for the first adventitious roots, adventitious roots are short and have many lateral roots; together these roots are prolific, giving rise to the appearance that they were sometimes interpreted in ecological studies as feathery compound leaves [[30, 35]; published plant guides [36]]; they are roots [1, 28]. Our findings are similar to those reported long ago in illustrations by Schenck [17, 18], although Schenck [17] reported primary root elongation; by our anatomical analysis, this is really hypocotylar elongation in his illustrations as the radicle remains embedded in the fruit/seed [28]. Roots of both species are typical for plants growing in aquatic/wetland conditions with typical endodermis, exodermis, and aerenchyma. Both species also exhibit root apical meristems that Heimsch and Seago [33] classified as tiered dicot with

separate initials for the stele, overlying tier of cortical initials, and epidermal-rootcap initials (not presented here).

Lewis [11] found that *J. americana* could reproduce easily by stolon, especially when stolons and young, vertical shoots were not covered by debris. Stolons extend from the base of erect shoots into the river water along the surface of the sand and rocks and among the boulders; some adventitious roots penetrated the sandy-rocky river shore bottom.

In both species, the structures in our photographs are similar to the drawings of Ogden [9], except that we have identified the structures in the organs; clearly, *Trapa* was already well enough known in New York waterways in 1974 for Ogden [9] to include it in his article. Metcalfe and Chalk [23–25, p. 216] noted “conspicuous” endodermis in the stem of three genera (*Andrographis*, *Barleria*, *Thunbergia*) of the Acanthaceae and “Casparian thickenings” in some members of the Lythraceae (*Adenaria*, *Cuphea*, *Lagerstroemia*, *Peplis*); their diagram [24, p. 1018] of *Justicia* stem is similar to our photographs.

However, vascular tissue arrangements of *Trapa natans* and *Justicia americana* are unusual for angiosperms, but Scott [37] had earlier reported polystelic stems in aquatic dicots derived from terrestrial plants. In *Trapa*, the hypocotyl superficially resembles a modified root stele in that only a few apparent tracheary cells are centrally located and surrounded by parenchyma, but it does not contain a typical root vasculature with arms of xylem, interspersed with batches of phloem, radiating outward to a pericycle; phloem encircles parenchyma and the limited xylem. While Fahn [38] stated that the primary root had monarch pattern, clearly a radicle never emerges into a primary root in *T. natans*; we interpret the axis as the transition zone of the hypocotyl. Hypocotyls never produce much mature tissue. Thus, after adventitious roots take over the anchorage function, the hypocotyl and fruit effectively may no longer function.

The stems of *Trapa* are siphonostelic with one layer of endodermis surrounding all vascular tissue. In the peduncle, where xylem cells are closely appressed, vascular tissue arrangement is best described as a kind of ectophloic siphonostele [38]; stolons and peduncles differ slightly in their positions of phloem. The early development of the vascular system in the stem of *Justicia americana* was described long ago by Jones [39, named *Dianthera americana* therein]. It has also been deemed to have a monocot-like atactostele [26], but we have shown that each complex vascular bundle or stele is surrounded by an endodermis; therefore, the stem is a polystele with each stele having parenchyma, primary and secondary xylem, and partially surrounding primary and secondary phloem—all within an endodermis. Other species of *Justicia* do not show the same polystelic vascular anatomy in their stems [40, 41], although O’Neill [40] noted what could be endodermis. The interest in the kind of vasculatures which characterize *Trapa* and *Justicia* was addressed long ago by Scott [37], but has not received much attention in recent decades [23, 24]. Our findings of fern-like (not identical to such steles) siphonosteles and polysteles clearly indicate a need for further study of these structural features in other members of their families since they are so prevalent in stems of aquatic and wetland plants [24].

Another distinctive feature of both species is the presence of a wide band of collenchyma under the epidermis in the stems (and even petioles), even when there is considerable secondary

vascular tissue, as in *J. americana*; both O'Neill [40] and Zottele and Aoyama [41] noted fairly extensive collenchyma under the epidermis [23, 24]. Collenchyma is clearly a substantive supportive tissue for these plants occupying riverine habitats. The air spaces do not occur within this tissue but internal to it in the next zone of cortex or ground tissue. Aerenchymatous tissue does not occur within individual steles of *Justicia* or in the hypocotyl and most stolons of *Trapa*, although lysigenous cortical cavities and protoxylem lacunae occur in *Trapa*, and schizogenous-expansigenous lacunae occur in the uppermost stolon and its continuation into the peduncle of *Trapa*; small lacunae occur throughout the ground tissue of *Justicia* stems.

While we have reported on the air spaces within these two species, we have not attempted to analyze the presence of an air space continuum between their organs [42]. We note that at the water-air interface, the distal stolons and peduncles show pith aerenchyma, in addition to cortical air spaces [28, 43]. Our descriptions of aerenchyma differ somewhat from Van der Valk [44], but we agree that floating leaves, such as *T. natans*, have enlarged mesophyll spaces which we believe can properly be termed aerenchyma because they have typical aerenchymatous lacunae. Leaves submersed in water during development do not develop typical leaf structures in *T. natans* and lack barrier layers in both *T. natans* and *J. americana*.

The multicellular trichomes which we observed along the petioles and on the abaxial surface of leaves, resembled those in drawings in Metcalfe and Chalk [25] and have been termed hydropoten because they presumably absorb water and minerals [25], but we did not test for this and we note that they are not at all like hydropoten in Nymphaeaceae (Seago, personal observation). The presence of crystals was not presented herein [for *T. bispinosa* 45, 46].

The nature of the stoloniferous growth and structural features of *T. natans*, including siphonostele, endodermis, collenchyma, and cortical air spaces, along with the anchorage of the extensive ramet systems by the fruit-hypocotyl axis and first adventitious roots, must contribute to its success in calmer waterways.

## 5. Conclusions

This study of the structural traits of both *Trapa natans* and *Justicia americana* reveals the ecological adaptations of each to their respective habitats. The organizations and structures of the tissues in roots, stolons, leaves, and peduncles of *T. natans* contribute to its characteristic sponginess, buoyancy, and flexibility in its floating habit, outpacing native species. The enormous production of ramets with their multiple floating leaves, along with the flowering/fruiting axis, can quickly cover a calm water's surface, probably monopolizing nutrients and space, while limiting light penetration and dissolved oxygen in the water column. The abundant adventitious roots undoubtedly aid in the absorption of nutrients and must contribute to its success in invading riverine habitats. The ability of *J. americana* to provide substrate stabilization and a barrier to shoreline erosion through its network of stolons can be attributed, in part, to its angular stems' structural characteristics, which surely give its stems (stolons and erect stems) strength. Its adventitious roots must also add to its ability to maintain substrate.

The unique stem steles of these two species, their endodermis delimiting these steles, their air space systems, and the peripheral, flexible collenchyma undoubtedly contribute to the respective ecosystem roles, including the respective roles of the invasive [10] versus the shoreline stabilizer [13] species. Unfortunately, we really do not know how extensive these anatomical patterns are in flowering plants [23, 24, 39]. The occurrence of endodermis-enclosed steles in stems, air space tissues and flexible collenchyma, found in these species of eudicots not near the base of the angiosperms, suggests that these structural traits have been conserved over evolution and can appear in more derived families, genera, and species of plants in response to environmental stimuli. The endodermis-enclosed steles of stems, however, are very different from the norm among eudicots.

## Acknowledgements

The authors wish to acknowledge the assistance of Dr. Carol A. Peterson, Daryl E. Enstone, and Dr. Simon Chuong, University of Waterloo, Ontario, Dr. Chris Meyer at University of Guelph, Dr. Hilary A. McManus at LeMoyne College, Dr. Julien B. Bachelier at SUNY Oswego, and Marilyn A. Seago for her continuing encouragement and support, especially in collecting specimens.

## Author details

James L. Seago Jr.<sup>1\*</sup>, Willow B. Eyres<sup>2</sup> and Matthew Volny<sup>3</sup>

\*Address all correspondence to: [jseago@twcny.rr.com](mailto:jseago@twcny.rr.com)

1 SUNY Oswego, Minetto, NY, USA

2 New York State Department of Environmental Conservation, Invasive Species Unit, Albany, NY, USA

3 Biology Department, University of Virginia, Charlottesville, VA, USA

## References

- [1] Crow, G. E., and C. B. Hellquist. Aquatic and wetland plants of northeastern North America, volume 1, pteridophytes, gymnosperms, and angiosperms: Dicotyledons. The University of Wisconsin Press, Madison, WI. 2000.
- [2] Naylor, M. Water chestnut in the Chesapeake Bay Watershed: A regional management plan. Maryland Department of Natural Resources. 2003.

- [3] Hummel, M., and S. Findlay. Effects of water chestnut (*T. natans*) beds on water chemistry and in the tidal freshwater Hudson River. *Hydrobiologia*. 2006; 559: 169–181. doi:10.1007/s10107-005-9201-0
- [4] Pemberton, R. W. Water chestnut. Invasive Plant Research Laboratory, US Department of Agriculture, Florida. 1999.
- [5] Britton, N. L., and A. Brown. An illustrated flora of the northern United States, Canada and the British Possessions. Vol. II Portulacaceae to Menyanthaceae. Charles Scribner's Sons, New York, NY. 1897.
- [6] Muenscher, W. C. Aquatic vegetation of the Mohawk watershed. NYSDEC: A biological survey of the Mohawk-Hudson watershed. NYSDEC Supplement to the Annual Report 1934. Biology Survey No. 9. 1934; 9: 228–249.
- [7] Winne, W. T. A study of the water chestnut, *Trapa natans*, with a view of its control in the Mohawk River. MS Thesis, Cornell University, Ithaca, NY. 1953.
- [8] Arber, A. Water plants: A study of aquatic angiosperms. Cambridge University Press, Cambridge, UK. 1920.
- [9] Ogden, E. C. Anatomical patterns of some aquatic vascular plants of New York. New York State Museum and Science Service Bulletin. 1974; 424: 1–133.
- [10] Groth, A. T., L. Lovett-Doust, and J. Lovett-Doust. Population density and module demography in *Trapa natans* (Trapaceae), an annual, clonally aquatic macrophyte. *American Journal of Botany*. 1996; 83: 1406–1415. Stable URL: <http://www.jstor.org/stable/2446095>
- [11] Lewis, K. P. Vegetative reproduction in populations of *Justicia americana* in Ohio and Alabama. *The Ohio Journal of Science*. 1980; 80: 134–137.
- [12] Penfound, W. T. The biology of *Dianthera americana* L. *American Midland Naturalist*. 1940; 24: 242–247.
- [13] Fritz, K. M., and J. W. Feminella. Substratum stability associated with the riverine macrophyte *Justicia americana*. *Freshwater Biology*. 2003; 48: 1630–1639. doi:10.1046/j.1365-2427.2003.01114.x
- [14] Fritz, K., M. Gangloff, and J. Feminella. Habitat modification by the stream macrophyte *Justicia americana* and its effects on biota. *Oecologia*. 2004; 140: 388–397. doi:10.1007/s00442-004-1594-3
- [15] Strakosh, T. R. Effects of water willow establishment on littoral assemblages in Kansas reservoirs: focus on age-0 largemouth bass. Ph.D. Dissertation, Kansas State University. 2006.
- [16] Strakosh, T. R., J. L. Eitzmann, K. B. Gido, and C. S. Guy. The response of water willow *Justicia americana* to different water inundation desiccation regimes. *North American Journal of Fisheries Management*. 2005; 25: 1476–1485.

- [17] Schenck, H. Die Biologie der Wassergewächse. Max Cohen & Sohn, Bonn. 1885.
- [18] Schenck, H. The biology of aquatic plants. A. R. G. Gantner Verlag K. G., Ruggell, Liechtenstein. Translation by D. H. Les. 2003.
- [19] Justin, S. H. F. W., and W. Armstrong. The anatomical characteristics of roots and plant response to soil flooding. *The New Phytologist*. 1987; 106: 465–495. doi:10.1111/j.1469-8137.1987.tb00153.x
- [20] Smirnov, N., and R. M. M. Crawford. Variation in the structure and response to flooding of root aerenchyma in some wetland plants. *Annals of Botany*. 1983; 51: 237–249.
- [21] Perumalla, C. J., C. A. Peterson, and D. E. Enstone. A survey of angiosperm species to detect hypodermal Casparian bands. I. Roots with a uniseriate hypodermis and epidermis. *Botanical Journal of the Linnean Society*. 1990; 103: 93–112. doi:10.1111/j.1095-8339.1990.tb00176.x
- [22] Peterson, C. A., and C. J. Perumalla. A survey of angiosperm species to detect hypodermal Casparian bands. II. Roots with a multiseriate hypodermis or epidermis. *Botanical Journal of the Linnean Society*. 1990; 103: 113–125. doi:10.1111/j.1095-8339.1990.tb00177.x
- [23] Metcalfe, C. R., and L. Chalk. *Anatomy of the dicotyledons. I.* Oxford University Press, London, UK. 1950a.
- [24] Metcalfe, C. R., and L. Chalk. *Anatomy of the dicotyledons. II.* Oxford University Press, London, UK. 1950b.
- [25] Metcalfe, C. R., and L. Chalk. *Anatomy of the dicotyledons. I. Systematic anatomy of leaf and stem, with a brief history of the subject.* Clarendon Press, Oxford, UK. 1979.
- [26] Popham, R. A. *Laboratory manual for plant anatomy.* C.V. Mosby, St. Louis, MO. 1966.
- [27] Menegus, F., L. Cattaruzza, L. Scaglioni, and E. Ragg. Effects of oxygen level on metabolism and development of seedlings of *Trapa natans* and two ecologically related species. *Physiologia Plantarum*. 1992; 86: 168–172. doi:10.1111/j.1399-3054.1992.tb01326.x
- [28] Sculthorpe, C. D. *The biology of aquatic vascular plants.* Edward Arnold, London, UK. 1967.
- [29] Bitonti, M. B., R. Cozza, G. Wang, M. Ruffini-Castiglione, S. Mazzuca, S. Castiglione, F. Sala, and A. M. Innocenti. Nuclear and genomic changes in floating and submerged buds and leaves of heterophyllous water chestnut (*Trapa natans*). *Physiologia Plantarum*. 1996; 97: 21–27. doi:10.1111/j.1399-3054.1996.tb00473.x
- [30] Caraco, N. F., and J. J. Cole. Contrasting impacts of a native and alien macrophyte on dissolved oxygen in a large river. *Ecological Applications*. 2002; 12: 1496–1509. doi:10.1890/1051-0761(2002)012[1496:CIOANA]2.0.CO;2



- [31] Seago, J. L., Jr., and L. C. Marsh. Adventitious root development in *Typha glauca*, with emphasis on the cortex. *American Journal of Botany*. 1989; 76: 909–923. Stable URL: <http://www.jstor.org/stable/2444547>
- [32] Seago, J. L., Jr., L. C. Marsh, K. J. Stevens, A. Soukup, O. Votrubová, and D. E. Enstone. A re-examination of the root cortex in wetland flowering plants with respect to aerenchyma. *Annals of Botany*. 2005; 96: 565–579. doi:10.1093/aob/mci211
- [33] Heimsch, C., and J. L. Seago, Jr. Organization of the root apical meristem in angiosperms. *American Journal of Botany*. 2008; 95: 1–21. doi:10.3732/ajb.95.1.1
- [34] Seago, J. L., Jr., C. A. Peterson, D. E. Enstone, and C. A. Scholey. Development of the endodermis and hypodermis of *Typha glauca* Godr. and *T. angustifolia* L. *Canadian Journal of Botany*. 1999; 77: 122–134.
- [35] Wu, M.-Y., and J. Wu. *In vitro* investigations on ultrasonic control of water chestnut. *Journal of Aquatic Plant Management*. 2007; 45: 76–83.
- [36] Campbell, S., P. Higman, B. Slaughter, and E. Schools. A field guide to invasive plants of aquatic and wetland habitats for Michigan. Michigan Natural Resources Inventory, Michigan State University Extension, Michigan. 2010.
- [37] Scott, D. H. Origin of polystely in dicotyledons. *Annals of Botany*. 1891; 5: 514–517.
- [38] Fahn, A. *Plant anatomy*. Pergamon Press, Oxford, UK. 1990.
- [39] Jones, W. R. The development of the vascular structure of *Dianthera Americana*. *Botanical Gazette*. 1912; 54: 1–30.
- [40] O'Neill, C. S. Anatomy of the shrimp plant, *Justicia brandegeana* (Acanthaceae). *Studies by Undergraduate Researchers at Guelph*. 2010; 3: 41–47.
- [41] Zottele, L., and E. M. Aoyama. Morfoanatomia e enraizamento de estacas caulinares de *Justicia wasshauseniana* Profice (Acanthaceae). *Natureza Online*. 2014; 12: 179–184. ESFA: <http://www.naturezaonline.com.br>
- [42] Jackson, M. B., K. Ishizawa, and O. Ito. Evolution and mechanisms of plant tolerance to flooding stress. *Annals of Botany*. 2009; 103: 137–142. doi:10.1093/aob/mcn242
- [43] Costantin, J. Recherches sur la structure de la tige des plantes aquatiques. *Annales des Sciences Naturelles, Botanique, Series 6*. 1884; 19: 287–331.
- [44] Van der Valk, A. G. *The biology of freshwater wetlands*. Oxford University Press, Oxford, UK. 2012.
- [45] Pandey, S. N., and A. Chadha. *Plant anatomy and embryology*. Vikas, New Delhi, India. 1997.
- [46] Bercu, R. Histoanatomy of the leaves of *Trapa natans* (Trapaceae). *Phytologia Balanica*. 2004; 10: 51–55.



---

# **Biodiversity of Floodplain Soils in the European North-East of Russia**

---

Alla Kolesnikova, Elena Lapteva, Svetlana Degteva,  
Anastasia Taskaeva, Alexey Kudrin,  
Yulia Vinogradova and Fluza Khabibullina

Additional information is available at the end of the chapter

<http://dx.doi.org/10.5772/63713>

---

## **Abstract**

River floodplains are unique nature landscapes. In contrast to zonal communities on watersheds, soil biota of river floodplains is studied in less degree. The research was conducted in the floodplain forests in the European North-East of Russia and showed high diversity of soil biota in alluvial forest soils. Floodplain forest soils are inhabited by 70 species of micromycetes, 53 genera of Nematoda, 60 species of Collembola, and 110 species of large invertebrates. Alluvial meadow soils with stable moisture and temperature conditions are characterised by high species diversity of micromycetes, nematodes and large invertebrates. Collembola prefer alluvial soddy soils. Soil microorganisms, meso- and macro-fauna can essentially increase taxonomic diversity and number in alluvial meadow-boggy soils at warming autumn.

**Keywords:** European North-East of Russia, Sysola River floodplain, aspen-birch forests, alluvial soils, soil microorganisms, meso- and macro-fauna

---

## **1. Introduction**

River floodplains are the most widely distributed habitats in the world, occurring from tropical to polar regions and from deserts to rainforests. Depending on their specific area of interest, various scientists view floodplains quite differently. Many ecologists perceive floodplains primarily as ecotonal extensions of river channels. Scientists who study plants and soils view floodplains as distinct habitats rather than simply ecotones between rivers and uplands. In fact,

---

floodplains are a mosaic of sub-habitats (some aquatic, some terrestrial, some wetland), and diverse sub-habitats potentially supporting a unique biota. While most work focuses on the aquatic biota of floodplains, the terrestrial component is being increasingly recognized [1].

Due to annual snowmelt floods, river floodplains have a specific 'terraqueous' regime [2] which creates particularly special conditions for vegetation cover, soils and soil organisms. Duration and regime of floods respond for the fact that floodplain soils largely differ from watershed soils not only concerning morphological structure and physical-chemical properties of soil profiles but also by life activity of soil biota which is involved into plant residues decomposition in terrestrial ecosystems. In contrast to zonal communities on watersheds, soil biota on river floodplains is less studied. In Russia, the role of soil biota on river floodplains was intensively studied in the 1960s–1980s of the twentieth century [3–6]. This was conditioned by the fact that floodplain soils were treated as to be used in engineering and agriculture. In the twenty-first century, floodplain landscapes gained high attention in both Russia and European countries [7–12]. These studies aim at identifying the dependence in population number of soil organisms from flood regime [13–15]; adaptations of invertebrates to moisture deficient or excess [16–18]. Complete descriptions of soil biota in river floodplains are lacking, and existing research tends to focus on a few groups of soil organisms. It is known that floodplains contribute significantly to the biodiversity of the world because so many species occur solely in floodplains or at least rely heavily on floodplains to satisfy important ecological needs [1].

Globally, the soil invertebrate fauna has been extensively researched only at a few temperate-zone floodplain ecosystems, mainly in the USA, Europe and Australia. The distinctive feature of European floodplains is that they have been transformed for centuries. As a consequence, 95% of riverine floodplains have been lost [1]. But it is known that soil biota in floodplain communities has higher diversity indices as compared to that in zonal communities. And geologically ancient soils (Central Amazonia) with long-term cycles of always alternating aboveground and water phases are inhabited with endemic invertebrates whereas young ecosystems (Central Europe)—with eurytopic species [19]. Floodplain forest ecosystems are key habitats for rare invertebrates, including the representatives of the postglacial period [20]. Overall, the knowledge of the soil biota in the northern floodplain communities remains incomplete and requires a sustained taxonomic and ecological research effort to provide better estimates of species diversity, distribution and evolutionary history.

River floodplains are 'oases of life' in the northern regions. Due to the warming effect of the river waters, highly productive grass-forb meadows and deciduous forests with grassy ground cover, which atypical for the watershed landscapes of the northern part of the taiga zone, are formed in the valleys of the boreal rivers [21]. At the same time, priority attention of ecologists has been paid to the identification of biodiversity and structure of soil biota in the coniferous forests occupied watersheds [22–24]. Alluvial soils of the northern river floodplains are studied fragmentarily in this respect, particularly soil biota of floodplain aspen-birch forests [9, 10]. This was conditioned by the fact that morphological and physico-chemical properties of alluvial soils as well as ways of preservation and increase of soils fertility of floodplain meadows were studied firstly at the European northeast of Russia. The high importance of

river ecosystems in shaping migration flows of substances in landscapes, the role of floodplain soils as biogeochemical barriers to the migration of chemicals, the specifics of vegetation cover at the floodplain terraces of the boreal zone and the importance of floodplains in maintaining of soil biota biodiversity are the conditions which are important to identify the features of formation of not only soil and plant cover at floodplain landscapes of the North but also the biodiversity of soil invertebrates and microorganisms, playing a leading role in the transformation of plant residues in terrestrial ecosystems. In this study, we focused at the variation of the soil biota in a river floodplain system with natural hydrological conditions and well-preserved forests that have not been modified by human disturbances. We assumed that a riverine landscape in the natural state exhibits a high level of complexity across a range of scales, which might contribute significantly to the species pool. So, the purpose of this study was to obtain new data about species diversity, number and structure of soil biota in the Sysola River floodplain located at the European North-East of Russia and to identify ecological and functional interlinks between alluvial forest soils in the taiga zone and soil biota.

## 2. Materials and methods

The studies were conducted in the Sysola River valley, middle taiga, Komi Republic and European North-East (**Figure 1**). The Sysola River (395 km long) is one of the largest left tributaries of the Vychegda River (1131 km) which, in turn, is a tributary of the Severnaya Dvina River (744 km), the White Sea basin. It is a typical plain river, which is occupied by meadows. Our researches were carried out in aspen-birch forest, which is located in middle part of floodplain terrace, low course of the Sysola River. This forest was divided into three plots which take different positions in relief of floodplain and greatly differ by ecological conditions as snow-melt water inundation period, ground water depth, soil type, plant composition in ground cover, etc. The plots form a natural ecological row along with increasing soil moisture content: Plot 1 (ridge top, high floodplain level) → Plot 2 (even part of floodplain, mean level) → Plot 3 (deep inter-ridge depression, low level). Spring flood regime in the Sysola River is unstable. High ridge tops soils do not become inundated or stay under water for a short period of time (1–1.5 weeks), while inter-ridge depressions sometimes stay under water for one and a half month or two months.

Morphological, physical-chemical soil properties and their hydrothermal regime were studied in accordance with the accepted methods [25, 26]. Reference sections for the morphological description of soil horizons and sampling were laid at key plots. Names of soil types and horizons indices are given according to the Russian standards [27]. Soil moisture content was identified gravimetrically, soil temperature—with an electronic transistor digital thermometer TET-TS11 (Russia) and loggers DS1921G (Russia). Carbon content was measured by the gas-chromatography method with CNHS-analyzer (Carlo Erba, Italy),  $\text{pH}_{\text{KCl}}$ —potentiometrically with glass and silver-chloride electrodes at soil:solution ratio of 1:2.5 for mineral and 1:25 for organic horizons, hydrolytic soil acidity (Ha)—by titration using  $\text{CH}_3\text{COONa}$  solution, exchangeable cations ( $\text{Ca}^{2+}$ ,  $\text{Mg}^{2+}$ )—by driving with  $\text{NH}_4\text{Cl}$  solution followed by atomic-

absorption identification at Hitachi 180–60, and texture—by the Kachinsky method with dispergation and boiling in the presence of NaOH.



**Figure 1.** Map scheme of research region.

Number of the principle ecologic-trophic groups of microorganisms was assessed by inoculation of solid nutrition media [28]. We identified concentration of ammonifiers (beef-peptone agar), oligonitrophilous (Aeshbi's medium), nitrifying (Vinogradsky's medium), and denitrifying (Giltai's medium) bacteria; microorganisms using mineral nitrogen compounds (starch-ammonia agar); oligotrophic (starvation agar) and pedotrophic (soil agar) microorganisms. Saccharolytic microscopic fungi were assessed using acid Chapek's medium, cellulose-decomposing fungi—Getchinson's medium, and oligotrophic fungi—starvation agar. Total microorganisms and micromycetes number was stated in CFU/g a.d.s. (colony-forming units per 1 g of absolutely dry soil). The microorganisms' biomass carbon was estimated by the rehydration technique on the base  $K_2SO_4$  extracts [29] in fresh samples of forest litter (A0, 0–3 cm deep) and humus horizon (A1, 3–15 cm deep). Samples were collected four times during vegetation period in threefold to fourfold replication. Taxa of micromycetes were identified after their extraction as pure cultures using Chapek-Dox medium with help of manual books for the identification of different taxonomic groups of micromycetes, interactive keys, and information Internet site (<http://www.indexfungarum.org>).

For the evaluation of taxonomic composition and number of nematodes, soil samples (5 cm in diameter, 5 cm deep) were collected in sevenfold replication monthly from June till August. Totally, 63 samples were collected. Nematodes were extracted from soil using modified

Bermann funnels, heat-killed and fixed in 4% formaldehyde. In each soil sample, at least 100 individuals were identified to the genera level using a Leica DM4000 B inverted microscope. Nematodes were identified following the taxonomic keys [30–32]. The abundance of nematodes was recalculated per 100 cc of soil. Nematodes were assigned to six trophic groups (bacterivores, fungivores, root-fungal feeders, plant parasites, omnivores and predators), according to classification [33]. In total, 190 soil samples (5 × 5 × 5 cm) were collected for identification of Collembola. Samples at each plot were collected in fivefold replication monthly from June till September 2003–2005. Extraction of Collembola was done in Berlese-Tulgren funnels. Quantitative accounting of large invertebrates was done by hand using of soil samples (25 × 25 × 5 cm). In total, 380 soil samples were collected by analogy to the sampling procedure of Collembola at the same time but in 10-fold replication at every plot. Characterization of soil organisms was done using general ecologic indices as occurrence frequency, relative abundance of species (P, %), species richness (S), Shannon's diversity (H') and evenness (J') indices, Simpson's index of dominance (D<sub>SM</sub>), Chekanovsky-Sjerenzen index of similarity (Ics). The obtained data were processed by standard methods of statistics using Microsoft Excel, STATISTICA 6.0 and PAST 3.1.

### 3. Characterization of plant and soil cover

River valleys of the taiga zone have two forest types, particularly birch and aspen forests [21]. From position of the Russian classification, these forests are considered as floodplain cycle of plant associations. They are divided into two, herbaceous—stone bramble and hair grass sedge series. Each of the two series is composed of two associations. Communities of the herbaceous—stone bramble series (*Betula sp.*—*Rubus saxatilis*—*Climacium dendroides* and *Populus tremula*—*Rubus saxatilis*—*Climacium dendroides*) form at ridge tops of the central floodplain. They grow on alluvial soddy or meadow soils. The phytocenoses of the hair grass sedge series (*Betula sp.*—*Carex cespitosa* and *Populus tremula*—*Carex cespitosa*) prefer moist habitats and occupy shores of former river beds, inter-ridge and near-terrace depressions on alluvial meadow-boggy soils. Deciduous forests formed in river floodplains have a well-developed and diverse underbrush. The most stable and often-met species in underbrush are *Rosa acicularis*, *R. majalis* and *Frangula alnus*. The underbrush of floodplain aspen forests includes *Viburnum opulus* and *Swida alba*. Totally, the study forests consist of 18 shrub species. The crown density for shrubs can sometimes reach 0.6–0.8. Water-loving plants dominate in ground cover of floodplain deciduous forests. The most valuable species of plants are *Rubus saxatilis* and *Carex cespitosa*. *Galium physocarpum*, *Lysimachia vulgaris*, *Ranunculus auricomus*, *Hylotelephium triphyllum*, *Moehringia lateriflora* are often noted but they are not abundant. Long flooding period, thick dead leaf layer and herbal plants inhibit the development of the moss cover. Total projective cover of moss seldom exceeds 5%. The most stable and abundant ground cover component in floodplain deciduous forests is *Climacium dendroides*. Characteristic of plant and soil cover at studied plots is presented in **Table 1**. Alluvial soils formed in floodplain deciduous forests have a forest litter horizon. It is formed due to the low mineralization rate of plant residues. Plant residues total at Plot 1 and Plot 2 equals 3.5–4.0 t/ha and at Plot 3—2.0–2.5 t/ha. Forest litter thickness in soils of the study plots is 3–5 cm. The lowest values (2–3 cm) are fixed for spring-early

summer period and the highest ones (5–6 cm)—for autumn due to the production of fresh leaf residues. The presence of herbs with a well-developed root system responds to the formation of a prominent humus horizon (12–23 cm thick) under find 2 have two layers. Loose well-textured dark-brown loam subhorizon A' being 5–10 cm thick lies immediately after forest litter. It gets gradually replaced by subhorizon A'' (about 10 cm) which is light-coloured loam with crumble-powder texture. The lower soil part (30 cm from soil surface) at Plot 1 is sandy alluvial layer. The lower soil part (25 cm from soil surface) at Plot 2 is gley. It has rusty and dove-coloured spots against brown background. Soil gleysation is related with a close groundwater occurrence. Soil profile at Plot 3 was cut before the depth of 80 cm only because beginning with 75 cm, and downwards, it was actively impacted by soil-ground waters. Humus horizon A1 does not have two sublayers. It is as gley as low soil profile due to high ground water level which increases in direction from ridge top (Plot 1) to inter-ridge depression (Plot 3). Depth and intensity of soil warming decrease along the same direction (**Figure 2**).

Parameter	Plot 1	Plot 2	Plot 3
Plot location	ridge top	even part of floodplain	deep inter-ridge depression
Altitude of floodplain terrace	high level	mean level	low level
Microrelief	Not expressed	Slightly expressed	Tussocks up to 15–20 cm high
Level of groundwater	Deeper than 2.5 m	About 1.5 m	0.75 m
Vegetation community	Aspen-birch herb-stone brumble forest	Aspen-birch herb-stone brumble forest	Aspen-birch hair grass sedge forest
Stand composition	7Asp3Birch	8Birch2Asp	8Birch2Asp
Canopy density	0.9	0.8–0.9	0.8–0.9
Stand age	I layer—VI age class II layer—IV age class	I layer—VII age class II layer—IV age class	I layer—VII age class II layer—IV age class
Stand height	I layer—20–22 m II layer—14–18 m	I layer—20–22 m II layer—14–18 m	I layer—20–22 m II layer—14–18 m
Underbrush	9 species, <i>Sorbus</i>	8 species, <i>Sorbus aucuparia</i> is dominant	4 species, <i>Padus avium</i> is dominant



Parameter	Plot 1	Plot 2	Plot 3
	<i>aucuparia</i> and <i>Frangula alnus</i> are dominants		
Herb cover (TPC, %)	25 species, <i>Rubus saxatilis</i> is dominant (TPC 15–40%)	27 species, <i>Rubus saxatilis</i> is dominant, <i>Carex cespitosa</i> is also abundant (TPC 20–40%)	16 species, <i>Carex cespitosa</i> is dominant, <i>Galium palustre</i> , <i>Filipendula ulmaria</i> , <i>Mentha arvensis</i> , <i>Lysimachia vulgaris</i> and <i>Rubus arcticus</i> are also abundant (TPC 20–40%)
Moss cover (TPC, %)	It is not expressed	It is expressed weakly, <i>Climacium dendroides</i> is registered (TPC up to 3%)	It is expressed weakly, <i>Climacium dendroides</i> and <i>Calliergon</i> species are registered (TPC up to 10%)
Type of soil	Alluvial soddy layered soil on sandy alluvium	Alluvial meadow soil on clay alluvium	Alluvial meadow-boggy soil on clay alluvium
The structure of the soil profile	$A0^{0-3}A1^{3-20}$ $AB^{20-30}I^{30-80}$ $II^{80-100}$	$A0^{0-5}A1^{5-25}$ $ABg^{26-38}Bg^{38-100}$	$A0^{0-5}A1g^{5-16}ABg^{16-28}Bg^{28-46}G^{46-80}$

Note: TPC – total projective cover.

**Table 1.** Characteristics of vegetation and soils at studied plots in the Sysola River valley.

Soil mineral horizons at Plot 1 have favourable moisture conditions for soil organisms – 40–60% of total moisture capacity (TMC). But forest litter suffers from moisture deficiency for practically whole summer period. Forest litter moisture degree equals 20–40% of TMC in summer. Plot 2 has best moisture conditions (within 40–60% of TMC) in upper soil horizons only towards July. In the other summer months and in autumn, soil moisture degree is 60–80% of TMC. At Plot 3, soil is seriously overmoistured due to close ground water occurrence. Additionally, this plot is under water for a long period of time during spring snow-melt period. But towards in July, it also decreases in soil moisture content of forest litter to 40–60% of TMC. It resists 60–65% of TMC to the end of vegetation period. Lower mineral horizons remain overmoistured towards late autumn (80–90% of TMC). The study soils are acid, base-unsaturated with a strongly decreasing organic carbon profile distribution (**Table 2**). At 20–30-cm depth, organic carbon content was 0.5–0.9% and from 4.5–4.8 (Plot 1, Plot 2) to 3.0% (Plot 3) in humus horizon. In direction from Plot 1 to Plot 3, soil acidity in forest litter increases. In autumn, forest litter acidity in all soil types decreases due to fresh plant residues. Thus, there

is a clear trend of worsening in living conditions of tree waste decomposing soil biota going from Plot 1 to Plot 3. Ecological conditions of biotopes undergo serious changes in direction from ridge top to inter-ridge depression. These changes respond for differences in qualitative and quantitative composition of plant waste, intensity of its mineralization and humification processes, structure of soil humus horizons. Upper organic soil horizons of alluvial forest soils are highly unstable by moisture content and heat provision. They are the principle habitat for invertebrates. Even overmoistured (meadow-boggy) soils have favourable conditions for soil biota life activity some time during summer-autumn.

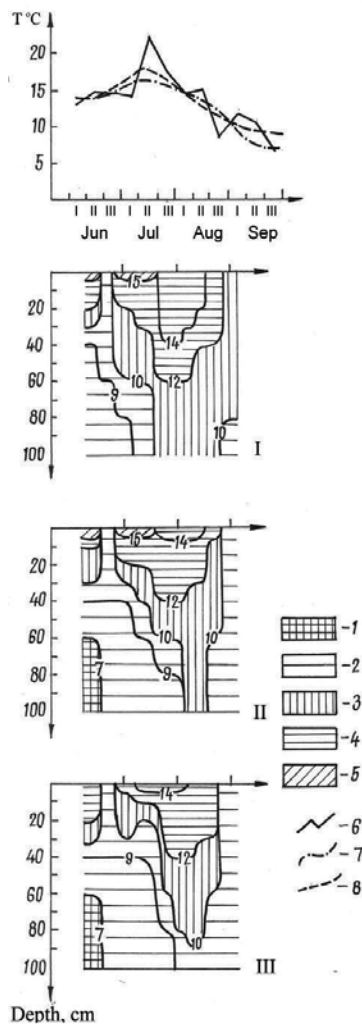


**Figure 2.** Temperature dynamics in alluvial forest soils of the Sysola River valley: I—alluvial soddy soil, II—alluvial meadow soil, III—alluvial meadow-boggy soil. Keys: 1 – <math>7^{\circ}\text{C}</math>; 2 –  $7\text{--}10^{\circ}\text{C}</math>; 3 –  $10\text{--}12^{\circ}\text{C}</math>; 4 –  $12\text{--}15^{\circ}\text{C}</math>; 5 –  $15\text{--}20^{\circ}\text{C}</math>; 6 – mean-decade air temperature (by data of 2003); 7 – mean-monthly long-time average annual air temperature; 8 – mean-monthly air temperature (by data of 2003).$$$$

Horizon	Depth, cm	pH <sub>KCl</sub>	Ha*	Exchangeable bases		S**	C	N	C/N	Sum of particles	
				Ca <sup>2+</sup>	Mg <sup>2+</sup>					<0.01 mm	<0.001 mm
				mmol/100 g soil						%	
Plot 1. Ridge top, alluvial soddy soil											
A0	0–3	4.8	27.5	30.6	5.0	56	21.7	1.5	14	–	–
A1	3–14	3.2	17.0	6.8	1.0	31	4.5	0.4	11	19	7
–“–	14–20	3.3	17.0	1.1	0.3	8	1.7	0.16	11	14	4
AB	20–30	3.6	7.4	0.6	0.2	10	0.5	0.04	13	16	6
I layer	30–50	3.6	6.5	0.9	0.3	15	0.2	–	–	0	0
Plot 2. Even floodplain part, alluvial meadow soil											
A0	0–3	4.8	25.0	40.9	8.1	66	38.9	2.2	18	–	–
A1	3–14	3.4	17.0	5.8	1.1	29	4.8	0.3	16	64	36
–“–	14–26	3.3	16.2	2.5	0.4	15	2.1	0.20	11	44	37
ABg	26–38	3.3	16.1	2.0	0.4	13	0.4	0.04	10	34	66
Bg	38–56	3.4	11.0	2.1	0.5	19	0.3	0.04	8	–	–
–“–	56–70	3.4	9.0	2.9	0.7	29	0.3	–	–	24	76
–“–	70–100	3.4	8.4	4.1	1.0	38	0.3	–	–	–	–
Plot 3. Deep inter-ridge depression, alluvial meadow-boggy soil											
A0	0–3	3.9	36.3	26.2	5.1	46	33.8	2.0	17	–	–
–“–	3–5	3.8	37.0	19.6	3.7	39	26.9	1.4	19	–	–
A1g	5–16	3.4	17.0	3.4	0.7	19	3.1	0.22	14	54	21
ABg	16–28	3.3	13.3	4.0	1.0	27	1.3	0.11	12	42	18
Bg	28–46	3.4	9.3	4.6	1.3	39	0.2	–	–	38	16
G	46–65	3.6	5.5	4.8	1.5	53	0.2	–	–	29	14
–“–	65–80	3.7	4.8	4.3	1.5	55	0.2	–	–	20	112

Note: «–» – not identified;

\* Ha – hydrolytic soil acidity;

\*\* S – base saturation by hydrolytic acidity:  $S(\%) = \frac{\sum (Ca^{2+} + Mg^{2+})}{\sum (Ha + Ca^{2+} + Mg^{2+})} \cdot 100$ .

**Table 2.** Physical-chemical properties of alluvial soils under floodplain deciduous forest.

#### 4. Diversity and structure of microbe communities in the alluvial forest soils

Microbe communities of alluvial soils differ from those of watershed soils [12] because of inundation of floodplain terrace and covering the surface of floodplain terrace with alluvial deposits [15]. Floodplain forest soils have a short bacterial profile. Bacteria are available within

upper 60–70 cm at Plot 2 and Plot 3. Single colonies were identified at a depth of 100 cm at Plot 1. In direction from Plot 1 to Plot 3, oligonitrophilous and denitrifying microorganisms become abundant. Nitrifying, ammonifiers and bacteria using mineral nitrogen compounds strongly decrease in number at Plot 3 (Figure 3). This normally proceeds in soils formed in conditions of excessive moisture content. Oligonitrophilous and oligotrophic microorganisms dominate at Plots 2 and 3 in the beginning of vegetation period. Ammonifiers, nitrifiers, denitrifiers, assimilators of mineral nitrogen compounds become abundant in July and towards the end of vegetation period. Their number and ratio significantly vary depending on soils type and weather conditions. When weather conditions are unfavourable (chilly weather with excessive rain precipitations), bacterial communities are presented by oligonitroflora. Unusually, warm weather with insufficient rain precipitations activates ammonifiers, assimilators of mineral nitrogen compounds and nitrifiers. Normally this increase in bacterial number also occurs in autumn when soil surface gets covered with plant waste products which decrease forest litter acidity. Microbial biomass carbon content in alluvial soils largely varies (Figure 4). Hydromorphic soils (Plot 2 and Plot 3) normally contain more microbe biomass carbon than automorphic soils (Plot 1). This situation is especially obvious in August and September when microbe communities in these soil types are highly active.

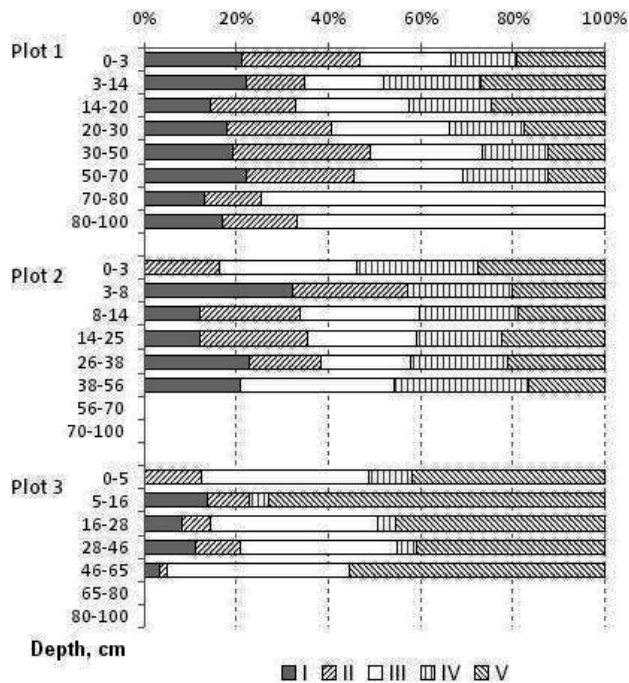


**Figure 3.** Profile distribution of ecologic-trophic bacterial groups in alluvial forest soils of the Sysola River valley. Microorganisms: I—on beef-peptone agar (ammonifiers); II—on starch-ammonia agar; III—on Aeshbi's medium (oligonitrophilous); IV—on Vinogradsky's medium (nitrifying microorganisms); V—on Giltai's medium (denitrifying microorganisms).

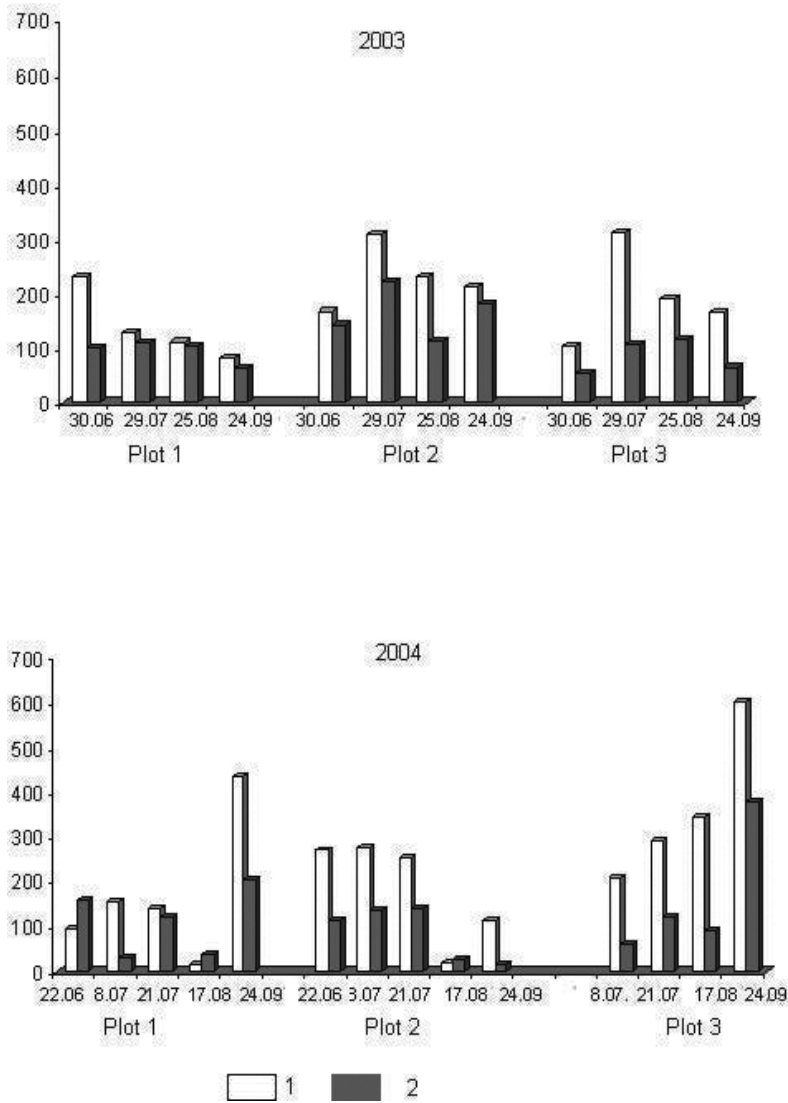


**Figure 4.** Microbial biomass carbon dynamics (mg C<sub>MB</sub> per 100 g of dry soil) in alluvial forest soils of the Sysola River valley.

## 5. Micromycetes activity in the alluvial forest soils

Micromycetes are the first inhabitants of plant waste products in forests [34, 35]. Soils of coniferous forests are rich in both microscopic and basidial fungi; their mycelium largely permeates forest litter [36]. Seventy-three species of micromycetes (including sterile forms) of 18 genera inhabit soils under spruce forests on watersheds of the Sysola and the Vychegda Rivers [22]. Leaf waste of birch-aspen forests differs from that of spruce and pine forests by

chemical composition and contains by 1.5–2 times more mineral elements as calcium, magnesium and nitrogen than pine or spruce needles [37]. So, deciduous leaf waste presents a well decomposition object for bacteria. Our data showed that floodplain forest soils have 70 species of micromycetes. But taxonomic diversity of microscopic fungi is truly higher in floodplain soils (31 genera). Practically, one half of micromycetes in floodplain forest soils (25 species) are species which were previously identified neither in taiga forest soils [36], nor in floodplain meadow soils of the middle taiga zone [38]. They are species of the *Penicillium* (*P. glaucogriseum*, *P. lapidosum*, *P. sclerotiorum*), *Paecilomyces* (*P. farinosus*, *P. carneus*, *P. variotii*), and *Trichoderma* (*T. reesei*, *T. longbrachiatum*, *T. crassumbissett*) genera, *Aureobasidium pullulans*, *Mycogone pernicioso*, *Monosporium silvaticum*, *Trichosporium fulvum*, *Geomyces pannorum*, *Botrytis pyramidalis*, *Alternaria alternate*, non-identified species of the *Coretropsis*, *Gliocladium*, *Circinella*, *Mycogone*, *Rhinochadiopsis*, *Rhizopus*, *Scopulariopsis*, *Phycomyces* genera. The genera of *Penicillium* (17 species), *Trichoderma* (7), *Chaetomium* (5) and *Paecilomyces* (4) are characterised by high species diversity in alluvial forest soils. The *Mucor*, *Cladosporium* and *Umbelopsis* genera count three species each, *Mycogone*, *Alternaria* and *Aureobasidium* — two, and the other genera — one species each. Spruce forest soils are characterised by high diversity of *Penicillium* genera (25 species), the constant presence of representatives of *Mucor* and *Trichoderma* genera, and domination of *Chaetomium* species [36]. *Trichoderma sympodianum*, *Umbelopsis vinacea*, *U. isabellina*, *U. ramanniana*, *Mucor racemosus*, *Chaetomium globosum*, *Ch. spirale*, *Geomyces pannorum*, as well as non-identified species of the *Mucor*, *Paecilomyces* and *Penicillium* genera are met in alluvial forest soils. Totally, there are 13 common species, including two sterile mycelium forms. In contrast to floodplain meadows [38], mycobiota taxonomic structure in floodplain forests is better represented (71 species of 22 genera). Micromycetes which inhabit only particular alluvial forest soils are characterized by the following features. Plant waste decomposition at Plots 2 and 3 is fulfilled by *Alternaria tenuis*, *A. alternata*, *Fusarium sp.*, *Paecilomyces farinosus*, *Trichoderma reesei*, at Plot 1 — *T. crassum*, *Chaetomium spiraliformum*, *Cladosporium potebniae*, *Gliocladium sp.*, *Mycogone sp.*, *Penicillium nigricans*, *Trichoderma koningii*. On the whole, microscopic fungi in alluvial forests soils form a specific complex: the Ics index is less than 50%. With increasing of soil moisture content in floodplain forest soils, number of micromycetes in forest litter (A0) and in mineral humus horizons (A1) becomes similar.

## 6. Communities structure and diversity of nematodes in the alluvial forest soils

Soil nematodes of the alluvial soils include 53 genera of 30 families. Number of nematodes varies between 635 inds./100 cm<sup>3</sup> (Plot 3) and 1105 inds./100 cm<sup>3</sup> (Plot 1). Diversity of nematodes in the floodplain forests is higher than that in non-flooded spruce (35) and pine forests (31 genera) in the study region (not-published data). Number of nematodes in the alluvial soils is also a little bit higher than that under watershed forests. It is 55–239 inds./100 cm<sup>3</sup> in pine forests [23] and 300 inds./100 cm<sup>3</sup> in deciduous forests. The greatest number of genera is found for soil at Plot 2 — 42 genera and the lowest one is noted for soil at Plot 3 — 32 genera (Table 3). Plot 3

is characterized by lowest diversity of nematodes. It is probably explained by unfavourable life conditions (overmoisture) for them. Excessive moisture of soil results into its poor aeration and reduction of qualitative and quantitative vegetation composition. Consequently, the taxonomic similarity of nematodes at the study plots is not high and it is equalled about 60%. Along with low diversity of nematodes, the rising of predomination of single taxa in soils of plot 3 is observed. All studied soils are characterized by high proportion of the *Filenchus* and *Eudorylaimus* genera. Soil at Plot 1 also has high relative abundance of *Plectus*, *Aphelenchoides*, *Acrobeloides* genera, soil at Plot 2—representatives of *Plectus*, *Teratocephalus*, *Metateratocephalus*, *Aphelenchoides*, *Alaimus* genera, and overmoistured soil at Plot 3—*Dorylaimus* representatives. Abundant genera of nematodes at Plot 1 and Plot 2 are typical for boreal ecosystems [39]. Ratio of dominants at Plot 3 is differed which seems to be related to overmoisture. Nematodes in studied soils belong to six trophic groups. Bacterivores nematodes are abundant at Plot 1 and Plot 2 (Figure 5). It is typical situation for different habitats [40]. Nematodes at Plot 3 are mainly omnivores. High soil moisture content at Plot 3 leads to massive reproduction of the hydrophilous and omnivores *Dorylaimus* genera.

Genera, parameter	Studied soils		
	Plot 1	Plot 2	Plot 3
<i>Filenchus</i>	21.0	17.0	7.0
<i>Eudorylaimus</i>	11.4	15.0	9.0
<i>Plectus</i>	9.6	6.0	3.7
<i>Metateratocephalus</i>	3.4	6.0	2.6
<i>Teratocephalus</i>	3.7	5.1	<1
<i>Aphelenchoides</i>	16.0	12.0	4.3
<i>Dorylaimus</i>	–	<1	52.9
<i>Acrobeloides</i>	5.1	2.0	2.9
<i>Alaimus</i>	4.3	5.8	1.0
Others	25.5	31.1	17.6
Number of genera	39	42	32
Density (inds./100 cm <sup>3</sup> )	1105 ± 185	745 ± 94	635 ± 90
Shannon diversity index (H')	2.30 ± 0.12	2.63 ± 0.13	1.93 ± 0.34
Simpson's index of dominance (DSM)	0.15 ± 0.03	0.12 ± 0.03	0.29 ± 0.12

Note: Table contains genera with relative abundance >5% at least at one plot.

Note: Values of abundance and index are mean ± SE, n=7.

**Table 3.** Characteristics of nematodes population in alluvial forest soils.

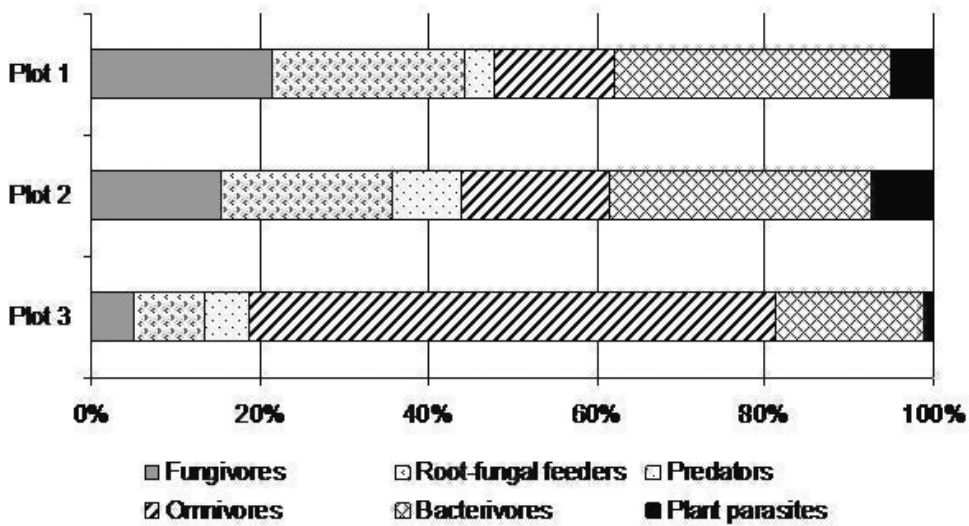


**Figure 5.** Trophic structure (ratio of group abundance) of nematodes communities in alluvial soils of the Sysola River valley: Plot 1—alluvial soddy soil, Plot 2—alluvial meadow soil, Plot 3—alluvial meadow-boggy soil.

## 7. Diversity and structure of Collembola in the alluvial soils

Collembola of floodplain communities in the taiga zone of the European part of Russia are understudied in comparison with coniferous forests on watersheds. For example, 65 Collembola species are registered in the floodplain ecosystems of the Komi Republic [11] whereas 173 species are noted in the coniferous forests of the European part of Russia [24]. The greatest number of species and stenobionts (species which exist only in particular habitats) are found at Plots 1 and 3 (Table 4). It is confirmed by the Shannon indices (2.70–2.94) that indicate their high taxonomic diversity. It is noticed that *Agrenia riparia* and *Ptenothrix atra* inhabit only Plot 1, whereas *Mesaphorura krausbaueri*, *Stenaphorura quadrispina*, *Brachystomella parvula*, *Folsomia kuznetsovae*, *Isotomurus fucicolus*, *Marisotoma tenuicornis* inhabit only Plot 3. Collembola groups of alluvial soils are quite similar by species composition, as widely distributed species form the basis of their communities. Springtails communities in alluvial forest soils have the same dominant species as in coniferous forests [24]. *Isotomiella minor* is typical species for boreal zone of the European part of Russia. *F. quadrioculata* prefers moist soils in Central Europe [41], but it is not met at moist forests of East Europe [42]. *Folsomia kuznetsovae* prefers moist and oligotrophic habitats [43]. It is revealed that soil moisture degree decreases number of epigeic species and increases ratio of euedaphic forms. Complexes of hemi- and euedaphic species are not much change from year to year and so form a stable part of Collembola group whereas epigeic species are most mobile in alluvial forest soils [9]. Collembola occupy upper soil horizons with high organic matter content and they are not found at depths under 20 cm from soil surface [10]. The population density of springtails varies during vegetation period and



observation years [9]. Average density of Collembola in alluvial soils is low, but it can reach 100 thous. inds./m<sup>2</sup> at some sampling terms and so significantly exceed that parameter in zonal communities. The highest population density of springtails is registered for Plot 2 (37.5 thous. inds./m<sup>2</sup>). It is 24.3 and 21.8 thous. inds./m<sup>2</sup> for Plots 3 and 1, correspondingly.

Species, parameter	Plot 1	Plot 2	Plot 3
<i>Folsomia quadrioculata</i>	41.7	59.2	24.3
<i>Isotomiella minor</i>	11.8	15.3	40.9
<i>Folsomia fimetarioides</i>	7.2	9.4	10.7
<i>Protaphorura boedvarrsoni</i>	3.5	5.5	<1
<i>Ceratophysella denticulata</i>	5.5	1.2	1.3
<i>Friesea mirabilis</i>	<1	<1	2.2
<i>Anurida ellipsoides</i>	<1	<1	5.7
<i>Folsomia kuznetsovae</i>	-	-	4.6
<i>Xenyllodes armatus</i>	6.8	<1	<1
<i>Folsomia manolachei</i>	3.1	<1	3.5
<i>Supraphorura fucifera</i>	1.5	1.4	<1
Total number of individuals	21,574	13,642	8248
Total number of species (S)	45	35	39
Shannon diversity index (H')	2.94	2.14	2.70
Shannon evenness index (J')	0.48	0.41	0.51

Note: Table contains species with relative abundance (%).

**Table 4.** Characteristics of Collembola population in alluvial forest soils.

## 8. Diversity and structure of soil macrofauna in the alluvial soils

Macrofauna of alluvial soils has a rich species composition (**Table 5**). Invertebrates in floodplain soils inhabit only the upper 30-cm soil layer. About 80% of large invertebrates occupy the upper 0–10-cm soil layer. Under the mark of 20 cm, there are only single individuals of earthworms [5]. Six species of Lumbricidae are registered in alluvial soils. *Octolasion lacteum* is dominant at Plot 3. It has high hemoglobin content in blood, so it inhabits badly aerating soils [6]. When litter became dry, soil at Plot 3 is inhabited by *Lumbricus rubellus*. Earthworms at Plot 2 are presented by *L. rubellus*, *Eisenia nordenskioldi*, *Dendrobaena octaedra*, *Aporrectodea*

Taxa	Plot 1	Plot 2	Plot 3
Gastropoda	+	+	+
Lumbricidae	4	6	2
Lithobiidae	1	1	1
Polyzoniidae	1	1	–
Carabidae, imago	31	33	16
Halyplidae, imago	1	1	–
Dytiscidae, imago	3	3	2
Silphidae, imago	2	1	–
Staphylinidae, imago	38	32	8
Scarabaeidae, imago	1	–	–
Cantharidae, imago	1	1	–
Elateridae, imago	12	8	1
Hymenoptera, larvae	+	+	–
Lepidoptera, larvae	+	+	–
Diptera, larvae	+	+	+
Aranei	+	+	+
Pseudoscorpiones	+	+	–
Total number of taxa	17	16	9
Total number of species	95	87	30

Note: «+» – taxa found, «–» – taxa not found.

**Table 5.** Taxonomical composition (species number) of soil macrofauna in alluvial forest soils.

*caliginosa*, *A. rosea*, *O. lacteum*. The abundant species of Lumbricidae at Plot 1 are *E. nordenskioldi*, *D. octaedra*, *L. rubellus*. These species inhabit litter of moist forests and clear cut areas. *A. caliginosa* is eurybiotic species, but it is seldom met at Plot 1. It prefers middle soil horizons with average soil moisture degree, and it can sink into anabiosis to survive in unfavourable conditions. The above distribution of Lumbricidae species by soil types is confirmed in literature [44]. The list of species can be considered complete because 12 Lumbricidae species were registered for periodically inundated beech forests in Germany [20]. Reduction in species diversity and number of Lumbricidae in inundated forests occurs regularly due to summer floods, not due to spring snow-melt floods [45]. Taxonomic composition of Myriapoda in alluvial soils is not as rich as in Central Europe. For example, 12 species of the *Lithobius*, *Geophilus*, *Strigamia* and *Schendyla* genera are found in different-aged (3, 30, and 80 years old) floodplain Czech forests [46]. Only two species *Lithobius curtipes* and *Polyzonium germanicum* are registered in studied soils. Spring, autumn, and summer floods greatly impact population structure of Myriapoda [18]. *Polyzonium germanicum* which is badly represented in floodplain forests and *Lithobius curtipes* which is abundant in long-inundated forests do best survive under water, for about 688.2 and 126.3 h, respectively [47]. The diversity of ground beetles (Carabidae) in alluvial forest soils is high. In compare, 28 Carabidae species were found in the floodplain of the Dnepr River middle course [5] and 42 Carabidae species were registered in the Czech floodplain forests [46]. *Carabus granulatus*, *Pterostichus oblongopunctatus*, *Pt. melanarius*, *Agonum fuliginosum*, *Amara brunnea* are often met in alluvial forest soils. The revealed

distribution of Carabidae at plots corresponds with species distribution in forest soils of the middle taiga. The abundant species (*C. granulatus*, *Pt. oblongopunctatus*, *A. brunnea*) in alluvial soils of Plots 1 and 2 are the same. *Elaphrus cupreus* is dominant at Plot 3. The high predominance of Carabidae community is noted at Plot 1, as high species richness and diversity is characterized for Plot 2 (Table 6). The species similarity of Carabidae communities in alluvial soils comprises over 60%. But ground beetles communities of Plots 1 and 2 show the highest similarity degree (about 75%). Ecological conditions at Plots 1 and 2 are equally favourable for Carabidae independently of soil type. The beetles can actively move and so look for better habitats. Rove beetles (Staphylinidae) are characterized by high species diversity in alluvial forest soils. The genera *Philonthus*, *Quedius*, *Tachyporus*, *Tachinus* and *Atheta* are abundant in floodplain forests. In autumn, alluvial soils are inhabited by *Arpedium* and *Omalium* genera which are best resistant to low temperatures. Staphylinidae communities at Plots 1 and 2 have a high species similarity (70%). But the absence of such similarity is noted for elevated Plots 1, 2 and Plot 3 (only 35%). The high diversity of rove beetles is characterized for Plots 1 and 2, but domination indices are extremely low (Table 6). Click beetles (Elateridae) in alluvial soils count 13 species, that is 25% of total fauna in the European North-East of Russia. The majority

Species, parameter	Plot 1	Plot 2	Plot 3
<b>Carabidae</b>			
<i>Carabus granulatus</i>	<b>21.6</b>	7.5	<b>26.5</b>
<i>Patrobus assimilis</i>	1.6	<b>17.8</b>	1.6
<i>Pterostichus oblongopunctatus</i>	<b>27</b>	<b>13.4</b>	1.6
<i>Amara brunnea</i>	6.5	<b>10.5</b>	2.2
<i>Elaphrus cupreus</i>	2.4	2.8	<b>15</b>
Shannon diversity index (H')	3.50	4.38	3.84
Shannon evenness index (J')	0.69	0.86	0.74
Simpson's index of dominance (D <sub>SM</sub> )	0.16	0.07	0.12
<b>Staphylinidae</b>			
<i>Geostiba circellaris</i>	<b>15.1</b>	2.4	<b>15</b>
<i>Atheta graminicola</i>	8.5	8.5	<b>27.5</b>
<i>Stenus flavipalpis</i>	-	-	<b>25</b>
Shannon diversity index (H')	4.55	4.72	2.58
Shannon evenness index (J')	0.87	0.94	0.86
Simpson's index of dominance (D <sub>SM</sub> )	0.06	0.03	0.18
<b>Elateridae</b>			
<i>Selatosomus impressus</i>	<b>27.2</b>	<b>38.7</b>	3.2
<i>Agriotes obscurus</i>	<b>20.4</b>	-	-
<i>Dalopius marginatus</i>	<b>18.4</b>	<b>11.9</b>	-
Shannon diversity index (H')	2.95	2.64	-
Shannon evenness index (J')	0.82	0.88	-
Simpson's index of dominance (D <sub>SM</sub> )	0.16	0.20	-

Note: Table contains species with relative abundance (%), «-» – species not found; bold indicates high domination degree.

**Table 6.** Characteristics of soil macrofauna in alluvial forest soils.

of species (4) belong to the *Selatosomus* genera. Larvae of click beetles prefer alluvial soddy soils. Abundant species are *Dalopius marginatus*, *Agriotes obscurus* and *Selatosomus impressus*. *S. impressus* is ecologically tolerant species, but it became abundant in alluvial meadow and meadow-boggy soils only at the warmest season, that is in July. The species similarity comprises 65% for Plots 1 and 2. But species richness is higher at Plot 2 (Table 6).

## 9. The impact of ecological conditions of the alluvial soils on soil biota

Deciduous birch and aspen forests in river floodplains cause development of specific biotopes. They, in turn, affect soil cover formation, species composition of plants, soil microorganisms, meso- and macro- fauna. But very similar floristic composition of plant communities within one series of floodplain forests evidences different tree species be not as pronounced edificators in specific floodplain ecotope conditions as those on watersheds. Ecological conditions considerably affect taxonomic diversity and number of biota in alluvial forest soils. The highest number of species and genera of micromycetes was found in alluvial meadow soil (Plot 2). Soil of this plot takes a transitional position between alluvial soddy soil (Plot 1) and alluvial meadow-boggy soil (Plot 3). It is well moistured, not extremely dry or moist. The large number of micromycetes species is found in alluvial soddy soil with moisture deficiency. The lowest number of species is found in alluvial meadow-boggy soil. Generally, complex of microscopic fungi is specific for each soil type. Taxonomic diversity of microscopic fungi in floodplain forest soils is higher than that in floodplain meadow and coniferous forest soils of the taiga zone. Nevertheless, species composition is practically the same. High taxonomic diversity of microscopic fungi in floodplain forests of the North could be conditioned by specific plant waste. Plant waste in spruce forests is homogenous and consists of moss and needle residues, so it has a specific biochemical composition and it is decomposed mainly by *Penicillium*. Taxonomic diversity of fungi in floodplain meadow soils is a bit higher (22 genera of micromycetes) possibly due to diverse plant waste (meadow grasses). Taxonomic diversity of fungi in floodplain forest soils is the highest (31 genera). Apparently, plant residues in floodplain forests is more diverse by chemical composition as consists of tree (aspen and birch) leaves, underbrush (mountain ash, dog rose, honeysuckle) leaves, dead grasses and branches. High taxonomic diversity of nematodes is revealed in alluvial meadow forest soil (Plot 2). Changes in nematode communities which happen at deviation from the ecological optimum (in alluvial soils of inter-ridge depression) fully correspond with the biocenotic principles on ratio between diversity and number of specimens in natural ecosystems. Collembola communities in floodplain forests occupy soil litter (which is typical of zonal communities) and differ by dominants and vital forms. Structure of such communities has a wide number of potential dominants, on one hand, and a high share of rare species, on the other. Due to this fact, high species diversity of Collembola is noted in alluvial soils of relief elevations (Plot 1) and depressions (Plot 3). In spite of low species richness of Collembola in floodplain ecosystems (relatively to zonal taiga communities), they do significantly contribute to biodiversity conservation of Collembola on the North [11]. Macrofauna in alluvial forest soils counts 17 taxa. Among them, Lumbricidae include six species, Myriapoda—two species, Carabidae—

40, Staphylinidae—49, Elateridae—13 species. High taxonomic diversity of macrofauna is revealed in alluvial soddy forest soil (Plot 1). But soil invertebrates can essentially increase taxonomic and species diversity in alluvial meadow-boggy soil (Plot 3) at warming autumn. This happens due to available fresh plant waste, low ground waters level, low moisture degree of upper soil horizons and, consequently, formation of appropriate ecological conditions for both soil fauna and microbiota [10]. High number and functional activity of bacteria at Plots 2 and 3 along with high number of meso- and macro-fauna leads to active mineralization of forest litter not only in alluvial soddy soils but also in alluvial meadow-boggy soils at inter-ridge depressions in the second half of vegetation period. For this reason, forest floodplain soils at deep inter-ridge depressions do not accumulate plant residues as a thick litter peaty layer like soils on watersheds. The obtained results well correspond with the idea about high biogenic potential of floodplain soils [48, 49]. Floodplain forests and wetlands are amongst the most diverse and species rich habitats on earth as the changing moisture conditions result in a wide variety of ecological niches. The banks of rivers and floodplains are in a permanent transformation. Many wetland areas in river valleys are 'biodiversity hotspots' containing high density of soil biota taxa [2, 14].

## 10. Conclusion

For the first time, we conducted a comprehensive study on major components of floodplain forests for middle taiga territory of European north-eastern Russia. Alluvial soils were shown to distinguish by ecological habitat conditions, particularly ridge top, levelled floodplain part and deep inter-ridge depression. Soils formed on different parts of floodplain terrace were revealed for different taxonomic composition of microorganisms, meso- and macro-fauna. Floodplain forest soils of the middle taiga subzone are inhabited 70 species from 31 genera of micromycetes, 53 genera from 30 families of nematodes, 60 species from 39 genera and 13 families of Collembola, 110 species from 17 taxa of large invertebrates. Alluvial meadow soils with stable moisture and temperature conditions are most diverse by species composition of micromycetes, nematodes, and large invertebrates. Springtails prefer alluvial soddy soils. Towards the end of vegetation period, every alluvial soil type increases in number of bacteria, microscopic fungi, and soil invertebrates in forest litter and becomes inhabited by new species. This is related with fresh plant waste and appropriate moisture conditions. So, fresh plant residues is actively transformed at this period not only in soils at elevated places (with favourable water-air regime at whole vegetation period) but also in overmoistured soils at inter-ridge depressions. Alluvial soils under floodplain forests in the European North-East of Russia are habitats with a high life density. In contrast with soils under coniferous forests on watersheds, alluvial soils in river valleys have a high taxonomic diversity of soil biota. Floodplain forest soils are habitats for rare species which cannot be met in soils under coniferous forests. As result of our research, 29 species of Collembola were noted at first for the Komi Republic, 2 species of Collembola were identified as new for science [11], 2 rare species of large invertebrates were included in the Red List of Komi Republic. The obtained data on quantitative and qualitative composition of micromycetes, nematodes, springtails and

large invertebrates can be used for assessment of spatial-temporal changes of floodplain soils under anthropogenic impacts.

## Acknowledgements

The research was financially supported by the UrD RAS Presidium Program 'Scientific Biodiversity Conservation Bases in Russia' (projects: 'Environmental Functions of Alluvial Soils and Biodiversity Formation of Floodplain Landscapes in the European North-East of Russia', 'Identification of Biodiversity Formation Mechanisms, Interdependences of Macro- and Microorganisms and their Role in Organic Matter Transformation in Soils of Floodplain Forests in the European North-East of Russia', 'The relationship of biodiversity and biological production potential of the terrestrial ecosystems of the European Arctic with the peculiarities of formation of permafrost soils and dynamic aspects of their transformation in the modern climate conditions', 'The diversity of plant and soil cover on the UNESCO World Heritage area "Virgin forests of Komi republic)', the Grants of the Government of the Komi Republic and the RFBR (09-04-98808 r\_sever\_a) 'Animal Population in Soils of Floodplain Ecosystems of the European North', (16-44-110989 r\_a) The creation of an information system "Soil fauna of Komi Republic".

## Author details

Alla Kolesnikova\*, Elena Lapteva, Svetlana Degteva, Anastasia Taskaeva, Alexey Kudrin, Yulia Vinogradova and Fluza Khabibullina

\*Address all correspondence to: kolesnikova@ib.komisc.ru

Institute of Biology, Komi Science Centre, Ural Department of Russian Academy of Sciences, Syktyvkar, Russia

## References

- [1] Batzer, D., Boix, D. (Eds.). Invertebrates in freshwater wetlands. An International Perspective on Their Ecology. New York, Dordrecht, London: Springer International Publishing Switzerland, 2016. 645 pp.
- [2] Dobrovoljskij, G.V. Soils of river floodplains in the central part of Russian Plane. Moskow, 1968. 298 p (In Russia).

- [3] Kryshstal, A.F. To study of soil and litter entomofauna dynamics in connection with the flood in the Dnepr river valley. *Entomological Review*, 1955. Vol. 34. No. 1. P. 120–139 (in Russia).
- [4] Geltser, Yu. A. About soil fauna in the Kljasjma River floodplain. *Floodplain Soils of Russian Plane*, M., 1963. Vol. 2. P. 141–145 (In Russia).
- [5] Striganova, B.R. Soil invertebrate complexes in the Dnestr River floodplain. *Entomological Review*, 1968. Vol. 47. No. 3. P. 360–368 (in Russia).
- [6] Perel, T.S. Differences of Lumbricidae organisation with their ecological features. *Adaptation of Soil Invertebrates to Environment Conditions*. M., 1977. P. 129–145 (In Russia).
- [7] Lessel, T., Marx, M.T., Eisenbeis, G. Effects of ecological flooding on the temporal and spatial dynamics of carabid beetles (Coleoptera: Carabidae) and springtails (Collembola) in a polder habitat. *ZooKeys*, 2011. Vol. 100. P. 421–446.
- [8] Busmachi, G. Collembola (Hexapoda) from the riparian habitats of the Dniester River. *Muzeul Olteniei, Craiova. Studii si comunicări. Stiintele Naturii.*, 2011. Vol. 27. No. 1. P. 63–70.
- [9] Taskaeva, A.A., Lapteva, E.M. The dynamics of Collembola communities in middle-taiga flood plain forests. *Povolzhsky ekologichesky zhurnal*, 2012. No. 4. P. 426–436 (In Russia).
- [10] Kolesnikova, A.A, Taskaeva, A.A., Lapteva, E. M., Degteva, S.V. Vertical distribution of Collembola, Lumbricidae and Elateridae in alluvial soils of floodplain forests. *Contemporary Problems of Ecology*, 2013. Vol. 6. No. 1. P. 34–42.
- [11] Taskaeva, A.A. Springtails (Collembola) assemblages in floodlands of the taiga zone of the Republic of Komi. *Entomological Review*, 2009. Vol. 89. No. 8. P. 965–974.
- [12] Golovchenko, A., Dobrovo'skaya, N. Population density and the reserves of microorganisms in floodplain soils of the protva river. *Eurasian Soil Science*. 2001. Vol. 34, No. 12. P. 1300–1304.
- [13] Russell, D., Hauth, A., Fox, O. Community dynamics of soil Collembola in ains of the Upper Rhine Valley. *Pedobiologia*. 2004. Vol. 48. No. 5–6. P. 527–536.
- [14] Sterzyńska, M. Assemblages of soil Collembola in wetlands in the floodplains of some Polish rivers. *Museum and Institute of Zoology PAS, Warszawa*. 2009. 96 pp.
- [15] Leontieva, M.V., Dobrovol'skaya, T.G., Pochatkova, T.N. Influence of flooding regime on the taxonomic structure of soil bacterial communities. *Bulletin of Moscow University. 17: Soil*. 2005. No. 1. P. 36–40 (in Russia).
- [16] Sterzyńska, M., Pižl, V., Tajovský, K., Stelmaszczyk, M., Okruszko, T. Soil fauna of peat-forming wetlands in a natural river floodplain. *Wetlands*. 2015. doi:10.1007/s13157-015-0672-0.

- [17] Russell, D., Schick, H., Nahrig, D. Reactions of soil Collembola communities to inundation in floodplain ecosystems of the Upper Rhine Valley. Broll, G., Merbach, W., Pfeiffer, E.-M. (Eds.). *Wetlands in Central Europe: Soil Organisms, Soil Ecological Processes and Trace Gas Emissions*. Görlitz: Springer, 2002. P. 35–70.
- [18] Tuf, I.H. Four-year development of a centipede (Chilopoda) community after a summer flood. *African Invertebrates*. 2003. Vol. 44. P. 265–276.
- [19] Adis, J., Junk, W. Terrestrial invertebrates inhabiting lowerland river floodplains of Central Amazonia and Central Europe: a review. *Freshwater Biology*. 2002. Vol. 47. P. 711–731.
- [20] Kuhle, J.C. Spatial patterns of distribution of earthworms in a hardwood floodplain forest. Pizl V., Tajovsky K. (Eds.). *Soil Zoological Problems in Central Europe*. Ceske Budejovice, 1998. P. 125–134.
- [21] Degteva, S.V. Parameters of ecological space and floristic diversity of forest formations in the northeast of European Russia. *Russian Journal of Ecology*, 2005. I. 36. No. 3. P. 158–163.
- [22] Khabibullina, F.M., Kuznetsova, E.G., Vaseneva, I.Z. Micromycetes in podzolic and bog-podzolic soils in the middle taiga subzone of northeastern European Russia. *Eurasian Soil Science*. 2014. Vol. 47. No. 10. P. 1027–1032.
- [23] Kudrin, A.A., Dolgin, M.M., Kolesnikova, A.A., Konakova, T.N., Taskaeva, A.A. Spatial distribution features of soils fauna in fine forests of the north taiga subzone (Komi Republic). *Bulletin of the North (Arctic) Federal University. Series: Natural Sciences*. 2014. No. 1. P. 72–83 (in Russia).
- [24] Kuznetsova, N.A. *Organization of springtails communities*. M., 2005. 244 p (in Russia).
- [25] Vorobyov, L.A. (Eds.). *M. Theory and practice of chemical analysis of soils*. GEOS Publicity 2006. 400 p (in Russia).
- [26] Vadyunina, A.F., Korchagina, Z.A. *The study methods of soil and ground physical properties*. M.: Vyssh.shkola, 1986. 345 p (in Russia).
- [27] *Classification and diagnostics of the USSR soils*. M.: Kolos, 1977. 224 p (in Russia).
- [28] Zvyagintsev, D.G. *Methods of Soil Microbiology and Biochemistry*. M.: MGU Publicity 1991. 304 p (in Russia).
- [29] Blagodatskiy, S.A., Blagodatskaya, E.V., Gorbenko, A.Y., Panikov, N.S. A re-hydration method of determining the biomass of microorganisms in soil. *Pochvovedenie* (Russian J. Soil Science). 1987. No. 19. P. 119–126 (in Russia).
- [30] Jairajpuri, M.S., Ahmad, W., Dorylaimida. *Free-living, Predaceous and Plant Parasitic Nematodes*. E.J. Brill, Leiden, 1992. 458 p.



- [31] Bongers, T., De nematoden van Nederland. Nederlandse Natuurhistorische Vereniging. Utrecht, The Netherlands, 194. 408 p.
- [32] Brzeski, M.W. Nematodes of Tylenchina in Poland and Temperate Europe. Muz. Inst. Zool. PAN. Warszawa, 1998. 397 p.
- [33] Yeates, G.W., Bongers, T., de Goede, R.G., Freckman, D.W., Georgieva, S.S. Feeding habits in soil nematode families and genera e an outline for soil ecologists. *Journal of Nematology*. 1993. Vol. 25. P. 315–331.
- [34] Dobrovol'skaya, T., Zvyagintsev, D., Chernov, I., et al. The role of microorganisms in the ecological functions of soils. *Eurasian Soil Science*. 2015. Vol. 48, No. 9. P. 959–967.
- [35] Berg, M.P., Kniese, J.P., Verhoef, H.A., Dynamics and stratification of bacteria and fungi in the organic layers of a scots pine forest soil. *Biol. Fert. Soils*. 1998. Vol. 26. P. 313–322.
- [36] Lindahl, B.D., Ihrmark, K., Boberg, J., Trumbore, S.E., Högberg, P., Stenlid, Ja., Finlay R.D. Spatial separation of litter decomposition and mycorrhizal nitrogen uptake in a boreal forest. *New Phytologist*, 2007. 173 pp.
- [37] Berger, T.W. Auswirkungen der Baumartenzusammensetzung auf den Waldbodenzustand von sekundären Fichtenwäldern und gemischten Fichten-Buchenbeständen. *Centralbl. Gesamte Forstw.* 2001. 118, No. 4. P. 193–215.
- [38] Lapteva, E.M., Khabibullina, F.M., Vinogradova, Yu. A. Diversity of micromycetes in flood plain meadow soils. *Mycology and Phytopathology J.*, 2009. Vol. 43. Issue 3. P. 200–206 (in Russia).
- [39] Sohlenius, B. Influence of clear-cutting and forest age on the nematode fauna in a Swedish pine forest soil. *Applied Soil Ecology*. 2002. Vol. 19. P. 261–277.
- [40] Zhao, J., Neher, D.A. Soil energy pathways of different ecosystems using nematode trophic group analysis: a meta analysis. *Nematology*. 2014. Vol. 16. No. 4. P. 379–385.
- [41] Raschmanová, N., Kováč, L., Miklisová, D. The effect of mesoclimate on Collembola diversity in the Zádiel Valley, Slovak Karst (Slovakia). *European Journal of Soil Biology*. 2008. Vol. 44. P. 463–472.
- [42] Kuznetsova, N.A. Humidity and distribution of springtails. *Entomological Review*, 2003. Vol. 83. No. 2. P. 230–238 (in Russia).
- [43] Potapov, M.B., Taskaeva, A.A. Analysis of vicarious species *Folsomia kuznetsovae* sp.n. and *F. bisetosa* Gisin (Collembola: Isotomidae). *Russian Entomological Journal*. 2009. Vol. 18. No. 1. P. 1–6 (in Russia).
- [44] Maculec, G. The effect of long term drainage of peat soil on earthworm communities (Oligochaeta: Lumbricidae). *Polish Ecological Studies*. 1991. Vol. 17. P. 203–219.

- [45] Pizl, V. Earthworm communities in Palava Biosphere Reserv (Southern Moravia) with special reference to the impact of floods. Pizl, V., Tajovsky, K. (Eds.). *Soil Zoological Problems in Central Europe*. Ceske Budejovice, 1998. P. 157–166.
- [46] Tajovsky, K. Impact of inundations on terrestrial arthropod assemblages in southern Moravia floodplain forests, the Czech Republic. *Ekologia*. 1999. Suppl. 18. No. 1. P. 77–184.
- [47] Tufova, J., Tuf, I.H. Survival under water – comparative study of millipedes (Diplopoda), centipedes (Chilopoda) and terrestrial isopods (Oniscidea). Tajovsky, K., Schlaghamersky, J., Pizl, V. (Eds.). *Contributions to Soil Zoology in Central Europe I*. Ceske Budejovice, 2005. P. 195–198.
- [48] Bayley, P. B. Understanding large river: floodplain ecosystems. *BioScience*. 1995. P. 153–158.
- [49] Tockner, K., Lorang, M. S., Stanford, J.A. River floodplains are model ecosystems to test general hydrogeomorphic and ecological concepts. *River Research and Applications*. 2010. Vol. 26. No. 1. P. 76–86.

---

# **Freshwater Prawns (Palaemonidae: *Macrobrachium*) with Abbreviated Larval Development in Rivers of Mexico: Uses, Management, and Conservation Opportunities**

---

Luis M. Mejía-Ortíz, Marilú López-Mejía,  
Antonio Chale Chim, Yazmín Perera-Pech,  
Keith A. Crandall, Oscar Frausto-Martínez and  
Luis C. Santander-Botello

Additional information is available at the end of the chapter

<http://dx.doi.org/10.5772/64400>

---

## **Abstract**

The *Macrobrachium* genus in Mexico is represented by two big groups: the first one, where the larval stages are extended, and the second one, has an abbreviated larval development. There are three main slopes in Mexico or exorheic basins and several endorheic basins such as lakes and inner lagoons. The species with extended larval stage are *M. carcinus*, *M. heterochirus*, *M. acanthurus*, *M. olfersii*, *M. hobbsi*, and *M. faustinum* in the Atlantic and Caribbean slope, while in the Pacific slope, these species are *M. americanum*, *M. occidentale*, *M. digueti*, *M. michoacanus*, *M. acanthochirus*, and *M. tenellum*. These species have important fishery activities on different basins because they live from oasis in desert to main rivers in the bigger basins. However, there are some rivers that have an extended region on their upstream such as Usumacinta, Grijalva, Papaloapan, and Coatzacoalcos basins that in general are considered as hydrological regions. Just in these extended regions, there are more caves in freshwater, springs, and primary or secondary streams, which are covered by short area rivers, and in these places, there are the following species: *M. totonacum*, *M. tuxtlaense*, *M. oaxacae*, *M. cosolapaense*, *M. oaxacae*, *M. jacatepecense*, *M. mazatecum*, and *M. vicconi*, while in the cave are *M. villalobosi*, *M. acherontium*, and *M. sbordonii*. However, for these species, the uses are more for the local groups mainly indigenous cultures such as Mayan, Lacandon, Zapotecs and Mixtecs, and others, and their commercial use is only in the local region depending on where these species are distributed.

**Keywords:** freshwater shrimp, Mexico, uses and management

---

## 1. Introduction

In the rivers, channels, and ponds in Mexico, there are several endemic crustaceans such as crabs, crayfishes, and freshwater shrimp species that are used by local people to obtain protein specifically by the indigenous cultures or these species are used by commercial fisheries in several basins around Mexico.

In first instance, the freshwater prawns from genus *Macrobrachium* in Mexico are represented by two big groups: the first one involved the species with a reproductive strategy “r” where the larval stages are extended, and the second one has an abbreviated larval development that is evidence of “k” strategy. There are three main slopes in Mexico or exorheic basins, on the Pacific, Atlantic and Caribbean Seas with several rivers, and several endorheic basins such as lakes and inner lagoons. The species with extended larval stages are in general bigger than those with abbreviated larval stages, and they have an important commercial use along the river basin where they inhabit and are possibly found in the big cities. The species members of this first group are *Macrobrachium carcinus*, *Macrobrachium heterochirus*, *Macrobrachium acanthurus*, *Macrobrachium olfersii*, *Macrobrachium hobbsi*, and *Macrobrachium faustinum* in the Atlantic and Caribbean slope, while in the Pacific slope, the species are *Macrobrachium americanum*, *Macrobrachium occidentale*, *Macrobrachium acanthochirus*, *Macrobrachium digueti*, *Macrobrachium michoacanus*, and (*Macrobrachium tenellum* **Table 1, Figure 1**) [1–3].

Pacific slope	Gulf of Mexico and Caribbean slopes
<i>Macrobrachium americanum</i>	<i>Macrobrachium carcinus</i>
<i>Macrobrachium tenellum</i>	<i>Macrobrachium acanthurus</i>
<i>Macrobrachium digueti</i>	<i>Macrobrachium olfersii</i>
<i>Macrobrachium occidentale</i>	<i>Macrobrachium heterochirus</i>
<i>Macrobrachium michoacanus</i>	<i>Macrobrachium hobbsi</i>
<i>Macrobrachium acanthochirus</i>	<i>Macrobrachium faustinum</i>

**Table 1.** Checklist of diadromous species of *Macrobrachium* in the three slopes in Mexico.

However, there are some rivers that have an extended region on their upstream such as Usumacinta, Grijalva, Papaloapan, and Coatzacoalcos basins that in general are considered as hydrological regions. Just in these extended region there are more caves with freshwater, springs, and primary or secondary streams that are covered by short area rivers; and in these places there are the following species: *Macrobrachium totonacum*, *Macrobrachium tuxtlaense*, *Macrobrachium oaxacae*, *Macrobrachium cosolapaense*, *Macrobrachium oaxacae*, *Macrobrachium jacatepecense*, *Macrobrachium mazatecum*, and *Macrobrachium vicconi*, and the cave represents *Macrobrachium villalobosi*, *Macrobrachium acherontium*, and *Macrobrachium sbordonii*, all of them with abbreviated larval development (**Table 2, Figure 2**) [3–12]. However, for these species, the uses are more for the local groups mainly indigenous cultures such as Lacandon, Zapotecs and

Mixtecs, and others, and their commercial use is only in the local region depending on where these species are distributed.

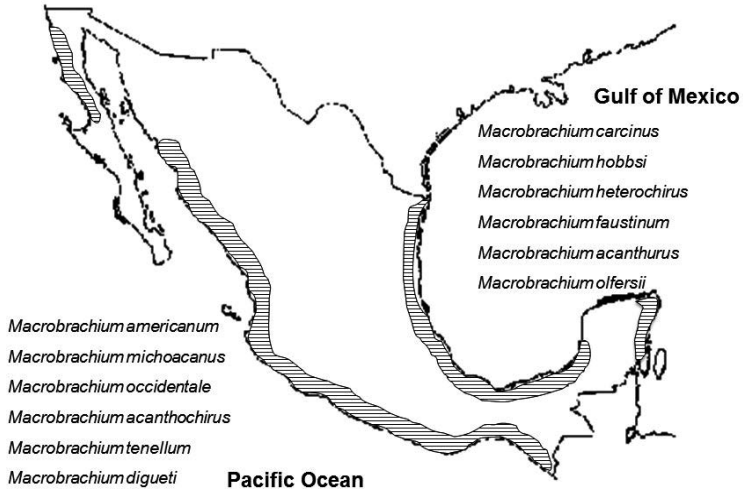


**Figure 1.** Distribution of freshwater prawns; valid species with extended larval development.

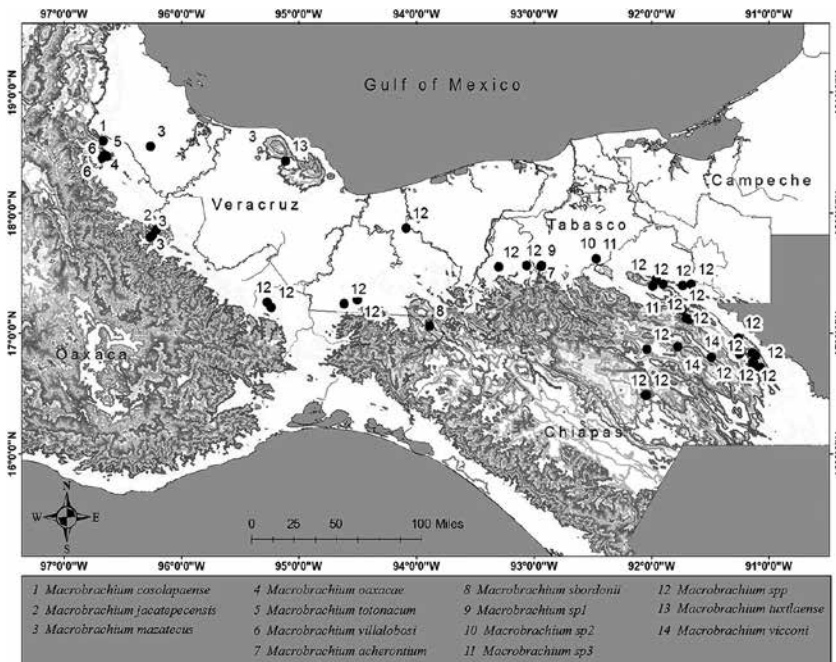


**Figure 2.** Distribution of freshwater prawns; described species, undescribed species and populations with abbreviated larval development.

The goal of this chapter is to show the distributional ranges of these species, as described in Section 2, which represents a holistic analysis that includes all species recognized in Mexico. Section 3 presents a normative frame analysis of the uses of natural resources such as freshwater prawns on river fisheries in Mexico and the river basin management programs according to the hydrological region in Mexico. Section 4 shows the commercial data specifically considering the bigger prawn species in the three slopes. Finally, Section 5 presents the uses and commercial opportunities to species with abbreviated larval development by the indigenous people and local markets in Mexico.

## 2. Distributional ranges of *Macrobrachium* species

In Mexico, these species are distributed into three exorheic basins: Pacific slope, Gulf of Mexico slope, and Caribbean slope. The first two basins are large with water flowing in the main river, and in the last one, due to the soil, the basins are subterranean and the freshwater flows underground to sea and the animals found the channels to inhabit in these places. It is interesting that in the Pacific and Gulf of Mexico or Caribbean Sea, there is one similar species inhabiting in each slope. In all cases, diadromous species need brackish water in some moments of their life cycle, while there are anadromous species that live their entire cycle in freshwater. In general, in these slopes, the climate is tropical wet, and tropical wet and dry and arid, because these species are present along the Pacific and Gulf of Mexico Coast; in general, the rivers still have the original riparian vegetation according to the location, but most of these basins are associated with a growing human population where the amount of sewage water has been increased in the past 50 years. Moreover, due to the water needs for agriculture, human consumption, and farmers, the dam construction occurred in the past years has produced diverse alterations in the normal migration conditions. For example, the species that need high content of oxygen dissolved, such as *Macrobrachium heterochirus* or *Macrobrachium occidentale*, cannot show more migration activity because the dam is an anthropogenic barrier and the distribution of these species is changed.

Caves and underground environments	Epigeal environments
<i>Macrobrachium villalobosi</i>	<i>Macrobrachium vicconi</i>
<i>Macrobrachium acherontium</i>	<i>Macrobrachium tuxtlaense</i>
<i>Macrobrachium sbordonii</i>	<i>Macrobrachium totonacum</i>
	<i>Macrobrachium cosolapaense</i>
	<i>Macrobrachium jacatepecense</i>
	<i>Macrobrachium oaxacae</i>
	<i>Macrobrachium mazatecum</i>

**Table 2.** Checklist of anadromous species of *Macrobrachium* with abbreviated larval development.

Species with abbreviated larval development trait in general live in the inner or endorheic basins mainly in springs. In general, these species inhabit areas between 100 and 300 m altitude around the mountain systems of hydrological basins. Because these mountain systems have emerged on Cretaceous and Tertiary and that the origin of *Macrobrachium* has been estimated in Cretaceous [13], the volcanic belt seems to be working as a geographical barrier for this group. The *Macrobrachium* species colonized these freshwater habitats together with *Creaseria morleyi* before the emergence of the Yucatan Peninsula [14].

Four habitat types are distinguished, where the freshwater prawns with abbreviated larval development have the following unifying characteristics: freshwater all time, tropical springs and streams, and important relationship with roots of riparian vegetation (trees or shrubs), the values of oxygen dissolved are high, and the pH trend toward alkalinity and few sites were recorded coexisting with another *Macrobrachium* species (complete larval development species). In general, all sites are clean without records of pollutants, both solids and dissolved.

### 3. Normative frame and management programs in Mexico

In Mexico, the normative frame for local fisheries is regulated by the Environment Secretary of Natural Resources (SEMARNAT, by Spanish acronyms). There are federal laws to protect the wildlife where it is stated that for some species that are examined with protected labels such as vulnerable, dangerous to extinct, or only dangerous, the fisheries are forbidden. In this case, for most *Macrobrachium* species, this law is not applicable because there are only two species *Macrobrachium villalobosi* and *Macrobrachium acherontium*, both protected from underground environments. So, each state establishes different regulations to grant the permissions to make a sustainable fishery. There are two main problems for the most species, the first one is the pollution that occurs in the high areas where the big cities are established because the regulations to eliminate the waste waters are null, so several elements such as heavy metals or nitrogenous or phosphorus species are released without any previous treatment. We suggest some sewage water treatment by using in first instance some local plants and increasing the treatment factories for this. However, the most important action is to prevent the indiscriminate water use because in the cities, small or big, there are few consciences about the implications on the water use. If we apply several strategies of environmental education, it is possible to attend the problem better. The other problem is establishing new dams in the middle of rivers to avoid the normal migrations to upstream and downstream as occur in several places. For those species that are living in the inner basins, the main problem is that they are living in specific places where they have a microdistribution and few species have several populations in different subbasins. So, any change in the environment could affect the populations that in some cases have been reported only in the locality type. A decrease has been reported in the population size of several species that normally live upstream. However, there are several records where the species of *Macrobrachium* walked out from rivers and climbed just beside the dam wall and then continued their migration upstream; so, if the dams include some passage or some strategies such as fish ladders, we cannot interrupt the normal migration.

#### 4. Fisheries and commercial data

In the slopes of Pacific and Gulf of Mexico, important fisheries on these resources exist. In general, the local people use local nets (atarrayas) or traps (nazas) to catch different species. The bigger species from both sides are *Macrobrachium carcinus* and *Macrobrachium americanum*; these species reach a maximum body length of 30 cm and a maximum weight surpassing 500 g. Another species from both sides are *Macrobrachium tenellum* and *Macrobrachium acanthurus*, both have a similar size to the most popular penaeid shrimps and several times they are sold as marine shrimps. Both species are very popular in the fisheries on the coastal areas, while for the first two species, the fisheries are more common in the middle of rivers where the ponds are deeper and the last important fisheries focus on *Macrobrachium heterochirus* and *Macrobrachium occidentale* that live in the waterfalls where the oxygen dissolved in water levels are higher in comparison with those reported in the coastal areas [15]. In Mexico, the fisheries are done mainly by local people and the average prices are shown in **Table 3**.

Species	Prices in US
<i>Macrobrachium carcinus</i>	\$ 35
<i>Macrobrachium americanum</i>	\$ 40
<i>Macrobrachium tenellum</i>	\$ 20
<i>Macrobrachium acanthurus</i>	
<i>Macrobrachium heterochirus</i>	\$ 15
<i>Macrobrachium occidentale</i>	
<i>Macrobrachium olfersii</i>	\$ 5
<i>Macrobrachium digueti</i>	
<i>Macrobrachium spp.</i>	

**Table 3.** Average prices for each species per kilogram.

#### 5. Local commercial uses of the *Macrobrachium* with abbreviated larval development

For the *Macrobrachium* species with abbreviated larval development, the main use is self-consumption, and for these cases, the indigenous cultures are the most important consumers; in the local market, it is possible to find some people that sale *Macrobrachium* species with this trait at a maximum value of US \$1.00 per kg; this is due to their small sizes and few people know it. There are different cultures that fishery this resource as shown in **Table 4**.

It is evident that the freshwater prawns of genus *Macrobrachium* in Mexico are an important natural resource because there are fisheries and local uses for self-consumption by indigenous



people, and the dangers to their population are relationship with the urban growth by human population because of the pollution levels and the energy needs (construction of dams in the rivers). However, the conservation actions include species with more danger to extinct due the habitat loss in the federal checklist to protect and monitor their populations.

Gulf of Mexico slope	
State	Indigenous cultures
Veracruz	Nahuas
	Totonacas
	Tepehuas
Oaxaca	Mazatecos
	Mixtecs
	Nahuas
	Zoques
	Amuzgos
Chiapas	Lacandones
	Mam
	Tzotziles
	Kanjobales
	Tojolabales
	Jalcatecos
	Zoques
	Chontales
Tabasco	Nahuas

**Table 4.** Indigenous cultures that used the *Macrobrachium* species with abbreviated larval development as self-consumer.

## Acknowledgements

The authors are grateful to the División of Desarrollo Sustentable from University of Quintana Roo and to Consorcio de Universidades Mexicanas (CUMEX) for supporting this collaboration through the International Exchange Program. This paper was also supported by the projects Diversidad del género *Macrobrachium* en el sureste de México (PROFI-2012-05-UQROO), Crustáceos Malacostracos del río Papalopan (CONABIO) and Sistemática molecular de los langostinos del género *Macrobrachium* con desarrollo larval abreviado en México y su relación con Guatemala y Belice (CONACYT-258494). The authors also thank Marilú and Maya Mejía Lopez and other undergraduate students who participated in the lab and fieldwork.

## Author details

Luis M. Mejía-Ortíz<sup>1,2\*</sup>, Marilú López-Mejía<sup>1</sup>, Antonio Chale Chim<sup>2</sup>, Yazmín Perera-Pech<sup>2</sup>, Keith A. Crandall<sup>3</sup>, Oscar Frausto-Martínez<sup>1</sup> and Luis C. Santander-Botello<sup>1</sup>

\*Address all correspondence to: [luismejia@uqroo.edu.mx](mailto:luismejia@uqroo.edu.mx)

1 Research Group of Aquatic Natural Resources Management, Sustainable Development Division, University of Quintana Roo, Cozumel, Quintana Roo, Mexico

2 Biospeleology and Carcinology Laboratory, Sustainable Development Division, University of Quintana Roo, Cozumel, Quintana Roo, Mexico

3 Computational Biology Institute, George Washington University and National Museum of Natural History, Smithsonian Institution, Washington, DC, USA

## References

- [1] Anger K. Neotropical *Macrobrachium* (Caridea: Palaemonidae): on the biology, origin, and radiation of freshwater-invading shrimp. *Journal of Crustacean Biology*. 2013; 33(2): 151–183.
- [2] Mejía-Ortíz LM, Alvarez F, Román R, & Viccon-Pale JA. Fecundity and distribution of freshwater prawns of the genus *Macrobrachium* in the Huitzilapan river, Veracruz, Mexico. *Crustaceana*. 2001; 74(1): 69–77.
- [3] Mejía-Ortíz LM & López-Mejía M. Freshwater prawns of the genus *Macrobrachium* (Decapoda, Palaemonidae) with abbreviated development from the Papaloapan River Basin, Veracruz, México: distribution and new species. *Crustaceana*. 2011; 84(8): 949–973.
- [4] Alvarez F, Villalobos JL, & Robles F. Abbreviated larval development of *Macrobrachium tuxtlaense* Villalobos and Alvarez, 1999, reared in the laboratory. *Crustaceana*. 2002; 75: 717–730.
- [5] Hobbs HH Jr. Two new troglobitic shrimps (Decapoda: Alpheidae and Palaemonidae) from Oaxaca, México. *Bulletin of the Association for Mexican Cave Studies*. 1973; 5: 73–80.
- [6] Holthuis LB. Cave shrimp (Crustacea, Decapoda, Natantia) from Mexico. *Accademia Nazionale dei Lincei*. 1977; 171: 173–195.
- [7] Mejía LM, Álvarez F, & Hartnoll RG. A new species of freshwater prawn, *Macrobrachium totonacum* (Decapoda: Palaemonidae), with abbreviated development from Mexico. *Crustaceana*. 2003; 76: 77–86.

- [8] Mejía-Ortíz LM, Baldari F, & López-Mejía M. *Macrobrachium sbordonii* (Decapoda: Palaemonidae), a new stygobitic species of freshwater prawn from Chiapas Mexico. *Zootaxa*. 2008; 1814: 49–57
- [9] Mejía-Ortíz LM Hartnoll RG, & López-Mejía M. The abbreviated larval development of *Macrobrachium totonacum* Mejia, Alvarez & Hartnoll, 2003 (Decapoda, Palaemonidae), reared in the laboratory. *Crustaceana*. 2010; 83(1): 1–16.
- [10] Roman R, Ortega AL, & Mejía LM. *Macrobrachium vicconi*, a new species of fresh-water shrimp from a rain forest in southeast Mexico, and comparison with congeners (Decapoda, Palaemonidae). *Journal of Crustacean Biology*. 2000; 20(1): 186–194.
- [11] Signoret GPB, Ortega ALM, & Brailovsky DS. Partially abbreviated larval development in an undescribed freshwater palaemonid prawn of the genus *Macrobrachium* from Chiapas, Mexico. *Crustaceana*. 2000; 73(3): 273–282.
- [12] Villalobos JL & Alvarez F. A new species of *Macrobrachium* (Crustacea: Decapoda: Palaemonidae), with abbreviated development, from Veracruz, Mexico. *Proceedings of the Biological Society of Washington*. 1999; 112(4): 746–753.
- [13] Porter ML, Pérez-Losada M, & Crandall KA. Model-based multi-locus estimation of decapod phylogeny and divergence times. *Molecular Phylogenetics and Evolution*. 2005; 37: 355–369.
- [14] Botello A & Alvarez F. Phylogenetic relationships among the freshwater genera of palaemonid shrimps (Crustacea: Decapoda) from Mexico: evidence of multiple invasions. *Latin American Journal of Aquatic Research*. 2013; 41(4): 773–780.
- [15] Mejía-Ortíz LM & Álvarez F. Seasonal effects on the distribution of three species of *Macrobrachium* along an altitudinal gradient. *Crustaceana*. 2010; 83(4): 385–397.







*Edited by Daniel Bucur*

Many of the challenges facing farmers and human communities from hydrographical basins are not new. But, due to the fact that the nature and extents of the problems vary from one region to another and from one basin to another, the responses are highly diversified. There is no generally valid solution for all the problems. However, in addressing issues on ensuring the prevention or mitigation of the destructive consequences of flood damage or prolonged drought as for the optimal use of water by consumers, sustainable basin land use, biodiversity conservation, and environment protection as well, fourteen specialists and their colleagues present the state of the art in these important matters and new possible solutions to solve, identified from the scientific investigations undertaken.

Photo by desertsolitaire / iStock

**IntechOpen**

